# HETEROMETALLIC ASSEMBLIES FROM RUTHENIUM 4-ETHYNYLPYRIDYL PRECURSORS

**GE QINGCHUN**

**NATIONAL UNIVERSITY OF SINGAPORE**

2010

# HETEROMETALLIC ASSEMBLIES FROM RUTHENIUM 4-ETHYNYLPYRIDYL PRECURSORS

BY

**GE QINGCHUN**

(*M.Sc.* Nankai University, P. R. China)

A THESIS SUBMITTED FOR THE DEGREE OF

**DOCTOR OF PHILOSOPHY**

DEPARTMENT OF CHEMISTRY

NATIONAL UNIVERSITY OF SINGAPORE

2010

# CONTENTS

# ACKNOWLEDGEMENTS

First of all, I am heartily thankful to my supervisor, Professor Hor Tzi Sum, Andy, whose guidance, encouragement and patience throughout the course of this project enabled me to develop an overall understanding of this subject. Without his support, this thesis would not have been possible. Saying that "the day as a teacher for life is the father", Prof Hor's spirit of hard working, his interest in chemistry and profound philosophy of life will have a lasting impact on my attitude towards life and career.

Secondly, I would like to express my gratitude to Professor Mark Humphrey at Australian National University. I appreciate his kind help on the nonlinear optical studies of this work, his helpful discussion and constructive suggestions. Thanks are extended to the staff of CMMAC (X-ray, Microananlytical, NMR and Mass spectrometry Laboratories) for their technical support and assistance.

Thirdly, I am indebted to many of my labmates in Prof Hor's group. Specifically I would like to thank Sheau Wei for her kind help and patience in my research and daily life; Dr. Weng Zhiqiang, Parag, Swee Kuan, Kian Eang, Jing Qiu, Hsiao Wei, Dr. Guo Yanhe, Dr. Li Fuwei, Dr. Zhang Jun, Dr. Bai Shiqiang, Dr. Zhao Jin, Ni Ni, Wen Hua, Gabriel, Xiao Yan, Shen Yu and Wang Jing for their help in one way or another. They make the research life in laboratory colorful and full of fun.

I would also like to thank National University of Singapore for granting me the research scholarship which provided me the opportunity to carry out the research for

this thesis.

Great gratitude is given to my beloved parents and family, for their great love and unselfish support during so many years' study.

Lastly, I offer my regards and blessings to all of those who supported me in all respects during the completion of the project.

# SUMMARY

The aim of this project is to synthesize and investigate the reactivity of a series of mononuclear Ru(II) 4-ethynylpyridine complexes: *trans*-[Ru(L)(C≡Cpy-4)(P-P)$_2$] or [Ru($\eta^5$-$C_5H_5$)(C≡Cpy-4)(P-P)] (L = Cl or H; P-P = 2PPh$_3$, dppm, dppe, dppf), which are used as "building blocks" to construct high nuclearity complexes with precisely controlled lengths.

A range of metal fragments, from square planar Pd(II)/Pt(II) chloride, paddlewheel geometrical dirhodium tetracetate to octahedral Re(I) diimine carbonyls, have been combined with mononuclear Ru(II) acetylides to yield a diverse range of architectures and properties. This project will address some of the deficiency in our knowledge of acetylide heterometallic assemblies.

**Chapter One** gives a general introduction of Ru(II) acetylide based mononuclear, oligo- and poly-nuclear complexes. Their synthetic methods, chemical reactivity, properties and applications are described.

**Chapter Two** describes the syntheses, characterization and general properties of Ru(II) 4-ethynylpyridine based mononuclear and heteronuclear complexes.

In this work, the mononuclear Ru(II) acetylides are obtained by incorporation of 4-ethynylpyridine into Ru(II) fragments. 4-Ethynylpyridine is the spacer of choice because it is chemically stable, conjugative, stereochemically active, geometrically directive, and able to support variety of metals in different redox states. It has been

shown to serve as versatile and powerful building blocks in the construction of heterometallic complexes. As a bridging ligand, 4-ethynylpyridine moiety plays an important role since it connects the donor and acceptor and is directly responsible for the degree of electronic communication between the metal centers.

Systematic studies on the spectroscopic properties of both mononuclear and heteronuclear systems have been conducted. They show the similarities and differences of these related complexes. Individual parameters from different spectroscopies reflect the subtle changes in the bonding, induced by the electronic properties of the electron-withdrawing metal fragments introduced. X-ray structural studies have been performed on most of the complexes under investigation, and could lead to their further development as molecular wires.

Nonlinearity can be enhanced by either increasing the conjugation length or increasing the strength of donor or acceptor groups. In this project, a series of transition metals of different nature, coordination geometry, coordination number, and oxidation states have been incorporated into Ru(II) 4-ethynylpyridine moieties and a change in the optical properties was anticipated. Linear and nonlinear optical properties of the mononuclear and heteronuclear complexes will be described in **Chapter Three**.

**Chapter Four** reports the electrochemical behavior of the complexes presented in **Chapter Two**. Incorporation of the redox center(s), mononuclear Ru(II) 4-ethynylpyridine complexes, into one-dimensional delocalized metal fragments

increases the electron delocalization, and enhances their electronic communication. Hence the heterometallic acetylide systems in this project exhibit more significant electrochemical properties. Electrochemical behavior of the mononuclear Ru(II) 4-ethynylpyridine complexes and their corresponding high nuclear (di-, tri- and tetra-nuclear) assemblies have been examined by cyclic voltammetry.

The experimental section is in **Chapter Five**. The collection and refinement details of X-ray diffraction studies are listed in **Tables 5.1** to **5.8**. The crystallographic analysis data (CIF files) of the structures presence in the thesis and spectra (ESI-MS and NMR) of all compounds are included in a companion CDROM placed at the back of the thesis.

# CHAPTER LIST

# LIST OF SCHEMES

# LIST OF TABLES

# LIST OF FIGURES

# LIST OF ABBREVIATIONS AND SYMBOLS

| | |
|---|---|
| br | broad |
| bpy | bipyridine |
| Bu | $C_4H_9$/phenyl |
| *ca.* | about (Latin *circa*) |
| Cp | $\eta^5$-Cyclopentadienyl |
| Cp* | 1,2,3,4,5-Pentamethylcyclopentadienyl |
| d | doublet |
| dbu | 1,8-diazabicyclo[5.4.0] undec-7-ene |
| dppm | bis(diphenylphosphino)methane |
| dppe | 1,2-bis(diphenylphosphino)ethane |
| dppf | 1,1'-bis(diphenylphosphino)ferrocene |
| ESI-MS | Electrospray Ionization Mass Spectrometry |
| Et | ethyl ($C_2H_5$) |
| *et al.* | and others (Latin *et alii*) |
| g | gram |
| h | hour(s) |
| IR | infrared |
| *J* | coupling |
| δ | chemical shift |
| m | medium (IR), multiplet ( NMR) |

| | |
|---|---|
| M | molecular weight |
| Me | $CH_3$/methyl |
| mg | milligram |
| min(s) | minute(s) |
| mL | milliliter |
| mmol | millimole |
| NLO | nonlinear optical |
| NMR | nuclear magnetic resonance |
| N-N | N,N- bridging ligands |
| OTf | $CF_3SO_3$/triflate/trifluoromethanesulfonate |
| P-P | P,P- bridging ligands |
| $PBu_3$ | tributylphosphine |
| Ph | $C_6H_5$/phenyl |
| $PPh_3$ | triphenylphosphine |
| py | pyridine |
| q | quartet |
| r.t. | room temperature |
| s | singlet ( NMR), strong (IR) |
| t | triplet |
| THF | tetrohydrofuran |
| tpy | tripyridine |
| v | very |

| | |
|---|---|
| V | voltage |
| v/v | volume/volume |
| vs | versus |
| w | weak |

# LIST OF NUMBERED COMPLEXES

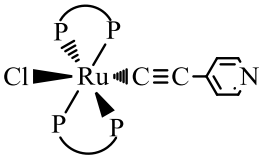


P⌒P = dppm **5.1**

P⌒P = dppe **5.3**

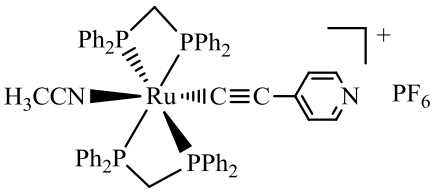


**5.2**

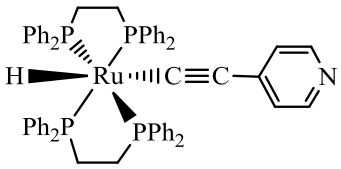


**5.4**

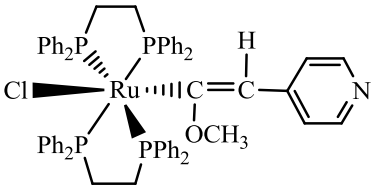


**5.5**

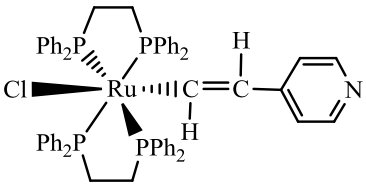


**5.6**

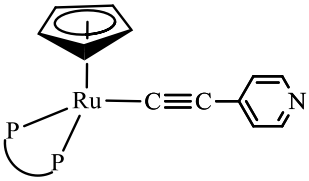


P⌒P = dppf **5.7**

P⌒P = 2PPh$_3$ **5.8**

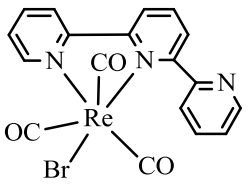


**5.9**

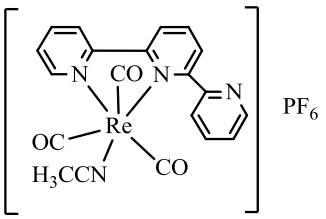


**5.10**

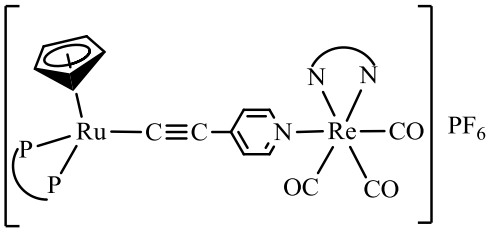

P P = dppf N N = bpy **5.11**, $Me_2$bpy **5.12**, $Bu_2$bpy **5.13**, phen **5.14**, P P = $2PPh_3$ N N = bpy **5.16**

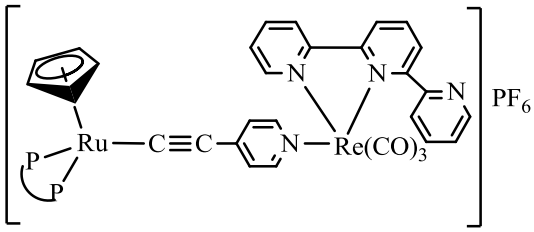

P P = dppf **5.15**

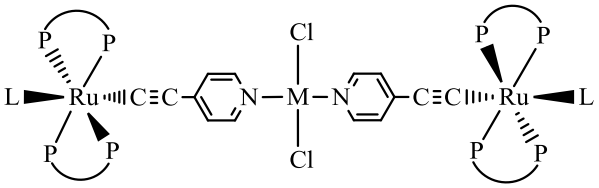

| M | P P | L | |
|---|---|---|---|
| Pd | dppm | Cl | **5.17** |
| Pt | dppm | Cl | **5.18** |
| Pd | dppe | Cl | **5.19** |
| Pt | dppe | Cl | **5.20** |
| Pd | dppe | H | **5.21** |

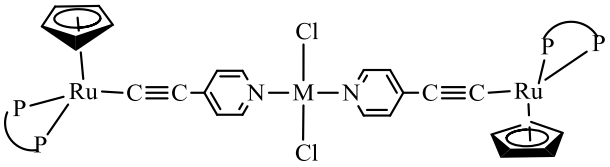

P P = dppf M = Pd **5.22**, M = Pt **5.23**

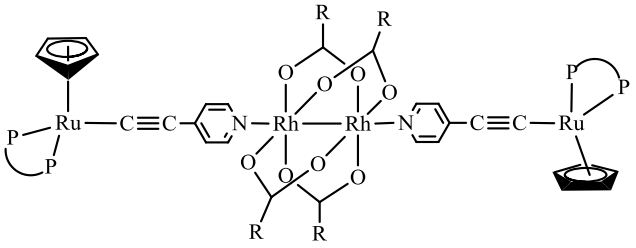

R = $CH_3$ **5.24**, $CH_2CH_3$ **5.25**, $(CH_2)_3CH_3$ **5.26**, $C(CH_3)_3$ **5.27**

P P = dppf

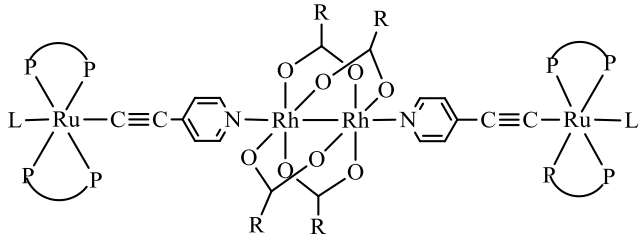

| R | P P | L | |
|---|---|---|---|
| $CH_3$ | dppm | Cl | **5.28** |
| $CH_2CH_3$ | dppm | Cl | **5.29** |
| $(CH_2)_3CH_3$ | dppm | Cl | **5.30** |
| $C(CH_3)_3$ | dppm | Cl | **5.31** |
| $CH_2CH_3$ | dppe | H | **5.32** |
| $(CH_2)_3CH_3$ | dppe | H | **5.33** |
| $C(CH_3)_3$ | dppe | H | **5.34** |

# LIST OF CONFERENCE PAPERS AND PUBLICATIONS

**Publications from this research work**:

**Journal Papers**

1 Q. Ge, T. C. Corkery, M. G. Humphrey, M. Samoc and T. S. A. Hor, "Organobimetallic $Ru^{II}$–$Re^{I}$ 4-ethynylpyridyl complexes: structures and non-linear optical properties", *Dalton Trans.*, 2009, 6192–6200.

2 Q. Ge, G. T. Dalton, M. G. Humphrey, M. Samoc and T. S. A. Hor, "Structural and Nonlinear Optical Properties of Aligned Heterotrinuclear [$Ru^{II}$-(Spacer)-$M^{II}$-(Spacer)-$Ru^{II}$] Complexes (M=Pd, Pt; spacer=4-ethynylpyridine)", *Chem. Asian J*. 2009, 4, 998 – 1005.

3 Q. Ge and T. S. A. Hor, "Stepwise assembly of linearly-aligned Ru–M–Ru (M = Pd, Pt) heterotrimetallic complexes with σ-4-ethynylpyridine spacer", *Dalton Trans.*, 2008, 2929–2936.

4 Q. Ge, G. T. Dalton, M. G. Humphrey, M. Samoc and T. S. A. Hor, "Structural, electrochemical, linear and nonlinear optical studies of $Ru^{II}$ σ-acetylide complexes and their heterometallic assembly with σ-4-ethynylpyridine-type spacers", manuscript in preparation.

5 Q. Ge, T. C. Corkery, M. G. Humphrey, M. Samoc and T. S. A. Hor, "Linear Heterotetranuclear $Ru^{II}$-$Rh^{II}$-$Rh^{II}$-$Ru^{II}$ Assembly: A Comprehensive Study of Their

Preparation, Structure, Electrochemistry, Optical Absorption and Nonlinear Optical Properties", submission in preparation.

**Conference Papers**

6 Q. Ge and T. S. A. Hor, "Use of Directional Bifunctional Spacers to Construct $\mu,\eta^2$-Alkynyl-Bridged Multinuclear Systems", *6th International Symposium by Chinese Inorganic Chemists (ISCIC-6) & 9th International Symposium by Chinese Organic Chemists (ISCOC-9)* (17 - 20 Dec 2006, Grand Copthorne Waterfront Hotel, -blank-, Singapore). Publication No. 0328723, (Poster Presentation)

7 Q. Ge and T. S. A. Hor, "Multimetallic assembly of Ru(II) complexes with sigma-4-ethynylpyridine-type spacers", in *XXXVIth International Conference on Coordination Chemistry* (13 - 18 Aug 2006, Cape Town International Convention Centre, Cape Town, South Africa), Publication No. 0309662, (Poster Presentation).

8 Q. Ge and T. S. A. Hor, "$Ru^{II}$-based Heterometallic Assembly with σ-Pyridylacetylide Spacer", in *Singapore-China Collaborative and Cooperative Chemistry Symposium (S=C=C=C=C=S)* (5 - 6 Jan 2006, National University of Singapore, Singapore), Publication No. 0226165, (Poster Presentation).

9 Q. Ge and T. S. A. Hor, "$Ru^{II}$-based Heterometallic Assembly with σ-4-Ethynylpyridine-type Spacers", in *Pacifichem 2005* (15 - 20 Dec 2005, Honolulu, Hawaii, United States) 168. Publication No. 0211723, (Poster Presentation).

10 Q. Ge and T. S. A. Hor, "$Ru^{II}$-based Heterometallic Assembly with σ-Ethynylpyridine Spacer", in *Singapore International Chemical Conference 4* (8 - 10 Dec 2005, Shangri-La Hotel, Singapore). Publication No. 0300186, (Poster Presentation).

11 Q. Ge and T. S. A. Hor, "Nitrito-bridged heterodinuclear complexes". In *The 8th International Symposium for Chinese Organic Chemists (ISCOC-8); The 5th International Symposium for Chinese Inorganic Chemists (ISCIC-5)* (19 - 22 Dec 2004, The Chinese University of Hong Kong, Hong Kong, China). Publication No. 0202954, (Poster Presentation).

# Chapter One

## *General Information of Ru(II) Acetylide Based Mononuclear, Oligo- and Poly-Nuclear Complexes*

## 1.1 Introduction

Organic materials with carbon-rich π-conjugation exhibit intriguing nonlinear optical (NLO) properties and can be potentially employed as polymeric conductors or liquid crystals.[1,2] This functionality can be attributed to the π-conjugation among the organic moieties, which allows π electron delocalization and hence electronic communication along the linear π-conjugated backbones. Although organics have dominated recent studies of molecular NLO materials,[1,3] they have several disadvantages: low energy transitions in the UV-vis region result in a trade-off between nonlinear efficiency and optical transparency; they have low thermal and chemical stability, and may be subject to random orientation.[1,4,5]

One possible strategy for altering and manipulating the properties of these materials is by incorporation of metal center units, $ML_n$, into the conjugated carbon-rich organic systems. This will introduce a range of properties, such as redox,[6-8] luminescence,[9-12] optical[5,13,14] and electronic properties,[15-17] since the electronic properties are modified by the incorporation of metal fragments due to the interplay among the metal ion, auxiliary ligands, and π-conjugated groups.[18,19] This

effect cannot be matched by the conventional π-conjugated organic systems. Moreover, compared to their organic molecules, the corresponding metal complexes, such as metal alkynyl complexes, have the advantage of much greater design flexibility, i.e. by variation in metal, oxidation state, ligand environment and geometry.[20-22]

Metal alkynyl complexes were first reported in 1960,[23] and the study of transition metal alkynyl complexes has been an intense area of research since the mid-1980's.[24] There are now over 20,000 papers focusing on metal alkynyl species and many carbon-rich organometallic systems are well documented.[5,18,25-29] The scope of the research not only covers traditional organometallic areas, but also reflects the interest in utilizing these species in materials science.[18,30,31] The chemistry of metal alkynyl complexes is a very topical and diverse area of interest and it is necessary to be selective in the coverage by concentrating on Ru(II) related acetylide complexes.

Ru(II) acetylide complexes have been playing a key role in the development of electrochemistry[14,32,33] and nonlinear optics.[4,5] These complexes have also highly contributed to the development of multimetallic electrochemistry[8,32,34] and nonlinearities,[5] and in particular to aspects related to photoinduced electron and energy transfer processes within multicomponent assemblies, including light-active dendrimers.[35-37] The chemistry of Ru(II) acetylide based mononuclear, oligonuclear and polynuclear assemblies is described in the following sections of this chapter.

## 1.2 Synthetic Methods

### 1.2.1 Mononuclear Ru(II) Acetylide Systems

Mononuclear Ru(II) complexes containing C≡C groups occupy a very important position in the development of oligo- and poly-nuclear organometallic chemistry. Efficient synthetic procedures to mononuclear Ru(II) acetylide complexes are therefore crucial. The synthetic scheme developed by Dixneuf *et al.*,[38,39] in which the reaction between a dichlororuthenium phosphine complex with a terminal alkyne in the presence of $NaPF_6$ and a base represents a significant breakthrough. Up to now, a number of synthetic strategies have been developed.[40-45]

Mononuclear Ru(II) acetylide complexes can be obtained from reactions of terminal alkynes or anionic alkynylating agents such as alkali-metal with a 16-electron Ru(II) metal species. The intermediate vinylidene metal complexes undergo deprotonation to yield the desirable metal acetylide analogues. The formation of these coordinatively unsaturated species from a suitable precursor complex is achieved by the following ways: (a) the dissociation of a halide ligand driven by the precipitation of an insoluble salt of the cationic vinylidene complex.[40,41] Some Ru(II) complexes have been proven to easily yield vinylidene species $Ru^{+}$=C=CHR by the displacement of a halide in the presence of both a non-coordinating anion and a terminal alkyne;[42] (b) the dissociation of a monodentate phosphine ligand;[43] (c) the dissociation of a solvent molecule coordinated to the metal center;[44,46] (d) the partial dissociation of hemilabile ligands,

which produces a vacant coordination site.[45] Some preparations used more than one of the above methods.[18]

## 1.2.2 Oligonuclear and Polynuclear Systems

There are a variety of methods to construct oligonuclear and polynuclear metal acetylide systems. One of the most attractive and convenient synthetic approaches is employing "metalloligands", i.e. "metal complexes as ligands"[47], as building blocks. Metal complexes with a basic pendant donor can serve as metalloligands.

The use of metalloligands as building blocks is very appealing for several reasons: (a) tremendous versatility due to the potentially large and diverse number of suitable transition metal complexes which can provide various spatial and electronic structures in accordance with their coordination numbers, geometries, and oxidation states; (b) the properties of each metal-containing subunit may undergo perturbation upon incorporation into the multicomponent system, and (c) a number of new processes involving different metal-containing units (intercomponent processes) may take place in the multinuclear complexes.

The design of metalloligands is important for the construction of multinuclear assemblies. A suitable choice of metalloligands leads to the possibility of controlling the overall structure and allows the occurrence of interesting and useful properties, such as electrochemical behavior, luminescence, optical characteristics, and function as catalysts. In order to produce defined architectures in a controlled fashion from

multiple subunits, special care must be devoted to the choice of metals, auxiliary ligands and bridging ligands. There are many known metalloligands.[48-51] However species containing both carbon-rich rigid bridging ligand and Ru(II) metal fragments are relatively sparse.[52-55] The donor group on mononuclear Ru(II) acetylides [Ru-C≡C-R] can help the Ru(II) acetylide complexes to serve as metalloligands to prepare high-nuclearity assemblies. Ru(II) acetylides containing terminal C≡C, C≡N, pyridyl, etc. are widely used as building blocks in the construction of high-nuclear complexes. Examples of mononuclear Ru(II) acetylides as metalloligands in the formation of oligo- or poly-nuclear assemblies are introduced based on different groups of the metals below.

### 1.2.2.1 Mononuclear Ru(II) Acetylides with Group 6 Metal Fragments

Ruthenium and Group 6 mixed metal acetylide complexes are usually prepared from Ru(II) acetylides containing uncoordinated CN or pyridyl moieties with Cr/Mo/W bound by carbonyl and labile ligands.[52,56] Reaction of complex **1** with [W(THF)(CO)$_5$] resulted in the displacement of the labile THF ligand and formation of the Ru-W binuclear complex **2** in moderate yield (**Scheme 1.1**).[57]

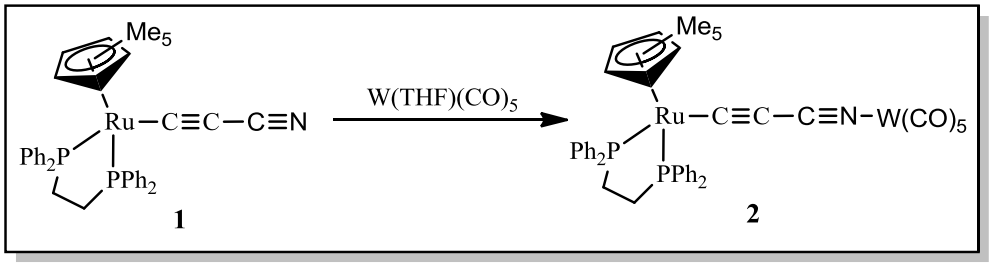


**Scheme 1.1** Synthesis of Ru-W binuclear complex **2** by the replacement of labile ligand

Treatment of octahedral cluster $[n\text{-}Bu_4N]_2[Mo_6Br_8(OTf)_6]$ (OTf = triflate) with metalloligand $[RuCp(C{\equiv}Cpy\text{-}4)(PPh_3)_2]$ afforded the metal-cluster-cored complex $[Mo_6Br_8][RuCp(C{\equiv}Cpy\text{-}4)(PPh_3)_2]_6(OTf)_4$.[53] The apical triflate ligands in the Mo-cluster undergo hexa-substitution by the ruthenium metalloligand.

### 1.2.2.2 Mononuclear Ru(II) Acetylides with Group 7 Metal Fragments

Only a few complexes formed from Ru(II) acetylides and metal fragments of Group 7 have been reported in the literature.[58,59] Most of them are constructed through 4-ethynylpyridine as the linker, as shown in **Scheme 1.2**. Treatment of Ru(II) biacetylide **3** with two equivalents of $[Re(^tBu_2bipy)(CO)_3(MeCN)](OTf)$ under reflux in THF afforded the trimetallic complex **4**.[58]

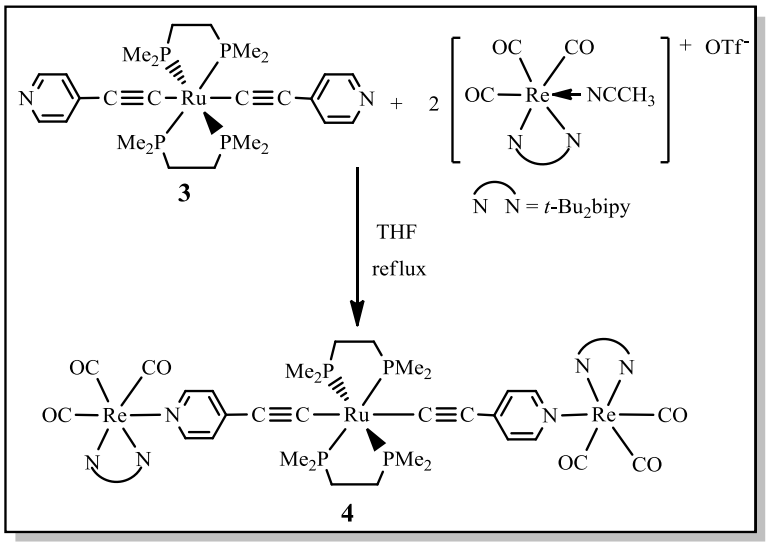


**Scheme 1.2** Formation of air and thermally stable trimetallic complex **4**

### 1.2.2.3 Mononuclear Ru(II) Acetylides with Group 8 Metal Fragments

There are a variety of homo- and hetero-metallic acetylide systems of Group 8

metals. Most of these complexes are obtained by the reaction of Ru(II) acetylides with terminal alkynes and metal fragments from the same group.[41,60] Ruthenium diynyl **5** was coupled with iron precursor [FeCp*Cl(dppe)] in $NEt_3$ in the presence of $NaBPh_4$ and 1,8-diazabicyclo[5.4.0] undec-7-ene (dbu) to give the Fe-Ru heterobimetallic complex **6** in high yield (**Scheme 1.3**).[54] This mixed Fe/Ru complex has been demonstrated to undergo three stepwise one-electron oxidations, allowing the investigation of the relative contributions of the metal and auxiliary ligands to the properties of the $[\{M\}\text{-}CC\text{-}CC\text{-}\{M\}]^{n+}$ assemblies.[54]

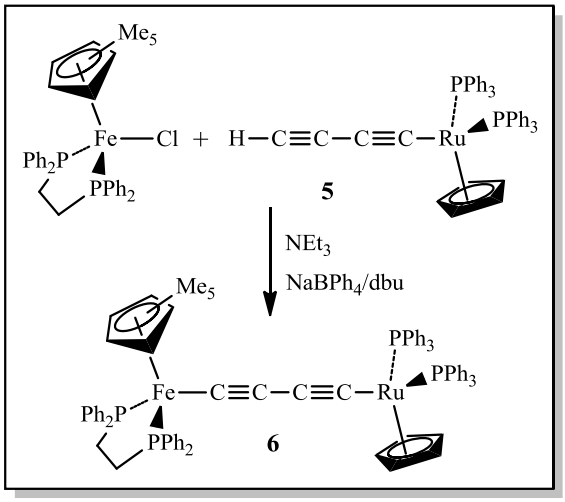


**Scheme 1.3** Synthesis of Fe-Ru diyndiyl complex **6** possessing three stepwise one-electron oxidation property

Due to its strong coordinating ability, the CN ligand can bond strongly with late transition metal ions compared to σ-only donor ligands or σ- and π-donor ligands, e.g. halide ions. Ru(II) acetylides carrying CN group are good building blocks for the fabrication of high nuclearity assemblies. The reactions shown in **Scheme 1.4** illustrate this reactivity. Reaction of compound **7** with $[RuCpCl(PPh_3)_2]$ and $NH_4PF_6$

in MeOH resulted in a conversion to the homobinuclear species **8**. A similar procedure with [FeCpCl(dppe)] led to the formation of the heterobimetallic species **9**.[61]

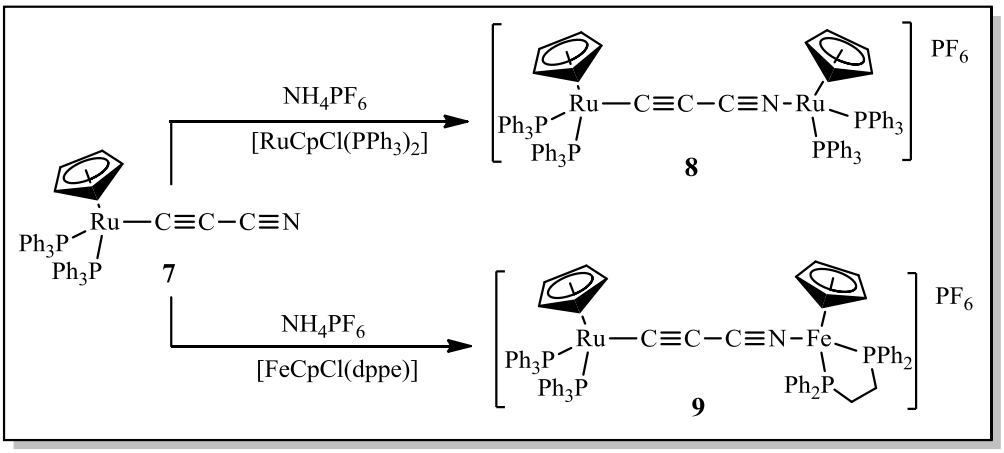


**Scheme 1.4** Formation of bimetallic complexes **8** & **9** from the metallocynoacetylide ligand **7**

Ru(II) acetylide complexes can also react with osmium carbonyl complexes through C≡C unit,[62] but this type of reaction is not as common as that of the Group 9 series.

### 1.2.2.4 Mononuclear Ru(II) Acetylides with Group 9 Metal Fragments

The reaction of Ru(II) acetylide complexes with metal fragments of Group 9 is depicted in **Scheme 1.5**, in which triyne **10** reacts with cobalt carbonyl complex $Co_2(CO)_8$ and mixed metal complex **11** was obtained.[62]

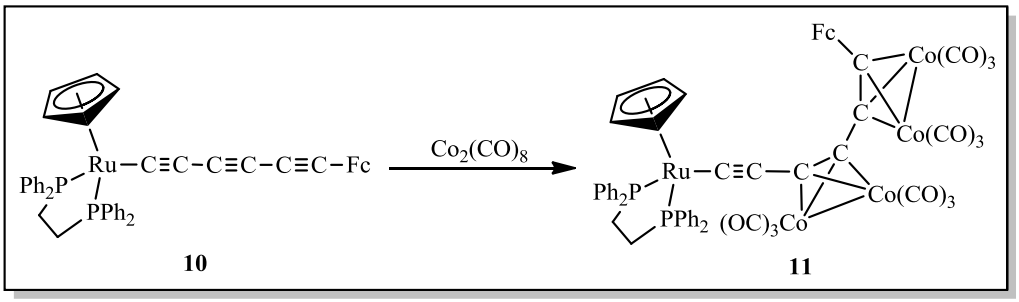


**Scheme 1.5** Synthesis of bimetallic cluster **11** by nucleophilic addition reation of complex **10**

The C≡C unit in Ru(II) acetylide complexes can react with other cobalt carbonyl complexes and metal carbonyls.[51,62,63]

### 1.2.2.5 Mononuclear Ru(II) Acetylides with Group 10 Metal Fragments

A $d^6/d^8$ Ru-Pd mixed-metal polymer **13** was prepared from Ru(II) tetrayne complex *trans*-[Ru(C≡C-*p*-$C_6H_4$-C≡CH)$_2$(dppe)$_2$] (**12**) and *trans*-[$PdCl_2(PBu_3)_2$] through a Cu-catalyzed dehydrohalogenation process.[64] Compound **13** represents the first Ru-Pd polymetallayne to be isolated in the literature and its trimetallic model compound **15** was also prepared from Ru(II) acetylide complex **14** and *trans*-[$PdCl_2(PBu_3)_2$] (**Scheme 1.6**).[65]

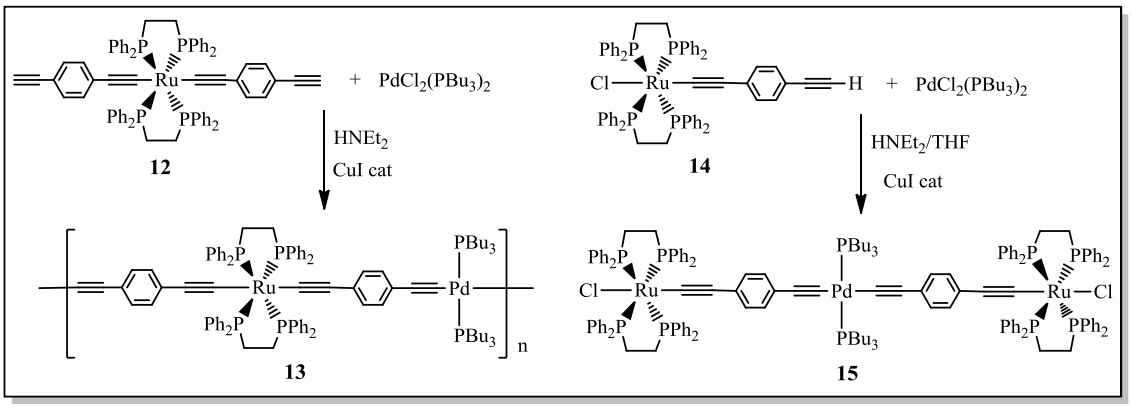


**Scheme 1.6** Formation of the first Ru-Pd polymetallayne **13** and its oligomer analogue **15**

Coupling of the triplatinum core complex **16** to three equivalents of the triruthenium complex **17** afforded a $Ru_6Pt_3$ dendrimer **18** (**Scheme 1.7**). This complex was prepared for its interesting NLO properties.[55] The synthetic methodology employed is applicable to higher generation species.

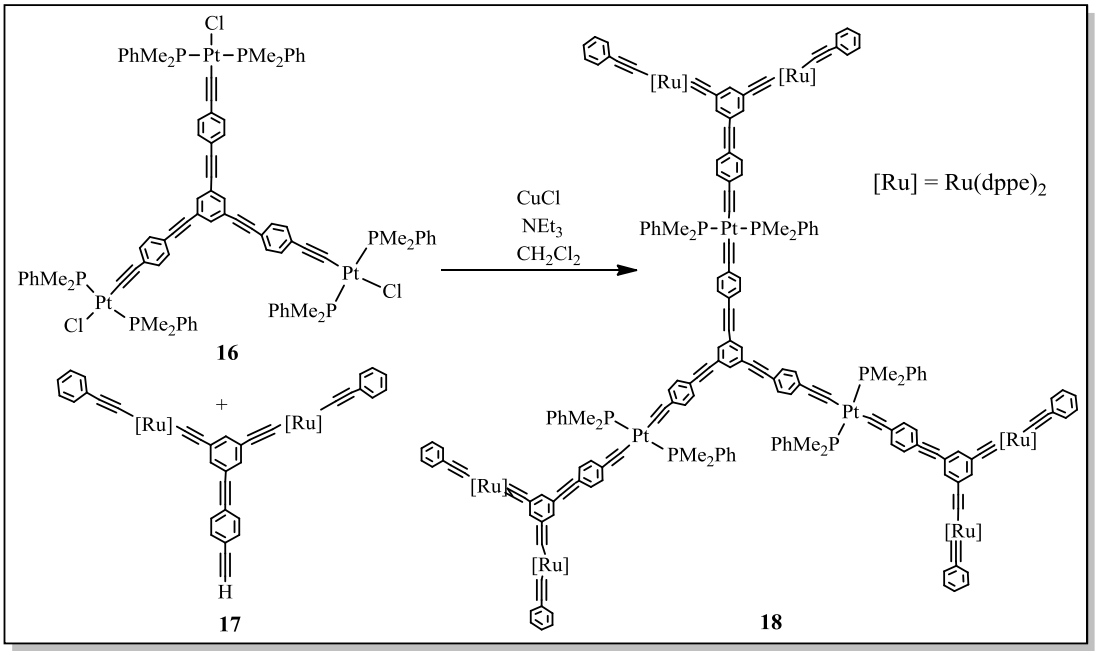


**Scheme 1.7** Synthesis of the $Ru_6Pt_3$ dendrimer **18** with interesting NLO properties

### 1.2.2.6 Mononuclear Ru(II) Acetylides with Group 11 Metal Fragments

Treatment of **19** with $AuCl(PPh_3)$ in the presence of NaOH in MeOH resulted in the formation of complex **20** as a light orange solid (**Scheme 1.8**).[63] This compound shows interesting interaction between ruthenium and ferrocene centers upon oxidation.

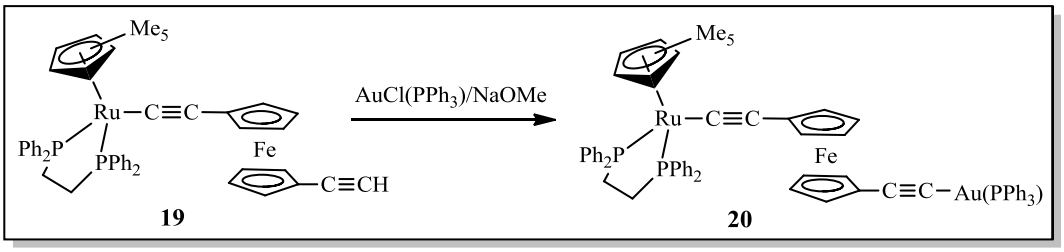


**Scheme 1.8** Synthesis of complex **20** which shows interation between Ru and Fe centers upon oxidation

The C≡C unit in Ru(II) acetylides can bind with low valent metal fragments of this group, such as CuI, AgCN, via π-interactions. Ru-Cu Complex **22** was prepared by reacting equimolar amounts of **21** with CuI in $CH_2Cl_2$ at r.t.. In this reaction, the C≡C electron-rich groups in **21** act as nucleophiles to coordinate to the electrophilic CuI. Isomerization occurs in **21** during the reaction (**Scheme 1.9**).[20]

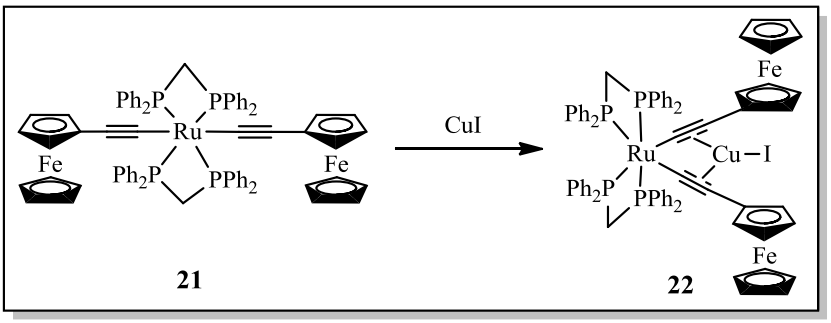


**Scheme 1.9** Nucleophilic reaction of C≡C in complex **21**

### 1.2.2.7 Mononuclear Ru(II) Acetylides With Group 12 Metal Fragments

Some Ru-Hg heterometallics have been reported in the literature.[66] A mixture of **23** and $Hg(OAc)_2$ was refluxed in THF overnight. Removal of the solvent followed by redissolving in $CH_2Cl_2$ and precipitation with hexane provided compound **24** in good yield (**Scheme 1.10**).[66]

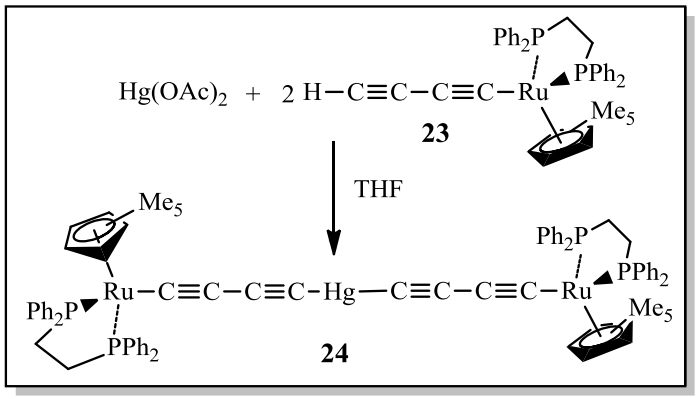


**Scheme 1.10** Synthesis of unusually bent bimetallic acetylide complex **24**

The approach of using mononuclear Ru(II) acetylides as metalloligands to construct oligo- or poly-nuclear systems demonstrates the feasibility of building mixed metal systems under simple reaction conditions. Other methods for the development of heterometallics based on Ru(II) acetylides have also attracted attention. Some typical and representative examples can be found in the literature.[67-69]

## 1.3 Chemical Reactivity

The chemical reactivity of metal acetylides is determined by their components. Much of the chemistry of Ru(II) acetylide based complexes is associated with their functional groups. For Ru(II) acetylide complexes $L_nRu$-C≡C-R, the reaction can occur on the Ru(II) metal center, or C≡C unit, or R moiety. Likewise, the chemical reactivity exhibited by the mononuclear Ru(II) acetylides can also be found in their corresponding oligo- or poly-nuclear acetylide systems. Moreover, these high nuclearity assemblies also exhibit other interesting reactivities due to the perturbation of metal fragments.

## 1.3.1 Reaction on Ru(II) Metal Center

### 1.3.1.1 Oxidation Reactions

For most complexes containing ruthenium acetylide fragments, the ruthenium metal centers are in O.S. +2 and easy to be oxidized. Oxidation of complex *trans*-[RuCl(C≡C-CHPh$_2$)(dppe)$_2$] (**25**) with ferrocenium salts gave a mixture of the corresponding allenylidene (**26**) and vinylidene species (**27**) (**Scheme 1.11**). However, oxidation of the same complex with the ferrocenium salt in the presence of pyridine gave exclusive product (**26**) (**Scheme 1.11**)[70] due to the function of pyridine in trapping the proton directly from the cationic radical during the reaction.

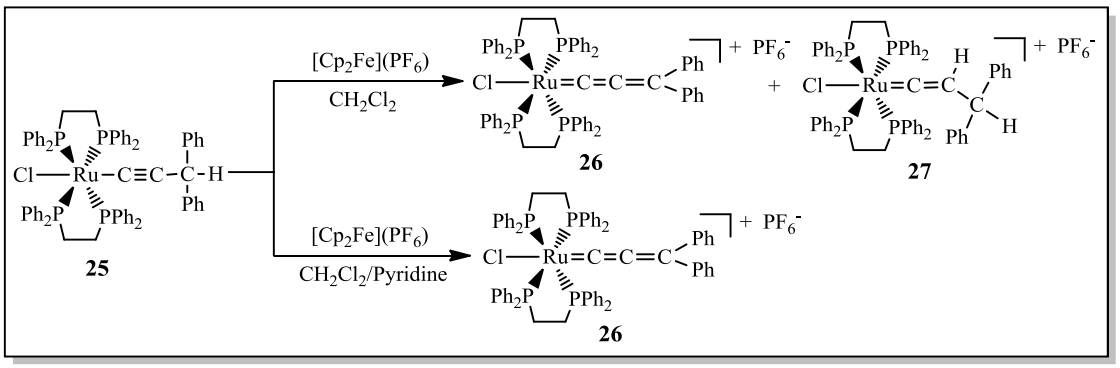


**Scheme 1.11** Oxidation reactions of complex **25**

Likewise, Ru(II) acetylide linked oligo- or poly-nuclear assemblies can also be readily oxidized by ferrocenium salt.[41] Treatment of the neutral tripodal complex **28** with equimolar amount of [Cp$_2$Fe](PF$_6$) yielded its cationic analogue (**Scheme 1.12**).[6]

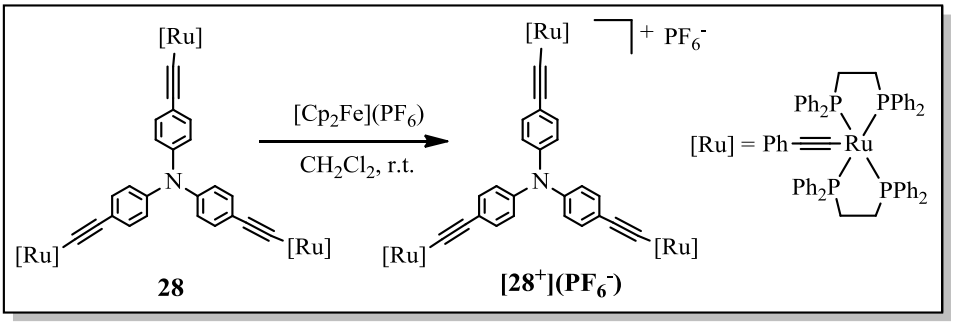


**Scheme 1.12** Oxidation reaction of dendrimer **28**

### 1.3.1.2 Ligand Exchange

As commonly observed in organometallic chemistry, coordinated halides and pseudohalides such as Cl can be replaced by solvent molecules or other ligands. These phenomena are illustrated in **Scheme 1.13**.[71,72]

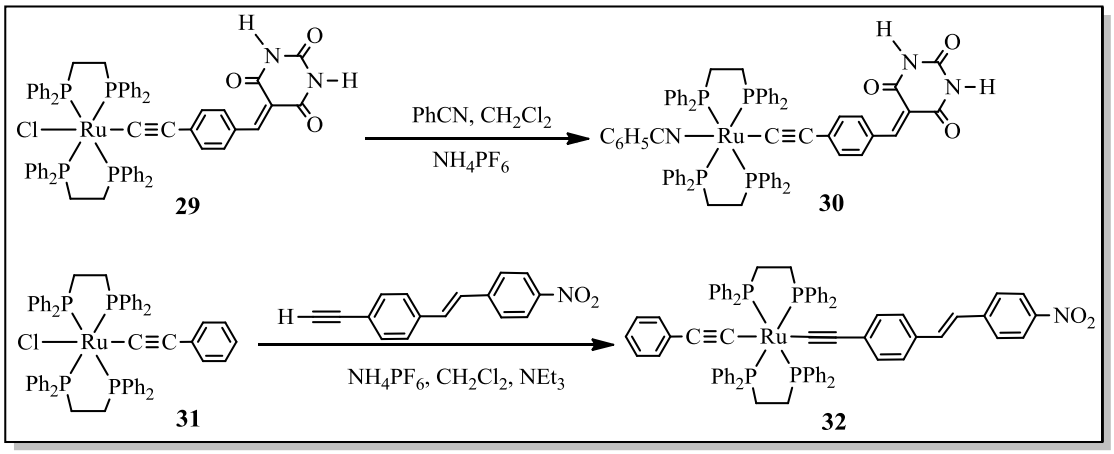


**Scheme 1.13** Ligand exchange reactions of complexes **29** & **31**

## 1.3.2 Reaction on the Spacer R

The most typical reaction occurred on the spacer R is to construct high nuclearity assemblies. In Ru(II) acetylide complexes, $L_nRu$-C≡C-R, the bridging ligand C≡C-R having a basic pendant donor can react with metal fragments to

construct high nuclearity systems through the linker R. These reactions have been illustrated in the construction of oligonuclear and polynuclear complexes described above.

## 1.3.3 Reaction on the C≡C Moiety

The C≡C moiety is also a focus of reactivity studies. The coordination of an acetylide anion to the Ru(II) metal center transfers the nucleophility from the $C_\alpha$ to the $C_\beta$ carbon atom,[73] therefore the addition of electrophiles to the $C_\beta$ and nucleophiles to the $C_\alpha$ of σ-acetylide complexes [Ru]-C≡C-R has been described as the most versatile entry into vinylidene complexes for a wide variety of systems.

### 1.3.3.1 Reactions with Electrophiles

Alkylations of complex **33** with $HC{\equiv}CCH_2Br$ in the presence of $KPF_6$ readily gave vinylidene complex **34** in high yield (**Scheme 1.14**).[74] Ru(II) acetylides with alkyl halides also react in a similar way.[75]

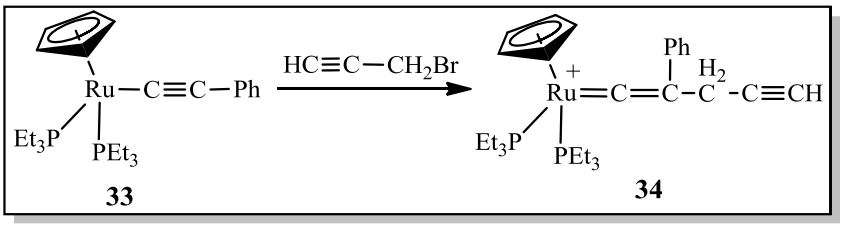


**Scheme 1.14** Ligand alkylation of complex **33**

Similarly, treatment of Ru(II) indenyl acetylide complexes

$[Ru(\eta^5\text{-}C_9H_7)(C{\equiv}CR)(PPh_3)_2]$ (R = $^t$Bu, $^n$Pr) with an excess of $HBF_4\,OEt_2$ led to the formation of the monosubstituted cationic vinylidene complexes $[Ru\{=C=C(H)R\}(PPh_3)_2(\eta^5\text{-}C_9H_7)]^+$.[76] This electrophilic addition, known as protonation reaction of metal acetylides, is the most common reaction with electrophilic reagents. By protonation of metal acetylide complexes, their corresponding metal vinylidene complexes can be obtained. This process is usually reversible as the elimination of proton at the $C_\beta$ in a metallic vinylidene complex produces an acetylide analogue.

Accordingly, one of the most familiar reactions of oligo- or poly-nuclear acetylides is electrophilic attack at the $C_\beta$ atom. The addition of cationic electrophiles, such as $H^+$ or $Me^+$, gives the corresponding vinylidene.[74,77,78] Reaction between **35** and MeI was carried out in THF in the presence of $NH_4BF_4$ to give the vinylidene derivative **36** in good yield (**Scheme 1.15**).[73]

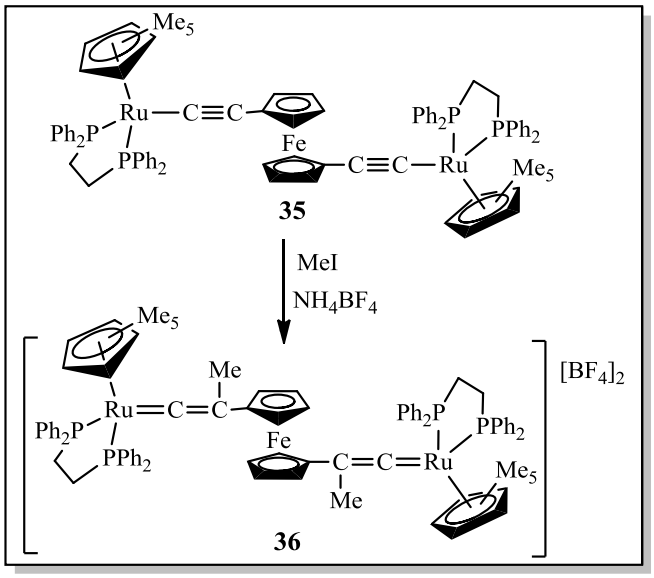


**Scheme 1.15** Electrophilic reaction of complex **35**

### 1.3.3.2 Reactions with Nucleophiles

In agreement with the above description, the attack of nucleophiles to metal acetylides mainly takes place at $C_\alpha$ due to its electron deficiency. The nucleophilic agents mostly used are hydrides, alcohols and water which lead to vinyl, alkoxycarbene and acyl complexes, accordingly.[42]

Complex $[Ru=C(OMe)(CH_2{}^tBu)(tpy)(bpy)]^{2+}$ (**38**) was synthesized by treatment of the corresponding acetylide complex $[Ru(C\equiv C{}^tBu)(tpy)(bpy)]^+$ (**37**) with MeOH under acidic conditions (**Scheme 1.16**).[79]

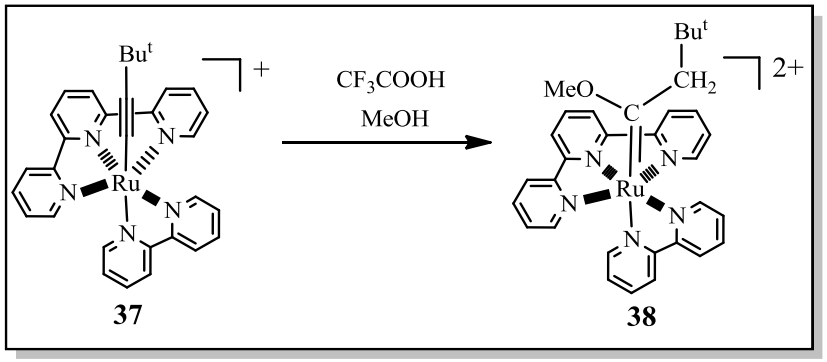


**Scheme 1.16** Nucleophilic reaction of complex **37**

### 1.3.3.3 Fabrication of Binuclear or Cluster Systems

The high degree of unsaturation in metal acetylide complexes increases their reactivity, and the presence of two sets of π-orbitals also allows the acetylide ligand to bridge two or more metal centers by combinations of σ- and π-bonding interactions.

In acetylide systems, the acetylide group binds terminally to a metal center, acting as a strong σ-donor. They can also serve as precursors to synthesize high nuclearity assemblies via the reaction of C≡C moieties. In the presence of a second

metal center, an acetylide ligand can bridge the two metals, acting either as a donor to both metals[50] or as a σ-donor to one metal and a π-donor to the other.[80,81] This method has proven to be useful for constructing heterometallic systems containing a large number of monovalent transition metal salts (such as CuI, AgCN, etc.)[82] and organometallic complexes ($Co_2(CO)_8$, $Ni(CO)_4$, etc.),[51] as illustrated in **Scheme 1.9**[20] and **Scheme 1.5**[62], respectively.

In addition, oligo- or poly-nuclear acetylides also exhibit other reactivities due to the perturbation of metal fragments introduced, which may not be found in their respective building blocks. Investigation in such aspects can be found in the works of Bruce *et al*.[63] and Griffith *et al*..[83]

## 1.4 Properties and Applications

Ru(II) acetylide based mononuclear and multinuclear complexes contain highly polarizable Ru(II) metal units. In their molecular systems, the π-system of the linear C≡C group provides a pathway for delocalization of electron density between the metal and ligand and, hence, an efficient mechanism for communication between two or more metal centers. Therefore, the Ru(II) acetylide based complexes have potential applications in electrochemistry and nonlinear optics,[4,5] in the development of conducting materials, and also in chromophores.

Ru(II) acetylide based complexes are one of the most extensively studied types of organometallic complexes, not only due to their ease of synthesis and versatility

of the reactions, but also because of their intriguing properties and applications, as illustrated below.

## 1.4.1 Electrochemical Properties

### 1.4.1.1 Mononuclear Ru(II) Acetylides

The electrochemical behavior of Ru(II) acetylide complexes has been extensively investigated by the groups of Bruce,[41,84] Dixneuf,[85] Humphrey,[86] Low,[87,88] Che[89,90] and others.[7,91,92]

Typically, mononuclear Ru(II) acetylides undergo single electron oxidation to give the corresponding cations. Their redox potential and chemical stability are sensitive to the supporting ligands on the ruthenium center as well as on the acetylide substituent.[20,84] Examples given in **Table 1.1** illustrate that the acetylide ligand and the auxiliary ligands share a role in determining the ease of oxidation at the Ru(II) metal center.

**Table 1.1** Cyclic voltammetric data of some Ru(II) acetylide complexes.[a]

| Complex | $E°_{ox}$(V) [$i_{pc}/i_{pa}$] $Ru^{II/III}$ | Complex | $E°_{ox}$(V) [$i_{pc}/i_{pa}$] $Ru^{II/III}$ |
|---|---|---|---|
| 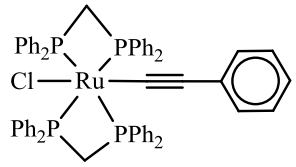 **39** | 0.55 [1][b] | 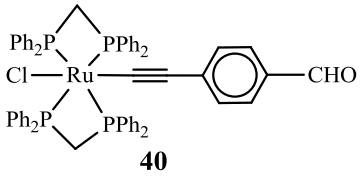 **40** | 0.66 [1][b] |
| 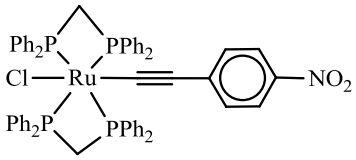 **41** | 0.72 [1][b] | 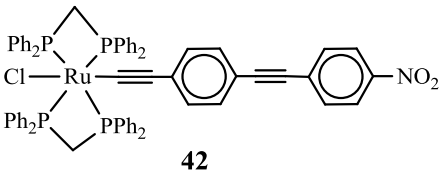 **42** | 0.57 [0.9][b] |
| 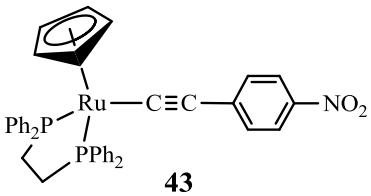 **43** | 0.67 [0.9][c] | 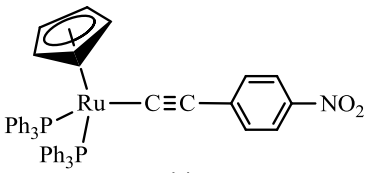 **44** | 0.73 [1][d] |
| 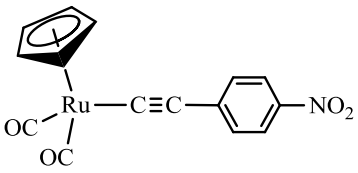 **45** | 0.86 [0.7][c] | | |

[a]Conditions: $CH_2Cl_2$; Pt-wire auxiliary, Pt working, and Ag/AgCl reference electrode ($FcH/FcH^+$ 0.56 V); [b]ref 85; [c]ref 90; [d]ref 91.

An examination of the cyclic voltammetric data for these acetylide complexes shows the following trends.

(1) An increase in the $Ru^{II/III}$ oxidation potential has been observed on addition of an electron-withdrawing substituent to the aryl ligand, and the stronger the electron-withdrawing ability, the greater the increscent magnitude, e.g. 0.55 V (**39**) vs 0.66 V (**40**) vs 0.72 V (**41**). This is consistent with the decrease in electron density

on ruthenium metal center.

(2) Chain lengthening of the nitro-containing acetylide ligand has been found to produce a decrease in the $Ru^{II/III}$ oxidation potential: i.e., from 0.72 V (**41**) to 0.57 V (**42**). This is caused by an increase in chain length that enhances the electron delocalization and consequently increases the ease of oxidation. A similar decrease has been observed in other systems.[89]

(3) The reversibility of the Ru(II) oxidation increases on replacing auxiliary ligand CO by $PPh_3$ or dppe (proceeding from **43/44** to **45**). Additionally, the ease of Ru(II) oxidation increases in the sequence **43** > **44** > **45**, in agreement with the trend in the electron-donating ability of the auxiliary ligands dppe > $PPh_3$ > CO. This is due to the stronger electron-donation of the auxiliary ligand which renders the Ru(II) center more electron-rich and the oxidized Ru(III) species higher stability.

In general, peripheral ligand substitution can provide a simple method to tune metal electron density, and hence its ease of oxidation. Oxidation of the Ru(II) complexes yields the corresponding Ru(III) species and gets a reversible or a quasi-reversible oxidation wave Ru(II)/Ru(III). This indicates Ru(II) acetylides could be useful for electrochemical switching[93] and isolation of the Ru(III) complexes may be possible due to the stability of the oxidized species. Theoretically the Ru(III) species can be reduced to its Ru(II) counterpart.

#### 1.4.1.2 Ru(II) Acetylide Based Oligo- and Poly-Nuclear Complexes

Linear multinuclear acetylide systems exhibit more intriguing electrochemical

properties. For instance, the dinuclear metal acetylide complexes often show electronic interaction between metal species, which stabilizes the mixed valence state, by changing the bonding mode of the "bridging ligand".[6,94] The electrochemical responses of complex **20** in **Scheme 1.8** examined by cyclic voltammetry revealed the interaction between ruthenium and ferrocene centers through the C≡C link.[63]

The Ru(II) acetylide based dinuclear complexes are viewed as model systems to evaluate the capability of communication between metal centers. The cyclic voltammogram for the diruthenium complex **46** in **Fig. 1.1** showed two reversible one-electron redox waves for the formation of the mono- and dicationic species, the $Ru^{III}/Ru^{II}$ and $Ru^{III}/Ru^{III}$ systems. The separation of 360 mV indicates the communication between the ruthenium centers through the 1,4-diethynylbenzene bridge.[64]

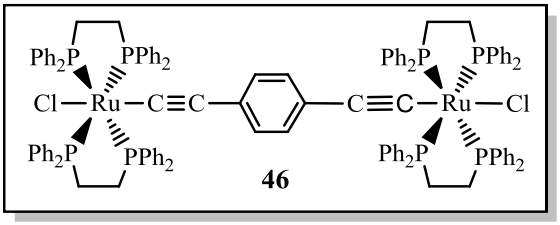


**Fig. 1.1** A bimetallic alkynyl complex as model for studying electron transfer properties

Due to the reversibility and difference in oxidation potentials of the metal centers, Ru(II) based binuclear acetylide molecular systems can serve as switches for the investigation of other properties. For example, the studies of Humphrey and co-workers have shown that Ru(II) acetylide based heterobinuclear complexes can act

as electrochemical switching of nonlinear properties through oxidation/reduction.[95] In the mixed Ru-Fe complex **47** (**Fig. 1.2**), the $Fe^{II}/Fe^{III}$ and $Ru^{II}/Ru^{III}$ couples are separated so far from one another that under electrochemical control, one can access the $Fe^{II}/Ru^{II}$, $Fe^{III}/Ru^{II}$, or $Fe^{III}/Ru^{III}$ states. Its NLO properties hence can be switched electrochemically through the reversible $Fe^{II}/Ru^{II}$, $Fe^{III}/Ru^{II}$, or $Fe^{III}/ Ru^{III}$ couples.[96]

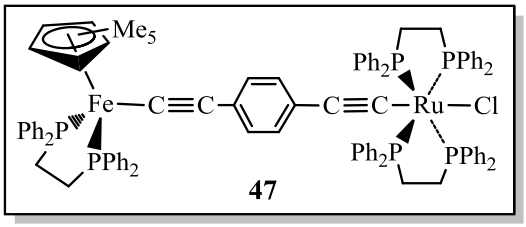

**47**

**Fig. 1.2** Mixed Ru-Fe complex **47** as an electrochemical switch for NLO

In the Ru(II) acetylide based oligo- and poly-nuclear complexes, however, the communication between metal centers does not always occur when they are oxidized. Electrochemical measurements of polymer **13** in **Scheme 1.6** show that there is only one redox wave for the $Ru^{II}/Ru^{III}$ couple, indicating a lack of communication between the Ru centers through the Pd bridges, which act as insulating units.[18]

## 1.4.2 Electronic Absorption and Photoluminescent Properties

### 1.4.2.1 Electronic Absorption Properties

The study on electronic absorption of Ru(II) acetylide based complexes is indispensable due to its fundamental importance in their nonlinear optical and luminescent studies.[93,96] As is expected of a highly delocalized organometallic π-system, the metal entities should determine the properties of the acetylide

compounds. Previous studies on metal acetylide systems[7] have shown that the highest occupied crystal orbital has predominantly metal *d* orbital character and is delocalized along the entire chain through $ML_n$ groups (n = 2, square planar; n = 4, octahedral). Hence the metal fragments in oligo- or poly-nuclear acetylides may affect the physical properties exhibited by their mononuclear precursors and organic ligands. Meanwhile, extension of the conjugation length of the alkynyl spacer group is suggested to lower the optical band gap by lowering the energy of the lowest unoccupied crystal orbital (predominantly alkynyl π* character).[90]

Ru(II) acetylide based complexes usually display at least two typical absorption bands in the UV-vis spectra: one in the UV region originated from intraligand and the other in the visible region with a large extinction coefficient due to metal-to-ligand charge transfer (MLCT) which is responsible for the usual yellow to orange color of these complexes.[7,35] Indeed, the highest occupied molecular orbital (HOMO) involved in the transition results from a considerable mixing of Ru(d$\pi$) orbitals with alkynyl $\pi$-orbitals, leading to an increase of the ligand character with length.

The UV-vis spectra of complexes **48**-**51** (**Fig. 1.3**) show a series of strong high-energy bands with high intensity in the UV region that correspond to intraligand ($\pi \rightarrow \pi^*$ or IL) transitions, either within the alkynyl ligands or within the phosphine coligands.[7,97] These complexes all exhibit long-wavelength transitions at about 400 nm originated from $d_{Ru} \rightarrow \pi^*_{alkynyl}$ metal-to-ligand charge transfer (MLCT). The MLCT bands exhibit a shift to lower energy with an increase in phenyl

ring number in complexes **48**-**50** along the series **48** > **49** > **50**. The lowest energy and highest intensity in the series of complexes **48**-**51** are found in trinuclear **51**. Both findings are consistent with the assignment of MLCT.[60]

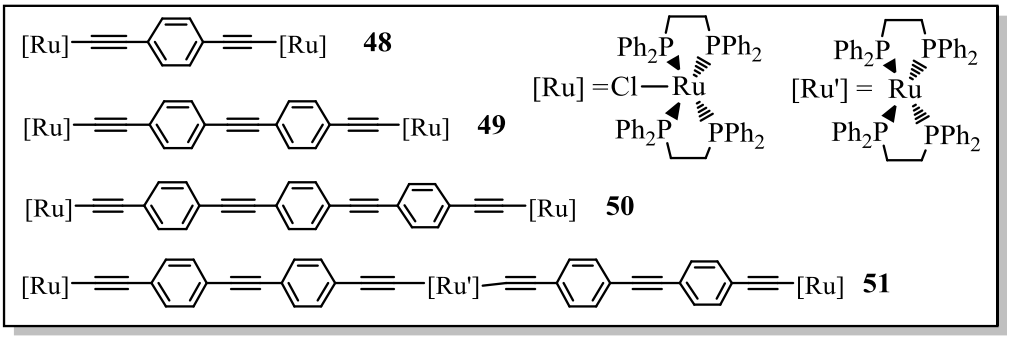


**Fig. 1.3** A series of organometallic wires with numbering of the presented complexes

### 1.4.2.2 Photoluminescent Properties

Although the photoluminescent properties of metal alkynyls of the Groups 10 and 11 transition metals have been extensively studied by Yam *et al.*,[98,99] reports on the luminescent properties of Ru(II) acetylide based complexes are rare.[69,79,100-102] This rarity is most probably attributed to Ru(II) acetylides being typically non-emissive or weakly emissive with short excited-state lifetimes at r.t..[79] This is also justified many Pt(II) or Au(I) acetylides are brightly emissive, but the luminescent behavior of the geometrically similar Ru(II) complexes are non-emissive or very weakly emissive.[69,100] For example, complexes $[Pt(C{\equiv}C\text{-}R)_2(^tBu_2bpy)]$ (R = py, CCpy, $C_6F_5$) have been shown to luminesce strongly from a $^3$MLCT excited state in both frozen and fluid solution.[103] However, their $d^6$ octahedral ruthenium analogues $[RuCl(C{\equiv}C\text{-}R)(Me_2bpy)(PPh_3)_2]$ (R = $^t$Bu, Ph, $C_6H_4Me$) do not appear to show the same emissive behavior, although they possess

the same MLCT spectral bands.[104] This could be due to the presence of the chloride ligand, which presumably dissociates in solution and may quench any emission.

The non-emissive or weakly emissive situation in Ru(II) monomer acetylides also occurs in the Ru(II) acetylide based oligo- and poly-nuclear complexes. The studies on the photoluminescent properties of complexes **52**, **53** and **54** (**Fig. 1.4**) in chloroform solutions were found to be non-emissive or very weakly emissive. In contrast, the gold acetylide analogue 2,4,6-[4-($PPh_3$)AuC≡$CC_6H_4$]$_3$-1,3,5-$C_3N_3$ was strongly emissive.[69] Theoretical computation on orbital pattern shows that these trimetallic Ru(II) acetylide complexes and their Au(I) analogue possess different lowest excited state with the MLCT state in the former and the $\pi \rightarrow \pi^*$ state in the latter, and the energy gap between the MLCT state and the ground state in the trimetallic Ru(II) acetylide complexes is smaller than that between the $\pi \rightarrow \pi^*$ state and the ground state in Au(I) analogue. Thus, quenching to the ground state is more efficient in these trimetallic Ru(II) acetylides, indicating that the radiationless process is easier in trimetallic Ru(II) acetylides than their Au(I) analogue.[69]

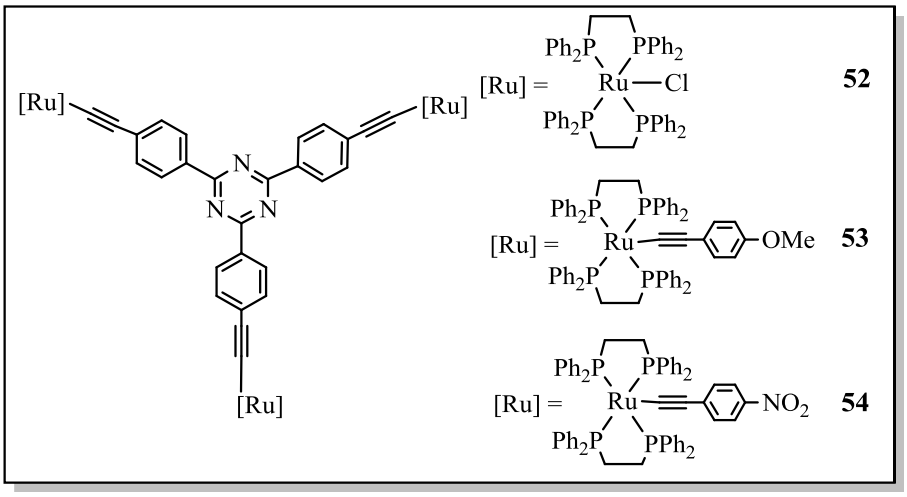


**Fig. 1.4** A series of organometallic wires with numbering of the presented complex

## 1.4.3 Nonlinear Optical (NLO) Properties

### 1.4.3.1 Ru(II) Mononuclear Acetylides

Detailed surveys of the NLO properties of Ru(II) acetylide based complexes have been reported.[4,5,105] Ru(II) acetylides with extended π conjugation exhibit interesting NLO properties The basic requirements for large NLO response are: (a) an increase in the conjugation length, and (b) an increase in the strength of donor and/or acceptor functional groups. Following this lead, many Ru(II) acetylides with significant NLO response have been synthesized and reported.[4,5,105] **Table 1.2** lists the $\beta$, $\beta_0$ (the second-order hyperpolarizability and its corrected value, respectively) and $\gamma_{real}$, $\gamma_{imag}$ (the real and imaginary components of the third-order hyperpolarizability, respectively ) values for some Ru(II) acetylides.[4]

**Table 1.2** NLO data of some Ru(II) acetylides.[a]

| Complex | $\beta$ ($10^{-30}$ esu) | $\beta_0$ ($10^{-30}$ esu) | $\gamma_{real}$ ($10^{-36}$ esu) | $\gamma_{imag}$ ($10^{-36}$ esu) |
|---|---|---|---|---|
| 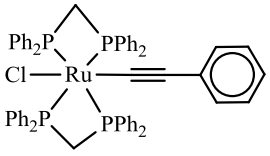 **39** | 20 | 12 | <120 | 0 |
| 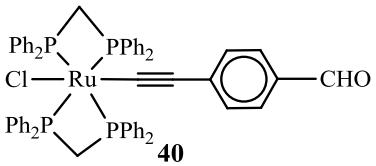 **40** | 106 | 38 | <120 | 210 ± 60 |
| 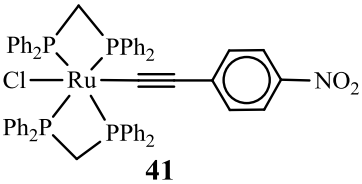 **41** | 767 | 129 | 170 ± 34 | 230 ± 46 |

| | | | | |
|---|---|---|---|---|
| 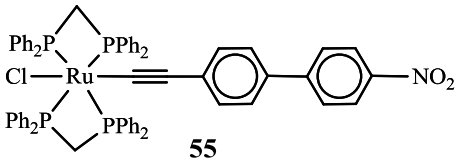 **55** | 933 | 178 | 140 ± 28 | 64 ± 13 |
| 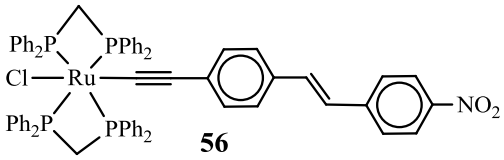 **56** | 1964 | 235 | 200 ± 40 | 1100 ± 220 |
| 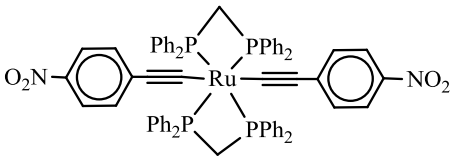 **57** | – | – | 300 ± 60 | 490 ± 98 |
| 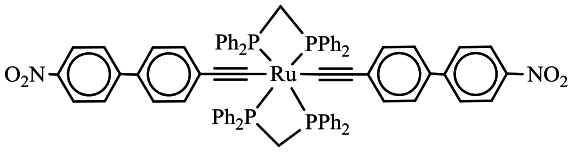 **58** | – | – | ≤800 | 2500 ± 500 |
| 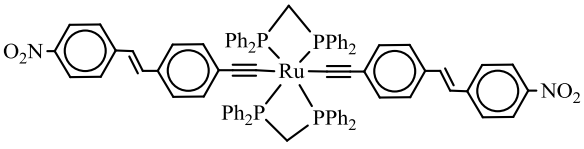 **59** | – | – | ≤1100 | 3400 ± 680 |

[a] ref. 4

The data in **Table 1.2** suggest that an increase in NLO response is resulted from an increase in the strength of the acceptors from H (**39**) to CHO (**40**) to $NO_2$ (**41**). Not surprisingly, an increase in both second- and third-order NLO values is seen to increase the conjugation length from **41** to **55** to **56**, and increase the π-delocalization length from **41** to **57**, **55** to **58** and **56** to **59**, leading to great enhancement in third-order nonlinearities.

Besides the modification in acetylide ligands (**Table 1.2**), one advantage of organometallic complexes over organic compounds is the possibility of tuning NLO

response by auxiliary ligand modification. For Ru(II) acetylide complexes, varying auxiliary ligand should modify donor strength or delocalization possibilities. Replacing two CO ligands in $[Ru(\eta^5\text{-}C_5H_5)(4\text{-}C{\equiv}CC_6H_4NO_2)(CO)_2]$ by dppe results in a significant increase in nonlinearity of $[Ru(\eta^5\text{-}C_5H_5)(4\text{-}C{\equiv}CC_6H_4NO_2)(dppe)]$.[106] The nonlinearity for the $PPh_3$ complex is greater than that of the $PMe_3$ analogue in $[Ru(\eta^5\text{-}C_5H_5)(4\text{-}C{\equiv}CC_6H_4NO_2)(L)_2]$, indicating that the greater delocalization possibilities of the former are more important for NLO response than the greater basicity of the latter.[107]

### 1.4.3.2 Ru(II) Acetylide Based Oligo- and Poly-Nuclear Complexes

Ru(II) acetylide based oligo- and poly-nuclear complexes with extended π-conjugation exhibit more interesting and significant NLO properties than their corresponding Ru(II) mononuclear precursors. They have large π-delocalization in contrast to mononuclear components, and an enhancement of the effective conjugation through increasing the π-delocalization length has been recognized as a way of achieving large third-order nonlinearities.[4,18] Incorporation of the second (in some cases third or more metal) center into Ru(II) acetylide molecular systems generally improves electron asymmetry greatly. These characteristics result in significant nonlinearity in oligo- and poly-nuclear acetylide complexes.

The 18-electron readily oxidizable Ru(II) centers in Ru(II) acetylides are very efficient donors. Therefore in the Ru(II) acetylide based donor-bridge-acceptor oligo- or poly-nuclear constructions, increasing the acceptor strength results in

enhancement in nonlinearity. These trends are illustrated in **Table 1.3**. The 4-pyridyl group in **60** has been metallated with $[Cr(CO)_5]$ and $[W(CO)_5]$ units. The respective products, **61** and **62,** possess significantly enhanced nonlinearities. Likewise, another series of Ru-Cr (**64**) and Ru-W (**65**) binuclear acetylide complexes obtained from **63** and respective $[Cr(CO)_5]$ and $[W(CO)_5]$ groups have also exhibited larger NLO properties than their precursor. This indicates that the addition of a Group 6 metal fragment proves to be a more effective route to enhancing nonlinearity. In both cases, the tungsten-containing complexes have stronger accepting ability than the chromium analogues, and hence, exhibit larger nonlinear responses.[4,5]

**Table 1.3** Comparison of second-order NLO between precursors and mixed metal complexes.[a]

| Complex | $\beta$ ($10^{-30}$ esu) | $\beta_0$ ($10^{-30}$ esu) | Complex | $\beta$ ($10^{-30}$ esu) | $\beta_0$ ($10^{-30}$ esu) |
|---|---|---|---|---|---|
| 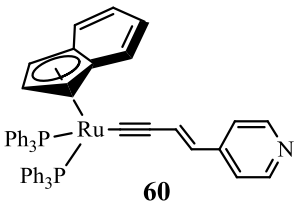 **60** | 100 | 37 | 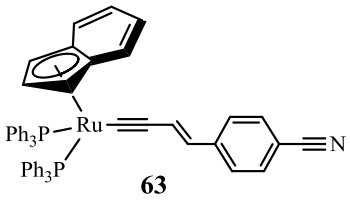 **63** | 238 | 71 |
| 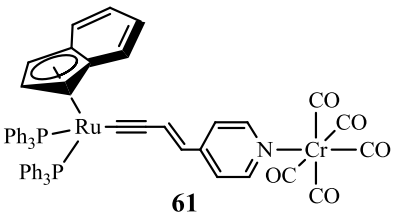 **61** | 260 | 60 | 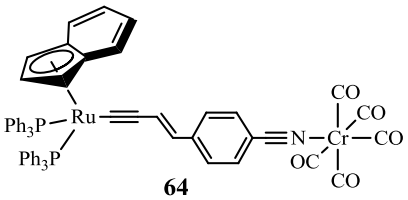 **64** | 465 | 119 |
| 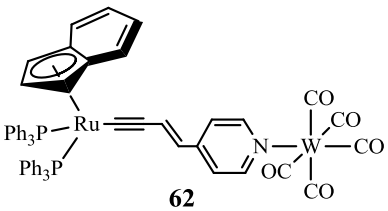 **62** | 535 | 71 | 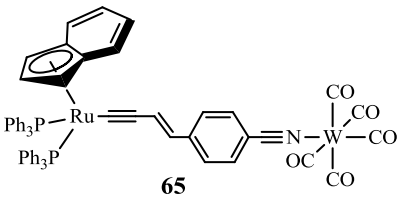 **65** | 700 | 150 |

[a] ref 4

Besides the modification by varying the length and composition of the π-system, another way to impact on NLO response significantly is "dimensional evolution".[102] Replacing the typical one-dimensional dipolar composition with a two-dimensional or three-dimensional octupolar arrangement has been proven to be an efficient way to increase NLO response greatly. This is the very reason that compounds with octupolar structures attract special attention nowadays.[6,35,55,108] **Table 1.4** lists the NLO values for the complexes with octupolar structures in **Fig. 1.5**.

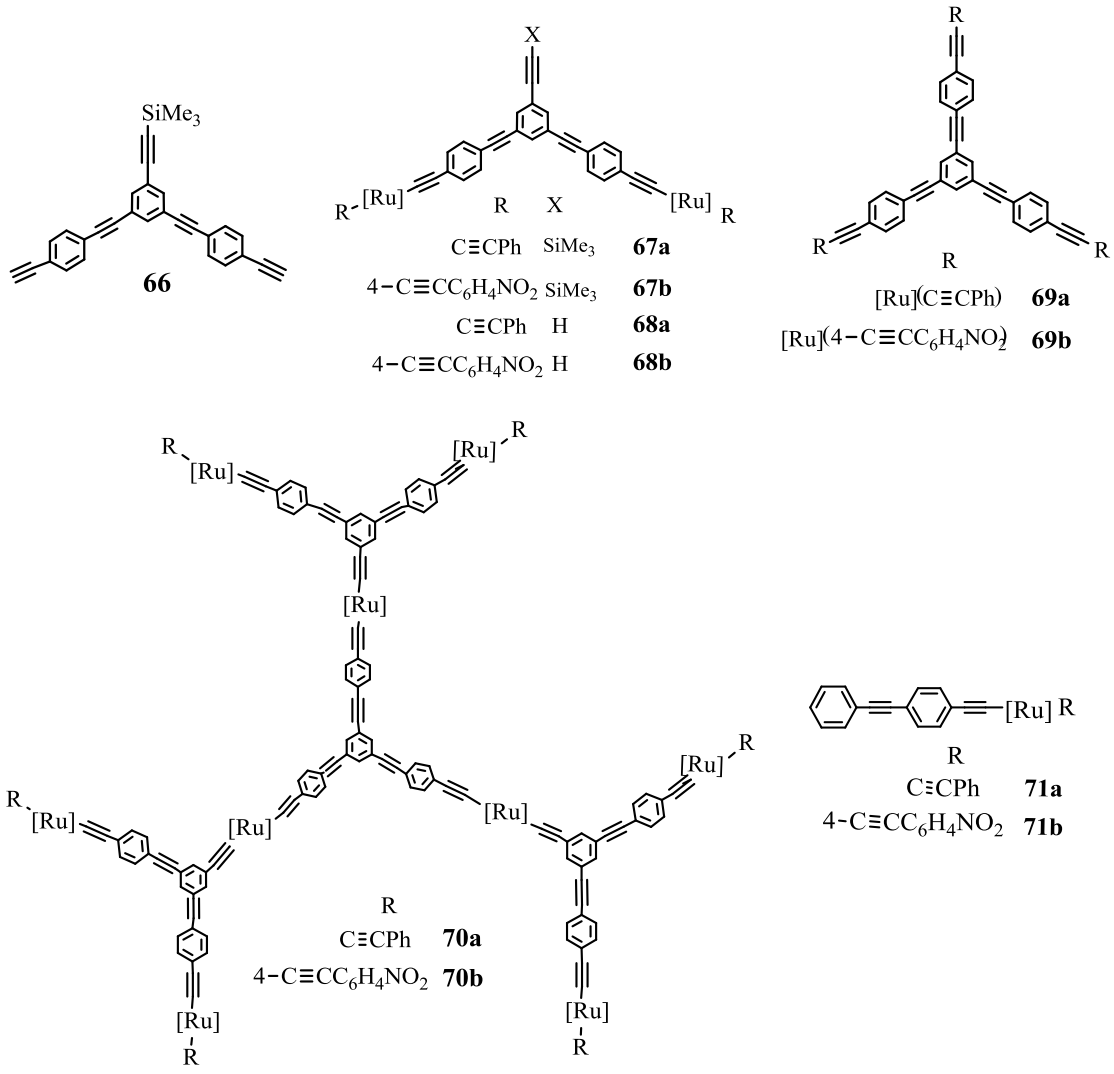


**Fig. 1.5** Octupolar compounds with significant NLO response ([Ru] = *trans*-Ru(dppe)$_2$)

**Table 1.4** NLO data of compounds with octupolar and dendrimer structures.[a]

| Complex | $\beta$ ($10^{-30}$ esu) | $\beta_0$ ($10^{-30}$ esu) | $\gamma_{real}$ ($10^{-36}$ esu) | $\gamma_{imag}$ ($10^{-36}$ esu) |
|---|---|---|---|---|
| **66** | 8 | 5 | 67 ± 30 | 7 ± 5 |
| **67a** | 105 | 37 | -700 ± 100 | 2270 ± 300 |
| **67b** | 900 | 182 | -5200 ± 1000 | 5200 ± 1000 |
| **68a** | 104 | 37 | -830 ± 100 | 2200 ± 300 |
| **68b** | 1120 | 220 | -4900 ± 1000 | 4900 ± 1000 |
| **69a** | 93 | 31 | -600 ± 200 | 2900 ± 500 |
| **69b** | 1220 | 254 | -5000 ± 1000 | 5600 ± 1000 |
| **70a** | 160 | 59 | -5050 ± 500 | 20100 ± 2000 |
| **70b** | 1880 | 350 | -14900 ± 3000 | 18200 ± 3000 |
| **71a** | 34 | 14 | -670 ± 300 | 1300 ± 300 |
| **71b** | – | – | – | – |

[a] ref 30

A number of observations from the data in **Table 1.4** can be made.

● Incorporation of the ligated metal fragment in proceeding from the organic acetylene **66** to the organometallic complexes **67a**, **67b** leads to a significant increase in both second- and third-order NLO responses, suggesting that the presence of the second electron-rich metal center being more important than the dipolar composition in enhancing NLO merit.

● The **b** series of compounds **67-70** have considerably higher nonlinearities than the corresponding **a** series, indicating that existence of acetylide ligands incorporating the strong acceptor group $NO_2$ gives rise to enhanced NLO responses.

● The $\gamma_{real}$ values for all complexes are negative, and the $\gamma_{imag}$ values for most are significant. This is consistent with two-photon effects contributing to the observed molecular nonlinearities, a result noted with other Ru(II) acetylide complexes.[86,108]

● Complexes **71** is the linear fragment of complexes **67**-**70**. A significant increase in their NLO responses is observed in progressing from **71** to **67**-**70**.

● Third-order nonlinearities of these compounds have error values too large to be neglected. Comment on the effect of structural variation on the magnitude of is therefore cautious, particularly in light of the error margins.

## 1.5 Conclusions & Objectives

Ru(II) acetylide based oligo- and poly-nuclear complexes can be synthesized by several strategies with mononuclear Ru(II) acetylides as "metalloligands" being the most popular and efficient method. In mononuclear Ru(II) acetylide complexes, electrochemical data ($Ru^{II}/Ru^{III}$ potentials) and NLO response are sensitive to auxiliary ligand variation of alkynyl electro-withdrawing substituents and alkynyl chain-lengthening. Similar to the mononuclear Ru(II) acetylide systems, the replacement of auxiliary ligands, the variation of the substituents, chain-length of alkynyl ligands, and the introduction of different metal fragments have significant influences on the properties of the oligo- and poly-nuclear acetylide complexes. The studies in photoluminescence of Ru(II) acetylide based mono-, oligo- and poly-nuclear complexes indicate that Ru(II) acetylide complexes are non-emissive or weakly emissive at r.t.. The reversibility of $Ru^{II}/Ru^{III}$ couples in these acetylide complexes allows reversible nonlinearity switching, complementing the vinylidene/alkynyl pair method.

Although some oligo- and poly-nuclear complexes containing mononuclear Ru(II) acetylides have been prepared as described above, the investigation of their

chemistry is far from complete, especially the effect of structure on third-order nonlinearities. Based on a thorough survey on this area, my work on "heterometallic assemblies from Ru(II) 4-ethynylpyridyl precursors" will be a worthwhile exploration.

### 1.5.1 Ru(II) Acetylide Based Mononuclear and Heteronuclear Complexes

Most Ru(II) acetylides are oxygen and moisture stable and therefore are easily prepared. From a design perspective, Ru(II) acetylide linkages are of interest because of the rigid nature of the acetylide ligands and the defined directionality in the case of *trans* substituted metal centers. Ru(II) acetylides, in particular, are excellent chromophores and electrophores,[109] which render them appealing building blocks for high nuclearity assemblies.

Ru(II) acetylides exhibit excellent electrochemical switching ability and significant nonlinear optical responses. In particular, due to their reversibility in protonation/deprotonation or oxidation/reduction reactions, Ru(II) acetylides are employed in NLO switching applications.[86,96] In addition, Ru(II) acetylide complexes are frequently more oxidatively stable and thermally robust than complexes containing other σ-bound carbon ligands, factors which are important considerations for potential devices.[16] These characteristics make Ru(II) acetylides more attractive than other metal acetylides. Studies by Humphrey and co-workers indicate that

second-order NLO response increases with increased ease of oxidation of the metal as well as increasing the metal valence electron count.[105] Therefore the 18-electron Ru(II) acetylides have larger NLO properties than 14-electron Au(I) acetylides and easily oxidizable Ru(II) acetylides possess more significant NLO responses than less readily oxidizable Ni(II) analogues.[64]

Ru(II) acetylides have a short history of about 30 years. Recent studies demonstrate their significance in chemistry and particularly materials chemistry. Despite the growing interests and investigations of Ru(II) acetylide systems, relatively little attention has been focused on the chemistry of their heterometallic assemblies. Compared to mixed metal acetylides of Groups 10 and 11,[28,98] heterometallic systems based on Ru(II) acetylides are poorly understood. In this project, my focus has been directed toward synthesizing and characterizing stable Ru(II) 4-ethynylpyridine based monometallic and heterometallic assemblies, in order to gain an understanding of their structural, electrochemical and optical properties. Use of mixed-metals would give the needed hybrid characters for certain advanced materials.

### 1.5.2 Diphosphine as Auxiliary Ligands

Ru(II) acetylide complexes supported by diphosphine ligands have attracted much attention.[4,110] Arylphosphine ligands, such as $PPh_3$, dppm, dppe, dppf, etc. have been extensively employed as auxiliary ligands in organometallic chemistry.

They are preferred over other ligands due to their electron-richness, bulkiness and stability. The study of Ru(II) complexes suggests that the bulkiness of the ligands is a determining factor for the stabilization of vinylidene or allenylidene Ru(II) intermediates of Ru(II) alkynyl complexes.[111,112] Besides, the aryl substituents in arylphosphine ligands increase electron delocalization and have a greater NLO response than their alkyl counterparts.[4] Finally, despite having identical substituents, diphosphine ligands, such as dppm and dppe, differ by imposing substantially different P-Ru-P angles. They hence, have different influence on the electron density at the metal center.[13] This will result in different properties of the metal center.

Encouraged by the rich chemistry of Ru(II) acetylide complexes and relative deficiency in heterometallic assemblies obtained from Ru(II) acetylide building blocks, I set out to systematically explore the chemistry of heterometallic assemblies containing Ru(II) acetylides. The aim of this project was to synthesize and investigate the reactivity of a series of mononuclear Ru(II) 4-ethynylpyridine complexes: *trans*-[Ru(L)(C≡Cpy-4)(P-P)$_2$] or [Ru($\eta^5$-$C_5H_5$)(C≡Cpy-4)(P-P)] (L = Cl or H; P-P = 2P$Ph_3$, dppm, dppe, dppf), which are used as "building blocks" to construct high nuclearity complexes with precisely controlled lengths.

A range of metal fragments, from square planar Pd(II)/Pt(II) chloride, paddlewheel geometrical dirhodium tetracetate to octahedral Re(I) diimine carbonyls, have been combined with mononuclear Ru(II) acetylides to yield a diverse range of architectures and properties. This project will address some of the deficiency in our knowledge of acetylide heterometallic assemblies.

# Chapter Two

# *Syntheses, Characterization and General Properties of Ru(II) 4-Ethynylpyridine Based Monometallic and Heterometallic Complexes*

## 2.1 Introduction

Ru(II) acetylides and their high nuclearity assemblies continue to be an active area of research since their first discovery.[5,114,115] These are also among the most important members in metal acetylide family.[16,32,35] The different components of {[Ru]-(C≡C-R)$_n$} or {[Ru]-(C≡C-R)$_n$-[M]} ([Ru] = Ru core and the auxiliary ligands; n = 1 or 2; [M] = other metal fragments) have been varied in an attempt to study their roles in influencing the physical and electronic properties of these Ru(II) acetylides.[4,20,52,60,84,87] Substituent effects are investigated by spectral methods, such as NMR, UV-vis spectroscopy,[6,87,92,116] as well as X-ray crystallography,[78] electrochemical measurement[91,117] and nonlinear optical technique.[4,5] In light of the significance of these compounds in organometallics, a detailed understanding of Ru(II) acetylides is clearly desirable. In this chapter, the syntheses, characterization and general properties of Ru(II) 4-ethynylpyridine based mononuclear and heteronuclear complexes are described.

# 2.2 Results and Discussion

## 2.2.1 Monometallic Ru(II) Acetylide and Vinylidene Complexes

### 2.2.1.1 Preparation

Monometallic Ru(II) acetylide complexes with a pendant pyridyl moiety, octahedral complexes *trans*-[RuR(C≡Cpy-4)(P-P)$_2$] (R = Cl, P-P = dppm **5.1**; R = Cl, P-P = dppe **5.3**; R = H, P-P = dppe **5.4**) and half-sandwich complexes [RuCp(C≡Cpy-4)(P-P)] (P-P = dppf **5.7**, P-P = 2PPh$_3$ **5.8**) were synthesized by the replacement of one of the Cl in *cis*-[RuCl$_2$(P-P)$_2$] or [RuCpCl(P-P)] by 4-ethynylpyridine when promoted by $NaPF_6$ in a basic medium $Al_2O_3$ (for **5.1** and **5.3**) or NaOH (for **5.4**, **5.7**, **5.8)** at r.t., as depicted in **Schemes 2.1** and **2.2**, respectively. The synthesis of **5.4** has been achieved through the reaction of 4-ethynylpyridine with *cis*-[RuCl$_2$(dppe)$_2$] and sodium in refluxing $CH_3OH$.[58] In this work, complex **5.4** was obtained in a simpler approach under milder conditions with comparative yield, and characterized by X-ray crystallography. *Trans*-[RuCl(C(OCH$_3$)=CHpy-4)(dppe)$_2$] **5.5** was obtained as a minor product in the preparative reaction of **5.4**. *Trans*-[RuCl(CH=CHpy-4)(dppe)$_2$] **5.6** was obtained when attempts were made to grow crystals of **5.5** in THF/hexane mixtures.

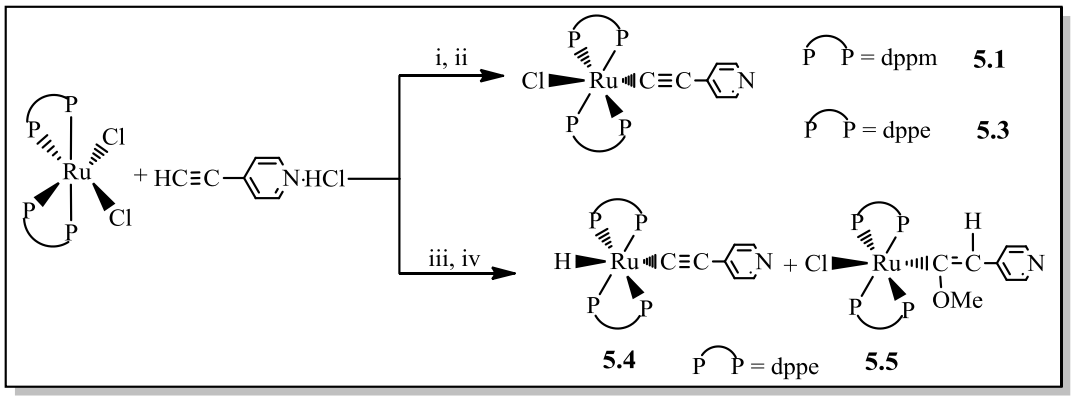


**Scheme 2.1** (i) $CH_2Cl_2$/MeOH/$NaPF_6$, overnight at r.t.; (ii) $Al_2O_3$; (iii) $CH_2Cl_2$/MeOH/$NaPF_6$, 5h at r.t.; (iv) NaOH, 2h at r.t..

The known compounds **5.7** and **5.8** were prepared by a modified method of Wu et.al.[52] with improved yields (~ 96%). They have been fully characterised.

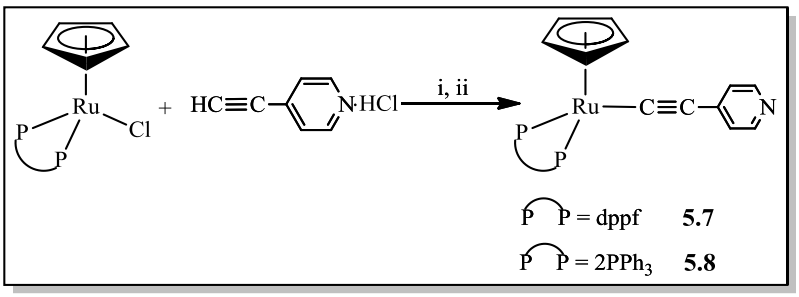


**Scheme 2.2** (i) $CH_2Cl_2$/MeOH/$NaPF_6$, 20h at r.t.; (ii) NaOH, 2h at r.t.

An attempt to synthesize a dendrimeric assembly such as $\{[RuCl(C{\equiv}Cpy\text{-}4)(dppm)_2]_4Pd\}(PF_6)_2$ from **5.1** and $[Pd(CH_3CN)_4](PF_6)_2$ was futile. Instead a ligand exchange reaction takes place giving *trans*-$[Ru(C{\equiv}Cpy\text{-}4)(CH_3CN)(dppm)_2]^+$, isolated as the $PF_6^-$ salt, **5.2** (**Scheme 2.3**). This is understandable since it could be energetically more favorable for the acidic solvento complex $[Pd(CH_3CN)_4](PF_6)_2$ to extract a basic chloride from **5.1** than to overcome the entropy barrier to give the sterically crowded $\{PdRu_4\}$ aggregate.

Complex **5.2** is unusual with its hybrid properties. Its dangling basic pyridyl function makes it a metalloligand whereas its labile $CH_3CN$ would enable it to be Lewis acid. Such dual presence of acidic and basic sites allows **5.2** to be a potential versatile building block in polymetallic coordination polymeric assembly.

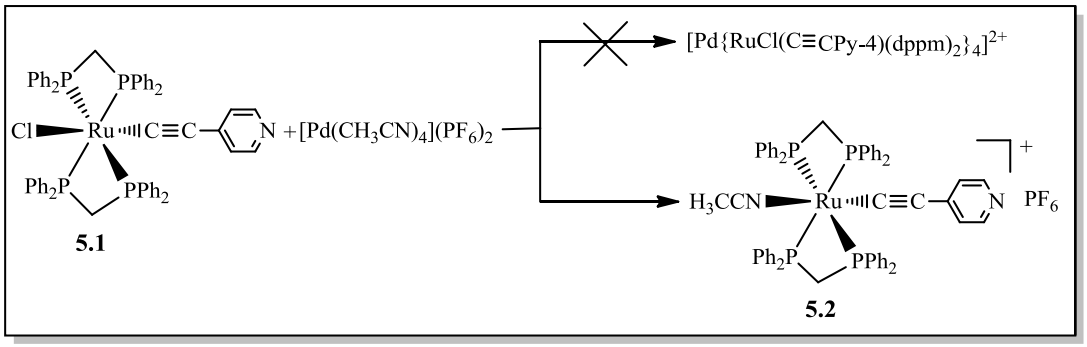


**Scheme 2.3** Formation of **5.2** from **5.1**: $CH_2Cl_2$, 12h at r.t.

### 2.2.1.2 Characterization and General Properties

All complexes **5.1 - 5.8** are air stable in solid state, but protonation occurs slowly in solution at the uncoordinated pyridine.[118,119] In particular, complex **5.5**, like other ether species, is not stable enough in solution and easy to be oxidized by $O_2$ when exposed to air. Complex **5.6** was actually formed during slow recrystallization of **5.5** from THF/hexane mixtures. Complex **5.6** was confirmed by its single X-ray crystal structure, as discussed below (Section **2.2.1c**).

All complexes readily dissolve in $CH_2Cl_2$. They show moderate solubility in THF but poor solubility in $CH_3CN$ and other common non-polar solvents. All complexes were characterized by $^{1}H$, $^{31}P$, $^{13}C$ NMR spectroscopy, IR, ESI-MS, and elemental analyses. The single crystal structures of complexes **5.1** – **5.4**, **5.6** and **5.7** were determined by X-ray single-crystal crystallography. The spectroscopic properties of

these complexes are consistent with their proposed formulae.

The C≡C IR vibration frequency of complexes **5.1** – **5.4**, **5.7** (2053 ~ 2092 $cm^{-1}$) varies slightly with the change of the diphosphine auxiliary ligands and the configuration of octahedral or half-sandwich in Ru(II) metal centers. The downfield shift of C≡C IR vibration frequency in these mononuclear Ru(II) acetylide complexes compared to free C≡C (2100 ~ 2250 $cm^{-1}$) is attributed to the electron-donor property of C≡Cpy and the back-donation from Ru core to the π* orbitals of C≡C, thus reducing the C≡C vibrational energy. The vibration frequency of complex **5.1** (2078 $cm^{-1}$) is similar to that of its analogue *trans*-[RuCl(C≡Cpy-2)$(dppm)_2$] (2080 $cm^{-1}$).[120] The higher energy C≡C absorption of **5.2** (2092 $cm^{-1}$) compared to its analogue **5.1** (2078 $cm^{-1}$) is consistent with a less basic metal center (Ru) resulting from the replacement of Cl by $CH_3CN$ and its cationic character. This decreases the back-donation from Ru to the π* orbitals of C≡C, and hence leads to stronger C≡C bond in **5.2**.

The signal of δ -10.03 (qn, $J_{P-H}$ = 19.0 Hz, 1H) in $^1$H NMR resonance of complex **5.4** indicates the presence of Ru-H bond. Likewise, δ 4.78 (d, 1H) in **5.5** and 6.51 (1H), 6.56 (1H) in **5.6** in their $^1$H NMR resonance confirm the existence of [Ru-$COCH_3$=C*H*py-4) and [Ru-C*H*=C*H*py-4] in **5.5** and **5.6**, respectively.

The chemical equivalence of the phosphines is indicated from a singlet $^{31}$P NMR resonance in the spectra (δ -6.0, -7.5, 49.5, 69.1, 53.4, 53.2, 55.5 and 50.8 ppm for **5.1**-**5.8,** respectively), suggesting the equivalent chemical environment of all P atoms in these complexes. In the octahedral complexes **5.1 – 5.4**, the two dppm or dppe

ligands occupy the equatorial plane with the Cl/$CH_3CN$/H ligand and alkynyl group *trans*-disposed at the axial plane. The blocking of the equatorial sites in an octahedral environment by dppm or dppe ensures that any incoming ligand or metal can only approach the axial sites. This conformational rigidity ensures a unidirectional coordination propagation.

The $^{13}C$ NMR resonances for the *α*-acetylide carbon in **5.1**, **5.3**, **5.4** and **5.7** are similar (δ 148.1 ~ 149.6 ppm), which are in accordance with other mononuclear Ru(II) σ-acetylide complexes (δ 148.0 ~ 149.7 ppm).[18,58,121] $^2J_{CP}$ cannot be detected in these complexes, presumably because of weak coupling between the near-orthogonal orientations of alkynyl and phosphine (T**ables 2.1** & **2.2**).

ESI-MS analysis of **5.1** – **5.4** and **5.7** gives their respective protonated parent ion peaks, {(m/z 1008, 100%) for **5.1 (Fig. 2.1)**; $([M] + H)^+$, m/z 1013, 100%) for **5.2**; $([M] + H + Cl)^+$, m/z 1070, 100%) for **5.3**, $(([M] + H)^+$, m/z 1002, 50%) for **5.4**; $(([M] + H)^+$, m/z 824, 100%) for **5.7**}. This indicates their good stability under the spectrometric conditions. The fragments ($[Ru(C{\equiv}Cpy)(dppm)_2]^+$, m/z 971, 40%), ($[Ru(dppm)_2]^+$, m/z 869, 20%) in **5.2**, ([RuCl(dppe)], m/z 536, 80%) in **5.3**, ($[RuH(dppe)_2]$, m/z 899, 100%) in **5.4** suggest that the Ru-C, Ru-Cl and Ru-$NCCH_3$ bonds are vulnerable to cleavage. All the ESI-MS data are consistent with the formulae proposed. They also substantiate the other spectroscopic data.

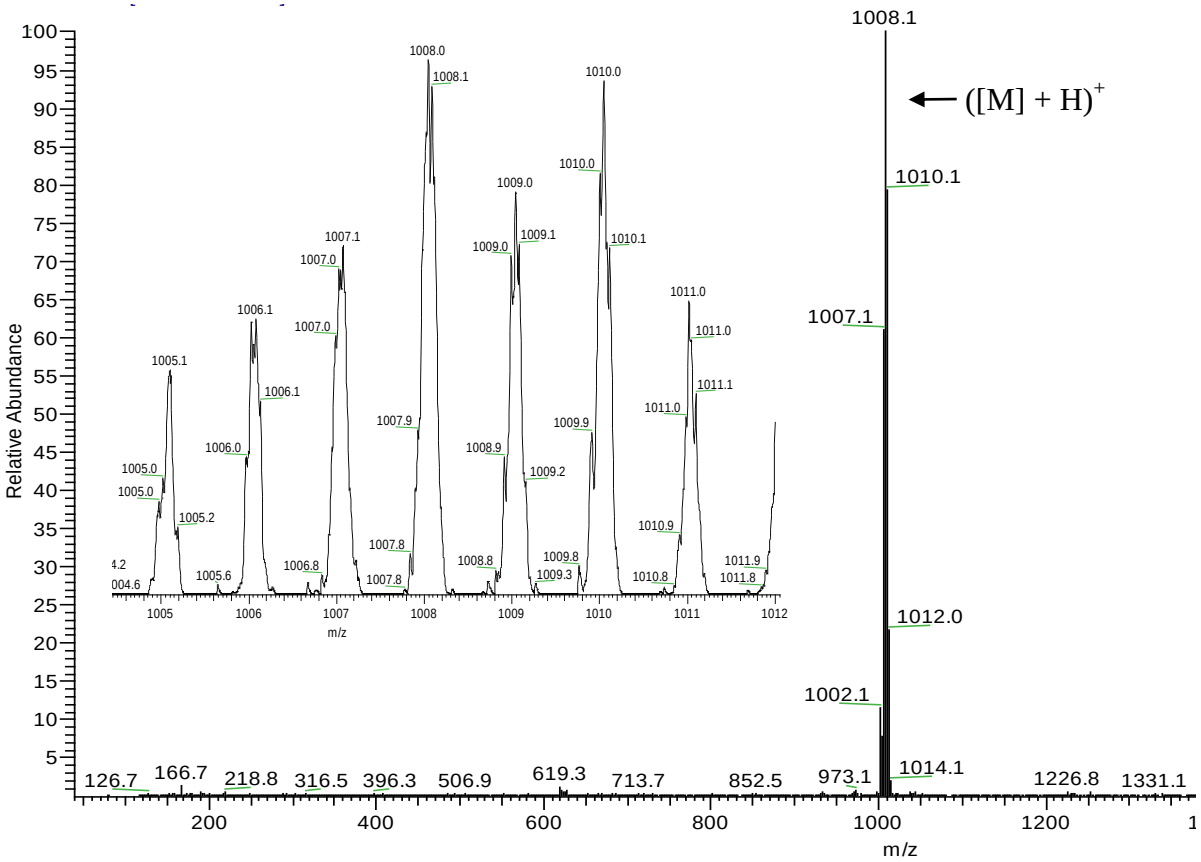


**Fig. 2.1** Positive-ion ESI mass spectrum of **5.1**

### 2.2.1.3 Structural and Reactivity Characteristics

The structures of **5.1 – 5.4**, **5.6** and **5.7** have been determined by X-ray single-crystal crystallography (**Fig. 2.2 – 2.7**; **Tables 2.1** & **2.2**). The relevant crystallographic data and refinement details are shown in **Tables 5.1 – 5.2** (**Chapter Five**).

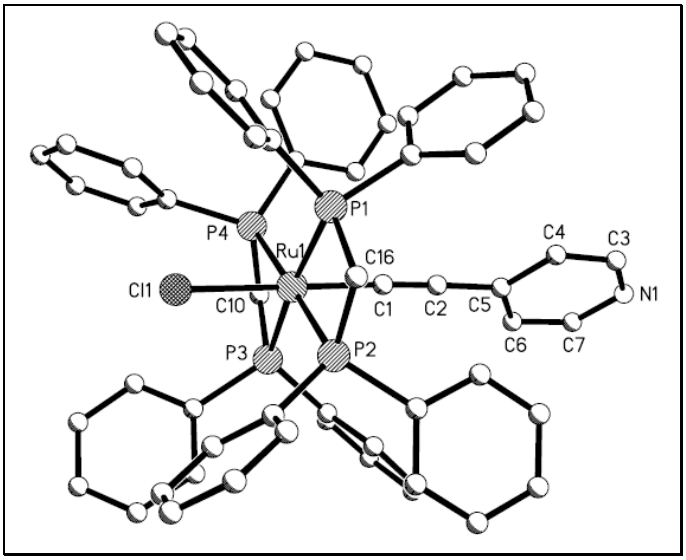


**Fig. 2.2** Crystal structure of *trans*-[RuCl(C≡Cpy-4)(dppm)$_2$] (**5.1**) with hydrogen atoms and solvent molecules omitted for clarity.

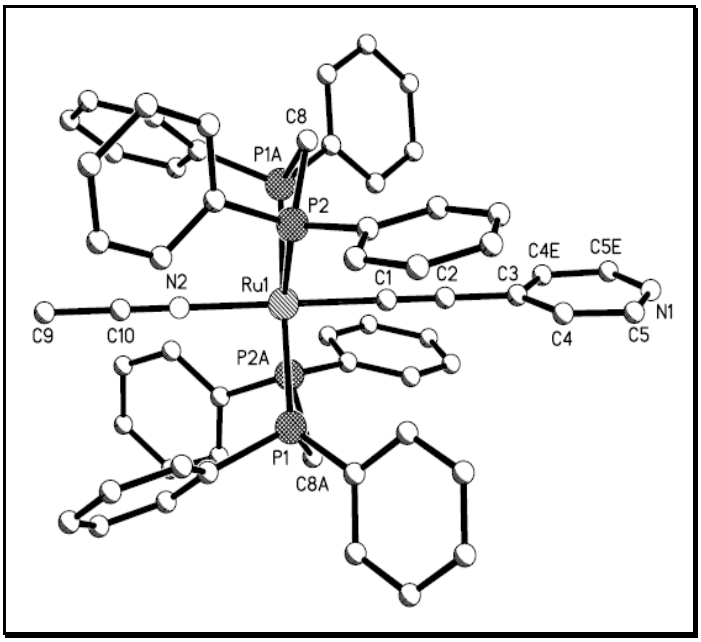


**Fig. 2.3** Crystal structure of *trans*-[Ru(C≡Cpy-4)(CH$_3$CN)(dppm)$_2$](PF$_6$) (**5.2**) with hydrogen atoms, anion and solvent molecules omitted for clarity.

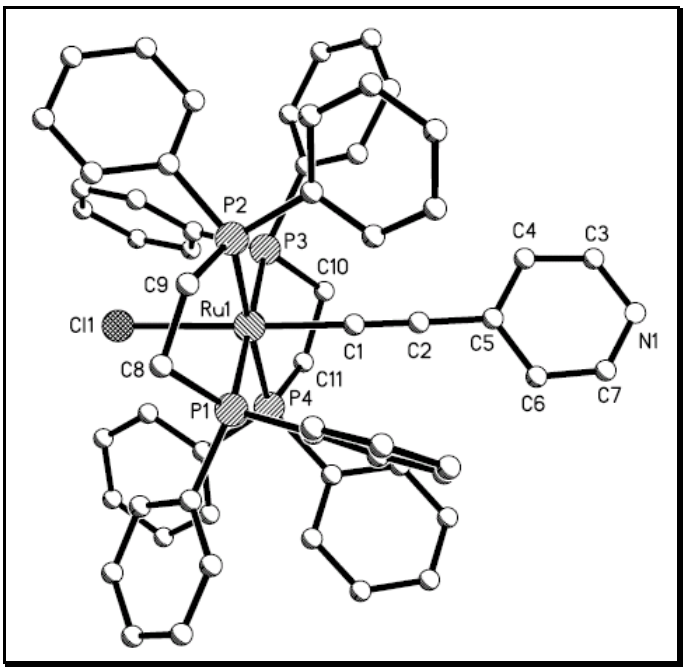


**Fig. 2.4** Crystal structure of *trans*-[RuCl(C≡Cpy-4)(dppe)$_2$] (**5.3**) with hydrogen atoms and solvent molecules omitted for clarity.

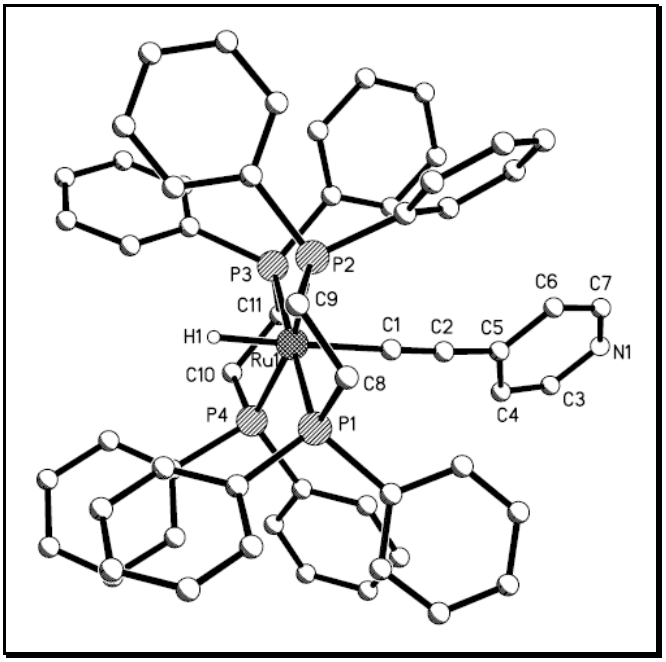


**Fig. 2.5** Crystal structure of *trans*-[RuH(C≡Cpy-4)(dppe)$_2$] (**5.4**) with hydrogen atoms and solvent molecules omitted for clarity.

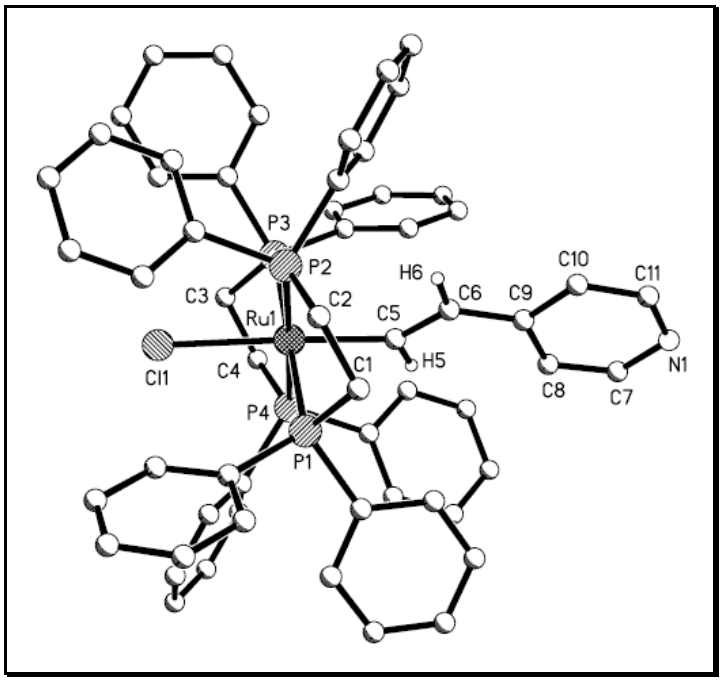


**Fig. 2.6** Crystal structure of *trans*-[RuCl(HC=CHpy-4)(dppe)$_2$] (**5.6**) with hydrogen atoms, anion and solvent molecules omitted for clarity.

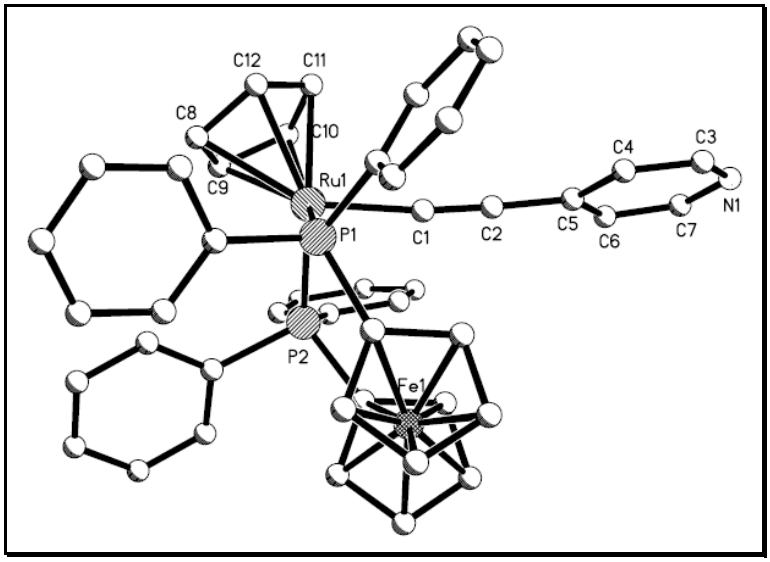


**Fig. 2.7** Crystal structure of [RuCp(C≡Cpy-4)(dppf)] (**5.7**) with hydrogen atoms and solvent molecules omitted for clarity.

**Table 2.1** Selected bond lengths (Å) and angles (°) of **5.1**, **5.2** and **5.7**.

| **5.1** | **5.2** | **5.7** |
|---|---|---|
| Ru(1)-C(1) 1.980(2) | Ru(1)-C(1) 2.04(1) | Ru(1)-C(1) 1.995(2) |
| Ru(1)-Cl(1) 2.4466(4) | Ru(1)-N(2) 2.052(8) | C(1)-C(2) 1.213(3) |
| C(1)-C(2) 1.212(3) | C(1)-C(2) 1.17(2) | C(2)-C(5) 1.425(3) |
| C(2)-C(5) 1.425(3) | C(2)-C(3) 1.45(2) | |
| | N(2)-C(10) 1.16(1) | |
| | C(9)-C(10) 1.48(2) | |
| C(1)-Ru(1)-Cl(1) 177.38(5) | C(1)-Ru(1)-N(2) 180 | C(2)-C(1)-Ru(1) 173.5(2) |
| C(2)-C(1)-Ru(1) 177.9(2) | C(10)-N(2)-Ru(1) 180 | C(1)-C(2)-C(5) 177.4(3) |
| C(1)-C(2)-C(5) 175.6(2) | N(2)-C(10)-C(9) 180 | |
| | C(2)-C(1)-Ru(1) 180 | |
| | C(1)-C(2)-C(3) 180 | |

**Table 2.2** Selected bond lengths (Å) and angles (°) of **5.3**, **5.4** and **5.6**.

| **5.3** | **5.4** | **5.6** |
|---|---|---|
| Ru(1)-C(1) 1.979(4) | Ru(1)-C(1) 2.071(5) | Ru(1)-C(5) 2.038(3) |
| Ru(1)-Cl(1) 2.495(1) | C(1)-C(2) 1.226(7) | Ru(1)-Cl(1) 2.5366(8) |
| C(1)-C(2) 1.231(5) | C(2)-C(5) 1.433(7) | C(5)-C(6) 1.357(4) |
| C(2)-C(5) 1.427(6) | | C(6)-C(9) 1.451(4) |
| C(1)-Ru(1)-Cl(1) 178.7(1) | C(2)-C(1)-Ru(1) 173.2(4) | C(5)-Ru(1)-Cl(1) 175.56(8) |
| C(2)-C(1)-Ru(1) 175.2(4) | C(1)-C(2)-C(5) 174.3(5) | C(6)-C(5)-Ru(1) 136.7(2) |
| C(1)-C(2)-C(5) 176.8(4) | | C(5)-C(6)-C(9) 126.5(3) |

Complexes **5.1** – **5.4** and **5.6** are mononuclear structures with octahedral Ru(II), whereas complex **5.7** has a half-sandwich configuration. All of them have a terminal 4-ethynylpyridine ligand coordinated at C leaving a free pyridyl pendant. For **5.1** – **5.4**, *trans* to the 4-ethynylpyridine ligand is either Cl (**5.1** & **5.3**), or $CH_3CN$ (**5.2**) or H (**5.4**). Two dppm (in **5.1** & **5.2**) or dppe (in **5.3** & **5.4**) chelates are locked onto a plane such that they force the two active functionalities, *viz*. Cl/$CH_3CN$/H and C≡Cpy,

to the perpendicular plane and *trans* to each other. This is a desirable scaffold as it complements the 1, 4 *(or trans)*-orientation of the donor atoms (C, N) at the spacer, thereby ensuring that any incoming metal must be aligned.

The Ru-C bond lengths in **5.1 – 5.4**, **5.6** and **5.7** (1.979(4) ~ 2.071(5) Å) are comparable to those of other known Ru(II) σ-acetylides (1.99(1) ~ 2.071(2) Å).[122] The C≡C distances in **5.1** – **5.4** and **5.7** (1.17(2) ~ 1.231(5) Å) fall within the range of those observed for related ruthenium (II) σ-acetlylide complexes.[123] Complex **5.2** has the shortest and presumably strongest bond (1.17(2) Å) in this series. The shorter C-C length in **5.2** than in its analogue **5.1**(1.212(3) Å) is in agreement with the C≡C IR absorption wavenumbers **5.2** (2092 $cm^{-1}$) > **5.1** (2078 $cm^{-1}$). It also indicates that Ru→C≡Cpy back-bonding is weaker in **5.2** because it is competing with a good π–acceptor $CH_3CN$ at the *trans* position.

The linear geometries of these monometallic acetylides are elucidated by the angles of Ru-C(1)-C(2)-C(5) with Ru-C(1)-C(2) (173.5(2) ~ 180°) and C(1)-C(2)-C(5) (174.3(5) ~ 180°). The angles of C(10)-N(2)-Ru(1) (180°), N(2)-C(10)-C(9) (180°), Ru-C(1)-C(2) (180°) and C(1)-C(2)-C(5) (180°) in complex **5.2** manifest its ideal linear feature along the C-N-Ru-C≡C-$C_{(py)}$ backbone.

The Ru-C and C=C bond distances in the vinylidene complex **5.6** are 2.038(3) and 1.357(4) Å, respectively, much longer than those in its acetylide analogue **5.3** (1.979(4) and 1.231(5) Å, respectively). The Ru-C bond distance (2.038(3) Å) in **5.6** is shorter than its analogue [Ru{(*Z*)-HC=CHPh}$(CO)_2(\eta^2$-$C_5Ph_5)$] (2.091(4) Å),[123] which is associated with the longer C=C distance (1.357(4) Å) in **5.6** than that in

[Ru{(*Z*)-HC=CHPh}$(CO)_2(\eta^2$-$C_5Ph_5)$] (1.329(6) Å).[124] The angles of C=C–Ru (136.7(2)°) and C=C–$C_{py}$ (126.5(3)°) in **5.6** indicate the much less linear structure than its acetylide analogue **5.3**. The nonlinear optical response exhibited by complex **5.3** rather than **5.6** testifies their structural difference (**Chapter Three**).

The incorporation of pyridine to the alkynyl unit in the monometallic Ru(II) acetylides would open up new avenues for the construction of multinuclear assemblies by employing the Ru(II) acetylides described above as building blocks. In view of this, three systems of heterometallic complexes containing different mononuclear Ru(II) acetylides including **5.1**, **5.3**, **5.4**, **5.7** and **5.8** have been developed. They will be introduced in the subsequent sections of this chapter.

## 2.2.2 Heterobimetallic Complexes of $d^5$ - $d^6$ Series

### 2.2.2.1 Preparation

Complexes of the formula *fac*-[$ReX(CO)_3$(N-N)] (X = Cl, Br, I; N-N: heterocyclic nitrogen ligand) can generally be prepared from $ReX(CO)_5$ and N-N ligand through CO dissociation by thermolytic method.[118,125] Under the promotion of a halide-extracting agent in a coordinating solvent, *fac*-[$Re(sol)(CO)_3$(N-N)]$^+$ can be obtained from *fac*-[$ReX(CO)_3$(N-N)] (**Scheme 2.4(a)**).[126,127] Complexes *fac*-[$ReBr(CO)_3$(tpy)] (**5.9**) and *fac*-[$Re(CH_3CN)(CO)_3$(tpy)]($PF_6$) (**5.10**) are conveniently obtained with quantitative yields by this approach (**Scheme 2.4(b)**). Complex **5.9** is prepared from carbonyl replacement of $ReBr(CO)_5$ by tpy under thermal conditions. Bromide abstraction and solvate entry of **5.9** facilitated by $AgPF_4$

would give **5.10**. Complexes **5.9** and **5.10** are not known in the literature although a derivative [ReBr(CO)$_3$(Ph-tpy)] has been reported.[128]

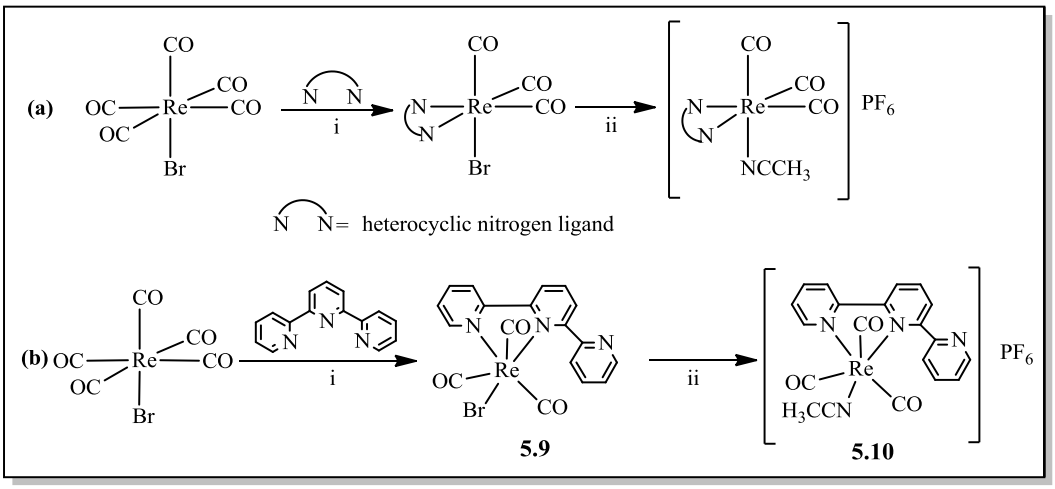


**Scheme 2.4** (i) toluene, 4h reflux; (ii) AgPF$_6$, CH$_3$CN, 12h reflux

The system of interest is represented by Lewis adducts formed between electron donors [RuCp(C≡Cpy-4)(P-P)] (P-P = dppf, **5.7**; 2PPh$_3$, **5.8**) and [Re$^I$(CO)$_3$] as acceptors represented by the diimine complexes *fac*-[ReBr(CO)$_3$(N-N)] (N-N: bpy, Me$_2$bpy, $^t$Bu$_2$bpy, phen), **5.9** and **5.10**.

The heterobimetallic adducts [RuCp(C≡Cpy-4)(P-P)][Re(CO)$_3$(N-N)](PF$_6$) **5.11** – **5.16** (P-P = dppf, N-N = bpy **5.11**, Me$_2$bpy **5.12**, $^t$Bu$_2$bpy **5.13**, phen, **5.14**, tpy, **5.15**; P-P = 2PPh$_3$, N-N = bpy **5.16**) are readily prepared from the Ru(II) metalloligands and the Re(I) CH$_3$CN solvent complexes in THF reflux (**Scheme 2.5**). The uncoordinated pyridyl nitrogen in **5.7** and **5.8** exhibits Lewis basicity, hence it can serve as the coordination sites for acceptors represented by Re(I) diimine carbonyl fragments *fac*-[Re(CH$_3$CN)(CO)$_3$(N-N)]$^+$. The weakly bound CH$_3$CN in these Re(I) moieties can easily dissociate to generate an empty coordination site.

Mixing equivalent amounts of **5.7** or **5.8** and *fac*-[Re($CH_3CN$)($CO$)$_3$(N-N)]($PF_6$) (N-N = bpy, $Me_2$bpy, $^tBu_2$bpy, phen, or tpy) in refluxing THF solution would give yellow to orange pure heterobimetallic Lewis adducts **5.11** – **5.16** (**Scheme 2.5**).

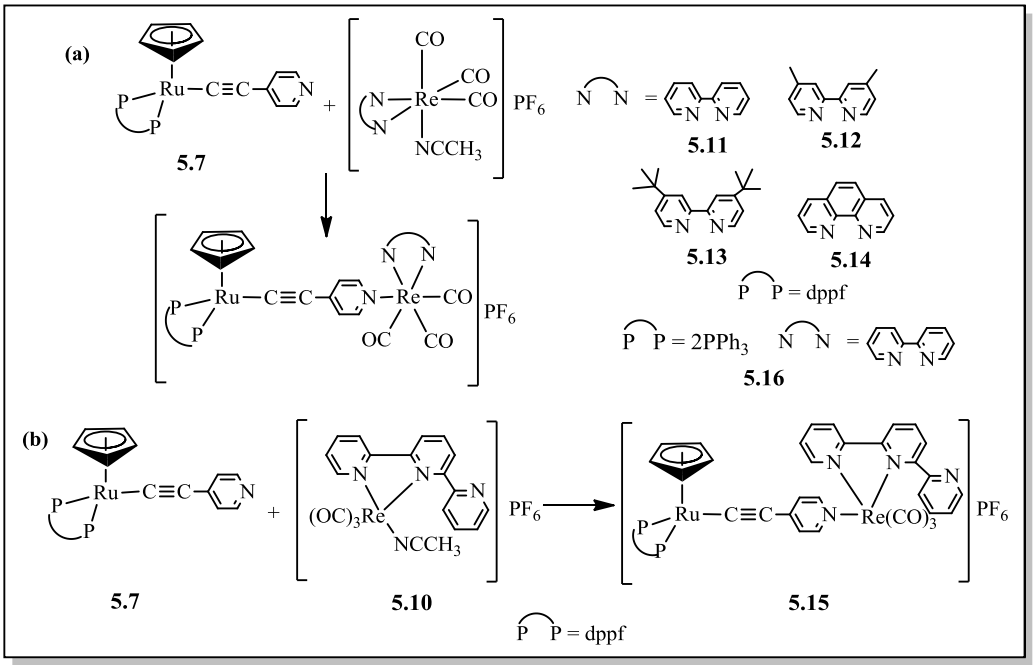


**Scheme 2.5** Formation of complexes **5.11**-**5.16**: THF, 12h, reflux

### 2.2.2.2 Characterization and General Properties

The characterization of monometallic Re(I) complexes **5.9**, **5.10** and the Ru(II)-Re(I) heterobimetallic assemblies was achieved by a variety of analytical techniques including IR, NMR, ESI-MS spectrometry, and elemental analysis. Complexes **5.9** and **5.11** – **5.15** were also characterized by X-ray crystallography.

The spectrometric data obtained for the complexes **5.9** – **5.16** are consistent with the expected structures of the products. The three strong IR active carbonyl peaks (2024, 1923 and 1899 $cm^{-1}$) of **5.9** are typical for *fac*-[ReX($CO$)$_3$(N-N)] complexes,[129] and consistent with a facial arrangement of the carbonyl

groups.[127,130,131] The higher CO stretching vibrations of **5.10** (2036 and 1928 $cm^{-1}$) than those of **5.9** suggested a higher electron back-donation from Re to the vacant **π*** orbitals of carbonyls in **5.9**, consistent with the observations in related systems.[126,131] They are also similar to the case of **5.2** and its Cl analogue **5.1** described in **2.2.1b**. The maintenance of the tricarbonyl moiety in both **5.9** and **5.10** would suggest that terpyridyl is bidentate and the third N donor is not able to compete for coordination with carbonyl, bromide or the $CH_3CN$ solvate in a 6-coordinate Re(I) core (**Scheme 2.4(b)**). No significant difference in the carbonyl stretching frequencies was observed among the various heterobimetallic complexes **5.11** – **5.16**, in which the Re(I) cation moieties exhibit two bands in the CO stretching region of the IR.

ESI-MS analysis of **5.9** shows a clean spectrum of the (protonated) parent ion ($[M + H]^+$, m/z 584, 100%), suggesting that the solid-state formulation is maintained in solution. For **5.10**, the parent ($[M]^+$, m/z 544, 25%) and desolvated complex ($[M\text{-}CH_3CN]^+$, m/z 504, 100%) have been detected (**Fig. 2.8**). The stronger intensity of the latter is within expectation because of the higher propensity for terpyridine to be tridentate upon the expulsion of the more labile $CH_3CN$.

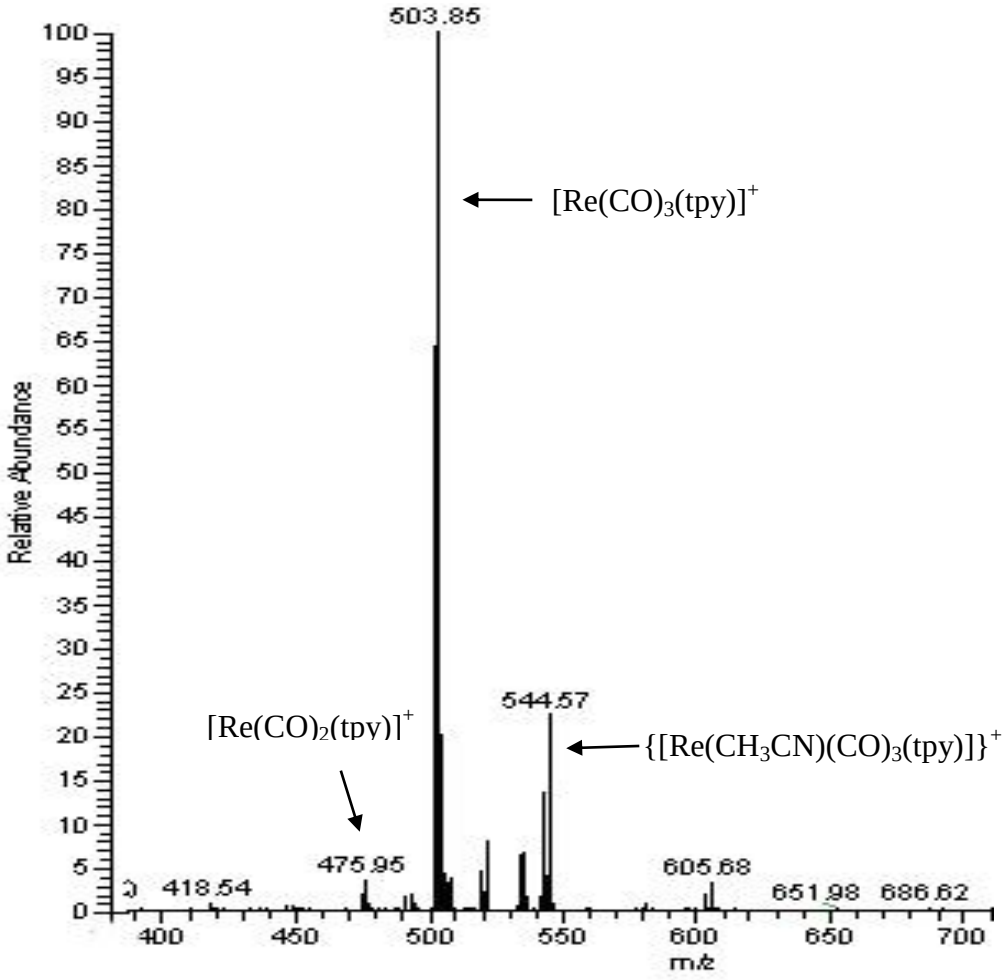


**Fig. 2.8** Positive-ion ESI mass spectrum of **5.10**

The good stability of these bimetallic assemblies **5.11**-**5.16** is evident in their ESI-MS spectra which invariably shows that the protonated parent ion $[M + H]^+$ as the principal peak (**Chapter Five**).

### 2.2.2.3 Structural and Reactivity Characteristics

Since terpyridine is rarely $\eta^2$-bidentate (e.g. [*cis*-Ru(bpy)($\eta^2$-tpy)$(CO)_2$]$(PF_6)_2$, [*cis*-Ru(bpy)($\eta^2$-tpy)$(CO)(CH_2OCH_3)$]$(PF_6)$ and [$AuBr(CN)_2(\eta^2$-tpy)]),[132-135] The proposal of structures of **5.9**, **5.10** and **5.15** would require verification from X-ray single-crystal crystallographic analysis. Single crystal X-ray diffraction studies have

provided geometric details of the solid state structures of **5.9** and **5.15**, as well as **5.11** – **5.14**. ORTEP diagrams for **5.9** and **5.11** – **5.15** are depicted in **Fig. 2.9** – **2.14**, selected bond lengths and bond angles are presented in **Tables 2.3** & **2.4**. The relevant crystallographic data and refinement details are shown in **Tables 5.3** – **5.4** (**Chapter Five**).

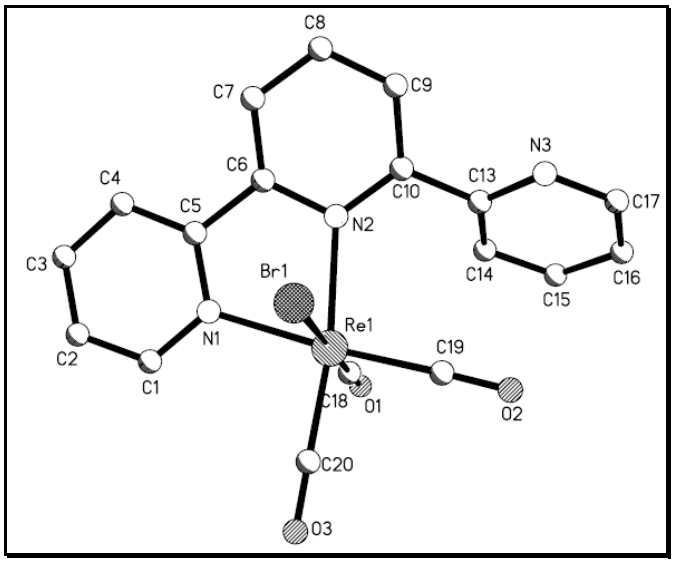


**Fig. 2.9** Crystal structure of $[ReBr(CO)_3(tpy)]$ (**5.9**) with hydrogen atoms and solvent molecules omitted for clarity

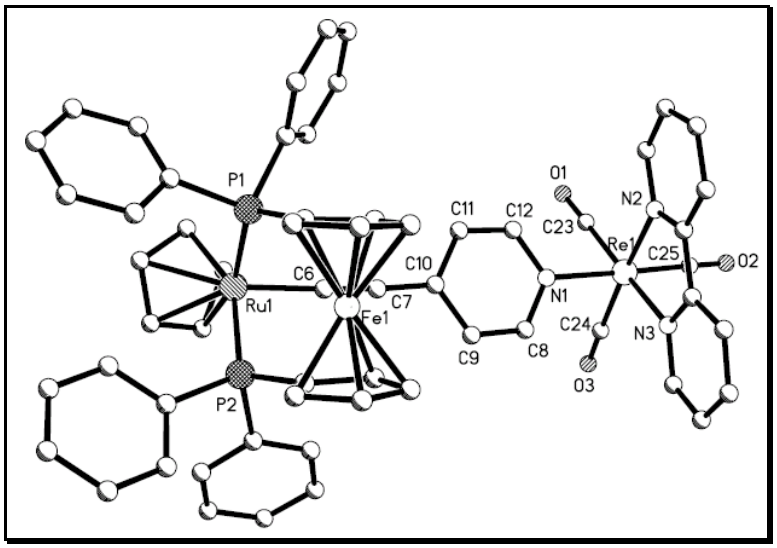


**Fig. 2.10** Crystal structure of $[RuCp(C{\equiv}Cpy\text{-}4)(dppf)][Re(CO)_3(bpy)](PF_6)$ (**5.11**) with hydrogen atoms, anion and solvent molecules omitted for clarity

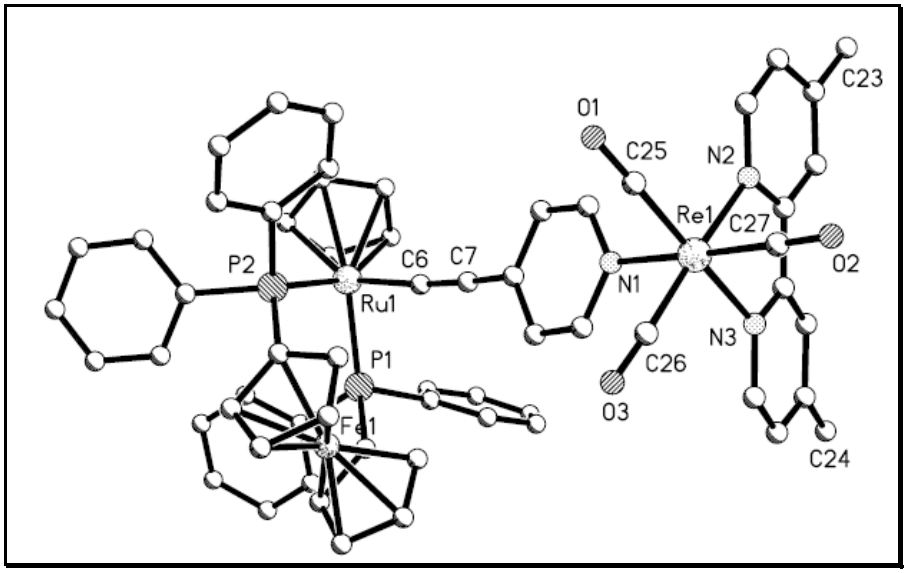


**Fig. 2.11** Crystal structure of [RuCp(C≡Cpy-4)(dppf)][Re(CO)$_3$(Me$_2$bpy)](PF$_6$) (**5.12**) with hydrogen atoms, anion and solvent molecules omitted for clarity

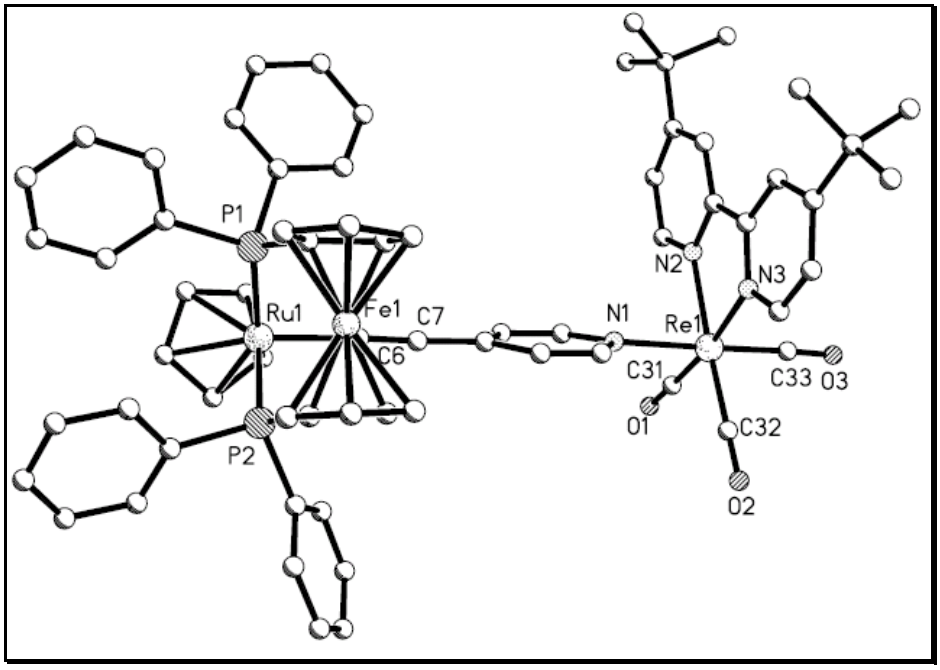


**Fig. 2.12** Crystal structure of [RuCp(C≡Cpy-4)(dppf)][Re(CO)$_3$($^t$Bu$_2$bpy)](PF$_6$) (**5.13**) with hydrogen atoms, anion and solvent molecules omitted for clarity

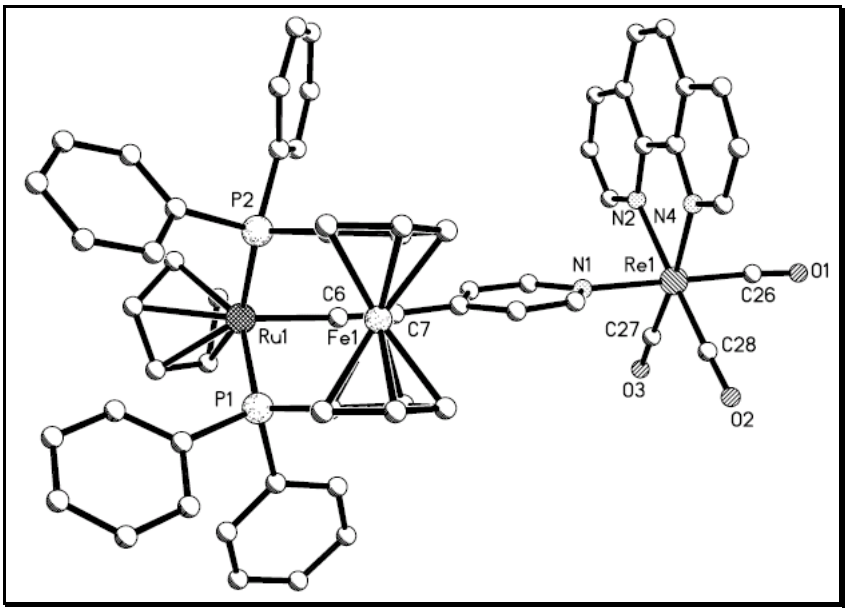


**Fig. 2.13** Crystal structure of [RuCp(C≡Cpy-4)(dppf)][Re(CO)$_3$(phen)](PF$_6$) (**5.14**) with hydrogen atoms, anion and solvent molecules omitted for clarity

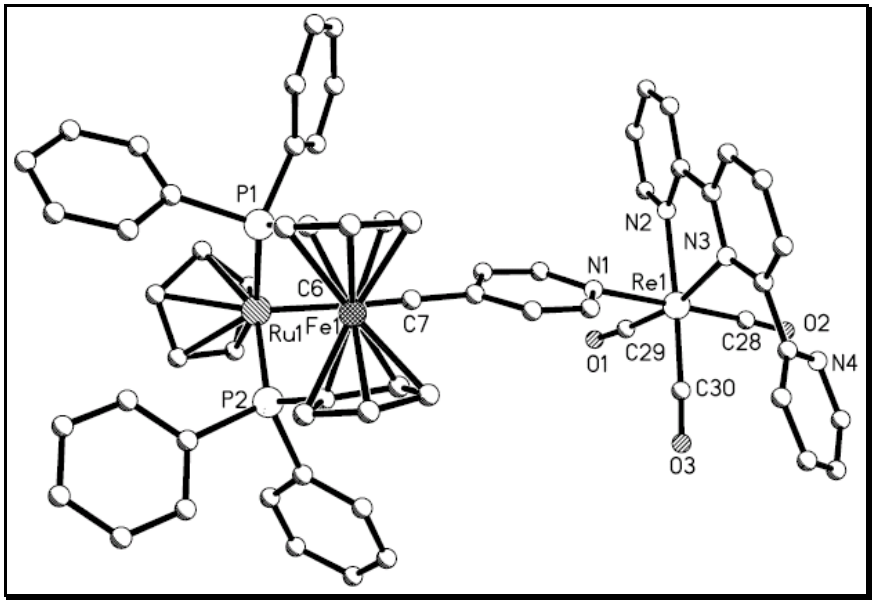


**Fig. 2.14** Crystal structure of [RuCp(C≡Cpy-4)(dppf)][Re(CO)$_3$(tpy)](PF$_6$) (**5.15**) with hydrogen atoms, anion and solvent molecules omitted for clarity

**Table 2.3** Selected bond lengths (Å) and angles (°) of **5.9**, **5.11** and **5.12**.

| **5.9** | **5.11** | **5.12** |
|---|---|---|
| Re(1)-N(1) 2.174(2) | Re(1)-N(1) 2.190(5) | Re(1)-N(1) 2.203(7) |
| Re(1)-N(2) 2.228(2) | Re(1)-N(2) 2.169(5) | Re(1)-N(2) 2.164(7) |

| | | |
|---|---|---|
| Re(1)-Br(1) 2.6409(3) | Re(1)-N(3) 2.176(5) | Re(1)-N(3) 2.162(8) |
| Re(1)-C(18) 1.886(3) | Re(1)-C(23) 1.913(7) | Re(1)-C(25) 1.89(1) |
| Re(1)-C(19) 1.922(3) | Re(1)-C(24) 1.923(7) | Re(1)-C(26) 1.91(1) |
| Re(1)-C(20) 1.913(3) | Re(1)-C(25) 1.912(7) | Re(1)-C(27) 1.89(1) |
| | Ru(1)-C(6) 1.972(6) | Ru(1)-C(6) 1.972(9) |
| | C(6)-C(7) 1.228(8) | C(6)-C(7) 1.24(1) |
| | | |
| N(1)-Re(1)-N(2) 74.80(8) | N(1)-Re(1)-N(2) 83.8(2) | N(1)-Re(1)-N(2) 84.5(2) |
| Br(1)-Re(1)-C(18) 177.89(8) | N(1)-Re(1)-N(3) 85.4 (2) | N(1)-Re(1)-N(3) 81.1(3) |
| Br(1)-Re(1)-C(19) 91.57(8) | N(2)-Re(1)-N(3) 74.5(2) | N(2)-Re(1)-N(3) 75.7(3) |
| Br(1)-Re(1)-C(20) 92.69(9) | N(1)-Re(1)-C(23) 89.7(2) | N(1)-Re(1)-C(25) 92.2(4) |
| N(1)-Re(1)-Br(1) 85.71(6) | N(1)-Re(1)-C(24) 94.0(2) | N(1)-Re(1)-C(26) 93.7(4) |
| N(2)-Re(1)-Br(1) 82.05(6) | N(1)-Re(1)-C(25) 178.7(3) | N(1)-Re(1)-C(27) 175.7(4) |
| | Ru(1)-C(6)-C(7) 170.7(5) | Ru(1)-C(6)-C(7) 174.7(8) |
| | C(6)-C(7)-C(10) 176.0(7) | C(6)-C(7)-C(10) 169(1) |

**Table 2.4** Selected bond lengths (Å) and angles (°) of **5.13** - **5.15**.

| **5.13** | **5.14** | **5.15** |
|---|---|---|
| Re(1)-N(1) 2.20 (1) | Re(1)-N(1) 2.181(7) | Re(1)-N(1) 2.202(5) |
| Re(1)-N(2) 2.155(9) | Re(1)-N(2) 2.171(8) | Re(1)-N(2) 2.151(5) |
| Re(1)-N(3) 2.178(8) | Re(1)-N(4) 2.171(8) | Re(1)-N(3) 2.208(5) |
| Re(1)-C(31) 1.92(1) | Re(1)-C(26) 1.907(9) | Re(1)-C(28) 1.927(7) |
| Re(1)-C(32) 1.93(1) | Re(1)-C(27) 1.89(1) | Re(1)-C(29) 1.890(8) |
| Re(1)-C(33) 1.92(1) | Re(1)-C(28) 1.90(1) | Re(1)-C(30) 1.923(8) |
| Ru(1)-C(6) 2.01(1) | Ru(1)-C(6) 1.978(8) | Ru(1)-C(6) 1.964(7) |
| C(6)-C(7) 1.19(2) | C(6)-C(7) 1.21(1) | C(6)-C(7) 1.220(8) |
| | | |
| N(1)-Re(1)-N(2) 85.3(3) | N(1)-Re(1)-N(2) 86.3(3) | N(1)-Re(1)-N(2) 83.4(2) |
| N(1)-Re(1)-N(3) 87.4(3) | N(1)-Re(1)-N(4) 85.1(3) | N(1)-Re(1)-N(3) 82.6(2) |
| N(2)-Re(1)-N(3) 74.7(3) | N(2)-Re(1)-N(4) 74.9(3) | N(2)-Re(1)-N(3) 75.0(2) |
| N(1)-Re(1)-C(31) 90.1(4) | N(1)-Re(1)-C(26) 178.3(4) | N(1)-Re(1)-C(28) 179.2(2) |
| N(1)-Re(1)-C(32) 92.7(4) | N(1)-Re(1)-C(27) 93.1(3) | N(1)-Re(1)-C(29) 90.0(2) |
| N(1)-Re(1)-C(33) 177.0(4) | N(1)-Re(1)-C(28) 92.0(3) | N(1)-Re(1)-C(30) 90.7(2) |
| Ru(1)-C(6)-C(7) 171(1) | Ru(1)-C(6)-C(7) 173.7(8) | Ru(1)-C(6)-C(7) 173.9(6) |
| C(6)-C(7)-C(10) 175 (1) | C(6)-C(7)-C(10) 177(1) | C(6)-C(7)-C(10) 170.4(7) |

The structure of **5.9** (**Fig. 2.9**) unequivocally shows a Re(I) octahedral sphere with the three carbonyls in *fac* configuration, and terpyridine in an unusual bidentate mode, *trans* to the carbonyls, and *cis* to the bromide. To avoid unfavorable ligand contacts, the third pyridyl ring that carries N(3) is twisted out and away from the equatorial plane. This results in an *anti*-like conformation with the two (N(2) & N(3)) pyridyl rings deviated significantly from being co-planar ($\delta$ 42.3$^{o}$). There are a few examples of bidentate tpy ligand or its derivatives[128,132-136] but, within our knowledge, **5.9** is the first crystallographically established example of such an occurrence at Re(I). The Re-$N_{diimine}$ bond distances in $\eta^2$-tpy Re(I) complex **5.9** (average ~ 2.20 Å) are longer than those in $\eta^3$-tpy Re(I) complexes *trans*-[Re(tpy)($^t$BuNC)$_2$($\eta^2$-Cp)](OTf) and *trans*-[Re(tpy)($^t$BuNC)$_2$($\eta^2$-acetophenone)](OTf) (average ~ 2.11 Å).[137] Apart from the rotational freedom of the C-C bond joining the pyridyl, **5.9** shows the high resistance of $Re^{I}(CO)_3$ to carbonyl substitution, and the reluctance of bromide dissociation to give an ionic species such as [Re(tpy)$(CO)_3$]Br.

Single-crystal X-ray diffraction analysis on **5.11**-**5.15** confirmed that the expected bimetallic complexes are formed with 4-ethynylpyridine serving as a single bridge between the heterometallic centers (**Fig. 2.10** – **2.14**, **Tables 2.3** & **2.4)**. Both the Re(I) and Ru(II) retain their ligands and maintain their expected geometries, with the *fac*-Re$(CO)_3$ moiety remaining undisturbed, similar to Ru(II)-Re(I) heterometallic complexes reported elsewhere.[58,59,138] The di-imine ligands keep their equatorial planar positions orthogonal to the spacer, thus imposing the latter to be *trans* to carbonyl at the axial position.

Angles involving the 4-ethynylpyridine unit in complexes **5.11** – **5.15** (N(1)-Re(1)-$C_{trans\ to\ py}$ 175.7(4) ~ 179.2(2)°) are close to linearity, as observed in related Re(I) involved bimetallic complexes.[58,139] In view of the fact that CO is a strong σ-donor and π-acceptor ligand, the *trans* effect of CO has influence on the ligand *trans* to it. It is reflected by the slightly longer bond lengths in Re-$N_{py}$ (average ~ 2.20 Å) than in Re-$N_{diimine}$ (average ~ 2.17 Å) in the series of complexes **5.11** – **5.15** (**Tables 2.3** & **2.4**). As commonly observed in other Re(I) tricarbonyl diimine systems, the N-Re-N bond angles (74.5(2) ~ 75.7(3)°) for **5.9** and **5.11 – 5.15** are found to be less than 90°, required by the bite distance exerted by the steric demand of the chelating diimine ligands.[8,12] The Re center in **5.15** is closer to an ideal octahedral structure with N(1)-Re(1)-C(28) 179.2(2)°, N(1)-Re(1)-C(29) 90.0(2)°, N(1)-Re(1)-C(30) 90.7(2)° than its precursor **5.9** and analogues **5.11 – 5.14**.

The bidentate coordination mode of terpyridine is also witnessed in **5.15**, leaving off one side pyridyl ring uncoordinated. The central pyridyl N atom is *syn* to the neighboring coordinated N atom and *anti* to the uncoordinated N atom. The N atom in the uncoordinated pyridyl ring is opposite to the Re center with a separation of 3.455 Å between them. Proximity of a bidentate tpy also does not appear to weaken the Re-$N_{spacer}$ bond (2.202(5) Å in **5.15** when compared to an average of 2.195 Å in **5.11-5.14**). Attempts to carry out decarbonylation to prepare [RuCp(C≡Cpy-4)(dppf)Re$(CO)_2(\eta^3$-tpy)](PF$_6$) from **5.15** through the use of trimethyamine N-oxide (TMNO) were futile, thus indicative of the high stability of the $Re(CO)_3$ core.

In the molecular systems of **5.11**, **5.12**, **5.14**, **5.15**, the Ru(1)-C(6) distances (1.964(7) ~ 1.978(8) Å) are slightly shorter than that reported in [RuH(C≡Cpy-4)(dppe)$_2$Re(CO)$_3$($^t$Bu$_2$bpy)](OTf) (2.004(5) Å),[58] but comparable to those in **5.13** (2.01 (1) Å) and another related complex {Ru(C≡Cpy-4)$_2$(16-TMC)[Re(CO)$_3$(bpy)]$_2$}(OTf)$_2$ (2.04(1) Å).[59] The bond distances of C≡C in **5.11** – **5.15** (1.19(2) ~ 1.24(1) Å), however, are much shorter than those in the two aforementioned complexes (1.298(9) and 1.41(1) Å, respectively).[58,59]

## 2.2.3 Heterotrimetallic Complexes of $d^6$ - $d^8$ - $d^6$ Series

### 2.2.3.1 Preparation

The metalloligand potentials of monometallic Ru(II) acetylides **5.1**, **5.3**, **5.4** and **5.7** are also illustrated in their reactions with [MCl$_2$(CH$_3$CN)$_2$] (M = Pd, Pt) at r.t. in CH$_2$Cl$_2$ to give a series of heterotrimetallic σ-acetylide complexes [*trans*-RuL(C≡Cpy-4)(P-P)$_2$]$_2$[MCl$_2$] (For P-P = dppm, L = Cl, M = Pd **5.17**, Pt **5.18**; For P-P = dppe, L = Cl, M = Pd **5.19**, Pt **5.20**; L = H, M = Pd **5.21**) (**Scheme 2.6**) or [RuCp(C≡Cpy-4)dppf]$_2$[MCl$_2$] (M = Pd **5.22**; M = Pt **5.23**) (**Scheme 2.7**). Through a systematic variation of the monometallic precursors and the square planar moieties, the properties of this class of complexes have been systematically tuned. These reactions are stoichiometrically controlled; use of 2-fold excess of the acidic [MCl$_2$(CH$_3$CN)$_2$] would result in the isolation of trimetallic {M$_2$Ru}complexes as yellow solids and the major products. Subsequent X-ray analysis (section **2.2.3c**) has established that these are linear coordination oligomers whereby the Ru-M-Ru

alignments are governed strictly by the directionality of the spacer, i.e. pyridyl acetylide and the geometric feature of the central metal M.

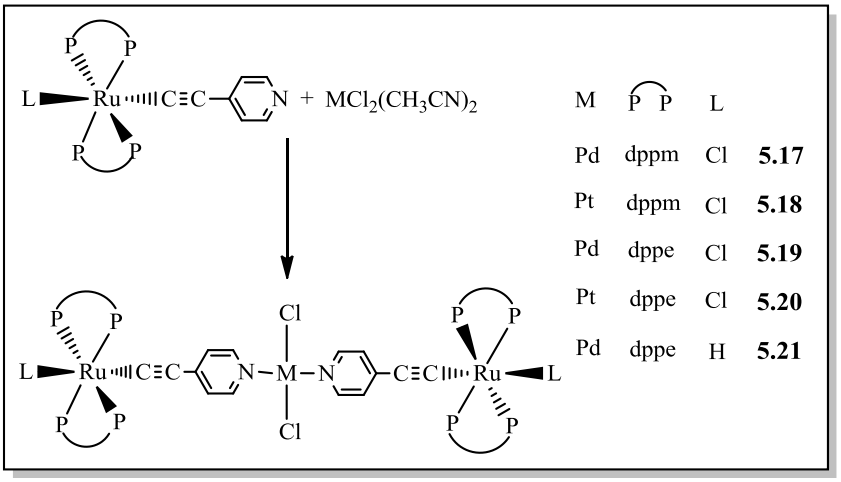


**Scheme 2.6** Formation of **5.17-5.21**: $CH_2Cl_2$, 12h at r.t.

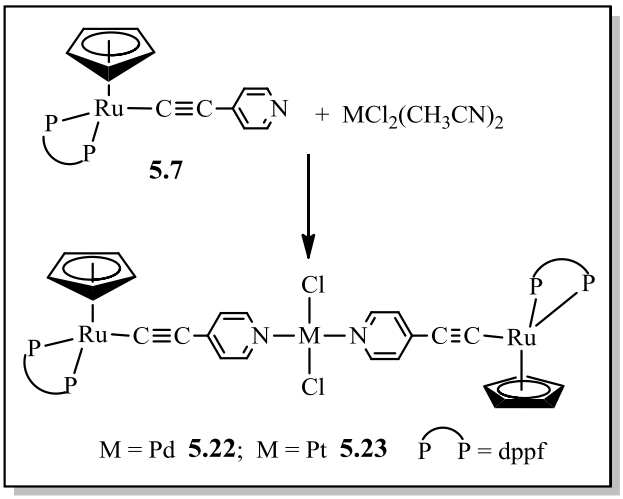


**Scheme 2.7** Formation of **5.22-5.23**: $CH_2Cl_2$, 12h at r.t.

### 2.2.3.2 Characterization and General Properties

All complexes **5.17 - 5.23** are air stable both in solid and solution states. All of them easily dissolve in $CH_2Cl_2$ without visible decomposition. They show poor solubility in THF and are insoluble in $CH_3CN$ and other common non-polar solvents.

All complexes were characterized by $^{1}H$, $^{31}P$, $^{13}C$ NMR spectroscopy, IR, ESI-MS, elemental analyses as well as single-crystal X-ray diffraction studies. The spectroscopic properties of all complexes are consistent with their proposed formulae.

The C≡C vibration frequency of complexes **5.17** – **5.23** are in the range of 2032 ~ 2049 $cm^{-1}$. The small difference between them indicates that the influence of the diphosphine ligands and the geometry of Ru(II) centers (octahedral or half-sandwich) or different square planar fragments on $IR_{(C\equiv C)}$ is insignificant. Compared to those in their respective monometallic Ru(II) acetylide precursors, the C≡C vibration frequency of complexes **5.17** – **5.23** undergoes a coordination-like down field shift with the magnitude of 20 ~ 35 $cm^{-1}$, suggesting that the perturbation at the pyridyl site by $PdCl_2$/$PtCl_2$ fragments leads to electron density dissipation at the triple bond through conjugation. Their $^{31}P$ NMR spectra show a singlet resonance (δ -6.3, -6.4, 49.2, 49.2, 69.1, 55.7 and 55.7 ppm for **5.17** – **5.23**, respectively) that indicates the equivalent phosphorus environment in the diphosphine ligands. Moreover, the coordination of pyridyl ligand on Pd(II)/Pt(II) centers has only slight influence on the chemical shifts of $^{31}P$ NMR resonance from Ru(II) monomers to Ru(II)-Pd(II)/Pt(II)-Ru(II) trinuclears. This is reasonable since the diphosphine ligands are non-coplanar with the Ru-C≡Cpy-M backbone, hence the lengthening of the conjugation along Ru-C≡Cpy-M axis has little effect on the spectra of the diphosphine ligands.

The $^{13}C$ NMR resonances for the *α*-acetylide carbon in **5.17** – **5.23** are similar (δ 151.0 ~ 151.7 ppm), which are downfield shifted compared to those of their

respective precursors **5.1**, **5.3**, **5.4** and **5.7** (δ 148.1 ~ 149.6 ppm) as well as other Ru(II) monomer σ-acetylide complexes (δ 148.0 ~ 149.7 ppm).[18,58,122] This suggests Ru(II) → C≡C π* back-bonding resulting from the Lewis acidic Pd(II)/Pt(II) centers withdrawing electron and lowering the electron density of C≡C. This interpretation is supported by the decrease of the C≡C stretching frequencies in the IR spectra of complexes **5.17** – **5.23 (**2032 ~ 2049 $cm^{-1}$) compared to those of **5.1**, **5.3**, **5.4**, **5.7** (2053 ~ 2078 $cm^{-1}$). $^{2}J_{CP}$ cannot also be detected in this series of complexes.

The heterotrimetallic formation is evident in the ESI spectra of **5.17** – **5.23**. ESI-MS analysis of **5.17** – **5.23** shows (m/z 1160, 100%) peak for **5.19 (Fig. 2.15)** and (1/2[M] – Cl) peak for **5.20** (m/z 1133, 45%) with a +2 charge state (*i.e.*, separation of peaks by 0.5 m/z), indicating that dppe-coordinate heterotrimetallic complexes are stable, and more stable than their dppm analogues in which ($[RuCl(C{\equiv}Cpy)(dppm)_2\text{-}PdCl\text{-}Py]^+$) and ($[RuCl(C{\equiv}Cpy)(dppm)_2\text{-}Pt]^+$) fragments were found in **5.17** and **5.18**, respectively. It is well known that the properties of organometallics may be modified dramatically by seemingly subtle changes in chemical structure. Indeed, despite having identical substituents, the dppm and dppe ligands differ by enforcing substantially difference PRuP angles at the metal, which render geometrically similar dppm and dppe compounds exhibiting different properties. This has been testified by previous studies.[13,111] Fragments of {$[RuCp(C{\equiv}Cpy)(dppf)\text{-}PdCl\text{-}py)]^+$ (m/z 1042, 100%) & ($[RuCp(C{\equiv}Cpy)(dppf) + H]^+$ (m/z 824, 35%)} in **5.22** and {$[RuCp(C{\equiv}Cpy)(dppf)\text{-}PtCl_2\text{-}RuCp(C{\equiv}Cpy)(dppf)]^+$ or $[M^+]$} (m/z 1912, 15%),

$[RuCp(C{\equiv}Cpy)(dppf)\text{-}PtCl\text{-}py]^+$ (m/z 1130, 20%) & $[RuCp(C{\equiv}Cpy)(dppf)\text{-}PtCl_2)]^+$ (m/z 1089, 20%)} in **5.23** were detected. The fragmentation patterns are in general agreement with the chemical formulation. The value of the soft ionization technique used in ESI is exemplified by the detection of the parent aggregate of **5.23**, which is also stabilized by extensive π-conjugation over the heterometallic network. Both the spectra of **5.22** and **5.23** show peaks of $[RuCp(C{\equiv}Cpy)(dppf)]^+$, suggesting its high stability even under applied voltage conditions.

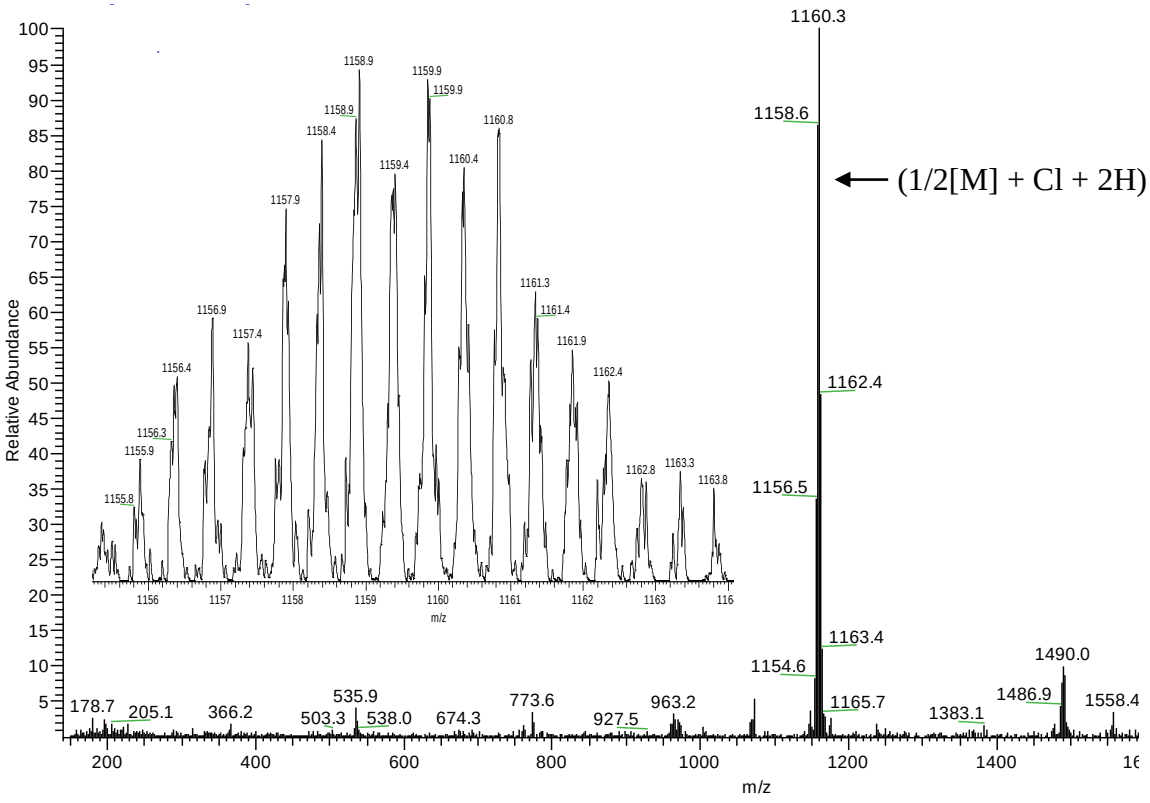


**Fig. 2.15** Positive-ion ESI mass spectrum of **5.19**

### 2.2.3.3 Structural and Reactivity Characteristics

In order to substantiate the analysis of the spectra data described above, single-crystal X-ray diffraction studies of all trinuclear complexes **5.17** – **5.23** were carried out to afford bond length and angle data about the donor-bridged-acceptor

linkage (**Fig. 2.16** – **2.22**, **Tables 2.5** & **2.6**. The relevant crystallographic data and refinement details are shown in **Tables 5.5** – **5.7** (**Chapter Five**)), as well as the degree of planarity and bond alternation of the π-system in the trinuclear system. They are consistent with the solution structures deducted from spectroscopic data.

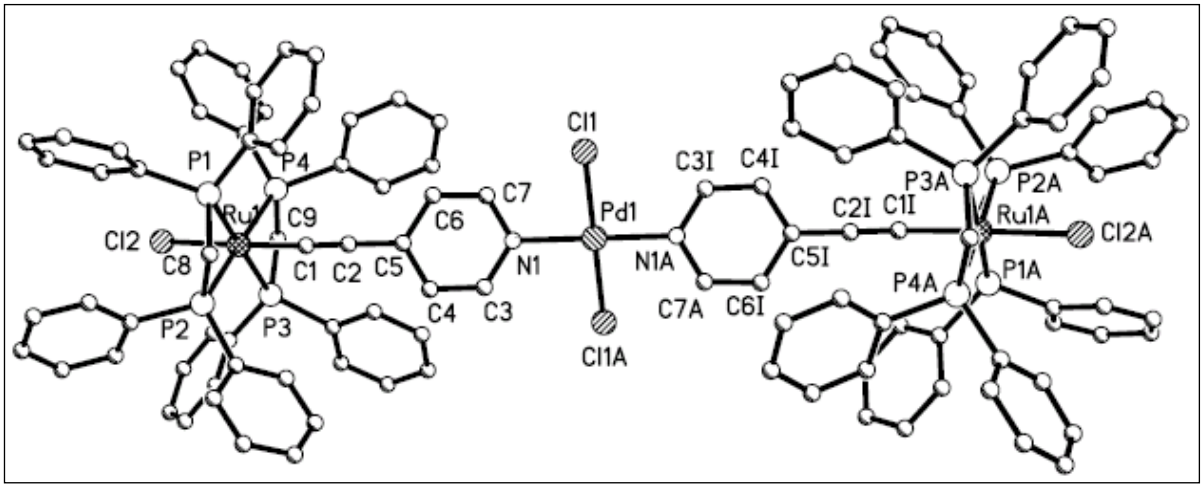


**Fig. 2.16** Crystal structure of [*trans*-RuCl(C≡Cpy-4)(dppm)$_2$]$_2$[PdCl$_2$] (**5.17**) with hydrogen atoms and solvent molecules omitted for clarity

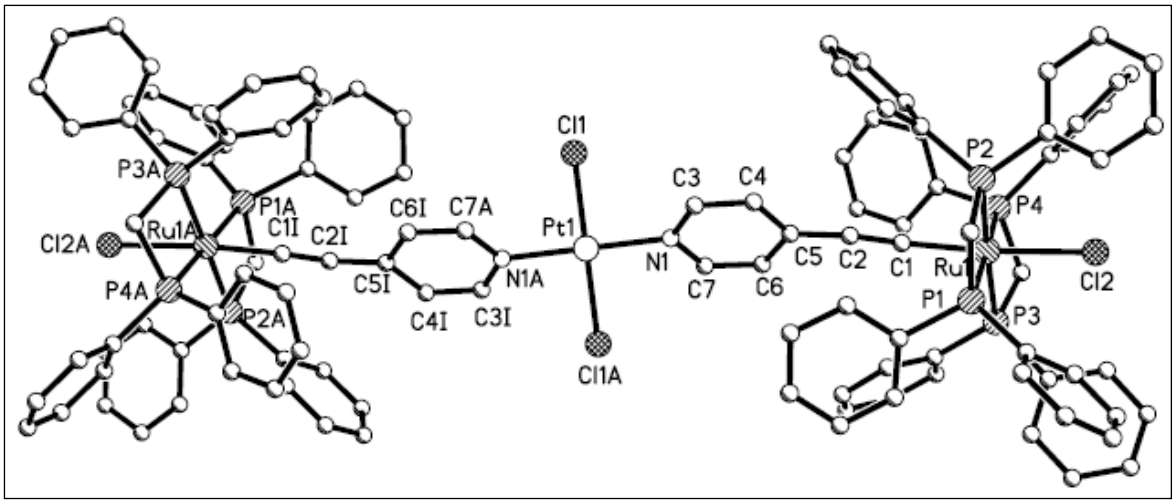


**Fig. 2.17** Crystal structure of [*trans*-RuCl(C≡Cpy-4)(dppm)$_2$]$_2$[PtCl$_2$] (**5.18**) with hydrogen atoms and solvent molecules omitted for clarity.

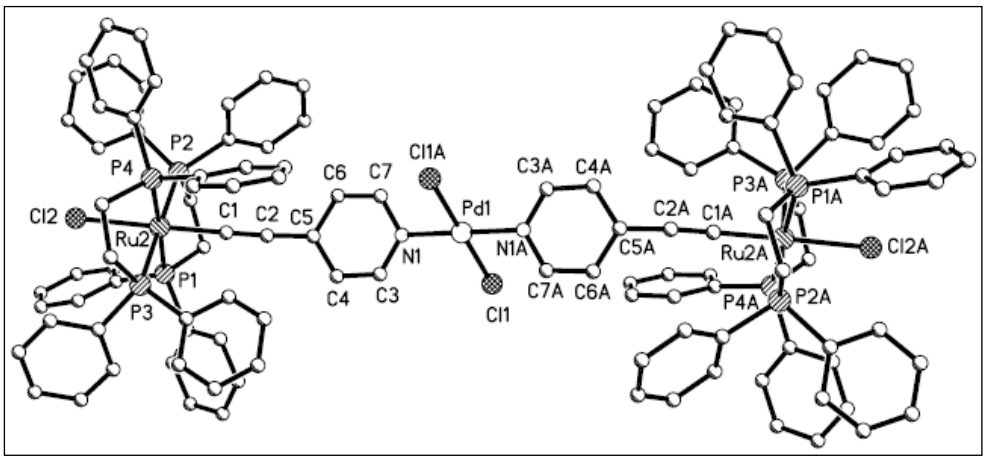


**Fig. 2.18** Crystal structure of [*trans*-RuCl(C≡Cpy-4)(dppe)$_2$]$_2$[PdCl$_2$] (**5.19**) with hydrogen atoms and solvent molecules omitted for clarity.

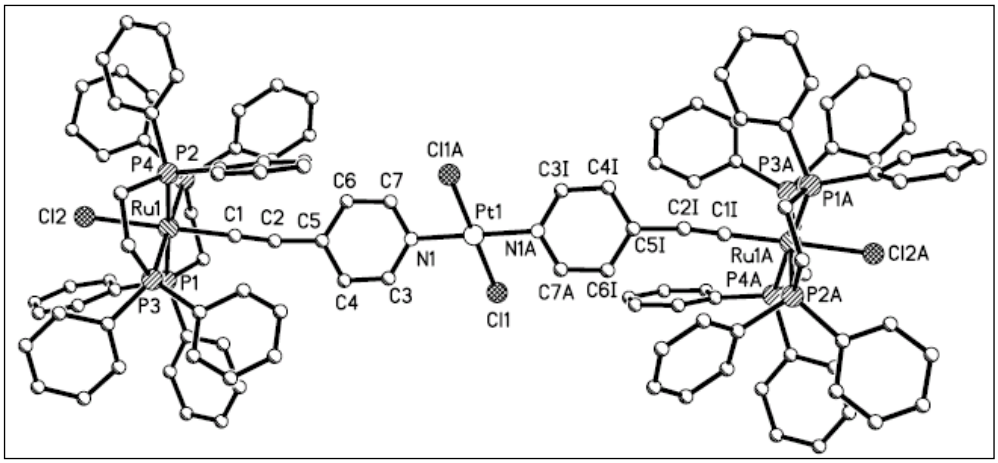


**Fig. 2.19** Crystal structure of [*trans*-RuCl(C≡Cpy-4)(dppe)$_2$]$_2$[PtCl$_2$] (**5.20**) with hydrogen atoms and solvent molecules omitted for clarity.

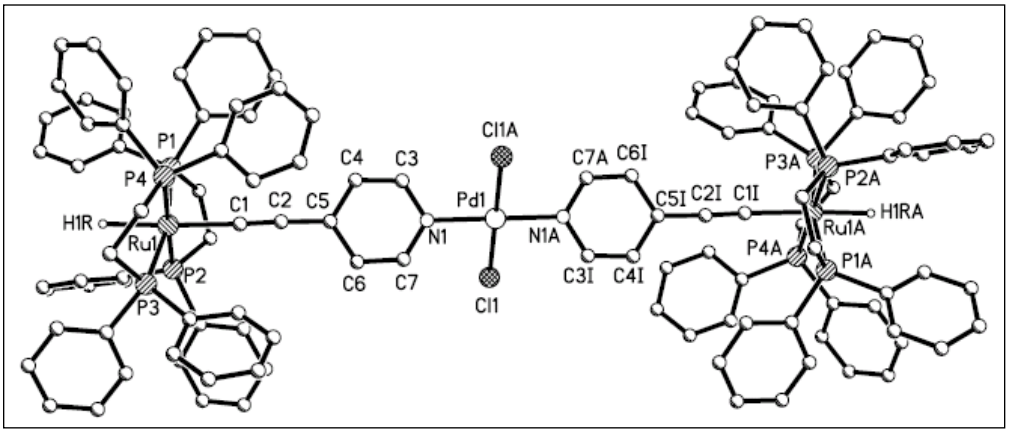


**Fig. 2.20** Crystal structure of [*trans*-RuH(C≡Cpy-4)(dppe)$_2$]$_2$[PdCl$_2$] (**5.21**) with hydrogen atoms and solvent molecules omitted for clarity

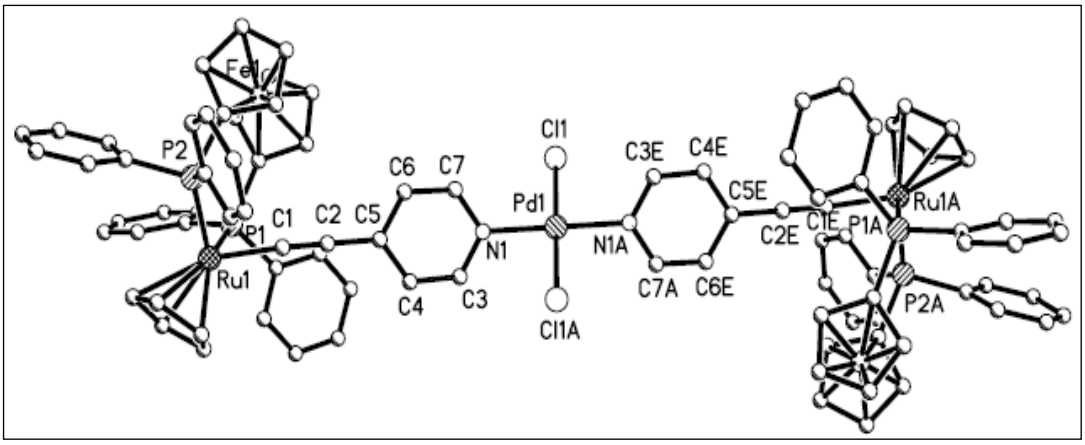


**Fig. 2.21** Crystal structure of $[RuCp(C{\equiv}Cpy\text{-}4)(dppf)]_2[PdCl_2]$ (**5.22**) with hydrogen atoms and solvent molecules omitted for clarity

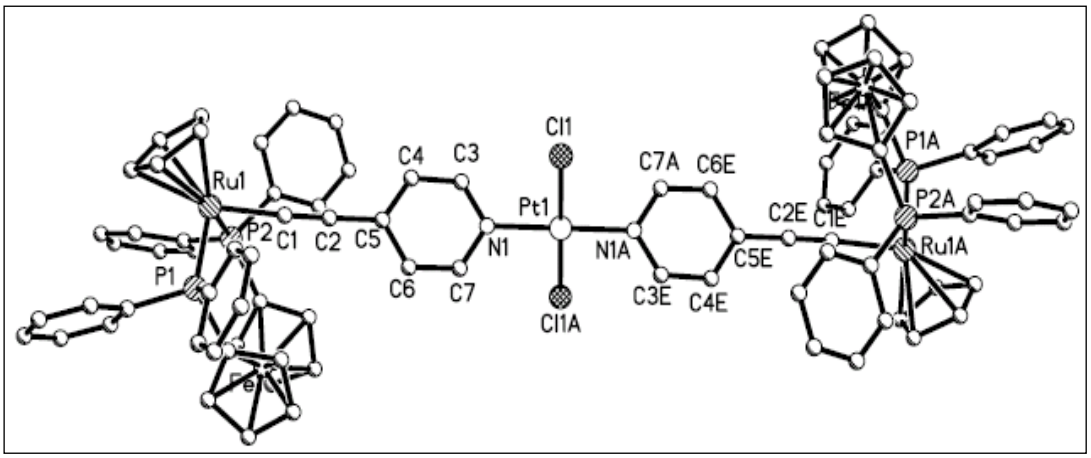


**Fig. 2.22** Crystal structure of $[RuCp(C{\equiv}Cpy\text{-}4)(dppf)]_2[PtCl_2]$ (**5.23**) with hydrogen atoms and solvent molecules omitted for clarity

**Table 2.5** Selected bond lengths (Å) and angles (°) of **5.17**, **5.18**, **5.22** and **5.23**.

| Complex | | | | |
|---|---|---|---|---|
| | Pd(1)-N(1) | 2.037(4) | Ru(1)-C(1) | 1.981(5) |
| | Pd(1)-Cl(1) | 2.304(2) | Ru(1)-Cl(2) | 2.483(1) |
| | C(1)-C(2) | 1.208(7) | C(2)-C(5) | 1.427(7) |
| **5.17** | N(1)-Pd(1)-N(1A) | 179.999(1) | Cl(1)-Pd(1)-Cl(1A) | 180.0 |
| | N(1)-Pd(1)-Cl(1) | 90.1(1) | C(1)-Ru(1)-Cl(2) | 174.8(2) |
| | N(1A)-Pd(1)-Cl(1) | 89.9(1) | C(2)-C(1)-Ru(1) | 177.4(5) |
| | | | C(1)-C(2)-C(5) | 170.6(6) |
| **5.18** | Pt(1)-N(1) | 2.020(5) | Ru(1)-C(1) | 1.970(6) |

| | | | | |
|---|---|---|---|---|
| | Pt(1)-Cl(1) | 2.282(2) | Ru(1)-Cl(2) | 2.456(2) |
| | C(1)-C(2) | 1.271(8) | C(2)-C(5) | 1.399(9) |
| | N(1)-Pt(1)-N(1A) | 180.0(3) | Cl(1)-Pt(1)-Cl(1A) | 180.0(1) |
| | N(1)-Pt(1)-Cl(1) | 90.4(2) | C(1)-Ru(1)-Cl(2) | 173.7(2) |
| | N(1A)-Pt(1)-Cl(1) | 89.6(2) | C(2)-C(1)-Ru(1) | 177.3(6) |
| | | | C(1)-C(2)-C(5) | 173.3(8) |
| **5.22** | Pd(1)-N(1) | 2.003(3) | Ru(1)-C(1) | 1.997(4) |
| | Pd(1)-Cl(1) | 2.296(1) | C(1)-C(2) | 1.210(5) |
| | | | C(2)-C(5) | 1.425(5) |
| | N(1)-Pd(1)-N(1A) | 180.0(3) | Cl(1)-Pd(1)-Cl(1A) | 80.00(7) |
| | N(1)-Pd(1)-Cl(1) | 90.9 (1) | C(2)-C(1)-Ru(1) | 173.4(3) |
| | N(1A)-Pd(1)-Cl(1) | 89.1(1) | C(1)-C(2)-C(5) | 177.7(4) |
| **5.23** | Pt(1)-N(1) | 1.989(7) | Ru(1)-C(1) | 2.008(9) |
| | Pt(1)-Cl(1) | 2.299(3) | C(1)-C(2) | 1.20(1) |
| | | | C(2)-C(5) | 1.42(1) |
| | N(1)-Pt(1)-N(1A) | 180.0(4) | Cl(1)-Pt(1)-Cl(1A) | 180.0 |
| | N(1)-Pt(1)-Cl(1) | 89.0(2) | C(2)-C(1)-Ru(1) | 173.2(7) |
| | N(1A)-Pt(1)-Cl(1) | 91.0(2) | C(1)-C(2)-C(5) | 177.3(9) |

**Table 2.6** Selected bond lengths (Å) and angles ( ᵒ) of **5.19** – **5.21**.

| **5.19** | **5.20** | **5.21** |
|---|---|---|
| Pd(1)-N(1) 2.001(4) | Pt(1)-N(1) 2.009(7) | Pd(1)-N(1) 2.020(7) |
| Pd(1)-Cl(1) 2.302(2) | Pt(1)-Cl(1) 2.307(3) | Pd(1)-Cl(1) 2.310(3) |
| Ru(2)-C(1) 1.970(5) | Ru(1)-C(1) 1.98(1) | Ru(1)-C(1) 2.06(1) |
| Ru(2)-Cl(2) 2.478(1) | Ru(1)-Cl(2) 2.478(2) | C(1)-C(2) 1.19(1) |
| C(1)-C(2) 1.209(7) | C(1)-C(2) 1.20(1) | C(2)-C(5) 1.42(1) |
| C(2)-C(5) 1.416(7) | C(2)-C(5) 1.44(1) | |
| N(1)-Pd(1)-N(1A) 179.997(1) | N(1)-Pt(1)-N(1A) 179.997(2) | N(1)-Pd(1)-N(1A) 180.0(7) |
| N(1)-Pd(1)-Cl(1) 89.9(1) | N(1)-Pt(1)-Cl(1) 90.2(3) | N(1)-Pd(1)-Cl(1) 89.4(2) |
| N(1A)-Pd(1)-Cl(1) 90.1(1) | N(1A)-Pt(1)-Cl(1) 90(1) | N(1A)-Pd(1)-Cl(1) 90.6(2) |
| Cl(1)-Pd(1)-Cl(1A) 180.0 | Cl(1)-Pt(1)-Cl(1A) 180.0 | Cl(1)-Pd(1)-Cl(1A) 180.0(2) |
| C(1)-Ru(2)-Cl(2) 178.3(1) | C(1)-Ru(1)-Cl(2) 178.4(3) | C(2)-C(1)-Ru(1) 177.8(9) |
| C(2)-C(1)-Ru(2) 177.6(5) | C(2)-C(1)-Ru(1) 177.6(8) | C(1)-C(2)-C(5) 176(1) |
| C(1)-C(2)-C(5) 162.6(6) | C(1)-C(2)-C(5) 162(1) | |

Complexes **5.17** – **5.23** are hetero-trinuclear complexes with a virtually linear arrangement of $Ru^{II}$-(spacer)-$Pd^{II}$/$Pt^{II}$-(spacer)-$Ru^{II}$ over a Ru-to-Ru separation of ~18.9 Å, and the heterometals Ru-to-Pd/Pt are bridged by spacers with a separation of ~ 9.4 Å. A slight lengthening of Ru···Fe distances were observed from **5.7** to **5.22** and **5.23** (4.38 vs 4.43 & 4.43 Å). These distances indicate no interaction between metals, consistent with the observation from their electrochemical properties (**Chapter Four**). These trinuclear complexes are centrosymmetric with the $d^8$ metal at the crystallographic inversion centers, and connected through two *trans*-configured octahedral spacers (in **5.17** – **5.21**) or two piano-stool units (in **5.22**, **5.23**) with cyclopentadienyl and diphosphine ligands in an *anti* configuration (**Fig. 2.21** & **2.22**). All the Pd/Pt atoms in **5.17** – **5.23** reside in an approximately square environment, ensuring the $180^o$ alignment in the complexes.

The overall geometries of trinuclear complexes are linear, but the attachment of Pd/Pt fragments in **5.19** and **5.20** causes a large deviation from a straight line along the axial orientation. They are much less linear than their mononuclear precursor **5.3** along the backbone {**5.19**/**5.20** vs **5.3**, 162.6(6)/162(1) vs 176.8(4) ° for C(1)-C(2)-C(5) angles}. The same phenomenon could be observed in their dppm analogues but only small deviation in the latter {**5.17**/**5.18** vs **5.1**, 170.6(6)/173.3(8) vs 175.6(2) ° for C(1)-C(2)-C(5) angles}. Contrary to its chloride analogues, the trinuclear hydrid complex **5.21** is even closer to linear than its mononuclear precursor **5.4**, where C(1)-C(2)-C(5) angles are 174.3(5) and 176(1) ° in **5.4** and **5.21**, respectively. Therefore, **5.21** is much closer to linear than its chloride analogues **5.19** and **5.20**. The

Ru-C bonds in this series of heterotrinuclears (1.970(5) ~ 2.008(9) A˚ ) except **5.21** (2.06(1) A˚) are shorter than those in the complexes [RuH(C≡Cpy)(dppe)$_2$-Rh$_2$(O$_2$CMe)$_4$-RuH(C≡Cpy)(dppe)$_2$] (2.071(2) A˚),[113] and *trans*-[Ru(C≡CC$_6$H$_4$OMe-*p*)$_2$(16-TMC)Re(CO)]$_3$(N-N)] (2.04(1) A˚).[59] Both of them are comparable to those in complex **5.21** (2.06(1) A˚). Complex **5.18** has the longest, and presumably weakest C≡C bond (1.271(8) A˚) in this series and longer than those in the two aforementioned complexes (1.197(3) and 1.20(1) Å, respectively),[59,113] and in [Re(C≡Cpy)(CO)$_3$($^t$Bu$_2$bpy)-Ru$_2$(form)$_4$-Re(C≡Cpy)(CO)$_3$($^t$Bu$_2$bpy)] (1.204(6) A˚).[138] The long C≡C bond in **5.18** is associated with a short Ru–C bond (1.970(6) A˚), which is expected for a strong metal to ligand (Ru→C≡C) back-bonding.

The M-N bonds in the trinuclear complexes have sufficient freedom to allow the pyridyl planes (and the connecting Ru units) to twist away from the M coordination plane, thus minimizing steric conflicts (dihedral angles between the M coordination (M-Cl-Cl-N-N) (M = Pd or Pt) and pyridyl planes in **5.17** – **5.23** are in the range of 36.3 ~ 58.7 º with **5.17** as the most coplanar (36.3 º) complexes.). As well known, coplanarity, along with efficient delocalization, is important for maximizing NLO response in the heterometallic complexes, as suggested by Humphrey[4,5]. In view of this, complex **5.17** is expected to have the largest NLO response in the trinuclear system presented here, in spite of the distortion from idealized coplanarity (0 º). The subsequent NLO results approved this prediction (**Chapter Three**).

## 2.2.4 Heterotetrametallic Complexes of $d^6$ - $d^7$ - $d^7$ - $d^6$ Series

### 2.2.4.1 Preparation

Since their first use as building blocks in the synthesis of polymeric species in 1981,[140] $[Rh_2(O_2CR)]$ entities have become attractive building blocks for coordination oligomers and polymers.[113,140-144] The series of $d^6$-$d^7$-$d^7$-$d^6$ heterotetrametallic assemblies in this work is constructed by metalloligand approach through the reaction of Ru(II) 4-ethynylpyridine precursors **5.1**, **5.4** and **5.7** with the dirhodium tetracarboxylates $[Rh_2(O_2CR)]$ which act as two-end Lewis acids, in a 2:1 molar ratio, lead to the formation of the heterotetrametallic complexes **5.24** – **5.34** (**Schemes 2.8** & **2.9**). The strategy of systematic variation of the monometallic precursors and the tetracarboxylate ligands on the $Rh_2$(IV) center is adopted to tune the properties of the tetrametallic products.

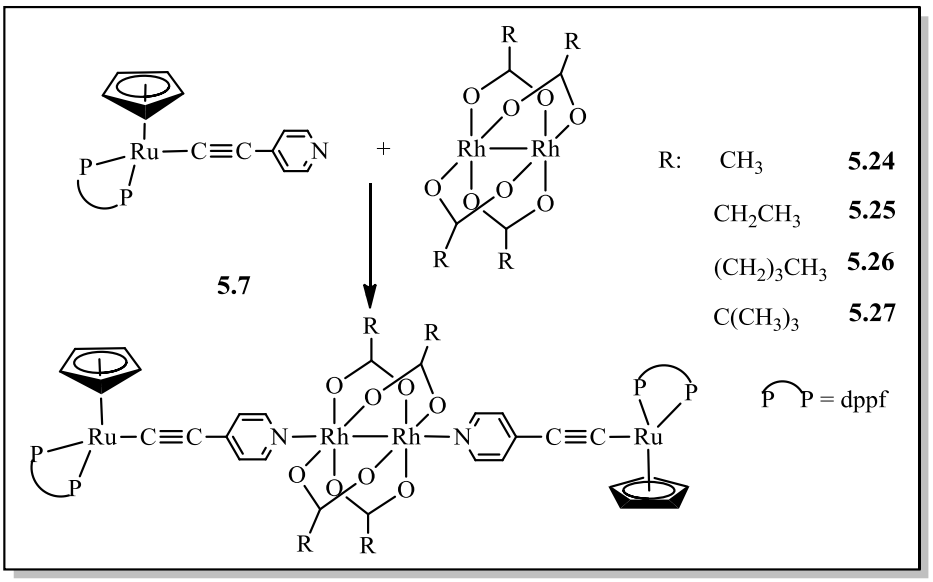


**Scheme 2.8** Formation of **5.24**-**5.27**: THF, 12h, reflux

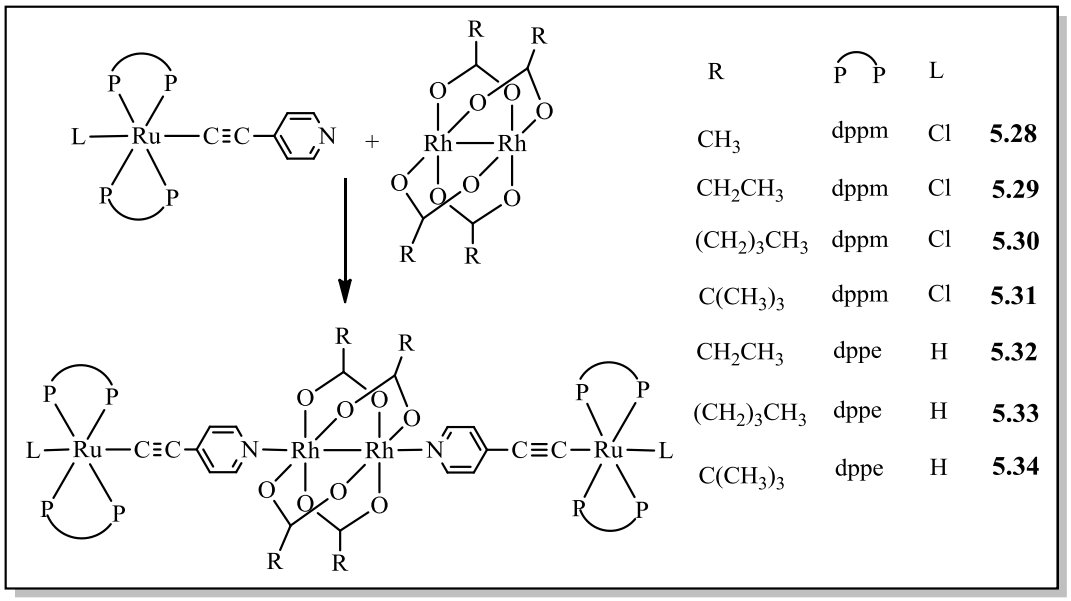


**Scheme 2.9** Formation of **5.28**-**5.34**: THF, 12h, reflux

### 2.2.4.2 Characterization and General Properties

All complexes were fully characterized by $^{1}H$, $^{31}P$, $^{13}C$ NMR spectroscopy, IR and elemental analyses. Complexes **5.24**, **5.27**, **5.31** and **5.34** were also characterized by single-crystal X-ray diffraction studies. The spectroscopic properties of all complexes are consistent with their proposed formulae.

Coordination of $[Rh_2(O_2CR)_4]$ to the pendant pyridyl N of monometallic Ru(II) 4-ethynylpyridine precursors causes chemical shifts in $^{1}H$, $^{31}P$ and $^{13}C$ NMR spectra and they are of diagnostic value. The resonance signals for the pyridyl protons of the tetranuclear complexes **5.24** – **5.34** appear at a lower field than those of their respective monometallic Ru(II) precursors. The obvious downfield shifts of the $\alpha$-pyridyl protons ($\Delta^{1}H$ = 0.4 ~ 0.7 ppm) reflect the Lewis acidity of $[Rh_2(O_2CR)_4]$ and their tendency to bind axial ligands. The magnitude of the shifts of $\alpha$-pyridyl protons decreases with the increase of the electron-donating ability of R in

$[Rh_2(O_2CR)_4]$, consistent with the decrease in electron-withdrawing ability of $[Rh_2(O_2CR)_4]$.

The $^{13}C$ NMR resonances for the $\alpha$-acetylide carbon in **5.24** – **5.34** are not significantly different ($\delta$ 148.8 ~ 150.0 ppm), which are slightly downfield shifted compared to their respective mononuclear precursors. Notably, the magnitude of downfield shifts is much smaller than that in their Ru-Pd/Pt-Ru analogues ($\delta$ 151.0 ~ 151.7 ppm),[145] consistent with the weaker electron-withdrawing ability of $[Rh_2(O_2CR)_4]$ fragments.

In metal acetylide systems, the C≡C stretching frequency is a sensitive probe for the electron density of the metal center. In the tetranuclear series of **5.24** – **5.34**, the IR active C≡C stretching vibration gives rise to bands at 2048 ~ 2073 $cm^{-1}$. This vibration is only slightly lower in energy (by 3 ~ 6 $cm^{-1}$) than that in their corresponding monometallic Ru precursors. This indicates that the influence of $[Rh_2(O_2CR)_4]$ on C≡C by coordination at the pyridyl site is insignificant, as observed in the literature.[113] In contrast, the trinuclear corresponding Ru(II)-Pd(II)/Pt(II)-Ru(II) analogues **5.17** – **5.23** have much stronger effect on C≡C (by 20 ~ 30 $cm^{-1}$), in accordance with the observation in $\alpha$-carbon $^{13}C$ NMR. The IR spectra of **5.24** – **5.34** all show two characteristic absorptions in the ranges 1583 ~ 1591 and 1414 ~ 1430 $cm^{-1}$, corresponding to the asymmetric and symmetric C-O stretching modes in a substance where acetate functions as a bidentate bridging group.[146] The difference between the asymmetric and symmetric C-O stretching frequencies is expected to be roughly the same ($\Delta$ = 162 ~ 170 $cm^{-1}$), which is consistent with those observed by

Johnson *et. al*.[147] and Endres *et. al*..[148]

### 2.2.4.3 Structural Analysis

The structures of complexes **5.24**, **5.27**, **5.31** and **5.34** were established by X-ray crystallography. **Fig. 2.23** – **2.26** illustrate the linear rigid-rod motif along the molecular axis and the coplanarity of the pyridine ring systems in these complexes. Selected bond distances and angles are listed in **Table 2.7**. The relevant crystallographic data and refinement details are shown in **Tables 5.7** – **5.8** (**Chapter Five**).

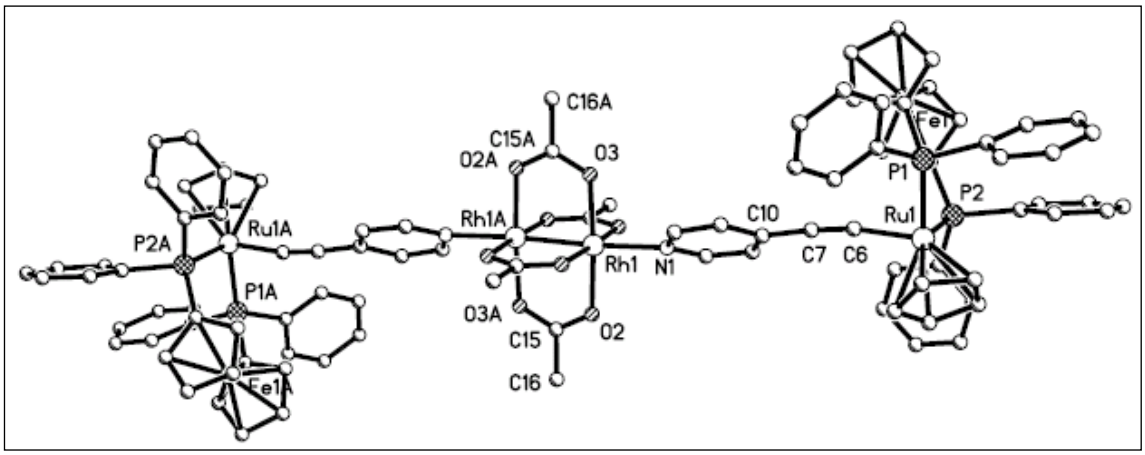


**Fig. 2.23** Crystal structure of $[RuCp(C{\equiv}Cpy\text{-}4)(dppf)]_2[Rh_2(O_2CCH_3)_4]$ (**5.24**) with hydrogen atoms and solvent molecules omitted for clarity.

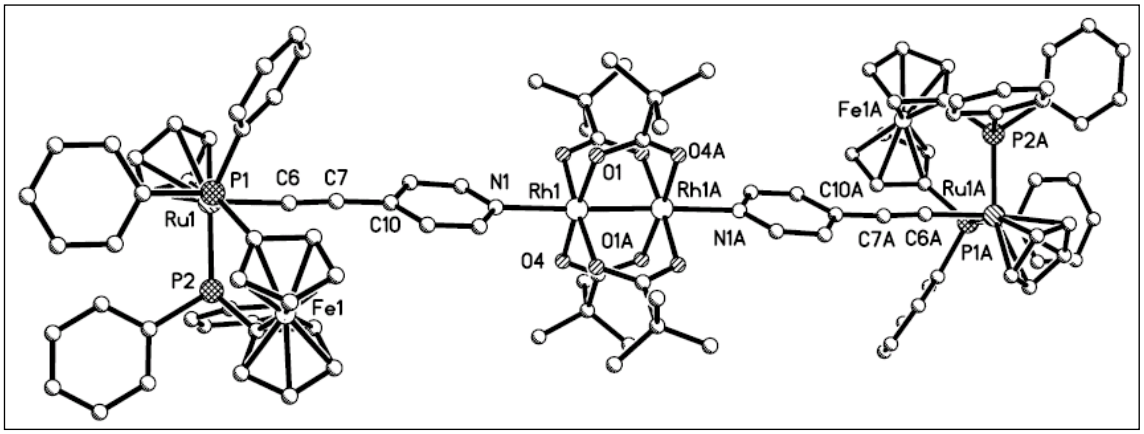


**Fig. 2.24** Crystal structure of $[RuCp(C{\equiv}Cpy\text{-}4)(dppf)]_2[Rh_2(O_2C(CH_3)_3)_4]$ (**5.27**) with hydrogen atoms and solvent molecules omitted for clarity

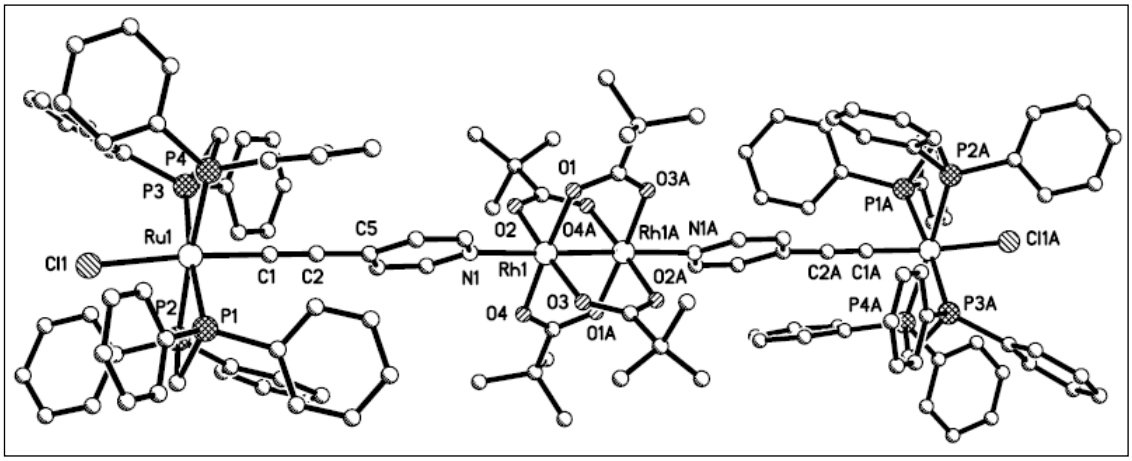


**Fig. 2.25** Crystal structure of [*trans*-RuCl(C≡Cpy-4)(dppm)$_2$]$_2$[Rh$_2$(O$_2$CC(CH$_3$)$_3$)$_4$] (**5.31**) with hydrogen atoms and solvent molecules omitted for clarity

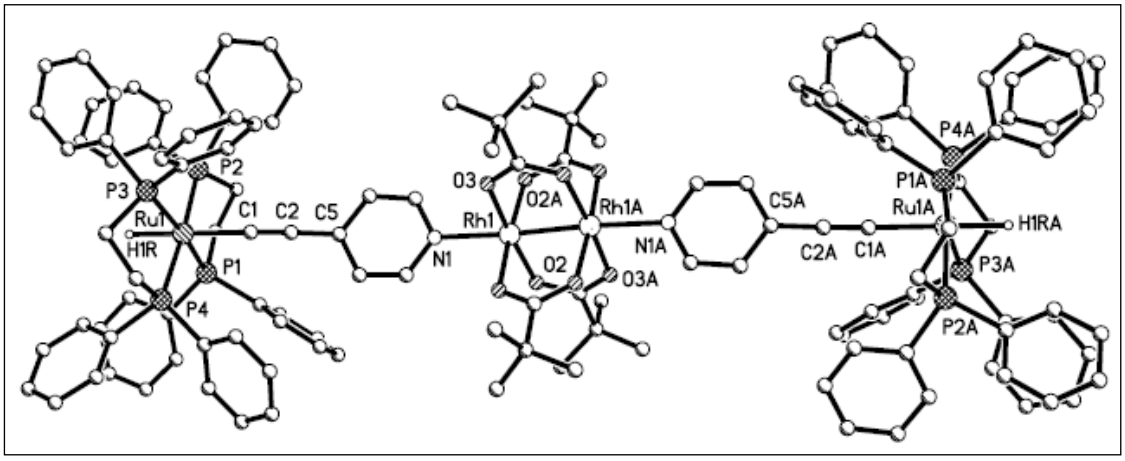


**Fig. 2.26** Crystal structure of [*trans*-RuH(C≡Cpy-4)(dppe)$_2$]$_2$[Rh$_2$(O$_2$CC(CH$_3$)$_3$)$_4$] (**5.34**) with hydrogen atoms and solvent molecules omitted for clarity.

**Table 2.7** Selected bond lengths (Å) and angles (°) of **5.24**, **5.27**, **5.31** and **5.34**.

| Complex | | | | |
|---|---|---|---|---|
| **5.24** | Rh(1)-O(1) | 2.037(5) | Rh(1)-Rh(1A) | 2.3947(9) |
| | Rh(1)-O(2) | 2.038(4) | Ru(1)-C(6) | 1.991(6) |
| | Rh(1)-O(3) | 2.037(5) | C(6)-C(7) | 1.212(8) |
| | Rh(1)-O(4) | 2.037(5) | C(7)-C(10) | 1.425(8) |
| | Rh(1)-N(1) | 2.222(5) | | |
| | O(1)-Rh(1)-O(4) | 175.4(2) | O(2)-Rh(1)-O(3) | 175.6(2) |
| | O(1)-Rh(1)-O(3) | 89.3(2) | N(1)-Rh(1)-Rh(1A) | 176.2(2) |
| | O(4)-Rh(1)-O(3) | 90.8(2) | C(7)-C(6)-Ru(1) | 170.2(5) |

| | | | | |
|---|---|---|---|---|
| | O(1)-Rh(1)-O(2) | 90.4(2) | C(6)-C(7)-C(10) | 175.2(7) |
| | O(4)-Rh(1)-O(2) | 89.1(2) | | |
| **5.27** | Rh(1)-O(1) | 2.032(4) | Rh(1)-Rh(1A) | 2.4023(7) |
| | Rh(1)-O(2) | 2.043(4) | Ru(1)-C(6) | 1.996(5) |
| | Rh(1)-O(3) | 2.032(4) | C(6)-C(7) | 1.221(6) |
| | Rh(1)-O(4) | 2.053(4) | C(7)-C(10) | 1.421(6) |
| | Rh(1)-N(1) | 2.234(4) | | |
| | O(1)-Rh(1)-O(4) | 175.7(1) | O(2)-Rh(1)-O(3) | 175.8(2) |
| | O(1)-Rh(1)-O(3) | 90.0(2) | N(1)-Rh(1)-Rh(1A) | 178.0(1) |
| | O(4)-Rh(1)-O(3) | 89.6(2) | C(7)-C(6)-Ru(1) | 174.0(4) |
| | O(1)-Rh(1)-O(2) | 90.2(2) | C(6)-C(7)-C(10) | 175.8(5) |
| | O(4)-Rh(1)-O(2) | 90.0(2) | | |
| **5.31** | Rh(1)-O(1) | 2.035(2) | Rh(1)-Rh(1A) | 2.3916(4) |
| | Rh(1)-O(2) | 2.029(2) | Ru(1)-Cl(1) | 2.4770(7) |
| | Rh(1)-O(3) | 2.043(2) | Ru(1)-C(1) | 1.983(3) |
| | Rh(1)-O(4) | 2.042(2) | C(6)-C(7) | 1.210(4) |
| | Rh(1)-N(1) | 2.214(2) | C(7)-C(10) | 1.423(4) |
| | O(1)-Rh(1)-O(4) | 88.57(9) | O(2)-Rh(1)-O(3) | 88.74(9) |
| | O(1)-Rh(1)-O(3) | 175.90(8) | N(1)-Rh(1)-Rh(1A) | 177.82(7) |
| | O(4)-Rh(1)-O(3) | 91.28(9) | C(1)-Ru(1)-Cl(1) | 174.92(8) |
| | O(1)-Rh(1)-O(2) | 91.11(9) | C(2)-C(1)-Ru(1) | 177.6(3) |
| | O(4)-Rh(1)-O(2) | 175.76(9) | C(1)-C(2)-C(5) | 176.2(3) |
| **5.34** | Rh(1)-O(1) | 2.040(3) | Rh(1)-Rh(1A) | 2.4044(7) |
| | Rh(1)-O(2) | 2.034(3) | Ru(1)-C(1) | 2.074(5) |
| | Rh(1)-O(3) | 2.025(3) | C(1)-C(2) | 1.219(6) |
| | Rh(1)-O(4) | 2.045(3) | C(2)-C(5) | 1.430(6) |
| | Rh(1)-N(1) | 2.245(4) | | |
| | O(1)-Rh(1)-O(4) | 88.6(1) | O(2)-Rh(1)-O(3) | 88.5(1) |
| | O(1)-Rh(1)-O(3) | 91.1(1) | N(1)-Rh(1)-Rh(1A) | 175.5(1) |
| | O(4)-Rh(1)-O(3) | 175.7(1) | C(2)-C(1)-Ru(1) | 178.2(4) |
| | O(1)-Rh(1)-O(2) | 175.5(1) | C(1)-C(2)-C(5) | 177.7(5) |
| | O(4)-Rh(1)-O(2) | 91.4(1) | | |

The overall geometries of complexes **5.24**, **5.27**, **5.31** and **5.34** are close to

linearity along the [Ru-C≡Cpy-Rh-Rh-pyC≡C-Ru] backbone with [N-Rh(1)-Rh(1A) 175.5(1) ~ 178.0(1)°; C≡C-Ru 170.2(5) ~ 178.2(4)°; $C_{py}$-C≡C 175.2(7) ~ 177.7(5)°] (**Table 2.7**). These tetrametallic complexes consist of one homobimetallic Rh-Rh paddle-wheel unit and two piano-stool (**5.24** & **5.27**) or octahedral (**5.31** & **5.34**) Ru units (**Fig. 2.23** – **2.26**). Each of the rhodium atoms changes its configuration from distorted square-pyramid in the rhodium dimer precursors to distorted octahedron in the heterotetrametallics. The Cp and dppf ligands in **5.24** and **5.27** are oriented in *anti* conformation (**Fig. 2.23** & **2.24**), similar to the instances in heterotrimetallic complexes **5.22** and **5.23** (Section **2.2.3c** ).

The Rh-N bond length in complex **5.34** (2.245(4) Å) is relatively longer than those in **5.24**, **5.27**, **5.31** (2.222(5), 2.234(4) and 2.214(2) Å, respectively) and its known analogue {[*trans*-[RuH(C≡Cpy-4)$(dppe)_2$]$_2$[$Rh_2(O_2CMe)_4$]} (2.225(2) Å),[113] indicating weaker rhodium-nitrogen interaction in **5.34**, whereas they are all typical for Rh-N bonds in such systems.[149-151] The distances of Rh-Rh in **5.24**, **5.27**, **5.31** and **5.34** (2.3916(4) ~ 2.4044(7) Å) are shorter than those in some dirhodium compounds,[152] but fall within the range reported for dirhodium compounds of comparable structures,[151,153,154] indicating metal-metal bonding interactions and consistent with the observation in their optical properties (**Chapter Three**). The angles of Rh-Rh-N in **5.24**, **5.27**, **5.31** and **5.34 (**175.5(1) ~ 178.0(1)°) are comparable to the reported complex [{*cis*-$Re_2Cl_2(O_2Cpy\text{-}4)_2(dppm)_2$}{$Rh_2(O_2CMe)_4$}] (177.6(7) and 176.3(7)°),[151] which also carries axial nitrogen donor ligands. The angle of C-C-Ru in complex

**5.24** (170.2(5)°) is smaller than those in the other three complexes (174.0(4), 177.6(3) and 178.2(4)° for **5.27**, **5.31** and **5.34**, respectively), indicating larger derivation from linear structure in **5.24** than in the latter three complexes; and half-sandwich Ru structural units distort larger than the octahedral Ru structural units (170.2(5), 174.0(4)° in **5.24** and **5.27** vs 177.6(3), 178.2(4)° in **5.31** and **5.34**). Similar observation is found in their heterotrimetallic analogue systems (Section **2.2.3c**). Attachment of $[Rh_2(O_2CCMe_3)_4]$ entity on **5.4** leads to more linear geometry in **5.34** along the axial orientation, where C≡C-C and Ru-C≡C angles are 174.3(5), 173.2(4)° and 177.7(5), 178.2(4)° in **5.4** and **5.34**, respectively. The variation of geometries in **5.24**, **5.27** and **5.31** compared to their respective precursors are less significant than **5.4**-**5.34** couple (**Table 2.7**).

## 2.3 Conclusions

A series of monometallic ruthenium 4-ethynylpyridine complexes has been synthesized. They are characterized by spectroscopy and crystallography. These ruthenium 4-ethynylpyridine complexes have proven to be versatile precursors in the construction of high nuclearity complexes. Three heterometallic systems are all prepared from the metalloligand approach by the reaction between ruthenium 4-ethynylpyridine precursors and the respective electron-withdrawing metal fragments. Some conclusions are drawn regarding the heterometallic systems.

(i) Syntheses: the systematically-varied series of organometallic donor-bridge-acceptor acetylide assemblies: heterobimetallics ($Ru^{II}$-$Re^{I}$),

heterotrimetallics ($Ru^{II}$-$Pd^{II}$/$Pt^{II}$-$Ru^{II}$) and heterotetrametallics ($Ru^{II}$-$Rh^{II}$-$Rh^{II}$-$Ru^{II}$) are all prepared through Lewis addition of $Ru^{II}$ 4-ethynylpyridine precursors and the corresponding $Re^{I}$, $Pd^{II}$/$Pt^{II}$ and $Rh^{II}$-$Rh^{II}$ fragments, in which the former acts as metalloligands, and the latter as Lewis acids.

(ii) Solubility: these heterometallic complexes are very soluble in common polar solvents, such as $CH_2Cl_2$, THF (for $Ru^{II}$-$Pd^{II}$/$Pt^{II}$-$Ru^{II}$ system, the complexes only moderately dissolve in $CH_2Cl_2$, and have poor solubility in THF), thus enabling a complete characterization and a detailed examination of their properties.

(iii) Structure: X-ray structural studies of most of the heterometallic complexes have been carried out. One dimensional organometallic oligomers are determined, in which the backbones consist of octahedral $Re^{I}$ carbonyl diimine (in heterobimetallics) or square planar $Pd^{II}$/$Pt^{II}$ chloride (in heterotrimetallics) or square-pyramid $Rh^{II}$-$Rh^{II}$ tetrcarboxylate (in heterotetrametallics) entities and two octahedral or half-sandwich $Ru^{II}$ acetylide units. The apparent lack of communication between the $Re^{I}$/$Pd^{II}$($Pt^{II}$)/$Rh^{II}$-$Rh^{II}$ metal centers with the steric crowding of the $Ru^{II}$ core might be responsible for the stability of the heterometallic systems that enables easy handling and characterization. Furthermore, slight variation in Ru-C and C≡C parameters was observed in these heterometallic assemblies compared to their respective monometallic $Ru^{II}$ acetylide precursors due to the electron-withdrawing properties of these metal entities.

(iv). Spectra: $^{13}C$ NMR (Ru-C chemical shifts) and $IR_{C\equiv C}$ spectral data are sensitive to the introduction of electron-withdrawing $Re^{I}$/$Pd^{II}$($Pt^{II}$)/$Rh^{II}$-$Rh^{II}$

fragments due to the extension of the electron delocalization along the backbone with the largest low-energy shifts in $Ru^{II}$-$Pd^{II}$/$Pt^{II}$-$Ru^{II}$ system. These data are therefore diagnostically valuable.

(v). Reactivity: trimetallic complexes **5.16** – **5.19** are terminated with four active chlorides – two at $d^6$ and two at $d^8$ metal sites at approximately orthogonal planes, while **5.21**, **5.22** and **5.27** – **5.30** possess two active chlorides – at $Pd^{II}$/$Pt^{II}$ and $Ru^{II}$ cores. Their presence and orientations present unique systems whereby the heterometallic oligomers can be propagated by introducing more heterometallic fragments, with the same or different spacer, at perpendicular directions. Such assembly would lead to the ultimate goal of constructing geometrically defined multiheterometallic polymers through a metal-by-metal and molecule-by-molecule control-growth pathway.

# Chapter Three

# *Optical Properties of Ru(II) 4-Ethynylpyridine Based Monometallic and Heterometallic Complexes*

## 3.1 Linear Optical Properties (UV-vis)

### 3.1.1 Introduction

UV-vis spectroscopy involves the spectroscopy of photons in the UV-vis region. In this region of the electromagnetic spectrum, molecules undergo electronic transitions. This technique is indispensable for the studies of other properties. It is complementary to fluorescence/phosphorescence spectroscopy because the latters deal with transitions of electrons from the excited state to the ground state and emission of photons, while UV-vis measures transitions of electrons from the ground state to the excited state.[155] This technique is also crucial to nonlinear optics since its study is based on UV-vis absorption.[4,5]

In this section, the optical absorption studies of both monometallic and heterometallic systems described in the previous chapter are discussed.

### 3.1.2 Results and Discussion

#### 3.1.2.1 Monometallic Ru(II) 4-Ethynylpyridine Complexes

The UV-vis absorption spectra of complexes **5.1** – **5.3** and **5.7** were recorded in

$CH_2Cl_2$ (**Fig. 3.1**). Each octahedral complex of **5.1** – **5.3** exhibits two high-energy absorption bands with $\lambda_{max}$ in the range 230 ~ 268 nm, whereas **5.7** contains only one absorption band at ca. 230 nm. They are characteristic of the presence of the phenyl substituents on the diphosphine ligands and are attributed to the ligand-centered $\pi \rightarrow \pi^*$ transition.[7,121,157] The broad absorption band at lower energy (> 330 nm) in **5.1**, **5.3** and **5.7**, which is absent in their chloro precursors,[158] is traced to $d_\pi(Ru) \rightarrow \pi^*(C{\equiv}Cpy)$ M $\rightarrow$ L charge transfer (MLCT) transitions. These MLCT transitions feature a large $\varepsilon$ value ($>10^4$ $dm^3mol^{-1}cm^{-1}$). Similar assignments have been made in related systems.[7,35,159] Herein the $\lambda_{max}$ in **5.1** is among the lowest in known mononuclear Ru σ-acetylide complexes.[27,121,160]

It is noted that the MLCT band in complex **5.3** is red shifted compared to that in its dppm analogue **5.1** (347 vs 336 nm), indicating the low C≡C energy in complex **5.3** which leads to the red shift of $d_\pi(Ru) \rightarrow \pi^*(C{\equiv}Cpy)$ transition. This red-shift is consistent with the $IR_{(C\equiv C)}$ value of **5.3** and **5.1** (2067 vs 2078 $cm^{-1}$).

Complex **5.2** shows two absorption bands at 312 nm ($\varepsilon = 1.2\times10^4$ $M^{-1}$ $cm^{-1}$) and 390 nm ($\varepsilon = 3.0\times10^3$ $M^{-1}$ $cm^{-1}$). The former is tentatively assigned as MLCT $d_\pi(Ru)\rightarrow\pi^*(C{\equiv}Cpy)$, whereas the latter represents the MLCT $d_\pi(Ru) \rightarrow \pi^*(NCCH_3)$. A similar lower energy transition in nitrile complexes has been reported by Low and co-workers.[161] The higher π back-bonding effect of CN in **5.2**, compared to Cl in **5.1**, stabilizes the $t_{2g}$ orbital and raises the energy difference between $d_\pi(Ru)$ and $\pi^*(C{\equiv}Cpy)$, giving a higher energy absorption in the $d_\pi(Ru) \rightarrow \pi^*(C{\equiv}Cpy)$ MLCT in **5.2**. This analysis is supported by the recent computational studies.[161,162] The longer

and presumably weaker Ru-C bond in **5.2** [2.04 (1) Å] compared to **5.1** [1.980 (2) Å] also supports the weaker back-donation from Ru to π*(C≡Cpy) in **5.2**.

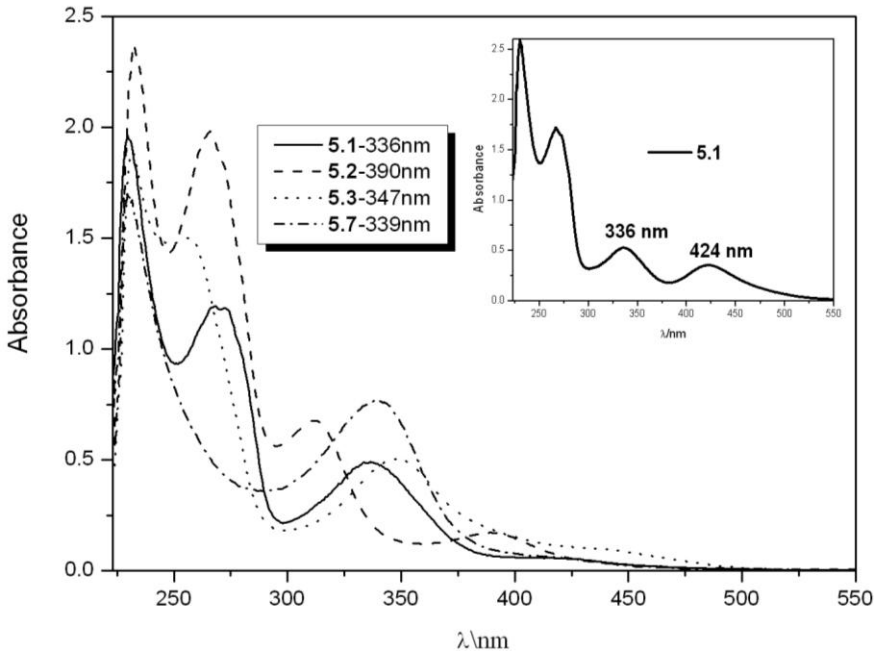


**Fig. 3.1** UV-vis absorption spectra of **5.1- 5.3** and **5.7** in $CH_2Cl_2$ at 298K (inset: The spectrum of **5.1** in $CH_2Cl_2$ solution upon standing over several days in air at 298K)

The solution of complex **5.1** in $CH_2Cl_2$ changes from yellow to orange after several days with a new absorption band at $\lambda_{max}$ = 424 nm ($\varepsilon = 7.0\times10^3$ $M^{-1}$ $cm^{-1}$), accompanied by $^1$H-NMR peaks at 9.41 ~ 9.46 ppm. This is tentatively assigned to partial protonation of the pendant pyridyl N, which is supported by Wrighton's study that nonligated N atom in pyridine is a site of protonation.[118] An acid-base titration experiment of **5.1** has been carried out in an attempt to assay the protonation of pendant pyridyl N.

**Acid-Base Titration Studies**

The solution of **5.1** in $CH_2Cl_2$ shows instantaneous color change from yellow to

orange upon addition of *p*-toluenesulfonic acid, with orange color becoming more intense as the acid concentration increases. An electronic absorption titration shows that the absorption band at 336 nm steadily gives way to a new band at 424 nm (**Fig 3.2**). The latter increases in absorbance with increasing the acid concentration. When the acid concentration is equivalent to that of **5.1**, the band at 336 nm disappears completely, which suggests quantitative conversion of the pendant pyridine to its pyridinium form. Similar color changes are noted in other systems[52,163] upon complex neutralization. The red shift of $\lambda_{max}$ associated with pyridine to pyridinium conversion is accounted for by the strong electron-withdrawal effect of $H^+$ which stabilizes the $\pi^*$(C≡Cpy) and lowers the energy of the MLCT transition, as reported by Wu *et al*..[52]

Upon further acid addition, 4-ethynyl pyridinium transforms to vinylidene pyridinium (**Scheme 3.1**). This leads to a blue shift of the band at 424 nm to a new band at 377 nm. Formation of a vinylidene pyridinium imparts a higher positive charge on Ru, which lowers the energy of both the Ru $t_{2g}$ orbital and $\pi^*$(C≡Cpy). The larger drop in $t_{2g}$ orbital effectively increases the net energy of MLCT resulting in blue shift. The formation of vinylidene pyridinium from acetylide pyridine suggests that both C≡C and uncoordinated pyridyl moieties are possible protonation sites, similar to those reported.[13,42,118] The higher basicity of pyridine compared to C≡C provides a rationale for sequential protonation starting with the former (**Scheme 3.1**).

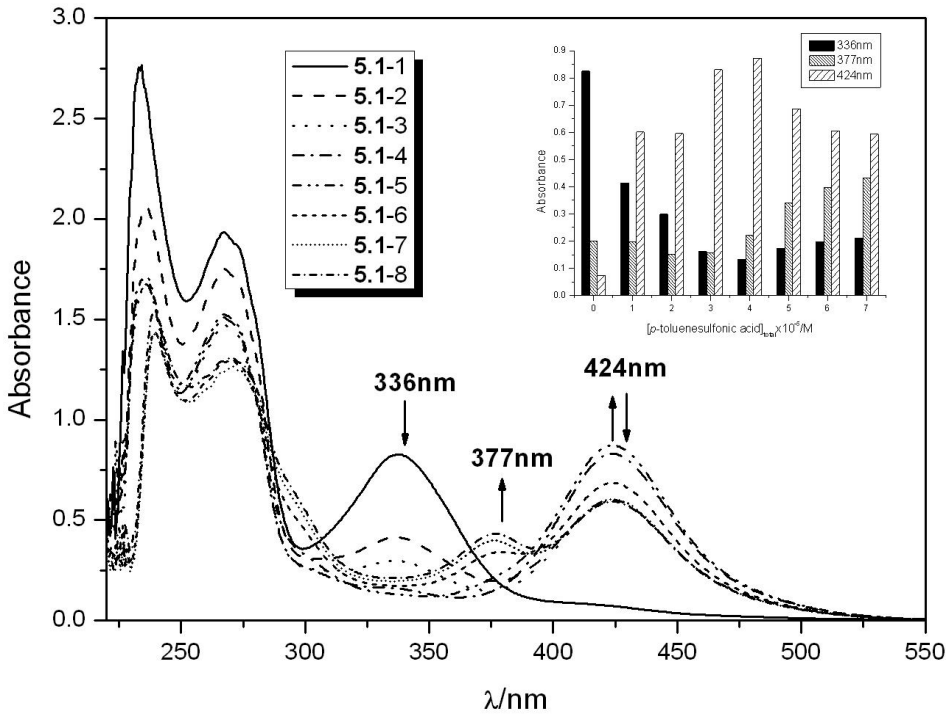


**Fig. 3.2** UV-vis absorption changes of **5.1** (concentration = 4.0 x $10^{-5}$ M) in $CH_2Cl_2$ with various concentrations of *p*-toluenesulfonic acid (from **5.1**-1 to **5.1**-8, representing 8 samples): 0, 1.0, 2.0, 3.0, 4.0, 5.0, 6.0, 7.0 (x$10^{-5}$ M) (inset: Plots of absorbance at 336, 377 and 424 nm against the total concentration of *p*-toluenesulfonic acid)

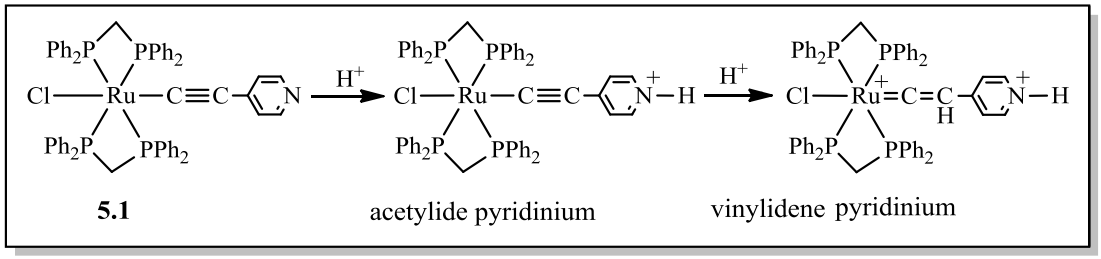


**Scheme 3.1** Structural changes of **5.1** upon addition of *p*-toluenesulfonic acid

### 3.1.2.2 Heterometallic Assemblies

The optical absorption spectra of binuclear ($Ru^{II}$-$Re^{I}$), trinuclear ($Ru^{II}$-$Pd^{II}$/$Pt^{II}$-$Ru^{II}$) and tetranuclear ($Ru^{II}$-$Rh^{II}$-$Rh^{II}$-$Ru^{II}$) assemblies were recorded in $CH_2Cl_2$ at r.t.. The absorption spectra of representative complexes [RuCp(C≡Cpy-4)(dppf)][Re(CO)$_3$(bpy)](PF$_6$) **(5.11)**, [RuCp(C≡Cpy-4)(dppf)]$_2$[PtCl$_2$]

**(5.23)** and [RuCp(C≡Cpy-4)(dppf)]$_2$[Rh$_2$(O$_2$CCH$_2$CH$_3$)$_4$] **(5.25)**, together with [RuCp(C≡Cpy-4)(dppf)] (**5.7**) as comparison, are depicted in **Fig. 3.3**. Generally, there are two main features in the UV-vis spectra of these heterometallic systems. The high-energy absorptions at wavelength < 300 nm, which are also found in their respective monometallic Ru(II) acetylide precursors, are assigned as intraligand-centered $\pi \rightarrow \pi^*$ transition. In contrast to those in their corresponding monometallic precursors, the spectra in high-energy region of the tri- and tetra-nuclear complexes are stronger in absorptions but no obvious change in energy. This is reasonable since the abundance of the diphosphine ligands in these complexes contributes to these strong absorptions and in turn supports the assignment of diphosphine-centered intraligand transition.

The observation of MLCT $d_\pi$(Ru) $\rightarrow$ $\pi^*$(C≡Cpy) in the monometallic Ru acetylides suggests that any perturbation of the electronic structure of the pendant pyridyl ligand will lead to an absorption shift in the MLCT. It is proved by the spectra of the heterometallic complexes. A red shift occurs in the spectra of the heterometallic complexes compared to their respective monometallic precursors due to the electron-withdrawing properties of the incoming Re(I) diimine carbonyl or Pd/Pt chloride or dirhodium tetraacetate fragments in bi-, tri- and tetra-nuclear systems. The coordination of these metal fragments on pyridyl ligand extends the conjugation network across the complex framework, thereby stabilizing $\pi^*$ of C≡Cpy and lowering the energy of the MLCT transition. This is consistent with the changes in the IR absorption of C≡C in the heterometallic systems. For example, 20

~ 30 $cm^{-1}$ lower in energy in the trinuclear Ru-Pd/Pt-Ru complexes than those in their respective mononuclear Ru acetylide precursors (**Chapter Five**). **Fig. 3.3** shows that the magnitude of the red shift of the $d_{\pi}(Ru) \rightarrow \pi^*(C{\equiv}Cpy)$ MLCT transition, compared to their precursor **5.7** (339 nm), is in the order **5.11** > **5.23** > **5.25** (407 vs 393 vs 370 nm). This sequence is not surprising since Re(I) cationic fragments exhibit stronger Lewis acidity than the neutral $[PtCl_2]$ and $[Rh_2(O_2CCH_2CH_3)_4]$ fragments, which renders the former to induce electron delocalization along the backbone more effectively than the latter.

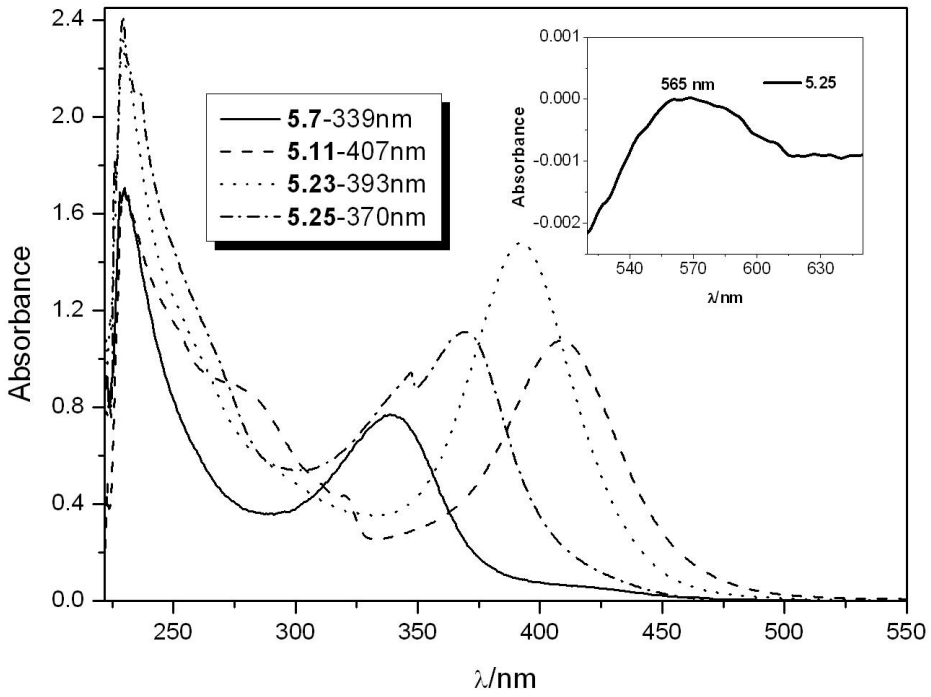


**Fig. 3.3** UV-vis absorption spectra of **5.7**, **5.11**, **5.23** and **5.25** in $CH_2Cl_2$ at 298K (inset: The spectrum of **5.25** in $CH_2Cl_2$ solution upon enlarging 400-times in the range of 520 ~ 650 nm)

Besides the high energy absorption at < 300 nm and the $d_{\pi}(Ru) \rightarrow \pi^*(C{\equiv}Cpy)$ MLCT transition in the visible region, each of the binuclear $Ru^{II}$-$Re^{I}$ system and tetranuclear $Ru^{II}$-$Rh^{II}$-$Rh^{II}$-$Ru^{II}$ system exhibits its own features in the optical

absorption spectra.

In the binuclear $Ru^{II}$-$Re^{I}$ system, the absorption bands at 275 ~ 327 nm could be a mixture of intraligand [$\pi \rightarrow \pi^*$ (diimine)] and [$d_\pi$(Re) $\rightarrow$ $\pi^*$(pyridine)] MLCT transition (**Fig. 3.3**),[129,130] With reference to previous spectroscopic work on related Re(I) diimine systems,[139,164,165] the absorption band at lower energy 350 ~ 400nm is characteristic of the Re(I) diimine moieties with extinction coefficients of the order of $10^3$ $dm^3 \cdot mol^{-1} \cdot cm^{-1}$. It is apparent that this absorption band is considerable superposition with the $d_\pi$(Ru) $\rightarrow$ $\pi^*$(C≡Cpy) MLCT transition, hence the $d_\pi$(Re) $\rightarrow$ $\pi^*$(diimine) bands must be obscured by the much more intense $d_\pi$(Ru) $\rightarrow$ $\pi^*$(C≡Cpy) MLCT absorption bands and cannot be directly located.

In the tetranuclear $Ru^{II}$-$Rh^{II}$-$Rh^{II}$-$Ru^{II}$ system, two more groups of absorption bands at ~ 347 nm (sh) and ~ 565 nm are also observed (**Fig. 3.3**). The low-energy absorption bands at ~565 nm are assigned to the $\pi^*(Rh_2) \rightarrow \sigma^*(Rh_2)$, similar to those in related systems.[153,166] This low-energy absorption band is probably responsible for the light red color of this series of tetranuclear complexes. The transition between the two rhodium centers is caused by the short Rh-Rh bond distance (~ 2.4 Å), indicating metal-metal interactions.

**Acid-Base Titration Studies**

The titration result of **5.1** suggested that having a pendant pyridyl group is not a prerequisite for protonation to take place. Indeed, the heterometallic complexes, with no pyridine pendant, could also convert to the corresponding vinylidene forms when

titrated with acid. When complex **5.22** is titrated with acid, its absorption band at 388 nm undergoes a gradual blue-shift to 338 nm, with growing intensity at higher acid concentration (**Fig. 3.4**). This is interpreted by the transformation of Ru-C≡C-py to $Ru^{+}$=C=CH-py upon acid addition (**Scheme 3.2**).

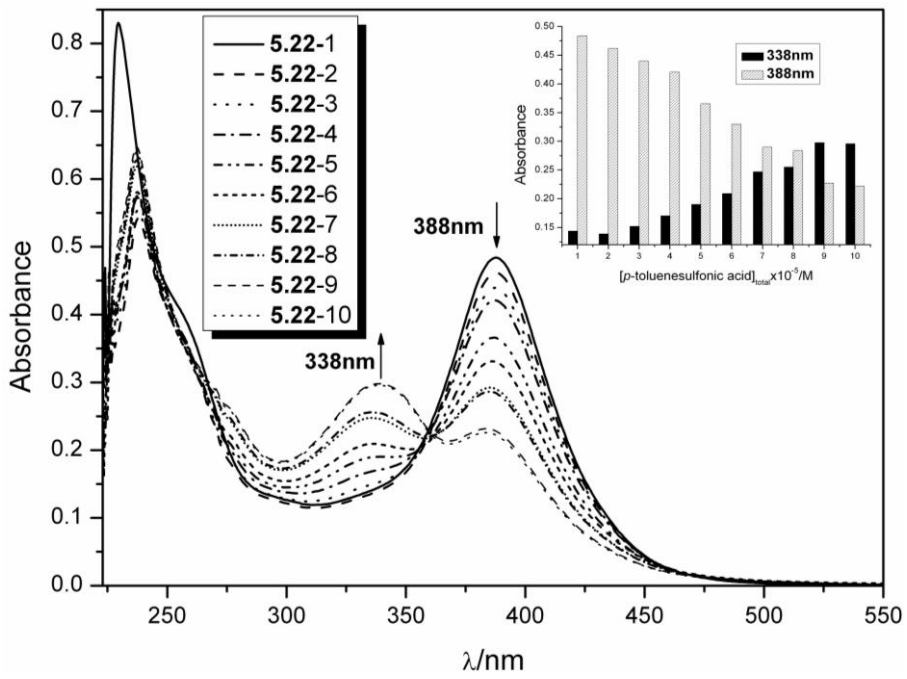


**Fig. 3.4** UV-vis absorption changes of **5.22** (concentration = 8.0 x $10^{-6}$ M) in $CH_2Cl_2$ with various concentrations of *p*-toluenesulfonic acid (from **5.22**-1 to **5.22**-10, representing 10 samples): 0, 0.20, 0.40, 0.60, 0.80, 1.00, 1.20, 1.40, 1.60, 1.80 (x$10^{-5}$ M) (inset: Plots of absorbance at 338 and 388 nm against the total concentration of *p*-toluenesulfonic acid)

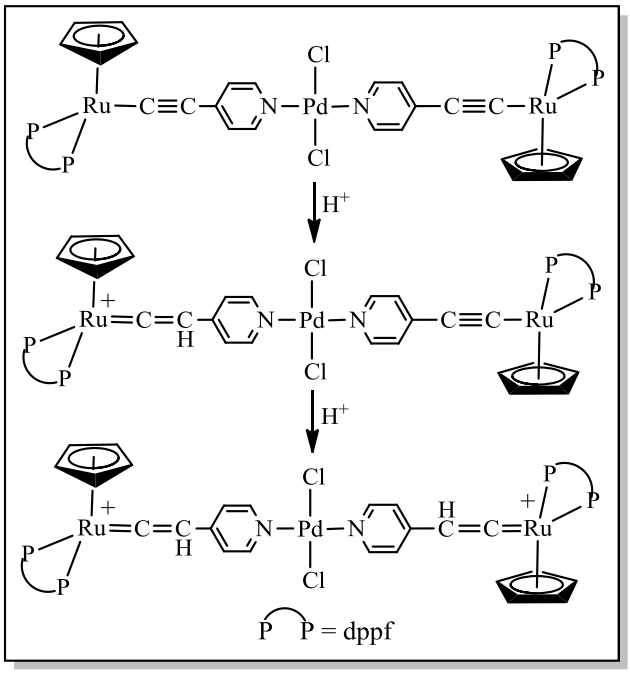


**Scheme 3.2** Structural changes of **5.22** upon addion of *p*-toluenesulfonic acid

Like monometallic Ru(II) acetylide complexes described above, [RuCp(C≡Cpy-4)(dppf)][Re(CO)$_3$(tpy)](PF$_6$) **(5.15)** also possesses two protonation sites viz. C≡C and the pendant pyridine from tpy ligand, but these two protonation sites belong to separate ligand groups. This leads to different observation when **5.15** is titrated with acid.

Acid titration of **5.15** shows no obvious change in the solution color or the absorption band at 407 nm as the pendant pyridine steadily converts to its pyridinium form upon addition of *p*-toluenesulfonic acid (**Scheme 3.3**). This is a sharp contrast to *trans*-[RuCl(C≡Cpy-4)(dppm)$_2$] (**5.1**), which shows an immediate color response as the pendant pyridyl ring is involved in the $d_{Ru} \rightarrow \pi^*$(C≡Cpy) transition. In complex **5.15**, the Re-bound protonated pyridyl has little communication with Ru, thereby showing little effect on the $d_{Ru} \rightarrow \pi^*$(C≡Cpy) transition. Upon further acid addition,

the acetylide pyridinium transforms to the vinylidene pyridinium form, which leads to a blue shift of the band at 407 nm to 355 nm accompanied by increases in absorption with increasing acid concentration (**Fig. 3.5**). Such a transformation of Ru-C≡C-py to $Ru^{+}$=C=CH-py upon acid addition (**Scheme 3.3**) has been described in the titration of **5.22** and other systems.[42,145]

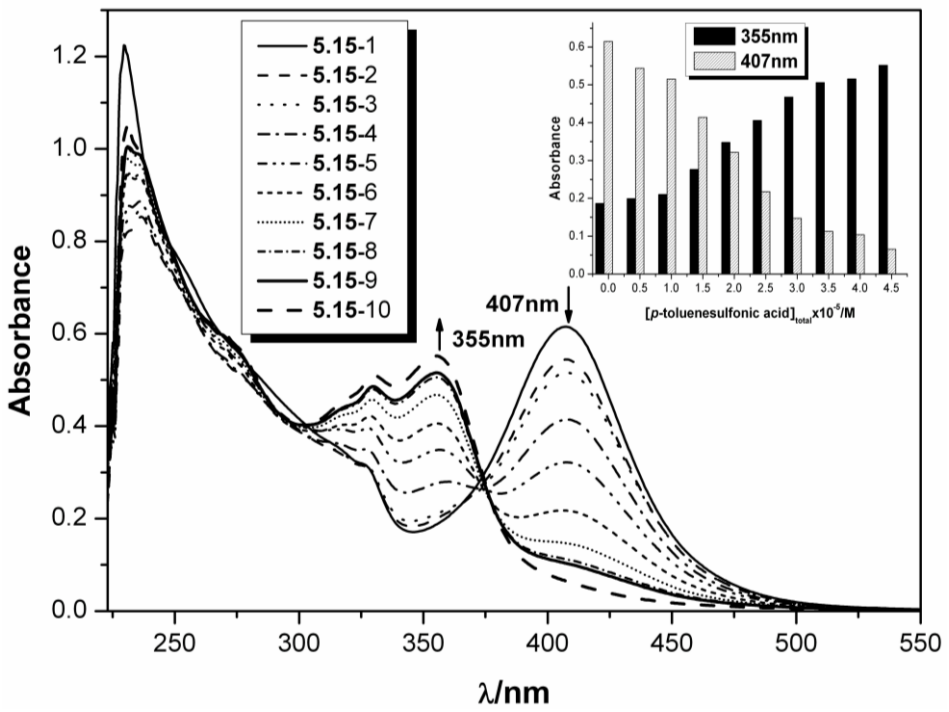


**Fig. 3.5** UV-vis absorption changes of **5.15** (concentration = 2.0 x $10^{-5}$ M) in $CH_2Cl_2$ with various concentrations of *p*-toluenesulfonic acid (from **5.15**-1 to **5.15**-10, representing 10 samples): 0, 0.5, 1.0, 1.5, 2.0, 2.5, 3.0, 3.5, 4.0, 4.5 (x$10^{-5}$ M) (inset: Plots of absorbance at 407 and 355 nm against the total concentration of *p*-toluenesulfonic acid)

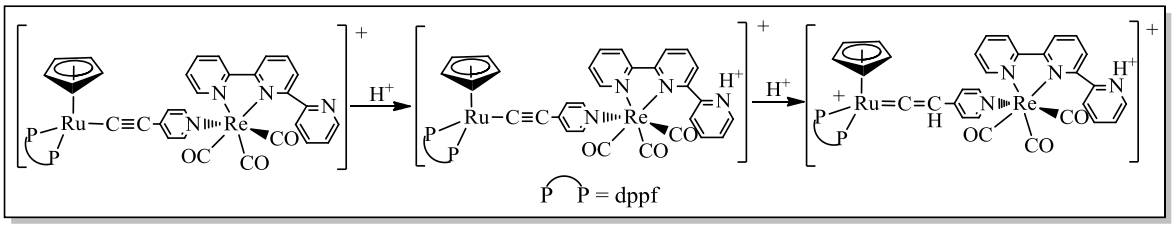


**Scheme 3.3** Structural changes of **5.15** upon addion of *p*-toluenesulfonic acid

### 3.1.3 Conclusions

Two main features in the UV-vis region are observed: the high energy ligand-centered $\pi \rightarrow \pi^*$ absorption (in the UV region), and the low energy absorption of $d_\pi(Ru) \rightarrow \pi^*(C{\equiv}Cpy)$ MLCT transition (in the visible region). Several points are concluded from the studies described above.

(i) Introduction of an electron-withdrawing group on pyridyl N atom has no observed influence on the intra-ligand $\pi \rightarrow \pi^*$ transition but leads to a red shift in $d_\pi(Ru) \rightarrow \pi^*(C{\equiv}Cpy)$ MLCT transition. The magnitude of the red shift in the heterometallic analogues follows the order $Ru^{II}$-$Re^{I}$ > $Ru^{II}$-$Pd^{II}$/$Pt^{II}$-$Ru^{II}$ > $Ru^{II}$-$Rh^{II}$-$Rh^{II}$-$Ru^{II}$.

(ii) In monometallic system, proceeding from the acetylide pyridine to acetylide pyridinium then to vinylidene pyridinium results in change of $d_\pi(Ru) \rightarrow \pi^*(C{\equiv}Cpy)$ MLCT transition (a red shift in the first process and a blue shift in the second one). Accordingly, a blue shift occurs in proceeding from the acetylide complex to its vinylidene analogue in heterometallic systems.

## 3.2 Nonlinear Optical Properties

### 3.2.1 Introduction

As described in the section of **1.4.3** in **Chapter One**, Ru acetylide complexes have attracted particular attention in the studies of their NLO properties.[4,5] Ru acetylides and their derivatives have been an important subset of organometallic complexes for nonlinear optics.[4,5] However, despite considerable studies concerned with second-order optical nonlinearities of Ru acetylide complexes,[4,5,105,167] their third-order NLO responses are comparatively little investigated over the past decade.[4,5] As such, only a extremely small number of heterometallic acetylide complexes have been investigated for their third-order NLO properties.[55] Investigations correlating third-order NLO response with systematically varying structural elements of heterometallic complexes are still unexplored.

In this chapter, the third-order NLO properties of monometallic Ru complexes and their corresponding high nuclear (bi-, tri- and tetra-nuclear) assemblies are reported. Since the heterometallic complexes have different π-conjugated systems, and the metal centers range from Group 7 to Group 10 with different coordination modes and geometries which have great effect on nonlinear response, the present study might be probing how structural modification of heterometallic acetylide complexes modifies the optical nonlinearities in a systematic fashion.

### 3.2.1.1 Theory for Nonlinear Optics

Optical nonlinearity is the study of the interaction of strong electric fields with materials possessing NLO properties.[4] A local electric field $\boldsymbol{E}_{\text{loc}}$ acting on a species will distort its electron density distribution $\rho(\boldsymbol{r})$, described in the dipole moment $\boldsymbol{\mu}$. When $\boldsymbol{E}_{\text{loc}}$ is comparable in strength to the internal electric fields within the molecule, at which point the distortion and the induced dipole moment should be treated as nonlinear functions of the field strength, usually being presented as a power series:[4]

$$\boldsymbol{\mu} = \boldsymbol{\mu}_0 + \alpha \boldsymbol{E}_{\text{loc}} + \beta \boldsymbol{E}_{\text{loc}}\, \boldsymbol{E}_{\text{loc}} + \gamma \boldsymbol{E}_{\text{loc}}\, \boldsymbol{E}_{\text{loc}}\, \boldsymbol{E}_{\text{loc}} + \ldots$$

The tensors $\alpha$, $\beta$ and $\gamma$ defined by the above equation are the linear polarizability, the second-order or quadratic hyperpolarizability (the first hyperpolarizability) and the third-order or cubic hyperpolarizability (the second hyperpolarizability), respectively.

The third-order hyperpolarizabilities can be described by perturbation theory as below:[4]

$$\gamma \propto \frac{-\mu_{ge}^{4}}{E_{ge}^{3}} + \frac{\mu_{ge}^{2}\mu_{ee'}^{2}}{E_{ge}^{2}E_{ge'}} + \frac{\mu_{ge}^{2}\left(\mu_{ee}-\mu_{gg}\right)^{2}}{E_{ge}^{3}}$$

where $\mu_{\text{gg}}$ is the ground state dipole moment, $\mu_{\text{ee}}$ is the excited state dipole moment, $\mu_{\text{ee'}}$ and $\mu_{\text{ge}}$ are transition dipole moments, and $E_{\text{ge}}$ and $E_{\text{ge'}}$ are optical absorption energies. This provides a useful indication of factors influencing NLO merit. For

example, the former expression suggests that an intense (large $\mu_{ge}$) charge-transfer (large $\mu_{ee}$ - $\mu_{gg}$) transition at long wavelength (low $E_{ge}$) will correspond to a significant γ coefficient.

### 3.2.1.2 Experimental Technique

Several techniques have been employed to measure third-order nonlinearities of metal acetylide complexes.[4] Among them, the Z-scan technique is a relatively simple and convenient way of investigating nonlinear response. It is also the most popular way to measure the third-order NLO merit of metal acetylides to date.[4,5]

Z-scan experiments for determining the NLO properties of metal acetylides are usually carried out in cells containing solutions of the complexes in common solvents. The NLO data are obtained from the conjunct contribution of the cell walls and the solvent, in addition to those of the dissolved complex. Usually both closed-aperture and open-aperture Z-scan measurements are undertaken. They are analyzed using equations derived by Sheikh-Bahae *et al.*.[168] The sample nonlinearity as a function of concentration is determined. The concentration dependence is then used to derive the extrapolated nonlinear parameters of the pure solute, and the components of the complex hyperpolarizability γ can be obtained eventually. An alternative way of expressing the molecular NLO parameters is by quoting the appropriate molecular absorption cross-sections, and referring to the absorption process responsible for the observed effects, e.g. two-photon absorption (TPA) cross-section.

The advantages of the Z-scan technique in determining the third-order NLO properties are obvious: the signs of the NLO susceptibility components are accessible without the need to carry out measurements on many solutions with a wide range of concentrations compared with other techniques, such as DFWM.[5] However, this technique cannot provide information about the temporal behavior of the NLO response, so that it may lead to uncertainties about the origin of nonlinear effects.

### 3.2.2 Results and Discussion

The Z-scan technique is employed to measure the third-order NLO response of the monometallic and heterometallic complexes in this work. Since third-order NLO measurements are affected by cell walls and solubility in addition to the nonlinearities of complexes, it is common that the resultant data are with large error margins in some cases, as observed in related systems,[30,35,72] which render meaningful comparisons difficult and development of structure-property relationships challenging. Accordingly, the discussion that follows needs to be cautious.

Third-order nonlinearities of these complexes were assessed by Z-scan studies at 750 nm. The systematic variation in their structures of these compounds permits assessment of the effects of sequential combination of metal centers with different geometries. It also allows for electron-withdrawing abilities, $\pi$-system lengthening

through the metal center, and progression from octahedral to half-sandwich Ru configuration on the NLO properties. All of the complexes absorb, to varying extents, at 375 nm, and hence the possibility of two-photon absorption was of particular interest. Both closed-aperture and open-aperture Z-scan measurements were undertaken, thus permitting simultaneous evaluation of spectral dependences of both imaginary and real components of the hyperpolarizability since the imaginary component ($\gamma_{imag}$) is available from the open-aperture signal, and the real part ($\gamma_{real}$) is determined by closed-aperture Z scan.[96] The third-order NLO response parameters, together with the linear optical data, are summarized in **Table 3.1**.

### 3.2.2.1 Features of Real Components ($\gamma_{real}$) of the Nonlinearities

Negative real components ($\gamma_{real}$) of the nonlinearities are observed in most instances (**Table 3.1**). The negative $\gamma_{real}$ values are likely to result from two-photon dispersion effects (resonant behavior of the third-order hyperpolarizability involving a rapidly changing real part and an enhanced imaginary part), a ubiquitous phenomenon observed in metal acetylide systems.[30,35,55,93] Two-photon absorption (TPA) is a third-order NLO property that is of interest for applications in multiphoton microscopy, optical limiting and optical data storage.[86] Although the negative $\gamma_{real}$ values result from two-photon dispersion effects, the sign of $\gamma_{real}$ is quite sensitive to small differences in the energies of absorption bands of the complexes, which might account for why *trans*-[RuH(C≡Cpy-4)$(dppe)_2$] (**5.4**), [RuCp(C≡Cpy-4)(dppf)] (**5.7**), and [RuCp(C≡Cpy-4)$(dppf)]_2[PtCl_2$] (**5.23**) exhibit

positive $\gamma_{real}$ values (**Table 3.1**).

The monometallic Ru and trimetallic Ru-Pd/Pt-Ru complexes generally show low solubilities in $CH_2Cl_2$ and large error margins in the real component $\gamma_{real}$ of the nonlinearities. This is due to the fact that the real components correspond to the refractive parts of the third-order nonlinearities, which are measured as increments to contributions from the solvent and windows of the cell used for the measurement. It is impossible to obtain a precise value if the solubility is inadequate.[93] This imprecision renders extraction of structure-NLO activity correlations particularly challenging, a ubiquitous problem for metal acetylide complexes.[30,104] Nevertheless, it is clear that, at this wavelength, the Ru-Rh-Rh-Ru complexes exhibit larger (in absolute terms) refractive nonlinearity than other complexes. All data that are larger than the error margins are negative – the largest values correspond to this series of complexes with absorption maxima closest to half the measurement wavelength (the Ru-Rh-Rh-Ru-containing complexes all have $\lambda_{max}$ in the range 370 ~ 373 nm), and consistent with the observed nonlinearities being dependent on the dispersion of the two-photon states.

#### 3.2.2.2 Features of Imaginary Components ($\gamma_{imag}$) of the Nonlinearities

In contrast to the $\gamma_{real}$ data, the solvent and cell windows do not contribute to the imaginary components $\gamma_{imag}$ of the nonlinearities, for which data are therefore available with greater precision. Hence, the differences between the values of the imaginary parts $\gamma_{imag}$ afford meaningful comparisons. The following conclusions can

be drawn from the data in **Table 3.1**:

(i) Mononuclear complexes

Generally, nonlinearities for the mononuclear Ru complexes are low in the imaginary components $\gamma_{imag}$, a result noted with their phenylethynyl or other diphosphine ligand analogues.[4,93] Differences in optical nonlinearities on replacing bidentate diphosphine are minor and significantly less than errors in data. In fact, the effect of structural variations (e.g. replacement of dppe with dppm, chloro with hydrido, or octahedral geometries with half-sandwich moieties) is subtle and within the error margins of the present studies.

(ii) Comparison between mononuclear and heteronuclear complexes

In contrast to the low nonlinearities and large error margins for the monometallic acetylide complexes, their heterometallic products are much more NLO active. Significant increases in nonlinearity of $\gamma_{imag}$ values are found in moving from the monometallic Ru complexes to N-complexed heterometallic derivatives, with the largest $\gamma_{imag}$ values being found for the Ru-Rh-Rh-Ru complexes (**Table 3.1**). This is evident when **5.11**-**5.15** or **5.23** or **5.24**-**5.27** are compared with their monometallic precursor **5.7** in which coordination and accompanied formation of a longer conjugation system result in a significant increase in third-order nonlinearities. A similar conclusion has been drawn earlier.[4] The significantly larger $\gamma_{imag}$ values of heterometallic complexes compared to those of their respective monometallic Ru

components indicate electronic communication between the Ru 4-ethynylpyridine moieties and the metal fragments introduced, manifesting that the cubic responses are not simply the sums of nonlinearities of their respective components.[169] Furthermore, previous studies have showed that any modification of the absorption spectrum of a complex contributes to the modification of the nonlinear polarizabilities.[93,96] This conclusion is testified by the present study. Incorporation of the electron-withdrawing metal fragments of $[Re(CO)_3(N\text{-}N)]^+$, $PdCl_2/PtCl_2$, or $[Rh_2(O_2CR)_4]$ into the monometallic Ru molecular systems results in significant red shifts in their optical absorptions (refer to Section **3.1.2.2**), consequently gives rise to significant increases in NLO response (**Table 3.1**). Notably, the NLO data for several complexes are markedly different, although their linear optical absorption data are very similar – further insight into this observation would require a complete wavelength dependence study of the cubic nonlinearities of these complexes, but this is prohibitive because of the time required.

(iii) Comparison among heterometallics

The heterometallic complexes shown in **Table 3.1** differ greatly in their third-order NLO response. For Ru-Re binuclear system, the complexes exhibit moderate third-order NLO response with small error margins. Extending the π-system through the metal center in proceeding from Ru-Re binuclear complexes to Ru-Pd/Pt-Ru trinuclear analogues, significant increases are observed in their third-order nonlinearities. This suggests that extending π-delocalization is the crucial factor

influencing NLO response, in accordance with the observation in organic systems.[170] The Ru-Rh-Rh-Ru tetranuclear complexes exhibit largest third-order NLO response. These largest values correspond to this series of complexes with absorption maxima closest to half the measurement wavelength (750 nm in this study). The Ru-Rh-Rh-Ru tetranuclear complexes all have $\lambda_{max}$ in the range 370 ~ 373 nm (**Table 3.1**), consistent with the observed nonlinearities being dependent on the dispersion of the two-photon states.

### 3.2.2.3 Two-Photon Absorption (TPA) Cross-Section $\sigma_2$

TPA cross-sections $\sigma_2$ are also listed in **Table 3.1**. They are related to $\gamma_{imag}$,[108,171] and both of them are calculated from the nonlinear absorption coefficients $\beta$. Since the measurements in this study were carried out with low repetition rate fs pulses, excited state absorption should be negligible, and the data should be an accurate reflection of TPA merit. TPA cross-section tends to scale with the size of the $\pi$-system in metal acetylide-based complexes. Structure-activity trends of $\sigma_2$ values are identical with those of $\gamma_{imag}$. The $\sigma_2$ values for the mononuclear Ru complexes are small, and progression from mononuclear Ru complexes to Ru-Re binuclear and Ru-Pd/Pt-Ru trinuclear heterometallic complexes results in increases in $\sigma_2$ with the largest $\sigma_2$ value being found in the Ru-Rh-Rh-Ru system.

### 3.2.2.4 Comparison of Third-Order Nonlinearities between Complexes in the Present Studies and Related Complexes Reported

The resultant data in **Table 3.1** demonstrate that the introduction of an electron-withdrawing group to the electron-donor Ru moiety leads to an increase in its third-order NLO response. The Ru acetylide molecular system gives a higher third-order response upon the introduction of a second (third or more in some cases) metal fragment compared to the influence of incorporating a non-metal or metalloid group.[4,5] For example, the introduction of strong electron acceptors such as $NO_2$, CHO, *etc*. into the acetylide ligands of linear mononuclear Ru complexes gives lower third-order NLO enhancement even though it is assisted by high π-delocalization in the mononuclear complexes. An alternative to achieve significant third-order responses is to use a functional acetylide with a sufficiently large π-delocalized ligand network (**Fig. 3.6**).[4,5]

It is difficult to make a good comparison between this work and other Ru acetylide based heterometallics due to the sparse study of their third-order NLO response. The multinuclear Ru-Pt dendrimer 1,3,5-$C_6H_3$(C≡C$C_6H_4$-4-C≡C-*trans*-[Pt($PMe_2Ph)_2$]C≡C-4-$C_6H_4$-3,5-$C_6H_3${C≡C-*trans*-[Ru(C≡CPh)$(dppe)_2$]}$_2)_3$ exhibits larger third-order NLO response ($\gamma_{real}$ = -6700 ± 2600 $10^{-36}$esu, $\gamma_{imag}$ = -2500 ± 1300 $10^{-36}$esu)[55] than the linear trinuclear Ru-Pd/Pt complexes in this work although the $\gamma_{real}$ value for **5.19** is amongst the largest for linear organometallic complexes,[4,171] indicating that large π-conjugation system and two dimensional configuration result in large third-order NLO response. Among the

few Ru-Re binuclear[58] or Ru-Rh-Rh-Ru tetranuclear[113] acetylide compounds known, there are no third-order NLO responses reported. The notable third-order NLO responses of heterometallic complexes in this study show promising NLO properties and highlight the potential of heterometallic systems.

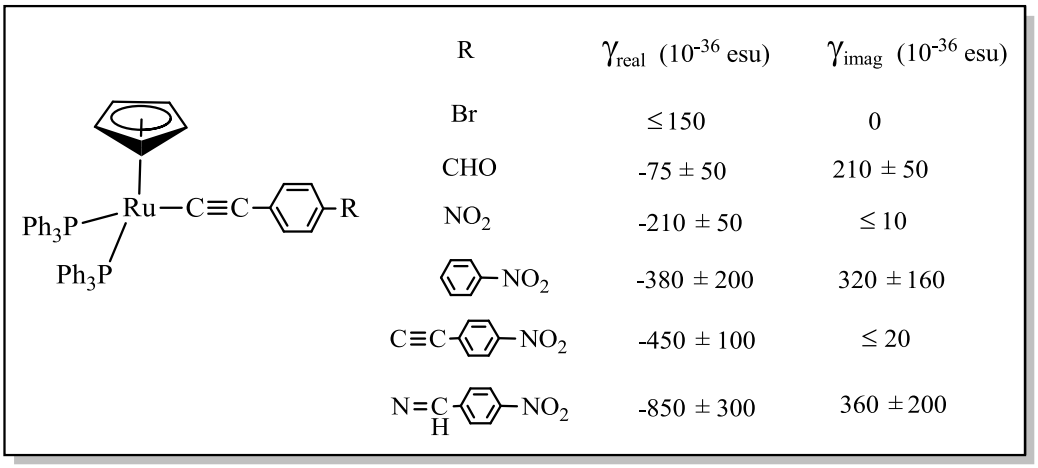


**Fig. 3.6** Selected mononuclear complexes with different acetylide ligands

**Table 3.1** Linear and third-order nonlinear optical data

| Complex | $\lambda_{max}$ (nm) ($\varepsilon$ ($10^4$ $M^{-1}cm^{-1}$) | $\gamma_{real}$ ($10^{-36}$ esu) | $\gamma_{imag}$ ($10^{-36}$ esu) | $\sigma_2$ (GM) |
|---|---|---|---|---|
| Mononuclear | | | | |
| **5.1** | 336 (2.0) | -100 ± 200 | 13 ± 10 | 4 ± 3 |
| **5.3** | 345 (2.4) | -160 ± 200 | 10 ± 10 | 3 ± 3 |
| **5.4** | 344 (1.8) | 55 ± 200 | 57 ± 30 | 16 ± 10 |
| **5.7** | 339 (2.5) | 40 ± 100 | 10 ± 4 | 3 ± 1 |
| Binuclear | | | | |
| **5.11** | 409 (3.2) | -590 ± 250 | 230 ± 40 | 65 ± 10 |
| **5.12** | 407 (3.4) | -230 ± 60 | 280 ± 20 | 80 ± 6 |
| **5.13** | 407 (3.0) | -480 ± 200 | 200 ± 40 | 55 ± 10 |
| **5.14** | 408 (3.5) | -460 ± 150 | 280 ± 50 | 80 ± 15 |
| **5.15** | 407 (2.3) | -570 ± 250 | 180 ± 30 | 50 ± 6 |

| | | | | |
|---|---|---|---|---|
| **5.16** | 410 (2.1) | -560 ± 150 | 280 ± 40 | 80 ± 10 |
| Trinuclear | | | | |
| **5.17** | 385 (5.6) | -9900 ± 3000 | 800 ± 100 | 220 ± 30 |
| **5.19** | 396 (8.6) | -17000 ± 10000 | 910 ± 400 | 250 ± 10 |
| **5.21** | 392 (8.5) | -460 ± 700 | 350 ± 80 | 100 ± 20 |
| **5.23** | 393 (5.3) | 1800 ± 3000 | 600 ± 200 | 170 ± 50 |
| Tetranuclear | | | | |
| **5.24** | 370 (4.8) | -600 ± 200 | 220 ± 50 | 60 ± 15 |
| **5.25** | 370 (5.6) | -650 ± 250 | 240 ± 40 | 65 ± 10 |
| **5.26** | 370 (4.6) | -880 ± 300 | 460 ± 100 | 130 ± 25 |
| **5.27** | 370 (4.5) | -1600 ± 800 | 1050 ± 400 | 290 ± 100 |
| **5.28** | 371 (4.4) | -1100 ± 400 | 1300 ± 350 | 360 ± 100 |
| **5.29** | 371 (4.7) | -3350 ± 750 | 1170 ± 250 | 320 ± 80 |
| **5.30** | 371 (4.6) | -940 ± 300 | 500 ± 50 | 140 ± 15 |
| **5.31** | 371 (4.0) | -1100 ± 800 | 770 ± 250 | 210 ± 80 |
| **5.32** | 373 (5.1) | -1300 ± 400 | 270 ± 40 | 75 ± 10 |
| **5.33** | 373 (4.8) | -1100 ± 500 | 220 ± 60 | 60 ± 20 |

### 3.2.3 Conclusions

The significantly higher third-order NLO responses upon introduction of strong metal-based electron acceptors suggest potential applications of heterometallic complexes in growing areas such as optical signal processing. Although the remaining problems in some complexes, such as solubility, make it difficult to pinpoint the effect of structural variations on third-order nonlinearity, nevertheless, in view of the paucity of NLO data on heterometallic acetylides,[55] these heterometallic systems show sufficient promise that NLO enhancement can be achieved in a multimetallic network.

Future exploration of these types of material will need to include a study of the temporal nature of the NLO response, its wavelength dependence, and its dependence on the chemical manipulations at both the spacer and the metal acceptor. The current systems, based on a simple and hence potentially versatile synthetic pathway, could allow the introduction of a range of heterometals that can carry ligands of different electronic characteristics. The use of an unusual bidentate terpyridine in **5.15** in the present study is just one of the many possibilities. It is noteworthy that the active chlorides distributed at the metal centers in the trinuclear Ru-Pd/Pt-Ru complexes potentially offer a mechanism to design materials for electronic and optical applications through structural and dimensional manipulations.

## 3.2.4 Experimental Section

The experiments were done by Prof. Mark Humphrey and his coworkers at Australian National Univeristy.

The compounds were investigated as $CH_2Cl_2$ solutions at concentrations in the range 0.1 – 2% w/w. Typically, three different concentrations of each compound were examined in a 1 mm path length Starna glass cell, the highest concentration being prepared first, measured, and the solution being progressively diluted for each subsequent measurement. The Z-scans were carried out using a femtosecond laser system consisting of a Clark-MXR CPA-2001 regenerative amplifier acting as a 775 nm pump and a Light Conversion TOPAS optical parametric amplifier. The system

was operated at a repetition rate of 250 Hz (reduced from the usual default rate of 1 KHz to minimize potential problems with thermal effects and sample photodecomposition[172]). The experiments were performed at a wavelength of 750 nm, which was obtained by doubling the 1500 nm signal output of the TOPAS.

The laser beam was attenuated to energies in the μJ/pulse range and directed through a standard Z-scan set-up equipped with a beam splitter, allowing one to record open-aperture and closed-aperture Z-scans simultaneously. The beam was focused so as to provide a spot size of about $w_0 \approx 50$ μm, ensuring that the Rayleigh range $z_R = \pi w_0^2/\lambda$ was larger than the total thickness of the sample (≈ 3 mm which includes two glass walls and the solution inside the cell). The data were recorded using three photodiodes monitoring the input pulse energy, the open aperture signal and the closed aperture signal, respectively, whose outputs were fed into three channels of a boxcar averager, which was GPIB-interfaced with a data collection computer; this also controlled the motion controller, providing *z* position travel in the range -40 to +40 mm. The data were analyzed with the help of a custom fitting program that used equations derived by Sheik-Bahae *et al*. to calculate the theoretical closed and open aperture Z-scan curves.[168] The values of the real and imaginary part of the nonlinear phase shift $\Delta\Phi_0$ (corresponding to the refractive and absorptive nonlinearity, respectively) were obtained for each scan involving the cell with different concentrations of the solute, an identical cell with just the solvent and a 3 mm thick fused silica plate serving as a calibration standard. The nonlinear refractive index, $n_2$, of silica at 750 nm, interpolated from the data analyzed by

Milam,[173] is 2.78 x $10^{-16}$ $cm^2/W$; the approximate value of 3 x $10^{-16}$ $cm^2/W$ has adopted throughout this work. The real part of the nonlinear phase shift obtained from the measurement on the silica can be used to calculate the light intensity; intensities of the order of 100 $GW/cm^2$ was employed.

The real and imaginary parts of the second hyperpolarizability, $\gamma$, of the solutes were computed from the concentration dependences of the real and imaginary parts of DF, assuming additivity of the nonlinear contributions of the solvent and the solute, and the applicability of the Lorentz local field approximation. The values of the two-photon absorption (TPA) cross-section $\sigma_2$ were computed from the absorptive part of the nonlinearity determined from the Z-scans. In all cases, errors of the relevant quantities were estimated from the assessed accuracies of the parameters for the fitting of Z-scans for the solutions and the corresponding scans for the solvent.[172]

# Chapter Four

# *Electrochemical Behavior of Ru(II) 4-Ethynylpyridine Based Monometallic and Heterometallic Complexes*

## 4.1 Introduction

Metal acetylide complexes featuring the electron-rich and redox-active organometallics endgroups are potentially useful as electronic or optoelectronic materials,[10,27,174,175] and their electrochemical properties are an important indicator in this regard. Therefore the electrochemistry of metal acetylides is of significant interest.[35,73] This area is the focus of various groups involved in carbon-rich organometallics over the world.[63,87,114,176] Investigation shows that the degree of conjugation along the metal-acetylide backbone is limited for Groups 10 and 11 metal acetylides due to the closed shell nature of M(I) (M = Cu, Ag and Au) and stable $d^8$ configuration of M(II) (M = Pd and Pt).[177] Hence, efforts have been focused on acetylide compounds of middle transition metals,[116,176] such as Ru.[35,114] The ability of Ru to operate as a connector allows electron flow to occur between different elements in *trans*-ditopic carbon-rich systems. The ability of Ru(II) acetylide conjugated species to act as molecular wires is closely related to their redox properties. Many Ru(II) acetylide containing systems have been probed by cyclic voltammetry (CV).[20,117] Although a number of reports have focused on the electrochemical

properties of ruthenium[89,122] and multimetallic acetylide complexes,[59,113,178,179] there are little systematic studies on ruthenium acetylide based heterometallic assemblies.

In this chapter, cyclic voltammetric method was applied to investigate the electrochemical properties of momo- and hetero- metallic systems. Since several factors exert significant influence on the electrochemical properties: the nature of the transition metal atom M and its coordination, the conjugation of the π-system for the bridging ligands, -C≡C-R, and the nature of the ancillary ligand field, $L_n$, the effect of the coordination mode and ligand environment of metal centers in both monometallic and heterometallic systems on electronic conductivity will be described.

## 4.2 Results and Discussion

In order to gain insight into the electronic environment of the new complexes, the redox properties of monometallic Ru(II) acetylide and heterometallic complexes were examined by CV. All complexes exhibit electroactivity due to the oxidation of $Ru^{II/III}$ couple. For heterobimetallic ($Ru^{II}$-$Re^{I}$) and heterotetrametallic ($Ru^{II}$-$Rh^{II}$-$Rh^{II}$-$Ru^{II}$) systems, the oxidation waves of $Re^{I/II}$ and $Rh_2^{IV/V}$ were also observed, respectively, whereas for the heterotrimetallic ($Ru^{II}$-$Pd^{II}$/$Pt^{II}$-$Ru^{II}$) system, the $Pd^{II/III}$ or $Pt^{II/III}$ oxidation potential was not detected, which might be due to the limit of the $CH_2Cl_2$ windows in the experimental conditions. For the sake of clarity, the electrochemical data will be discussed separately under the classes of mono- and

tri- metallic systems, bimetallic system, and tetrametallic system.

### 4.2.1 Mono- and Tri- metallic Systems

The electrochemical data for complexes **5.1**, **5.3**, **5.7**, **5.17 – 5.19**, **5.22** and **5.23 (**refer to **Chapter Five)** are summarized in **Table 4.1**, together with data of complexes *trans*-[$RuCl_2(dppm)_2$] and *trans*-[$RuCl_2(dppe)_2$] for comparison. A single Ru-centered oxidation in the positive potential region in **5.1**, **5.3**, **5.17 – 5.19** is observed, whereas complexes **5.7**, **5.22** and **5.23** give two oxidation waves, corresponding to the redox couples of $Ru^{II/III}$ and $Fe^{II/III}$ (**Table 4.1**). Similar assignments have been reported.[180-182] There is no indication of metal-metal electrochemical communication in the trinuclear complexes. All oxidation waves in complexes **5.1**, **5.3**, **5.7**, **5.17 – 5.19**, **5.22** and **5.23** exhibit quasi-reversible or irreversible oxidation process ($\Delta E$ = 100-140 mV, under standard conditions of 100 $mV \cdot s^{-1}$ scan rate at r.t.). **Fig. 4.1** gives a comparison of the CV responses of complexes **5.1**, **5.18** and **5.22**.

**Table 4.1** Cyclic voltammetric data for complexes **5.1**, **5.3**, **5.7**, **5.17** – **5.19**, **5.22** and **5.23**[a]

| Complex | $E_{1/2ox}$, V ($\Delta E$, mV; $i_{pc}/i_{pa}$)[b] | |
|---|---|---|
| | $Fe^{II/III}$ | $Ru^{II/III}$ |
| *trans*-[$RuCl_2(dppm)_2$] | | 0.53[c] |
| *trans*-[$RuCl_2(dppe)_2$] | | 0.50[d] |
| *trans*-[RuCl(C≡Cpy-4)$(dppm)_2$] (**5.1**) | | 0.57(100, 0.5) |
| *trans*-[RuCl(C≡Cpy-4)$(dppe)_2$] (**5.3**) | | 0.62(100, 0.8) |
| [RuCp(C≡Cpy-4)(dppf)] (**5.7**) | 0.94(104)[e] | 0.56(106)[e] |
| [*trans*-RuCl(C≡Cpy-4)$(dppm)_2]_2[PdCl_2]$ (**5.17**) | | 0.66(110, 1.0) |
| [*trans*-RuCl(C≡Cpy-4)$(dppm)_2]_2[PtCl_2]$ (**5.18**) | | 0.66(140, 0.9) |
| [*trans*-RuCl(C≡Cpy-4)$(dppe)_2]_2[PdCl_2]$ (**5.19**) | | 0.71 (120) |
| [RuCp(C≡Cpy-4)$(dppf)]_2[PdCl_2]$ (**5.22**) | 0.94[f] | 0.68(120, 1.0) |
| [RuCp(C≡Cpy-4)$(dppf)]_2[PtCl_2]$ (**5.23**) | 0.95[f] | 0.68(110, 0.7) |

[a]All potentials vs SCE with a rate of 100 mV $s^{-1}$, ferrocene/ferrocenium couple located at 0.56 V. Data obtained from room temperature $CH_2Cl_2$ solutions with 0.1 M $^nBu_4NPF_6$ as supporting electrolyte. [b]$E_{1/2ox} = (E_{ox} + E_{red})/2$; $\Delta E = E_{ox} - E_{red}$. [c]ref 189. [d]ref 188. [e]ref 187. [f]$E_{pa}$ for nonreversible process.

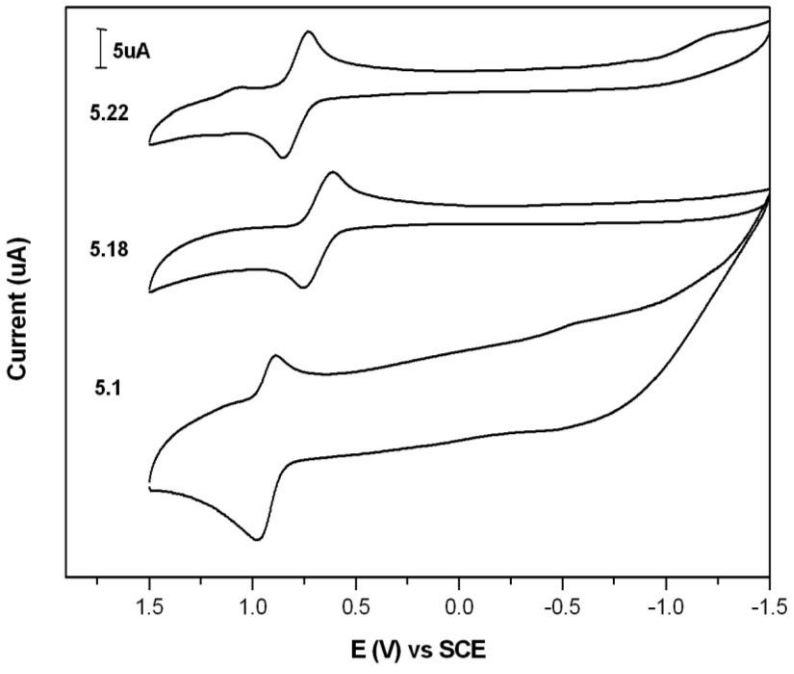


**Fig. 4.1** Cyclic voltammograms of **5.1**, **5.18** and **5.22** in $CH_2Cl_2$ (0.1 M $^nBu_4NPF_6$) at r. t.

**Table 4.1** shows that the $Ru^{II}/Ru^{III}$ oxidation couple in *trans*-[RuCl(C≡Cpy-4)$(dppe)_2$] (**5.3**) is slightly anodic shifted by 50 mV with respect to that in its dppm analogue *trans*-[RuCl(C≡Cpy-4)$(dppm)_2$] (**5.1**) (0.62 vs 0.57 V). This indicates that there is less electron density on Ru core in **5.3** than in **5.1**, which render Ru center in **5.3** not as easy to be oxidized as in **5.1**. This result is consistent with the $\nu_{C\equiv C}$ vibrational frequencies in **5.3** and **5.1** (2067 vs 2078 $cm^{-1}$), suggesting that the Ru center in **5.3** is more electrophilic and accepts more electron density from C≡C unit. This leads to a lower $\nu_{C\equiv C}$ vibrational frequency.

Replacing chloride by 4-ethynylpyridine from *trans*-[$RuCl_2(dppe)_2$][183] to *trans*-[RuCl(C≡Cpy-4)$(dppe)_2$] (**5.3**) results in an increase of 120 mV in the oxidation potential of $Ru^{II/III}$, indicating that 4-ethynylpyridine is better in stabilizing the lower oxidation state. This is within expectation in view of its stronger π-acceptor character compared to chloride. A similar effect is observed in dppm analogues when comparing *trans*-[$RuCl_2(dppm)_2$][184] with *trans*-[RuCl(C≡Cpy-4)$(dppm)_2$] (**5.1**) and other closely related systems.[185]

The effect of the pyridyl function (in *trans*-[RuCl(C≡Cpy-4)$(dppm)_2$] (**5.1**) and *trans*-[RuCl(C≡Cpy-4)$(dppe)_2$] **(5.3**)) is evident when a comparison is made with their phenyl analogues *trans*-[RuCl(C≡CPh)$(dppm)_2$] (+0.45 V vs SCE)[186] and *trans*-[RuCl(C≡CPh)$(dppe)_2$] (+0.46 V vs SCE)[183], respectively. The $Ru^{II/III}$ potentials in **5.1** and **5.3** increase by 120 mV and 160 mV, respectively, as a result of the electron-withdrawal effect of pyridyl acetylide. This increase is similar to that found in other ruthenium acetylide complexes.[187] Such oxidation potentials are generally

uniform across different pyridyl acetylide isomers, as evident in *trans*-[RuCl(C≡Cpy-2)(dppm)$_2$] (+0.57 V vs SCE)[184] and *trans*-[RuCl(C≡Cpy-4)(dppm)$_2$] (+0.57 V vs SCE) (**5.1**) (**Table 4.1**).

Examination of **5.17** – **5.19**, **5.22** and **5.23** revealed that changes between Pd(II) and Pt(II) or between the octahedral and half-sandwich spheres are insignificant (**Table 4.1**). The oxidation potentials of $Ru^{II/III}$ in **5.17** – **5.19** and **5.22**, **5.23** undergo an anodic shift by 90 ~ 120 mV compared to their corresponding Ru mononuclear precursors **5.1**, **5.3** and **5.7** (**Table 4.1**). This is in agreement with the peak assignment (vide supra) as the coordination of pyridyl at the Lewis acidic Pd/Pt centers should lower the electron density in Ru through inductive effect, thereby stabilizing $Ru^{II}$ and making it less susceptible to oxidation. Other supporting evidence for the decrease of electron density character of heterotrimetallic complexes includes: (1) low C≡C stretching frequency (2078, 2068 vs ~ 2046 $cm^{-1}$ in **5.1**, **5.3** and **5.17** – **5.19**/**5.22**/**5.23**, respectively); (2) downfield shift of Ru-*C* (~ 149 vs ~ 151 ppm) in $^{13}C$ NMR.

Coordination of the metalloligands **5.1**, **5.3** and **5.7** has a pronounced effect on the reversibility of the redox process. Indeed, as shown in **Fig. 4.2**, the $Ru^{II}$ oxidation of complex **5.1** is chemically irreversible with $i_{pc}/i_{pa}$ = 0.5, but reversible in **5.17** with $i_{pc}/i_{pa} \approx 1$ (**Table 4.1**). This suggests a higher chemical stability of **5.17** than its monometallic precursor **5.1** after one electron removal. Similar phenomena were observed in other heterotrimetallic complexes and their respective monometallic precursors (**Table 4.1**). The higher degree of conjugation across the spacer-linked hetero-trinuclear network could make it less vulnerable to the redox process.

Comparison with the trinuclear analogue $[RuCl(C{\equiv}CC_6H_4C{\equiv}C)(dppe)_2]_2[Pd(PBu_3)_2]$ ($Ru^{II/III}$: +0.33 V vs SCE)[65] shows that the series of trinuclear complexes in this work have higher oxidation potentials of $Ru^{II/III}$ (~ +0.66 V). This is not unexpected since $PdCl_2$ is more efficient in electron-withdrawing than $Pd(PBu_3)_2$.

## 4.2.2 Bi- and Tetra- Metallic Systems

### 4.2.2.1 Bimetallic System ($Ru^{II}$-$Re^{I}$)

For the $Ru^{II}$-$Re^{I}$ bimetallic complexes **5.11** – **5.16**, the remotely electroactive ends possess different redox states (the donor and the acceptor sites). The electrochemical features of **5.11** – **5.16** were studied by cyclic voltammetry (CV). The CV data of **5.7** and **5.8**[182] are included for comparison (**Table 4.2**). A representative CV of **5.12** is shown in **Fig. 4.2**. In general, all complexes exhibit a single ligand-centered reduction in the negative potential region. Complexes **5.11**-**5.14** show three successive steps of metal oxidation of $Ru^{II/III}$ (0.69 ~ 0.73 V), $Fe^{II/III}$ (0.98 ~ 1.08 V) and $Re^{I/II}$ (1.31 ~ 1.38 V) in the positive potential region. Similar observations have also been reported.[129,164,182,188] Only two oxidation potentials are observed in **5.15** (**Table 4.2).** Absence of the $Re^{I/II}$ oxidation step in **5.15** could suggest that the Re(I) center is more resistive to oxidation. The absence of the intermediate oxidation step in **5.16** is within expectation when dppf is replaced by two $PPh_3$ ligands (**Table 4.2**). This supports the assignment of oxidation potentials in complexes **5.11** – **5.15**. Comparing these results with those of the reductions of the diimine ligands, the observed electrochemical processes can be

assigned (**Scheme 4.1**; complex **5.11** as a representative), from the literature:[189]

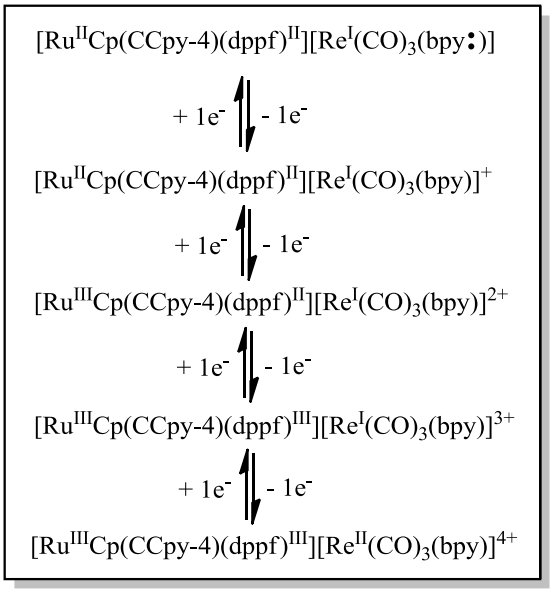


**Scheme 4.1** Electrochemical processes of **5.11**

**Table 4.2** Cyclic voltammetric data for complexes **5.7**, **5.8** and **5.11** – **5.16**[a]

| Complex | $E_{1/2}$(ox)(V) vs. SCE[b] | | | $E_{1/2}$(red)(V) vs SCE ($\Delta E_p$(mV))[c] |
|---|---|---|---|---|
| | $Ru^{II/III}$ | $Fe^{II/III}$ | $Re^{I/II}$ | |
| [RuCp(C≡Cpy-4)(dppf)] (**5.7**) | +0.56[d] | +0.94[d] | | |
| [RuCp(C≡Cpy-4)($PPh_3$)$_2$] (**5.8**) | +0.61[d] | | | |
| [RuCp(C≡Cpy-4)(dppf)][Re(CO)$_3$(bpy)]($PF_6$) (**5.11**) | +0.69 | +0.98 | +1.33 | -1.17(140) |
| [RuCp(C≡Cpy-4)(dppf)][Re(CO)$_3$($Me_2$bpy)]($PF_6$) (**5.12**) | +0.69 | +0.99 | +1.32 | -1.27(150) |
| [RuCp(C≡Cpy-4)(dppf)][Re(CO)$_3$($^t$Bu$_2$bpy)]($PF_6$) (**5.13**) | +0.69 | +0.98 | +1.31 | -1.28(140) |
| [RuCp(C≡Cpy-4)(dppf)][Re(CO)$_3$(phen)]($PF_6$) (**5.14**) | +0.73 | +1.00 | +1.38 | -1.13(180) |
| [RuCp(C≡Cpy-4)(dppf)][Re(CO)$_3$(tpy)]($PF_6$) (**5.15**) | +0.78 | +1.07 | | -1.14(260)[e] |
| [RuCp(C≡Cpy-4)($PPh_3$)$_2$][Re(CO)$_3$(bpy)]($PF_6$) (**5.16**) | +0.75 | | +1.35[f] | -1.17(180) |

[a]All potentials vs SCE with a rate of 100 mV $s^{-1}$, ferrocene/ferrocenium couple located at 0.56 V. Data obtained from room temperature $CH_2Cl_2$ solutions with 0.1 M $^n$Bu$_4$N$PF_6$ as supporting electrolyte. [b]$E_{1/2ox} = (E_{ox} + E_{red})/2$. [c]$\Delta E = E_{ox} - E_{red}$. [d]ref 188. [e]irreversible. [f]nonreversible

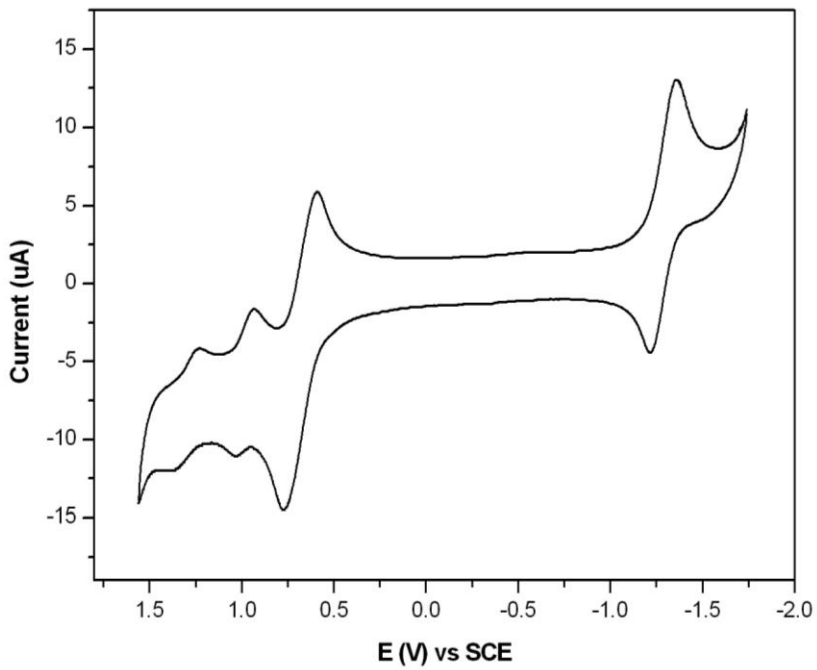


**Fig. 4.2** Cyclic voltammogram of **5.12** in $CH_2Cl_2$ (0.1 M $^nBu_4NPF_6$) at r. t.

The oxidation potentials of $Ru^{II/III}$ in **5.11 – 5.16** undergo an anodic shift of 130 ~ 170 mV compared to their respective precursors **5.7** and **5.8**. This indicates the inductive effect imposed by the electron-withdrawing $Re^{I}$ fragment and the cation formation, which decreases the electron density of $Ru^{II}$ metal, and hence decreases their ease of oxidation. The coordination, on the other hand, reduces the oxidation potentials of $Re^{I/II}$ in **5.11**-**5.16** compared to their respective Re(I) precursors[127,190] due to electron-donation from pyridyl of the spacer. For example, the $Re^{I/II}$ oxidation potential in **5.11** undergoes a cathodic shift of 0.44 V from its precursor $[Re(CH_3CN)(CO)_3(bpy)](PF_6)$ (1.77 V vs SCE).[127] Comparison with the $[Au(C{\equiv}Cpy\text{-}4)(PR_3)][Re(CO)_3(N\text{-}N)](OTf)$ system ($Re^{I/II}$ 1.66 ~ 1.79 V)[164] points to a more ready Re(I) oxidation in **5.11**-**5.16**, indicating that [RuCp(C≡Cpy-4)(P-P)] is probably more efficient in electron-donation than $[(PR_3)Au(C{\equiv}Cpy\text{-}4)]$. There is no

clear evidence of communication across the metal centers.

The sole quasi-reversible reduction couple in **5.11**-**5.16** (-1.13 ~ -1.28 V vs SCE) (**Table 4.2**) is tentatively assigned as ligand-centered reduction of the diimine.[164,188] The more negative reduction potentials in **5.12** (-1.27 V) and **5.13** (-1.28 V) compared to **5.11** and **5.16** (-1.17 V) could be rationalized by the presence of electron-donating substituents of methyl and *tert*-butyl groups in the former, which makes bpy ligand more electron rich and less electron-accepting, and hence decreases its ease of reduction. Likewise, the lower electron density on phen and tpy in **5.14** (-1.13 V) and **5.15** (-1.14 V) leads to a cathodic shift compared to **5.11.** The terpyridine reduction in **5.15** is electrochemically irreversible, possibly due to some secondary processes of the pendant pyridyl such as polymerization on the electrode surface.

#### 4.2.2.2 Tetrametallic Sytem ($Ru^{II}$-$Rh^{II}$-$Rh^{II}$-$Ru^{II}$)

The redox potentials of complexes **5.24**, **5.26** – **5.29** and **5.34** are collected in **Table 4.3**. **Fig. 4.3** gives the representative CV of complex **5.24**. Complexes **5.24**, **5.26** and **5.27** undergo three successive electrochemically quasi-reversible (120 ~ 220 mV) oxidation processes, ascribed to the $Ru^{II} \rightarrow Ru^{III}$ (~ +0.63 V), $Fe^{II} \rightarrow Fe^{III}$ (~ +0.95 V) and $Rh_2^{IV} \rightarrow Rh_2^{V}$ (+1.12 ~ +1.18 V) redox change, respectively. Similar assignments have been made in closely related systems,[143,191] and $Ru^{II}$-$Re^{I}$ dinuclear and $Ru^{II}$-$Pd^{II}$/$Pt^{II}$-$Ru^{II}$ trinuclear systems described above. Accordingly, the CV of complexes **5.28** and **5.29**, in which the dppf ligand is absent, exhibits two subsequent oxidation couples with $E_{1/2} \approx +0.63$ V from the oxidation of the two ruthenium units,

and $E_{1/2}$ ≈ +1.10 V from the oxidation process of $Rh_2^{IV} \rightarrow Rh_2^{V}$. The oxidation waves of $Rh_2^{IV} \rightarrow Rh_2^{V}$ are broad, possibly owing to the coupling between the two rhodium cores (Rh-Rh: ~ 2.40 Å). Specially, an irreversible oxidation wave was observed at $E_{pa}$ = +1.38 V in complex **5.34** besides the oxidation couple of $Rh_2^{IV} \rightarrow Rh_2^{V}$ at $E_{1/2}$ = +1.12 V. The oxidation process in $E_{pa}$ = +1.38 V is tentatively ascribed to the irreversible $Ru^{III} \rightarrow Ru^{IV}$ oxidation, as reported in related system.[58] The $Ru^{II/III}$ oxidation potential is missing in the CV of **5.34** possibly due to the unstable molecular system of hydride complex by reason of one electron removal from $Ru^{II}$.

**Table 4.3** Cyclic voltammetric data for complexes **5.24**, **5.26** – **5.29** and **5.34**[a]

| Complex | $E_{1/2}$(ox)(V) vs. SCE[b] | | |
|---|---|---|---|
| | $Ru^{II/III}$ | $Fe^{II/III}$ | $Rh_2^{IV/V}$ |
| [RuCp(C≡Cpy-4)(dppf)]$_2$[$Rh_2(O_2CCH_3)_4$] **(5.24)** | +0.63 | +0.94 | 1.17 |
| [RuCp(C≡Cpy-4)(dppf]]$_2$[$Rh_2(O_2C(CH_2)_3CH_3)_4$] **(5.26)** | +0.64 | +0.95 | +1.18 |
| [RuCp(C≡Cpy-4)(dppf)]$_2$[$Rh_2(O_2C(CH_3)_3)_4$] **(5.27)** | +0.62 | +0.95 | +1.12 |
| *trans*-[RuCl(C≡Cpy-4)(dppm)$_2$]$_2$[$Rh_2(O_2CCH_3)_4$] **(5.28)** | +0.63 | | ~ +1.09 |
| *trans*-[RuCl(C≡Cpy-4)(dppm)$_2$]$_2$[$Rh_2(O_2CCH_2CH_3)_4$] **(5.29)** | +0.65 | | +1.10 |
| *trans*-[RuH(C≡Cpy-4)(dppe)$_2$]$_2$[$Rh_2(O_2CC(CH_3)_3)_4$] **(5.34)** | +1.38[c] | | +1.12 |

[a]All potentials vs SCE with a rate of 100 mV $s^{-1}$, ferrocene/ferrocenium couple located at 0.56 V. Data obtained from room temperature $CH_2Cl_2$ solutions with 0.1 M $^nBu_4NPF_6$ as supporting electrolyte. [b]$E_{1/2ox} = (E_{ox} + E_{red})/2$; $\Delta E = E_{ox} - E_{red}$, [c]nonreversible of $Ru^{III} \rightarrow Ru^{IV}$ oxidation process.

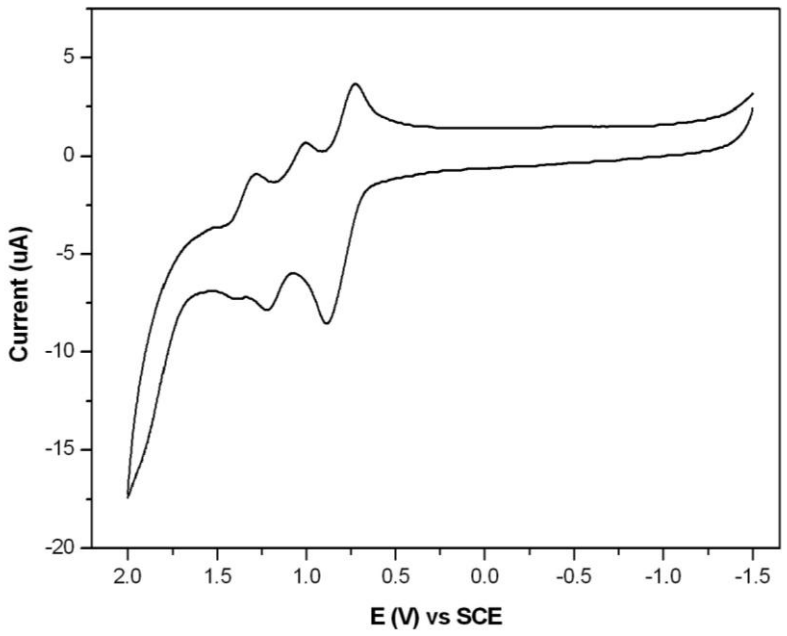


**Fig. 4.3** Cyclic voltammogram of **5.24** in $CH_2Cl_2$ (0.1 M $^nBu_4NPF_6$) at r. t.

The coordination of dirhodium(II) by metalloligands of Ru(II) 4-ethynylpyridine complexes results in a pronounced cathodic shift of $Rh_2^{IV} \rightarrow Rh_2^{V}$ (1.10 ~ 1.18 V) from the parent $[Rh_2(O_2CCH_3)_4]$ (1.36 V)[191] due to the strong electron-donating ability of ruthenium acetylide precursors, which increase the electron density of Rh(II) core, and hence enhance the ease of $Rh_2^{IV}$ oxidation. This shift reflects an increased stabilization of the higher oxidation state of the $Rh_2$-core. The oxidation potentials of $Ru^{II/III}$ (~ +0.63 V) in this series of tetranuclear complexes are comparable to those in the $Ru^{II}$-$Re^{I}$ dinuclear (~ +0.70 V) and $Ru^{II}$-$Pd^{II}$/$Pt^{II}$-$Ru^{II}$ trinuclear (~ +0.66 V) systems described above. They all undergo an anodic shift compared to their corresponding Ru(II) 4-ethynylpyridine precursors (~ +0.57 V). This anodic shift can likely be attributed to the delocalization of electrons along the backbone in the heterometallic systems. Similar phenomena have been observed in other heterometallic systems.[138] Comparison between **5.24** ($Rh_2^{IV/V}$ 1.17 V) and

$[Fc(C\equiv Cpy\text{-}4)]_2[Rh_2(O_2CCH_3)_4]$ ($Rh_2^{IV/V}$ 0.62 V vs SCE),[192] $[Fcpy\text{-}4]_2[Rh_2(O_2CCH_3)_4]$ ($Rh_2^{IV/V}$ 0.58 V vs SCE)[192] indicates that [RuCp(C≡Cpy-4)(dppf)] is lower in electron-donation ability than [Fc(C≡Cpy-4)] and [Fcpy-4].

## 4.3 Conclusions

Generally the CV data suggest that the electron rich heterometallic species tend to be oxidized easier. Some specific summaries are given below:

(i) In the heterometallic systems, the introduction of Lewis acidic electron-withdrawing metal fragments, $[Re(CO)_3(N\text{-}N)]^+$, or $PdCl_2/PtCl_2$, or $[Rh_2(O_2CR)_4]$, leads to an increase in the oxidation potential of $Ru^{II/III}$ compared to their respective Ru(II) 4-ethynylpyridine precursors. $Ru^{II}$-$Re^{I}$ dinuclear system possesses the greatest increase, consistent with the strongest electron-withdrawing ability of rhenium cation fragments.

(ii) In contrast, the oxidation potentials of $Re^{I/II}$ and $Rh_2^{IV/V}$ in the di- and tetra-nuclear systems, respectively, decrease compared to their corresponding $[Re(CO)_3(N\text{-}N)]^+$ and $[Rh_2(O_2CR)_4]$ fragments. This indicates the electron-donation properties of Ru(II) 4-ethynylpyridine precursors increase the electron density of the Re(I) or $Rh_2$(IV) centers and hence enhance their ease of oxidation.

(iii) The introduction of electron-withdrawing metal fragments on Ru(II) 4-ethynylpyridine precursors results in not only the change in the oxidation potentials of metal centers, but also the stability of the molecular systems. The Lewis acidic metal fragments are efficient in stabilizing the high oxidation state species. The successive two or three electron oxidations in bi- and tetra- nuclear systems also indicate their high stability.

The results reported here support the concept that the introduction of metal fragments into the acetylide π system could enhance charge transfer along the backbone of metal coordination oligomers and polymers. These results also suggest that systems containing Ru centers could be conductive, and hetero-assemblies containing donor-bridge-acceptor based on Ru unit can lend stability and raise conductivity of the systems. This could be a valuable reference for the construction of electronic conductive materials.

## 4.4 Experimental Section

The experiments in this section were done at Department of Chemistry, National University of Singapore. Standard electrochemical techniques were employed. Electrochemical measurements were conducted on an Autolab PGSTAT 30 electrochemical system. Cyclic voltammetry was performed in a three-electrode cell containing a glassy carbon working electrode surrounded by a platinum-spiral

auxiliary electrode, and an aqueous saturated clomel reference electrode (SCE).

The cyclic voltammetric experiments were conducted in $CH_2Cl_2$ solutions at room temperature by using $^{n}Bu_4NPF_6$ (0.1 M) as supporting electrolyte. $CH_2Cl_2$ was dried by refluxing over $CaH_2$, followed by distillation. All scans were performed under a nitrogen atmosphere at the rate of 100 mV/s. Under the applied experimental conditions, the one electron oxidation of ferrocene occurs at 0.56 V.

# Chapter Five

# *Experimental Section*

## 5.1 General Techniques

### 5.1.1 Reagents and Solvents

Unless otherwise stated, all chemicals are commercial reagents and used as supplied. All reactions and manipulations were carried out under $N_2$ with the use of standard inert-atmosphere and Schlenk techniques. Solvents used for synthesis were distilled over appropriate drying reagents and deoxygenated prior to use. Chemical reagents, unless otherwise specified, were commercial products and were used without further purification.

### 5.1.2 Nuclear Magnetic Resonance Spectroscopy

NMR spectra were measured on Bruker ACF300 300 MHz FT NMR spectrometers ($^{1}H$ at 300.14 MHz, $^{13}C$ at 75.43 MHz, $^{31}P$ at 121.50 MHz). Chemical shifts in the $^{1}H$ and $^{13}C\{^{1}H\}$-NMR spectra were measured relative to partially deuterated solvent peaks which are reported relative to TMS. $^{31}P$ chemical shifts were measured relative to 85% $H_3PO_4$. Unless otherwise specified, all NMR spectra were recorded in $CDCl_3$ solutions at room temperature.

### 5.1.3 Electrospray Mass Spectra

Electrospray mass spectra were obtained in positive-ion mode with a Finnigan/MAT LCQ mass spectrometer coupled with TSP4000 HPLC system and the crystal 310 CE system. The mobile phase was 80% MeOH/20% $H_2O$ pumped at a flow-rate of 0.4 ml/min. The spectrometer employed a quadrupole mass filter with an m/z range of 0 ~ 2000. The capillary temperature was 150°C. Peaks were assigned from the m/z values and from the isotope distribution patterns.

### 5.1.4 Infra-red Spectroscopy

Fourier transform infra-red spectra were recorded on a Bruker IFS 48 FTIR spectrometer. All experiments were done in $CH_2Cl_2$ solution using liquid cell with KBr windows for solution measurement.

### 5.1.5 Elemental Analyses

Elemental analyses were performed on a Perkin–Elmer PE 2400 CHNS Elemental Analyzer at the Elemental Analysis Laboratory. For some compounds, it is difficult to obtain satisfactory analytical data. This could be attributed to their inherent instability and/or possible contamination by trace quantity of their corresponding precursors which cannot be removed.

Unless otherwised stated, all theoretical values of elemental analyses are given

without taking into consideration of the solvates. This is because the elemental analysis data obtained in experiments are without solvents in most cases.

## 5.2 X-Ray Crystal Structure Determination and Refinement

The X-ray structure determinations were carried out by Ms. Tan Geok Kheng at the X-Ray Diffraction laboratory, Department of Chemistry, National University of Singapore.

The diffraction experiments were carried out on a Bruker SMART CCD diffractometer using Mo-K$\alpha$ radiation ($\lambda$ = 0.71073 Å). The program SMART[193] was used for collecting frames of data, indexing reflections and determination of lattice parameters, SAINT[194] for integration of the intensity of reflections and scaling, SADABS[2] for empirical absorption correction, and SHELXTL[195] for space group and structure determination, refinements, graphics, and structure reporting. The structures were refined by full-matrix least squares on $F^2$ with anisotropic thermal parameters for non-hydrogen atoms, unless otherwise indicated [$R = \Sigma||F_o| - |F_c||/\Sigma|F_o|$, and $w$R = $\{\Sigma[w(F_o^2 - F_c^2)^2]/\Sigma[w(F_o^2)^2]\}^{1/2}$ (where $w^{-1} = \sigma^2(F_o^2) + (aP)^2 + (bP)$). The relevant crystallographic data and refinement details are shown in **Tables 5.1** – **5.8**.

**Table 5.1** Crystal data and structure refinement of **5.1**, **5.2** and **5.7**.[a,b]

| Complex | **5.1** | **5.2** | **5.7** |
|---|---|---|---|
| empirical formula | $C_{57}H_{48}ClNP_4Ru$ | $C_{59}H_{51}F_6N_2O_{2.50}P_5Ru$ | $C_{50}H_{45}FeNOP_2Ru$ |
| fw | 1007.36 | 1197.94 | 894.73 |
| cryst system | Triclinic | Tetragonal | Monoclinic |
| space group | P-1 | I-42d | P2(1)/n |
| unit cell dimens | *a* = 13.5514(6) Å, α = 108.138(1)° *b* = 13.5933(6) Å, β = 94.060(1)° *c* = 13.8171(7) Å, γ = 94.729(1)° | *a* = 25.6097(6) Å, α =90° *b* = 25.6097(6) Å, β = 90° *c* = 27.9465(8) Å, γ = 90° | *a* = 11.4423(4) Å, α =90° *b* = 21.6175(8) Å, β = 108.615(1)° *c* = 17.4386(7) Å, γ = 90° |
| cell vol ($Å^3$) | 2398.0(2) | 18328.9(8) | 4087.8(3) |
| *Z* | 2 | 8 | 4 |
| D(calcd), $Mg/m^3$ | 1.395 | 0.868 | 1.454 |
| abs coeff, $mm^{-1}$ | 0.556 | 0.298 | 0.842 |
| *F*(000) | 1036 | 4896 | 1840 |
| crystal size ($mm^3$) | 0.46 x 0.24 x 0.20 | 0.44 x 0.30 x 0.20 | 0.30 x 0.20 x 0.08 |
| $\theta$ range for data collection (°) | 1.52-27.50 | 1.59-25.00 | 1.55-27.50 |
| index ranges | -17 ≤ h ≤ 17, -17 ≤ k ≤17, -17 ≤ l ≤ 17 | -30 ≤ h ≤ 30, -30 ≤ k ≤21, -33 ≤ l ≤ 28 | -14 ≤ h ≤ 14, -22 ≤ k ≤28, -22 ≤ l ≤ 22 |
| reflcns collcd | 31494 | 53176 | 28800 |
| indepdt reflcns | 10991 [*R*(int) = 0.0820] | 8072 [*R*(int) = 0.0791] | 9391 [*R*(int) = 0.0322] |
| max and min transm | 0.8970 and 0.7841 | 0.9428 and 0.8800 | 0.9357 and 0.7863 |
| data/restraints/params | 10991/0/577 | 8072/47/316 | 9391/0/505 |
| goodness-of-fit on $F^2$ | 1.035 | 1.090 | 1.038 |
| final *R* indices [$I>2\sigma(I)$] | *R*1 = 0.0323, w*R*2 = 0.0781 | *R*1 = 0.0861, w*R*2 = 0.2398 | *R*1 = 0.0363, w*R*2 = 0.0846 |
| *R* indices (all data) | *R*1 = 0.0372, w*R*2 = 0.0806 | *R*1 = 0.1074, w*R*2 = 0.2629 | *R*1 = 0.0448, w*R*2 = 0.0884 |
| largest diff peak and hole (e. $Å^{-3}$) | 0.496 and -0.262 | 1.124 and -0.453 | 0.801 and -0.448 |

[a]Temperature 223(2) K. [b]Crystals of **5.1**, **5.7** were grown by slow diffusion of hexane into their concentrated THF solutions whereas suitable crystal **5.2** was obtained similarly from the DMF–$Et_2O$ mixture.

**Table 5.2** Crystal data and structure refinement of **5.3**, **5.4** and **5.6**.[a,b]

| Complex | **5.3** | **5.4** | **5.6** |
|---|---|---|---|
| empirical formula | $C_{67}H_{68}ClNO_2P_4Ru$ | $C_{59}H_{53}NOP_4Ru$ | $C_{63}H_{62}ClNOP_4Ru$ |
| fw | 1179.62 | 1000.97 | 1109.54 |
| cryst system | Triclinic | Monoclinic | Triclinic |
| space group | P-1 | P2(1)/n | P-1 |
| unit cell dimens | *a* = 9.9872(6) Å, α = 79.508(1)° *b* = 13.2164(8) Å, β = 84.714(1)° *c* = 22.948(1) Å, γ = 76.250(1)° | *a* = 15.2171(7) Å, α = 90° *b* = 18.624(1) Å, β = 107.979(1)° *c* = 18.0947(9) Å, γ = 90° | *a* = 10.3088(9) Å, α = 97.011(2)° *b* = 12.477(1) Å, β = 97.048(2)° *c* = 22.117(2) Å, γ = 105.021(2)° |
| cell vol (Å$^3$) | 2889.2(3) | 4877.6(4) | 2691.3(4) |
| *Z* | 2 | 4 | 2 |
| D(calcd) (Mg/m$^3$) | 1.356 | 1.363 | 1.369 |
| abs coeff (mm$^{-1}$) | 0.475 | 0.493 | 0.503 |
| crystal size (mm$^3$) | 0.54 x 0.10 x 0.08 | 0.30 x 0.10 x 0.08 | 0.38 x 0.16 x 0.10 |
| $\theta$ range for data collection (°) | 0.90-27.50 | 1.61-25.00 | 0.94-27.49 |
| index ranges | -12 ≤ h ≤ 12, -17 ≤ k ≤17, -29 ≤ l ≤ 29 | -18 ≤ h ≤ 17, -22 ≤ k ≤15, -21 ≤ l ≤ 21 | -13 ≤ h ≤ 13, -16 ≤ k ≤16, -28 ≤ l ≤ 28 |
| reflcns collcd | 37788 | 28413 | 35862 |
| indepdt reflcns | 13258 [*R*(int) = 0.0820] | 8587 [*R*(int) = 0.0704] | 12358 [*R*(int) = 0.0820] |
| max and min transm | 0.9630 and 0.7837 | 0.9616 and 0.8662 | 0.9514 and 0.8317 |
| data/restraints/params | 13258/0/685 | 8587/0/590 | 12358/5/640 |
| goodness-of-fit on $F^2$ | 1.008 | 1.179 | 1.105 |
| final *R* indices [$I>2\sigma(I)$] | *R*1 = 0.0621, w*R*2 = 0.1256 | *R*1 = 0.0665, w*R*2 = 0.1280 | *R*1 = 0.0538, w*R*2 = 0.1174 |
| *R* indices (all data) | *R*1 = 0.1091, w*R*2 = 0.1455 | *R*1 = 0.0873, w*R*2 = 0.1352 | *R*1 = 0.0692, w*R*2 = 0.1244 |
| largest diff peak and hole (e. Å$^{-3}$) | 1.095 and -0.683 | 0.822 and -0.921 | 1.322 and -0.711 |

[a]Temperature 223(2) K. [b]Crystals of **5.3**, **5.4** and **5.6** were all grown by slow diffusion of hexane into their concentrated THF solutions.

**Table 5.3** Crystal data and structure refinement of **5.9**, **5.14** and **5.15**.[a,b]

| Complex | **5.9** | **5.14** | **5.15** |
|---|---|---|---|
| empirical formula | $C_{18}H_{11}BrN_3O_3Re$ | $C_{67}H_{55}F_6FeN_3O_{4.5}P_3ReRu$ | $C_{72}H_{64}F_6FeN_4O_5P_3ReRu$ |
| fw | 583.41 | 1526.19 | 1615.30 |
| cryst system | Monoclinic | Triclinic | Monoclinic |
| space group | C2/c | P-1 | P2(1)/n |
| unit cell dimens | *a* = 31.169(2) Å, α = 90° *b* = 7.1260(4) Å, β = 110.967(2)° *c* = 16.8518(8) Å, γ = 90° | *a* = 10.9936(4) Å, α = 76.837(1)° *b* = 15.0032(5) Å, β = 87.376(1)° *c* = 19.5116(6) Å, γ = 76.478(1)° | *a* = 10.7232(4) Å, α = 90° *b* = 16.4535(5) Å, β = 93.891(1)° *c* = 37.860(1) Å, γ = 90° |
| cell vol ($Å^3$) | 3495.1(3) | 3046.7(2) | 6664.3(4) |
| *Z* | 8 | 2 | 4 |
| D(calcd) ($Mg/m^3$) | 2.217 | 1.644 | 1.610 |
| abs coeff ($mm^{-1}$) | 9.263 | 2.610 | 2.394 |
| *F*(000) | 2192 | 1500 | 3232 |
| crystal size ($mm^3$) | 0.26 x 0.12 x 0.10 | 0.33 x 0.20 x 0.12 | 0.36 x 0.16 x 0.12 |
| $\theta$ range for data collection (°) | 2.46-27.47 | 1.43-26.00 | 1.64-25.00 |
| index ranges | $-40 \le h \le 40$, $-9 \le k \le 9$, $-19 \le l \le 21$ | $-13 \le h \le 12$, $-18 \le k \le 18$, $-23 \le l \le 24$ | $-12 \le h \le 12$, $-15 \le k \le 19$, $-45 \le l \le 45$ |
| reflcns collcd | 11888 | 19681 | 38909 |
| indepdt reflcns | 3994 [*R*(int) = 0.0225] | 11983 [*R*(int) = 0.0675] | 11738 [*R*(int) = 0.0797] |
| max and min transm | 0.4577 and 0.1968 | 0.7447 and 0.4534 | 0.7621 and 0.4795 |
| data/restraints/params | 3994/0/235 | 11983/13/778 | 11738/20/838 |
| goodness-of-fit on $F^2$ | 1.052 | 0.997 | 1.001 |
| final *R* indices [$I>2\sigma(I)$] | *R*1 = 0.0177, w*R*2 = 0.0415 | *R*1 = 0.0737, w*R*2 = 0.1319 | *R*1 = 0.0490, w*R*2 = 0.0989 |
| *R* indices (all data) | *R*1 = 0.0204, w*R*2 = 0.0423 | *R*1 = 0.1181, w*R*2 = 0.1652 | *R*1 = 0.0790, w*R*2 = 0.1093 |
| largest diff peak and hole (e. $Å^{-3}$) | 0.595 and -0.547 | 1.251 and -0.984 | 1.087 and -0.533 |

[a]Temperature 223(2) K. [b]Suitable crystals of **5.9**, **5.14** and **5.15** were obtained by slow diffusion from $CH_2Cl_2$/hexane, THF/hexane and THF/$Et_2O$ mixtures, respectively.

**Table 5.4** Crystal data and structure refinement of **5.11** – **5.13**.[a]

| Complex | **5.11** | **5.12**[b] | **5.13** |
|---|---|---|---|
| empirical formula | $C_{62}H_{51}Cl_6F_6FeN_3O_3P_3ReRu$ | $C_{63}H_{52}F_6FeN_4O_3P_3ReRu$ | $C_{68}H_{63}Cl_2F_6FeN_3O_3P_3ReRu$ |
| fw | 1648.79 | 1463.12 | 1591.14 |
| temp (K) | 243(2) | 223(2) | 223(2) |
| cryst system | Triclinic | Orthorhombic | Monoclinic |
| space group | P-1 | Pna2(1) | P2(1)/c |
| unit cell dimens | *a* = 11.3707(6) Å, α = 74.436(1)° *b* = 16.6896(8) Å, β = 83.073(1)° *c* = 17.4696(9) Å, γ = 82.149(1)° | *a* = 16.589(1) Å, α = 90° *b* = 14.2533(9) Å, β = 90° *c* = 24.617(2) Å, γ = 90° | *a* = 11.8417(3) Å, α = 90° *b* = 10.4494(3) Å, β = 93.128(1)° *c* = 54.218(2) Å, γ = 90° |
| cell vol (Å$^3$) | 3151.5(3) | 5820.5(7) | 6698.8(3) |
| *Z* | 2 | 4 | 4 |
| D(calcd) (Mg/m$^3$) | 1.738 | 1.670 | 1.578 |
| abs coeff (mm$^{-1}$) | 2.776 | 2.728 | 2.454 |
| *F*(000) | 1628 | 2904 | 3176 |
| crystal size (mm$^3$) | 0.28 x 0.24 x 0.10 | 0.40 x 0.08 x 0.02 | 0.34 x 0.20 x 0.08 |
| $\theta$ range for data collection (°) | 1.52-27.47 | 0.83-27.49 | 1.50-25.00 |
| index ranges | -14 ≤ h ≤ 14, -21 ≤ k ≤21, -22 ≤ l ≤ 22 | -21 ≤ h ≤ 21, -18 ≤ k ≤16, -28 ≤ l ≤ 31 | -14 ≤ h ≤ 11, -12 ≤ k ≤12, -64 ≤ l ≤ 64 |
| reflcns collcd | 41593 | 42083 | 38509 |
| indepdt reflcns | 14407 [*R*(int) = 0.0609] | 12734 [*R*(int) = 0.0947] | 11798 [*R*(int) = 0.0833] |
| max and min transm | 0.7688 and 0.5104 | 0.9475 and 0.4083 | 0.8278 and 0.4891 |
| data/restraints/params | 14407/13/783 | 12734/1/741 | 11798/4/808 |
| goodness-of-fit on $F^2$ | 1.070 | 1.052 | 1.234 |
| final *R* indices [$I>2\sigma(I)$] | *R*1 = 0.0588, w*R*2 = 0.1319 | *R*1 = 0.0651, w*R*2 = 0.0997 | *R*1 = 0.0886, w*R*2 = 0.1788 |
| *R* indices (all data) | *R*1 = 0.0762, w*R*2 = 0.1382 | *R*1 = 0.0911, w*R*2 = 0.1107 | *R*1 = 0.1045, w*R*2 = 0.1796 |
| largest diff peak and hole (e. Å$^{-3}$) | 1.621 and -1.246 | 2.175 and -1.086 | 1.557 and -3.591 |

[a]Crystals of **5.11** and **5.13** were grown by slow diffusion of $Et_2O$ into their concentrated $CH_2Cl_2$ solutions whereas suitable crystal **5.12** was obtained similarly from the THF/hexane mixture. [b]The Flack parameter for complex **5.12** is 0.00(8).

**Table 5.5** Crystal data and structure refinement of **5.19** – **5.21**.[a]

| Complex | **5.19** | **5.20** | **5.21** |
|---|---|---|---|
| empirical formula | $C_{119}H_{106}Cl_6N_2P_8PdRu_2$ | $C_{119}H_{106}Cl_6N_2P_8PtRu_2$ | $C_{125}H_{121}Cl_2N_2OP_8PdRu_2$ |
| fw | 2333.06 | 2421.75 | 2294.44 |
| temp (K) | 243(2) | 223(2) | 223(2) |
| cryst system | Triclinic | Triclinic | Triclinic |
| space group | P-1 | P-1 | P-1 |
| unit cell dimens | *a* = 13.0704(5) Å, α = 76.016(1)° *b* = 13.6102(5) Å, β = 74.898(1)° *c* = 16.9427(6) Å, γ = 63.853(1)° | *a* = 13.0498(8) Å, α = 75.932(1)° *b* = 13.5372(8) Å, β = 74.578(2)° *c* = 16.919(1) Å, γ = 64.164(2)° | *a* = 12.367(6) Å, α = 89.16(4)° *b* = 18.184(8) Å, β = 76.40(4)° *c* = 25.43(1) Å, γ = 86.06(4)° |
| cell vol (Å$^3$) | 2584.0(2) | 2565.2(3) | 5545(4) |
| *Z* | 1 | 1 | 2 |
| D(calcd) (Mg/m$^3$) | 1.499 | 1.568 | 1.374 |
| abs coeff (mm$^{-1}$) | 0.792 | 1.984 | 0.644 |
| *F*(000) | 1190 | 1222 | 2362 |
| crystal size (mm$^3$) | 0.14 x 0.10 x 0.08 | 0.30 x 0.08 x 0.06 | 0.38 x 0.20 x 0.10 |
| $\theta$ range for data collection (°) | 1.88-26.00 | 1.69-25.00 | 1.65-25.00 |
| index ranges | $-16 \le h \le 16$, $-16 \le k \le 16$, $-20 \le l \le 20$ | $-15 \le h \le 15$, $-16 \le k \le 16$, $-20 \le l \le 20$ | $-14 \le h \le 14$, $-21 \le k \le 21$, $-30 \le l \le 30$ |
| reflcns collcd | 30561 | 27968 | 44471 |
| indepdt reflcns | 10149 [*R*(int) = 0.0791] | 9037 [*R*(int) = 0.1114] | 19532 [*R*(int) = 0.1018] |
| max and min transm | 0.9394 and 0.8972 | 0.8902 and 0.5875 | 0.9384 and 0.7919 |
| data/restraints/params | 10149/6/628 | 9037/15/628 | 19532/18/1251 |
| goodness-of-fit on $F^2$ | 1.010 | 1.145 | 1.121 |
| final *R* indices [$I>2\sigma(I)$] | *R*1 = 0.0600, w*R*2 = 0.1210 | *R*1 = 0.0829, w*R*2 = 0.1574 | *R*1 = 0.1042, w*R*2 = 0.1948 |
| *R* indices (all data) | *R*1 = 0.0943, w*R*2 = 0.1338 | *R*1 = 0.1070, w*R*2 = 0.1671 | *R*1 = 0.1601, w*R*2 = 0.2171 |
| largest diff peak and hole (e. Å$^{-3}$) | 0.675 and -0.774 | 1.715 and -2.461 | 1.088 and -1.272 |

[a]Crystals of **5.19** and **5.20** were obtained from their concentrated $CH_2Cl_2$ solutions whereas suitable crystal **5.21** was grown by slow diffusion of hexane into its concentrated THF solution.

**Table 5.6** Crystal data and structure refinement of **5.17**, **5.18** and **5.22**.[a]

| Complex | **5.17** | **5.18** | **5.22** |
|---|---|---|---|
| empirical formula | $C_{117}H_{102}Cl_{10}N_2P_8PdRu_2$ | $C_{118}H_{104}Cl_4N_2OP_8PtRu_2$ | $C_{100}H_{90}Cl_2Fe_2N_2O_2P_4PdRu_2$ |
| fw | 2446.81 | 2352.82 | 1966.76 |
| temp (K) | 223(2) | 293(2) | 223(2) |
| cryst system | Triclinic | Monoclinic | Triclinic |
| space group | P-1 | P2(1)/n | P-1 |
| unit cell dimens | *a* = 10.7826(6) Å, α = 94.691(1)° *b* = 11.4946(6) Å, β = 102.727(1)° *c* = 24.089(1) Å, γ = 106.061(1)° | *a* = 10.177(2) Å, α = 90° *b* = 31.291(5) Å, β = 97.706(4)° *c* = 17.958(3) Å, γ = 90° | *a* = 10.9644(6) Å, α = 82.092(1)° *b* = 13.7758(7) Å, β = 80.015(1)° *c* = 14.6407(8) Å, γ = 76.863(1)° |
| cell vol ($Å^3$) | 2765.9(3) | 5667(2) | 2109.7(2) |
| *Z* | 1 | 2 | 1 |
| D(calcd) ($Mg/m^3$) | 1.469 | 1.379 | 1.548 |
| abs coeff ($mm^{-1}$) | 0.8376 | 1.749 | 1.087 |
| *F*(000) | 1242 | 2376 | 1000 |
| crystal size ($mm^3$) | 0.20 x 0.14 x 0.04 | 0.16 x 0.08 x 0.06 | 0.28 x 0.10 x 0.10 |
| $\theta$ range for data collection (°) | 1.87-27.50 | 1.73-25.00 | 1.42-27.50 |
| index ranges | $-13 \le h \le 13$, $-14 \le k \le 14$, $-31 \le l \le 17$ | $-12 \le h \le 11$, $-36 \le k \le 37$, $-21 \le l \le 21$ | $-14 \le h \le 14$, $-17 \le k \le 17$, $-19 \le l \le 19$ |
| reflcns collcd | 19911 | 32602 | 28081 |
| indepdt reflcns | 12637 [*R*(int) = 0.0539] | 9949 [*R*(int) = 0.0585] | 9691 [*R*(int) = 0.0505] |
| max and min transm | 0.9673 and 0.8505 | 0.9023 and 0.7672 | 0.8991 and 0.7506 |
| data/restraints/params | 12637/8/646 | 9949/39/638 | 9691/0/520 |
| goodness-of-fit on $F^2$ | 0.968 | 1.097 | 1.086 |
| final *R* indices [$I>2\sigma(I)$] | *R*1 = 0.0669, w*R*2 = 0.1241 | *R*1 = 0.0593, w*R*2 = 0.1357 | *R*1 = 0.0508, w*R*2 = 0.1112 |
| *R* indices (all data) | *R*1 = 0.1251, w*R*2 = 0.1425 | *R*1 = 0.0801, w*R*2 = 0.1453 | *R*1 = 0.0674, w*R*2 = 0.1182 |
| largest diff peak and hole (e. $Å^{-3}$) | 0.890 and -0.573 | 1.106 and -1.296 | 0.901 and -0.409 |

[a]Crystals of **5.17**, **5.18** and **5.22** were grown by slow diffusion from THF/hexane, $CH_2Cl_2$/hexane and THF/hexane mixtures, respectively.

**Table 5.7** Crystal data and structure refinement of **5.23**, **5.24** and **5.27**.[a,b]

| Complex | **5.23** | **5.24** | **5.27** |
|---|---|---|---|
| Empirical formula | $C_{100}H_{90}Cl_2Fe_2N_2O_2P_4PtRu_2$ | $C_{102}H_{90}Cl_4Fe_2N_2O_{12}P_4Rh_2Ru_2$ | $C_{136}H_{158}Fe_2N_2O_{14}P_4Rh_2Ru_2$ |
| fw | 2055.45 | 2321.10 | 2688.18 |
| cryst system | Triclinic | Orthorhombic | Monoclinic |
| space group | P-1 | Pbcn | P2(1)/n |
| unit cell dimens | *a* = 10.9657(7) Å, α = 82.104(1)° *b* = 13.7951(9) Å, β = 80.018(1)° *c* = 14.642(1) Å, γ = 76.837(1)° | *a* = 34.3174(9) Å, α = 90° *b* = 20.5762(6) Å, β = 90° *c* = 16.9894(5) Å, γ = 90° | *a* = 10.1081(9) Å, α = 90° *b* = 38.924(4) Å, β = 92.817(2)° *c* = 17.839(2) Å, γ = 90° |
| cell vol (Å$^3$) | 2113.0(2) | 11996.6(6) | 7010(1) |
| *Z* | 1 | 4 | 2 |
| D(calcd) (Mg/m$^3$) | 1.615 | 1.285 | 1.274 |
| abs coeff (mm$^{-1}$) | 2.526 | 0.942 | 0.743 |
| *F*(000) | 1032 | 4680 | 2780 |
| crystal size (mm$^3$) | 0.46 x 0.24 x 0.20 | 0.42 x 0.20 x 0.10 | 0.60 x 0.30 x 0.10 |
| $\theta$ range for data collection (°) | 1.93-27.50 | 1.66-25.00 | 1.55-25.00 |
| index ranges | $-14 \le h \le 14$, $-17 \le k \le 17$, $-19 \le l \le 19$ | $-30 \le h \le 40$, $-24 \le k \le 24$, $-20 \le l \le 20$ | $-10 \le h \le 12$, $-46 \le k \le 46$, $-14 \le l \le 21$ |
| reflcns collcd | 25891 | 68370 | 40997 |
| indepdt reflcns | 9700[*R*(int) = 0.1145] | 10562 [*R*(int) = 0.0859] | 12313[*R*(int)=0.0481] |
| max and min transm | 0.6321 and 0.3896 | 0.9117 and 0.6931 | 0.9294 and 0.6642 |
| data/restraints/ params | 9700/35/521 | 10562/28/600 | 12313/28/740 |
| goodness-of-fit on $F^2$ | 1.005 | 1.049 | 1.080 |
| final *R* indices [$I>2\sigma(I)$] | *R*1 = 0.0778, w*R*2 = 0.1277 | *R*1 = 0.0605, w*R*2 = 0.1691 | *R*1 = 0.0577, w*R*2 = 0.1422 |
| *R* indices (all data) | *R*1 = 0.1490, w*R*2 = 0.1484 | *R*1 = 0.0810, w*R*2 = 0.1815 | *R*1 = 0.0756, w*R*2 = 0.1510 |
| largest diff peak and hole (e.Å$^{-3}$) | 1.536 and -0.819 | 1.755 and -1.129 | 0.771 and -0.456 |

[a]Temperature 223(2) K. [b]Crystals of **5.23** and **5.27** were grown by slow diffusion of hexane into their concentrated THF solutions whereas suitable crystal **5.24** was obtained similarly from the $CH_2Cl_2$/hexane mixture.

**Table 5.8** Crystal data and structure refinement of **5.31** and **5.34**.[a,b]

| Complex | **5.31** | **5.34** |
|---|---|---|
| empirical formula | $C_{141.18}H_{146.36}Cl_{17.18}N_2O_{8.41}P_8Rh_2Ru_2$ | $C_{163}H_{194}N_2O_{15}P_8Rh_2Ru_2$ |
| fw | 3270.43 | 3076.92 |
| cryst system | Triclinic | Monoclinic |
| space group | P-1 | P2(1)/c |
| unit cell dimens | *a* = 13.2564(6) Å, α = 110.676(1)° *b* = 17.1649(7) Å, β = 104.478(1)° *c* = 19.4726(8) Å, γ = 100.279(1)° | *a* = 12.397(1) Å, α = 90° *b* = 35.814(3) Å, β = 102.968(2)° *c* = 18.361(2) Å, γ = 90° |
| cell vol ($Å^3$) | 3835.9(3) | 7944(1) |
| *Z* | 1 | 2 |
| D(calcd) ($Mg/m^3$) | 1.416 | 1.286 |
| abs coeff ($mm^{-1}$) | 0.840 | 0.530 |
| *F*(000) | 1665 | 3208 |
| crystal size ($mm^3$) | 0.50 x 0.40 x 0.20 | 0.50 x 0.14 x 0.14 |
| $\theta$ range for data collection (°) | 1.68-25.00 | 1.61-23.30 |
| index ranges | -15 ≤ h ≤ 15, -20 ≤ k ≤20, -23 ≤ l ≤ 23 | -13 ≤ h ≤ 13, -39 ≤ k ≤39, -14 ≤ l ≤ 20 |
| reflcns collcd | 41936 | 39661 |
| indepdt reflcns | 13494 [*R*(int) = 0.0287] | 11420 [*R*(int) = 0.0482] |
| max and min transm | 0.8500 and 0.6788 | 0.9295 and 0.7774 |
| data/restraints/params | 13494/50/930 | 11420/112/932 |
| goodness-of-fit on $F^2$ | 1.059 | 1.079 |
| final *R* indices [$I>2\sigma(I)$] | *R*1 = 0.0367, w*R*2 = 0.0963 | *R*1 = 0.0491, w*R*2 = 0.1203 |
| *R* indices (all data) | *R*1 = 0.0438, w*R*2 = 0.1002 | *R*1 = 0.0610, w*R*2 = 0.1264 |
| largest diff peak and hole(e. $Å^{-3}$) | 0.869 and -0.498 | 0.635 and -0.376 |

[a]Temperature 223(2) K. [b]Crystal of **5.31** was grown by slow diffusion of hexane into their concentrated THF solution whereas suitable crystal **5.34** was obtained similarly from the $CH_2Cl_2$/hexane mixture.

Most of complexes were crystallized as solvated molecules. They are summarized in **Table 5.9**.

**Table 5.9** Complexes crystallized as solvated molecules

| Complex | No. of solvent molecules | | | | | |
|---|---|---|---|---|---|---|
| | THF | $CH_2Cl_2$ | $H_2O$ | $CH_3CN$ | Hexane | MeOH |
| **5.2** | | | 2 | | | |
| **5.3** | 2 | | | | | |
| **5.6** | 1 | | | | | |
| **5.7** | 1 | | | | | |
| **5.11** | | 3 | | | | |
| **5.12** | | | | 1 | | |
| **5.13** | | 2 | | | | |
| **5.14** | 2 | | | | | |
| **5.15** | 2 | | | | | |
| **5.17** | | $1^1/_2$ | | | | |
| **5.18** | 1 | | | | | |
| **5.19** | | 1/2 | | | | |
| **5.20** | | 1/2 | | | | |
| **5.21** | 1 | | | | 1/2 | |
| **5.22** | 1 | | | | | |
| **5.23** | 1 | | | | | |
| **5.24** | | 1 | 2 | | | |
| **5.27** | 4 | | | | | |
| **5.31** | | 4 | | | | |
| **5.34** | 3 | | | | | 1/2 |

Several molecules show disordered atoms. Two of the $CH_2Cl_2$ out of the three molecules in **5.11** are slightly disordered and one THF molecule in **5.14** disordered. In **5.19**, one half of $CH_2Cl_2$ is disordered. The $CH_2Cl_2$ in **5.20** is disordered into two positions at 75:25 ratio. The four THF in **5.27,** three THF and half a MeOH in **5.34** have large thermal parameters and are not stable towards to refinement, indicating that the solvents are loosely held. In **5.24**, the $CH_2Cl_2$ is disordered into two parts sharing one Cl (Cl1A). The $CH_2Cl_2$ solvent molecules in **5.31** have bad thermal

parameters and with a number of large residual peaks. A disorder scheme was introduced to reduce the residual peaks and the overall R values. This disorder scheme involves splitting of two of the $CH_2Cl_2$ and partial replacement of the remaining two by $CH_2Cl_2$ and $H_2O$. This disorder is probably due to partial losing of the solvent during data collection.

## 5.3 Syntheses and Reactions

### 5.3.1 Syntheses of Monometallic Ru(II) Acetylide or Vinylidene Complexes

#### 5.3.1.1 Material Information

4-Ethynylpyridine hydrochloride, NaOH, $NaPF_6$ and $AgPF_6$ were obtained from Aldrich and used without further purification. *trans*- and *cis*-$[RuCl_2(dppm)_2]$,[196,197] *trans*- and *cis*-$[RuCl_2(dppe)_2]$[196,198] $[RuCpCl(dppf)]$[199] and $[RuCpCl(PPh_3)_2]$[200] were prepared according to the literature methods.

#### 5.3.1.2 Syntheses

***trans*-[RuCl(C≡Cpy-4)(dppm)$_2$] (5.1)**

A mixture of *cis*-$[RuCl_2(dppm)_2]$ (197 mg, 0.21 mmol), $NaPF_6$ (102 mg, 0.61 mmol) and HC≡Cpy-4·HCl (67 mg, 0.48 mmol) in $CH_2Cl_2$/MeOH (40 mL, 3:1 v/v) was stirred overnight at r.t. The solvent was then removed under reduced pressure and the resulting residue purified by column chromatography on neutral alumina using

THF-hexane (1:2) as eluent, giving **5.1** as a yellow product (95 mg (45%)). $^{1}$H NMR (300 MHz, $CDCl_3$, 25°C): δ 4.92 (m, 4H, PC*H*$_2$), 5.83 (d, $J_{H\text{-}H}$ = 6.1 Hz, 2H, py), 7.06-7.44 (m, 40H, Ph), 8.01 (d, $J_{H\text{-}H}$ = 6.1 Hz, 2H, py). $^{31}$P NMR (300 MHz, $CDCl_3$, 25°C): δ -6.0 (s, *P*-$CH_2$). $^{13}$C NMR (300 MHz, $CDCl_3$, 25°C): δ 148.1 (Ru-*C*), 135.7 ($C_\alpha$(py)), 134.7/134.5 (dt ($C_\alpha$-phenyl)), 133.7 ($C_\gamma$(py)), 133.2 (dt, $C_\beta$-phenyl), 129.4/129.2 (d, $C_\delta$-phenyl), 127.6 (dt, $C_\gamma$-phenyl), 125.5 ($C_\beta$(py)), 124.8 (s, Ru-C≡*C*), 50.2 (t, P-*C*$H_2$). ESI-MS ($CH_2Cl_2$, 15 V, 150°C): *m*/*z* (fragment, relative intensity): 1008 ($[M]^+$, 100), 971 ($[M\text{-}Cl]^+$, 10). IR: (KBr) ν(C≡C) 2078 $cm^{-1}$(m). Anal. Calcd for $C_{57}H_{48}ClNP_4Ru$: C 67.92, H 4.77, N 1.39%. Found: C 67.29, H 4.66, N 1.40%.

***trans*-[Ru(C≡Cpy-4)($CH_3CN$)(dppm)$_2$]($PF_6$) (5.2)**

[$PdCl_2(CH_3CN)_2$] (7 mg, 0.026 mmol) was added to a $CH_3CN$ (20 mL) solution of $AgPF_6$ (15 mg, 0.06 mmol) and the mixture refluxed with stirring for 1 h under the protection of light. The resultant yellow suspension was filtered through Celite and then concentrated to ~10 mL *in vacuo*. *trans*-[RuCl(C≡Cpy-4)(dppm)$_2$] (**5.1**) (108 mg, 0.10 mmol) in $CH_2Cl_2$ (30 mL) was added and the mixture stirred for 12 h at r.t. The solvent was removed under reduced pressure and the resulting residue purified by recrystallization from THF-hexane to give **5.2**. Yield 55 mg (47%). $^{1}$H NMR (300 MHz, $CDCl_3$, 25°C): δ 1.55(s, 3H, C*H*$_3$CN), 4.80-5.03 (m, 4H, C*H*$_2$), 6.26 (d, $J_{H\text{-}H}$ = 5.4 Hz, 2H, py), 7.11-7.55 (m, 40H, Ph), 8.25 (d, $J_{H\text{-}H}$ = 5.4 Hz, 2H, py). $^{31}$P NMR (300 MHz, $CDCl_3$, 25°C): δ -7.5 (s, *P*-$CH_2$), -132.0−155.5 (m, *P*$F_6$). $^{13}$C NMR (300 MHz, $CDCl_3$, 25°C): δ 133.1 (s ($C_\alpha$-phenyl)), 132.1 ($C_\gamma$(py)), 131.3 (s, $C_\beta$-phenyl),

130.6 (s, $C_\delta$-phenyl), 129.0 (s, $C_\gamma$-phenyl), 128.4 ($C_\beta$(py)), 124.8 (s, Ru-C≡*C*), 115.0 (s, $CH_3$*C*N), 30.3 (s, P-*C*$H_2$), 2.3 (s, *C*$H_3$CN). Ru-*C* and $C_\alpha$(py) were not detected. ESI-MS ($CH_2Cl_2$, 15 V, 150°C): m/z (fragment, relative intensity): 1012 ($[M]^+$, 100), 971 ($[M\text{-}CH_3CN]^+$, 40), 869 ($[M\text{-}CH_3CN\text{-}C{\equiv}Cpy]^+$, 20). IR: (KBr) ν(C≡C) 2092 $cm^{-1}$(s). Anal. Calcd for $C_{59}H_{51}F_6N_2P_5Ru$: C 61.14, H 4.40, N 2.42%. Found: C 60.87, H 4.53, N 2.48%.

***trans*-[RuCl(C≡Cpy-4)(dppe)$_2$] (5.3)**

A mixture of *cis*-[$RuCl_2$(dppe)$_2$] (203 mg, 0.21 mmol), $NaPF_6$ (102 mg, 0.61 mmol) and HC≡Cpy-4·HCl (67 mg, 0.48 mmol) in $CH_2Cl_2$/MeOH (40 mL, 3:1 v/v) were stirred overnight at r.t. The solvent was then removed under reduced pressure and the resulting residue purified by column chromatography on neutral alumina using THF-hexane (1:2) as eluent, giving **5.3** as a light yellow product (91 mg (42%)). $^1$H NMR (300 MHz, $CDCl_3$, 25°C): δ 2.68 (t, 8H, PC$H_2$), 6.34 (d, $J_{H\text{-}H}$ = 6.1 Hz, 2H, py), 6.92-7.35 (m, 40H, Ph), 8.20 (d, $J_{H\text{-}H}$ = 6.0 Hz, 2H, py). $^{31}$P NMR (300 MHz, $CDCl_3$, 25°C): δ 49.5 (s, *P*-$CH_2$). $^{13}$C NMR (300 MHz, $CDCl_3$, 25°C): δ 148.6 (Ru-*C*), 137.2 ($C_\alpha$(py)), 135.4/135.9 (dt ($C_\alpha$-phenyl)), 134.4 ($C_\gamma$(py)), 133.4 (dt, $C_\beta$-phenyl), 129.0 (d, $C_\delta$-phenyl), 127.0/127.3 (dt, $C_\gamma$-phenyl), 125.5 ($C_\beta$(py)), 124.7 (Ru-C≡*C*), 30.3 (P-*C*$H_2$). ESI-MS ($CH_2Cl_2$, 15 V, 150°C): m/z (fragment, relative intensity): 1070 ($[M+Cl]^+$, 100), 537 ($[RuCl(dppe)]^+$, 70). IR: ($CH_2Cl_2$) ν(C≡C) 2067 $cm^{-1}$ (s). Anal. Calcd for $C_{59}H_{52}ClNRuP_4$: C 68.44, H 5.03, N 1.35%. Found: C 67.93, H 5.17, N 1.38%.

***trans*-[RuH(C≡Cpy-4)(dppe)$_2$] (5.4)**

A mixture of *cis*-[$RuCl_2(dppe)_2$] (203 mg, 0.21 mmol), $NaPF_6$ (102 mg, 0.61 mmol) and HC≡Cpy-4·HCl (67 mg, 0.48 mmol) in $CH_2Cl_2$/MeOH (40 mL, 3:1 v/v) were stirred for 5 h at r.t.. Then NaOH (60 mg, 1.5 mmol) was added and the reaction continued to stir 30 min at r.t.. The solvent was then removed under reduced pressure and the resulting residue purified by column chromatography on neutral alumina using THF-hexane (1:2) as eluent, giving **5.4** as a pale yellow product (128 mg (61%)). $^1$H NMR (300 MHz, $CDCl_3$, 25°C): δ -10.03 (qn, $J_{P-H}$ = 19.0 Hz, 1H, Ru-*H*), 1.98 (m, 4H, C*H*$_2$), 2.46 (m, 4H, C*H*$_2$), 6.83 (d, $J_{H-H}$ = 6.2 Hz, 2H, py), 6.93-7.44 (m, 40H, Ph), 8.31(d, $J_{H-H}$ = 6.1 Hz, 2H, py). $^{31}$P NMR (300 MHz, $CDCl_3$, 25°C): δ 69.0 (s, *P*-$CH_2$). $^{13}$C NMR (300 MHz, $CDCl_3$, 25°C): δ 149.6 (Ru-*C*), 148.7 ($C_\alpha$(py)), 138.6/137.4 (dt ($C_\alpha$-phenyl)), 133.7/133.5 ($C_\gamma$(py)), 128.6/128.4 (dt, $C_\beta$-phenyl), 127.1/127.0 (d, $C_\delta$-phenyl), 125.5 (dt, $C_\gamma$-phenyl), 124.8 ($C_\beta$(py)), 115.3 (Ru-C≡*C*), 32.3 (P-*C*$H_2$). ESI-MS ($CH_2Cl_2$, 15 V, 150°C): m/z (fragment, relative intensity): 1002 ($[M + H]^+$ , 45), 899 ($[RuH(dppe)_2 + H]^+$, 100). IR: ($CH_2Cl_2$) ν(C≡C) 2053 $cm^{-1}$ (s). Anal. Calcd for $C_{59}H_{53}NRuP_4$: C 70.80, H 5.30, N 1.40%. Found: C 70.11, H 5.23, N 1.42%.

***trans*-[RuCl(COCH$_3$=CHpy-4)(dppe)$_2$] (5.5)**

Complex **5.5** was obtained as a minor product with 5% yield (11.0 mg) in the reaction of preparing **5.4**. $^1$H NMR (300 MHz, $CDCl_3$, 25°C): δ 2.66 (s, 8H, C*H*$_2$), 3.74 (3H, OC*H*$_3$), 4.78 (d, $J_{H-H}$ = 17.0 Hz, 1H, CH=C*H*)), 5.71 (d, $J_{H-H}$ = 6.1 Hz, 2H,

Py*H*), 6.91-7.73 (m, 40H, Ph), 8.00 (d, $J_{H\text{-}H}$ = 6.1 Hz, 2H, Py*H*). $^{31}$P NMR (300 MHz, $CDCl_3$, 25°C): δ 53.4 (s). $^{13}$C NMR (300 MHz, $CDCl_3$, 25°C): δ 148.4 (m, Ru-*C*), 145.6 ($C_\alpha$(py)), 137.6/137.7 (dt ($C_\alpha$-phenyl)), 134.8 ($C_\gamma$(py)), 133.6 (dt, $C_\beta$-phenyl), 128.9/129.0 (d, $C_\delta$-phenyl), 127.1/127.6 (dt, $C_\gamma$-phenyl), 125.5 ($C_\beta$(py)), 118.1 (s, Ru-C=*C*H), 30.2 (m, P-*C*$H_2$), 22.6 (CO*C*$H_3$=CH). ESI-MS ($CH_2Cl_2$, 15 V, 150°C): m/z (fragment, relative intensity): 1002 ([M]-Cl-$OCH_3$)$^+$, 35), 897 ([Ru(dppe)$_2$]$^+$, 100). Anal. Calcd for $C_{60}H_{56}ClNORuP_4$: C 67.54, H 5.25, N 1.31%. Found: C 66.01, H 5.43, N 1.32%.

***trans*-[RuCl(CH=CHpy-4)(dppe)$_2$] (5.6)**

Complex **5.6** was obtained during the slow crystallization experiment of a solution of **5.5** in THF/hexane mixture. $^1$H NMR (300 MHz, $CDCl_3$, 25°C): δ 2.66 (s, 8H, C*H*$_2$), 5.71 (d, $J_{H\text{-}H}$ = 6.1 Hz, 2H, py), 6.51 (1H, C*H*=CHpy), 6.56 (1H, CH=C*H*py), 6.91-7.72 (m, 40H, Ph), 8.00 (d, $J_{H\text{-}H}$ = 6.1 Hz, 2H, py). $^{31}$P NMR (300 MHz, $CDCl_3$, 25°C): δ 53.2 (s). ESI-MS ($CH_2Cl_2$, 15 V, 150°C): m/z (fragment, relative intensity): 1002 ([M]-Cl)$^+$, 55), 968 ([RuCl(dppe)$_2$ + Cl]$^+$, 100), 896 ([Ru(dppe)$_2$]$^+$, 50), 502 ([Ru(dppe) + H]$^+$, 80). Anal. Calcd for $C_{59}H_{54}ClNRuP_4$: C 68.34, H 5.21, N 1.35%. Found: C 67.12, H 5.32, N 1.33%.

**[RuCp(C≡Cpy-4)(dppf)] (5.7)**

A mixture of [RuCpCl(dppf)] (378 mg, 0.5 mmol), $NaPF_6$ (218 mg, 1.3 mmol) and HC≡Cpy-4·HCl (140 mg, 1.0 mmol) in $CH_2Cl_2$/MeOH (50 mL, 4:1 v/v) was

stirred for 20 h at r.t. NaOH (68 mg, 1.7 mmol) was added and stirred further for 1 hour. The solvent was then removed under reduced pressure, and the resulting residue purified by column chromatography on neutral alumina using THF-hexane (1:3 v/v) as eluent, giving **5.7** as an orange solid (395 mg, 96%). $^{1}$H NMR (300 MHz, $CDCl_3$, 25°C): δ 4.01 (s, 2H, dppf), 4.19 (s, 2H, dppf), 5.17 (s, 2H, dppf), 5.30 (s, 2H, dppf), 4.32 (s, 5H, Cp), 6.97 (d, $J_{H-H}$ = 6.1 Hz, 2H, py), 7.31-7.81 (m, 20H, Ph), 8.31 (d, $J_{H-H}$ = 6.1 Hz, 2H, py). $^{31}$P NMR (300 MHz, $CDCl_3$, 25°C): δ 55.5 (s, dppf). $^{13}$C NMR (300 MHz, $CDCl_3$, 25°C): δ 149.1(Ru-*C*), 137.6–125.3 (Ph, py), 111.8 (Cp) 73.2–68.1 (Fc). ESI-MS ($CH_2Cl_2$, 15 V, 150°C): m/z (fragment, relative intensity): 824 ($[M + H]^+$, 100). IR: ($CH_2Cl_2$) ν(C≡C) 2068 $cm^{-1}$(s). Anal. Calcd for $C_{46}H_{37}FeNRuP_2$: C 67.15, H 4.50, N 1.70%. Found: C 66.92, H 4.58, N 1.73%.

**[RuCp(C≡Cpy-4)($PPh_3$)$_2$] (5.8)**

Complex **5.8** was synthesized similar to the procedure for **5.7**, except that [RuCpCl($PPh_3$)$_2$] was used instead of [RuCpCl(dppf)]. The yellow product **5.8** was isolated in 95% yield. $^{1}$H NMR (300 MHz, $CDCl_3$, 25°C): δ 4.35 (s, 5H, Cp), 6.87 (d, $J_{H-H}$ = 6.2 Hz, 2H, py), 7.07-7.45 (m, 30H, Ph), 8.26 (d, $J_{H-H}$ = 6.1 Hz, 2H, py). $^{31}$P NMR (300 MHz, $CDCl_3$, 25°C): δ 50.8 (s, *P*$Ph_3$). ESI-MS ($CH_2Cl_2$, 15 V, 150°C): m/z (fragment, relative intensity): 793 ($[M + H]^+$, 100). Anal. Calcd for $C_{48}H_{39}NRuP_2$: C 72.73, H 4.92, N 1.77%. Found: C 71.09, H 5.13, N 1.80%.

## 5.3.2 Syntheses of $d^5 - d^6$ Heterobimetallic Complexes

### 5.3.2.1 Material Information

2,2'-Bipyridine (bpy), 4,4'-dimethyl-2,2'-bipyridine ($Me_2bpy$), 4,4'-di-tert-butyl-2,2'-bipyridine ($^tBu_2bpy$), 1,10-phenanthroline (phen) and 2,2',6,6'-terpyridine (tpy) were obtained from Aldrich and used as received. *fac*-[$ReBr(CO)_3(N\text{-}N)$] were prepared in quantitative yield from the reflux of an equimolar mixture of [$ReBr(CO)_5$][201] and the corresponding heterocyclic nitrogen ligands (bpy, $Me_2bpy$, $^tBu_2bpy$, phen, tpy) in toluene for 4 h.[202] *fac*-[$Re(CH_3CN)(CO)_3(N\text{-}N)](PF_6)$ were prepared by refluxing an equimolar amounts of *fac*-[$ReBr(CO)_3(N\text{-}N)$] and $AgPF_6$ in $CH_3CN$ overnight, which is a modification of the reported procedure for *fac*-[$Re(OTf)(CO)_3(bpy)$] (OTf = $CF_3SO_3^-$).[126] The synthesis and characterization data of the new compounds *fac*-[$ReBr(CO)_3(tpy)$] and *fac*-[$Re(CH_3CN)(CO)_3(tpy)](PF_6)$ are given below.

### 5.3.2.2 Syntheses

#### *fac*-[$ReBr(CO)_3(tpy)$] (5.9)

A mixture of [$ReBr(CO)_5$] (812 mg, 2.0 mmol) and tpy (466 mg, 2.0 mmol) in toluene (50 mL) was heated to reflux for 4 h. The solvent was removed under vacuum and the resultant residue washed 3 times with $Et_2O$ to afford **5.9** as a bright yellow solid with yield > 95% (> 1.1 g). $^1H$ NMR (300 MHz, $CDCl_3$, 25°C): δ 7.51 (q, $J_{H\text{-}H}$ = 6.1 Hz, 2H, tpy), 7.74 (d, $J_{H\text{-}H}$ = 7.2 Hz, 1H, tpy), 7.90 (m, 2H, tpy), 8.11 (m, 2H, tpy), 8.26 (t, $J_{H\text{-}H}$ = 7.7 Hz, 2H, tpy), 8.82 (d, $J_{H\text{-}H}$ = 4.6 Hz, 1H, tpy), 9.11 (d, $J_{H\text{-}H}$ = 5.8 Hz, 1H,

tpy). $^{13}$C NMR (300 MHz, $CDCl_3$, 25°C): δ 122.5-162.5 (tpy), 189.5, 193.2, 196.6 (*C*O). ESI-MS ($CH_2Cl_2$, 15 V, 150°C): m/z (fragment, relative intensity): 584 ([M + H]$^+$, 100), 503 ([M - Br]$^+$, 35). IR: ($CH_2Cl_2$) ν(C≡O) 2024(s), 1923(s), 1899(s) cm$^{-1}$. Anal. Calcd for $C_{18}H_{11}BrN_3O_3Re$: C 37.05, H 1.89, N 7.20%. Found: C 36.68, H 1.93, N 7.31%.

***fac*-[Re(CH$_3$CN)(CO)$_3$(tpy)](PF$_6$) (5.10)**

A mixture of *fac*-[ReBr(CO)$_3$(tpy)] (**5.9**) (583 mg, 1.0 mmol) and $AgPF_6$ (278 mg, 1.1 mmol) was heated to reflux in $CH_3CN$ (30 mL) with protection from light for 12 h. The solvent was removed under vacuum and the residue purified by recrystallization from $CH_2Cl_2$/$Et_2O$. Yield 620 mg (90%). $^1$H NMR (300 MHz, $CDCl_3$, 25°C): δ 1.58 (s, 3H, C*H*$_3$CN), 7.48 (m, 2H, tpy), 7.72 (d, $J_{H-H}$ = 7.0 Hz, 1H, tpy), 7.88 (m, 2H, tpy), 8.09 (m, 2H, tpy), 8.25 (t, $J_{H-H}$ = 7.6 Hz, 2H, tpy), 8.81 (d, $J_{H-H}$ = 4.4 Hz, 1H, tpy), 9.10 (d, $J_{H-H}$ = 5.5 Hz, 1H, tpy). $^{31}$P NMR (300 MHz, $CDCl_3$, 25°C): -143.6 (m, $J_{P-F}$ = 712.6 Hz, $PF_6$). $^{13}$C NMR (300 MHz, $CDCl_3$, 25°C): δ 65.8 (*C*H$_3$CN), 124.5-153.4 (tpy), 188.6, 192.9, 194.9 (*C*O). ESI-MS ($CH_2Cl_2$, 15 V, 150°C): m/z (fragment, relative intensity): 545 ([M + H]$^+$, 25), 504 ([M-CH$_3$CN]$^+$, 100). IR: ($CH_2Cl_2$) ν(C≡O) 2036(s), 1928(s) cm$^{-1}$. The ν(C≡N) is obscured by the strong ν(C≡O) at 2036(s) cm$^{-1}$. Anal. Calcd for $C_{20}H_{14}F_6N_4O_3PRe$: C 34.83, H 2.03, N 8.13%. Found: C 34.26, H 2.15, N 8.20%.

**[RuCp(C≡Cpy-4)(dppf)][Re(CO)$_3$(bpy)](PF$_6$) (5.11)**

[RuCp(C≡Cpy-4)(dppf)] (**5.7**) (82 mg, 0.1 mmol) and *fac*-[Re(CH$_3$CN)(CO)$_3$(bpy)](PF$_6$) (**5.10**) (61 mg, 0.10 mmol) were mixed and heated to reflux in THF (30 mL) under $N_2$ for 12 h. The solvent was removed under vacuum and the resulting residue purified by recrystallization from THF/hexane (5:1). Yield 80 mg (57%). $^1$H NMR (300 MHz, $CDCl_3$, 25°C): δ 4.03 (s, 2H, dppf), 4.25 (s, 2H, dppf), 4.31 (s, 2H, dppf), 4.97 (s, 2H, dppf), 4.29 (s, 5H, Cp), 6.79 (d, 2H, $J_{H-H}$ = 6.6 Hz, py), 7.24-7.65 (m, 22H, py & Ph), 7.72 (t, 2H, $J_{H-H}$ = 6.6 Hz, bpy), 8.35 (t, 2H, $J_{H-H}$ = 7.9 Hz, bpy), 8.69 (d, 2H, $J_{H-H}$ = 8.4 Hz, bpy), 9.05 (d, 2H, $J_{H-H}$ = 4.8 Hz, bpy). $^{31}$P NMR (300 MHz, $CDCl_3$, 25°C): δ 55.4 (s, dppf), -143.6 (m, $J_{P-F}$ = 712.6 Hz, $PF_6$). $^{13}$C NMR (300 MHz, $CDCl_3$, 25°C): δ 68.6-75.8 (Fc), 85.5 (Cp), 114.9 (Ru-C≡*C*), 125.5-133.9 (Ph), 129.4, 141.6, 152.5, 155.8 ($C_5H_4N$), 149.7 (Ru-*C*). Carbons from COs were not detected. ESI-MS ($CH_2Cl_2$, 15 V, 150°C): m/z (fragment, relative intensity): 1250 ([M + H]$^+$, 100). IR: ($CH_2Cl_2$) ν(C≡O) 2028(s), 1928(s) cm$^{-1}$. Anal. Calcd for $C_{59}H_{45}F_6N_3O_3P_3FeReRu$: C 50.83, H 3.23, N 3.02%. Found: C 51.09, H 3.68, N 3.00%.

Complexes **5.12**-**5.16** follow a synthetic procedure similar to that of **5.11**. Their data are given below.

**[RuCp(C≡Cpy-4)(dppf)][Re(CO)$_3$(Me$_2$bpy)](PF$_6$) (5.12)**

The orange solid of **5.12** was isolated in 77% yield (110 mg). $^1$H NMR (300 MHz, $CDCl_3$, 25°C): δ 2.68 (s, 6H, C*H*$_3$), 4.03 (s, 2H, dppf), 4.26-4.32 (9H, 4H from dppf and 5H from Cp), 4.99 (s, 2H, dppf), 6.80 (d, $J_{H\text{-}H}$ = 6.7 Hz, 2H, py), 7.27-7.66 (m, 24H, py & Ph & bpy), 8.59 (s, 2H, bpy), 8.81 (d, $J_{H\text{-}H}$ = 5.6 Hz, 2H, bpy). $^{31}$P NMR (300 MHz, $CDCl_3$, 25°C): δ 55.4 (s, dppf), -143.5 (m, $J_{P\text{-}F}$ = 712.6 Hz, $PF_6$). $^{13}$C NMR (300 MHz, $CDCl_3$, 25°C): δ 21.6 (*C*H$_3$), 68.6-75.8 (Fc), 85.5 (Cp), 114.7 (Ru-C≡*C*), 126.6-134.0 (Ph), 149.8 (Ru-*C*), 129.4, 140.2, 151.6, 154.8, 155.6 (bpy). Carbons from COs were not detected. ESI-MS ($CH_2Cl_2$, 15 V, 150°C): m/z (fragment, relative intensity): 1278 ($[M + H]^+$, 100). IR: ($CH_2Cl_2$) ν(C≡O) 2027(s), 1925(s) cm$^{-1}$. Anal. Calcd for $C_{61}H_{49}F_6N_3O_3P_3FeReRu$: C 51.51, H 3.45, N 2.96%. Found: C 51.94, H 3.29, N 2.92%.

**[RuCp(C≡Cpy-4)(dppf)][Re(CO)$_3$($^t$Bu$_2$bpy)](PF$_6$) (5.13)**

The orange solid of **5.13** was isolated in 50% yield (75 mg). $^1$H NMR (300 MHz, $CDCl_3$, 25°C): δ 1.43 (s, 18H, C*H*$_3$), 4.01 (s, 2H, dppf), 4.29 (7H, 2H from dppf & 5H from Cp)), 4.34 (s, 2H, dppf), 5.06 (s, 2H, dppf), 6.93 (d, $J_{H\text{-}H}$ = 6.6 Hz, 2H, py), 7.24-7.66 (m, 22H, py & Ph), 7.75 (d, $J_{H\text{-}H}$ = 6.6 Hz, 2H, bpy), 8.42 (s, 2H, bpy), 8.88 (d, $J_{H\text{-}H}$ = 5.9 Hz, 2H, bpy). $^{31}$P NMR (300 MHz, $CDCl_3$, 25°C): δ 55.6 (s, dppf), -143.8 (m, $J_{P\text{-}F}$ = 712.6 Hz, $PF_6$). $^{13}$C NMR (300 MHz, $CDCl_3$, 25°C): δ 30.1 (*C*H$_3$), 68.4-73.2 (Fc), 85.5 (Cp), 122.1 (Ru-C≡*C*), 125.5-134.1 (Ph), 150.3, 152.3, 155.8, 166.0 (bpy). Carbons from COs were not detected. ESI-MS ($CH_2Cl_2$, 15 V, 150°C):

m/z (fragment, relative intensity): 1362 ($[M + H]^+$, 100). IR: ($CH_2Cl_2$) ν(C≡O) 2027(s), 1926(s) $cm^{-1}$. Anal. Calcd for $C_{67}H_{61}F_6N_3O_3P_3FeReRu$: C 53.42, H 4.05, N 2.79%. Found: C 52.96, H 4.17, N 2.82%.

**[RuCp(C≡Cpy-4)(dppf)][Re(CO)$_3$(phen)](PF$_6$) (5.14)**

The orange solid of **5.14** was isolated in 56% yield (80 mg). $^1$H NMR (300 MHz, $CDCl_3$, 25°C): δ 4.01 (s, 2H, dppf), 4.25 (7H, 2H from dppf and 5H from Cp), 4.28 (s, 2H, dppf), 4.93 (s, 2H, dppf), 6.75 (d, $J_{H-H}$ = 6.8 Hz, 2H, py), 7.19-7.62 (m, 20H, Ph), 7.73 (d, $J_{H-H}$ = 6.8Hz, 2H, py), 8.15 (m, 4H, phen), 8.82 (d, $J_{H-H}$ = 6.9 Hz, 2H, phen), 9.52 (d, $J_{H-H}$ = 3.8 Hz, 2H, phen). $^{31}$P NMR (300 MHz, $CDCl_3$, 25°C): δ 55.4 (s, dppf), -143.6 (m, $J_{P-F}$ = 712.6 Hz, $PF_6$). $^{13}$C NMR (300 MHz, $CDCl_3$, 25°C): δ 68.6-73.2 (Fc), 85.5 (Cp), 114.7 (Ru-C≡*C*), 125.5-135.8 (Ph & phen), 140.4, 146.5, 153.4 (phen), 149.7 (Ru-*C*). Carbons from COs were not detected. ESI-MS ($CH_2Cl_2$, 15 V, 150°C): m/z (fragment, relative intensity): 1274 ($[M + H]^+$, 100). IR: ($CH_2Cl_2$) ν(C≡O) 2029(s), 1929(s) $cm^{-1}$. Anal. Calcd for $C_{61}H_{45}F_6N_3O_3P_3FeReRu$: C 51.66, H 3.18, N 2.96%. Found: C 51.49, H 3.58, N 2.92%.

**[RuCp(C≡Cpy-4)(dppf)][Re(CO)$_3$(tpy)](PF$_6$) (5.15)**

The orange product **5.15** was isolated in 48% yield (70 mg). $^1$H NMR (300 MHz, $CDCl_3$, 25°C): δ 4.03 (s, 2H, dppf), 4.23 (s, 2H, dppf), 4.30-4.32 (7H, 2H from dppf and 5H from Cp), 4.95 (s, 2H, dppf), 6.70 (d, $J_{H-H}$ = 6.8 Hz, 2H, py), 7.28-7.77 (m, 25H, py & Ph & tpy), 7.89 (d, $J_{H-H}$ = 7.1 Hz, 1H, tpy), 7.97 (t, $J_{H-H}$ = 7.6 Hz, 1H, tpy),

8.39 (t, $J_{H-H}$ = 7.9 Hz, 2H, tpy), 8.66 (q, $J_{H-H}$ = 7.7 Hz, 2H, tpy), 8.85 (d, $J_{H-H}$ = 4.0 Hz, 1H, tpy), 9.12 (d, $J_{H-H}$ = 5.1 Hz, 1H, tpy). $^{31}$P NMR (300 MHz, $CDCl_3$, 25°C): δ 55.3 (s, dppf), -143.6 (m, $J_{P-F}$ = 712.6 Hz, $PF_6$). $^{13}$C NMR (300 MHz, $CDCl_3$, 25°C): δ 68.6-75.7 (Fc), 85.5 (Cp), 114.9 (Ru-C≡*C*), 125.5-135.7 (Ph & tpy), 137.3, 140.0, 140.8, 141.7, 151.5 (tpy), 149.9 (Ru-*C*). Carbons from COs were not detected. ESI-MS ($CH_2Cl_2$, 15 V, 150°C): m/z (fragment, relative intensity): 1326 ($[M + H]^+$, 100). IR: ($CH_2Cl_2$) ν(C≡O) 2028(s), 1930(s) $cm^{-1}$. Anal. Calcd for $C_{64}H_{48}F_6N_4O_3P_3FeReRu$: C 52.24, H 3.27, N 3.81%. Found: C 51.87, H 3.79, N 3.95%.

**[RuCp(C≡Cpy-4)($PPh_3$)$_2$][Re(CO)$_3$(bpy)]($PF_6$) (5.16)**

The yellow product **5.16** was isolated in 53% yield (72 mg). $^1$H NMR (300 MHz, $CDCl_3$, 25°C): δ 4.32 (s, 5H, Cp), 6.65 (d, $J_{H-H}$ = 6.6 Hz, 2H, py), 7.05-7.32 (m, 30H, Ph), 7.56 (d, $J_{H-H}$ = 6.7 Hz, 2H, py), 7.71 (t, $J_{H-H}$ = 6.6 Hz, 2H, bpy), 8.35 (t, $J_{H-H}$ = 8.0 Hz, 2H, bpy), 8.69 (d, $J_{H-H}$ = 8.4 Hz, 2H, bpy), 9.03 (d, $J_{H-H}$ = 5.4 Hz, 2H, bpy). $^{31}$P NMR (300 MHz, $CDCl_3$, 25°C): δ 50.7 (s, *P*$Ph_3$), -143.6 (m, $J_{P-F}$ = 712.6 Hz, $PF_6$). $^{13}$C NMR (300 MHz, $CDCl_3$, 25°C): δ 86.2 (Cp), 116.5 (Ru-C≡*C*), 125.8-133.6 (Ph), 137.7, 138.2, 141.7, 152.4, 155.8 (bpy), 149.4 (Ru-*C*). Carbons from COs were not detected. ESI-MS ($CH_2Cl_2$, 15 V, 150°C): m/z (fragment, relative intensity): 1219 ($[M + H]^+$, 100). IR: ($CH_2Cl_2$) ν(C≡O) 2028(s), 1928(s) $cm^{-1}$. Anal. Calcd for $C_{61}H_{47}F_6N_3O_3P_3ReRu$: C 53.71, H 3.45, N 3.08%. Found: C 53.13, H 3.59, N 3.03%.

## 5.3.3 Syntheses of $d^6$ - $d^8$ - $d^6$ Heterotrimetallic Complexes

### 5.3.3.1 Material information

$PdCl_2(CH_3CN)_2$[203] and $PtCl_2(CH_3CN)_2$[203] were prepared according to the literature methods.

### 5.3.3.2 Syntheses

**[*trans*-RuCl(C≡Cpy-4)(dppm)$_2$]$_2$[PdCl$_2$] (5.17)**

*trans*-[RuCl(C≡Cpy-4)(dppm)$_2$] (**5.1**) (121 mg, 0.12 mmol) and $PdCl_2(CH_3CN)_2$ (16 mg, 0.06 mmol) in $CH_2Cl_2$ (30 mL) was stirred for 12 h at r.t. The solvent was removed under vacuum and the resulting residue purified by recrystallization from THF/hexane. Yield 59 mg (45%). $^1$H NMR (300 MHz, $CDCl_3$, 25°C): δ 4.88 (m, 8H, C*H*$_2$), 5.62 (d, $J_{H\text{-}H}$ = 6.7 Hz, 4H, py), 7.09-7.42 (m, 80H, Ph), 8.02 (d, $J_{H\text{-}H}$ = 6.7 Hz, 4H, py). $^{31}$P NMR (300 MHz, $CDCl_3$, 25°C): δ -6.3 (s, dppm). $^{13}$C NMR (300 MHz, $CDCl_3$, 25°C): δ 151.5 (s, Ru-*C*), 150.4 ($C_\alpha$(py)), 135.8/135.7 (dt ($C_\alpha$-phenyl)), 133.7 ($C_\gamma$(py)), 133.1 (dt, $C_\beta$-phenyl), 129.6/129.5 (d, $C_\delta$-phenyl), 128.2 (dt, $C_\gamma$-phenyl), 127.8/127.7 ($C_\beta$(py)), 125.5 (s, Ru-C≡*C*), 52.8 (t, P-*C*H$_2$). ESI-MS ($CH_2Cl_2$, 15 V, 150°C): m/z (fragment, relative intensity): 1226 ([RuCl(C≡Cpy)(dppm)$_2$-PdCl-py)]$^+$, 100), 1007 ([RuCl(C≡Cpy)(dppm)$_2$ + H]$^+$, 75). IR: (KBr) ν(C≡C) 2049 cm$^{-1}$(m). Anal. Calcd for $C_{114}H_{96}Cl_4N_2PdRu_2P_8$: C 62.44, H 4.38, N 1.28%. Found: C 62.18, H 4.36, N 1.36%.

**[*trans*-RuCl(C≡Cpy-4)(dppm)$_2$]$_2$[PtCl$_2$](5.18)**

Complex **5.18** was synthesized similar to the procedure for **5.17**, except that $PtCl_2(CH_3CN)_2$ was used instead of $PdCl_2(CH_3CN)_2$. The yellow solid of **5.18** was isolated in 23% yield. $^1$H NMR (300 MHz, $CDCl_3$, 25°C): δ 4.90 (m, 8H, C*H*$_2$), 5.61 (d, $J_{H-H}$ = 6.8 Hz, 4H, py), 7.08-7.42 (m, 80H, Ph), 8.13 (d, $J_{H-H}$ = 6.7 Hz, 4H, py). $^{31}$P NMR (300 MHz, $CDCl_3$, 25°C): δ -6.4 (s, dppm). $^{13}$C NMR (300 MHz, $CDCl_3$, 25°C): δ 151.5 (s, Ru-*C*), 150.6 ($C_\alpha$(py)), 135.8 (dt ($C_\alpha$-phenyl)), 133.7/133.6 ($C_\gamma$(py)), 133.1/133.0 (dt, $C_\beta$-phenyl), 129.6/129.5 (d, $C_\delta$-phenyl), 128.3 (dt, $C_\gamma$-phenyl), 127.8/127.7 ($C_\beta$(py)), 125.5 (s, Ru-C≡*C*), 53.4 (t, P-*C*H$_2$). ESI-MS ($CH_2Cl_2$, 15 V, 150°C): m/z (fragment, relative intensity): 1211 ([RuCl(dppm)$_2$(C≡Cpy)-Pt)]$^+$, 85), 929 ([RuCl(dppm)$_2$(C≡C)]$^+$, 100). IR: (KBr) ν(C≡C) 2046 cm$^{-1}$(m). Anal. Calcd for $C_{114}H_{96}Cl_4N_2PtRu_2P_8$: C 60.03, H 4.21, N 1.23%. Found: C 59.54, H 4.34, N 1.38%.

**[*trans*-RuCl(C≡Cpy-4)(dppe)$_2$]$_2$[PdCl$_2$] (5.19)**

Complex **5.19** was synthesized similar to the procedure for **5.17**, except that *trans*-[RuCl(C≡Cpy-4)(dppe)$_2$] (**5.3**) was used instead of *trans*-[RuCl(C≡Cpy-4)(dppm)$_2$] (**5.1**). The yellow solid of **5.19** was isolated in 45%. $^1$H NMR (300 MHz, $CDCl_3$, 25°C): δ 2.66 (t, 16H, C*H*$_2$), 6.12 (d, $J_{H-H}$ = 6.8 Hz, 4H, py), 6.95-7.37 (m, 80H, Ph), 8.24 (d, $J_{H-H}$ = 6.6 Hz, 4H, py). $^{31}$P NMR (300 MHz, $CDCl_3$, 25°C): δ 49.2 (s, dppe). $^{13}$C NMR (300 MHz, $CDCl_3$, 25°C): δ 150.9 (s, Ru-*C*), 135.4-125.6 (Ph & py), 30.4 (m, P-*C*H$_2$). Ru-C≡*C* could not be detected. ESI-MS: ($CH_2Cl_2$, 15 V, 150°C): m/z (fragment, relative intensity): 1160

(1/2[M+2Cl]$^{2+}$, 100). IR: ($CH_2Cl_2$) ν(C≡C) 2032 $cm^{-1}$ (s). Anal. Calcd for $C_{118}H_{104}Cl_4N_2PdRu_2P_8$: C 63.05, H 4.63, N 1.25%. Found: C 62.46, H 4.67, N 1.23%.

**[*trans*-RuCl(C≡Cpy-4)(dppe)$_2$]$_2$[PtCl$_2$] (5.20)**

Complex **5.20** was synthesized similar to the procedure for **5.18**, except that *trans*-[RuCl(C≡Cpy-4)(dppe)$_2$] (**5.3**) was used instead of *trans*-[RuCl(C≡Cpy-4)(dppm)$_2$] (**5.1**). The yellow complex **5.20** was isolated in 38% yield. $^1$H NMR (300 MHz, $CDCl_3$, 25°C): δ 2.66 (t, 16H, C*H*$_2$), 6.09 (d, $J_{H-H}$ = 5.9 Hz, 4H, py), 6.96-7.40 (m, 80H, Ph), 8.33 (d, $J_{H-H}$ = 5.9 Hz, 4H, py). $^{31}$P NMR (300 MHz, $CDCl_3$, 25°C): δ 49.2 (s, dppe). $^{13}$C NMR (300 MHz, $CDCl_3$, 25°C): δ 151.1 (s, Ru-*C*), 138.6-125.7 (Ph & py), 113.7 (Ru-C≡*C*), 30.4 (m, P-*C*H$_2$). ESI-MS ($CH_2Cl_2$, 15 V, 150°C): m/z (fragment, relative intensity): 1132 (1/2[M-2Cl]$^{2+}$, 100). IR: ($CH_2Cl_2$) ν(C≡C) 2037 $cm^{-1}$ (s). Anal. Calcd for $C_{118}H_{104}Cl_4N_2PtRu_2P_8$: C 60.64, H 4.45, N 1.20%. Found: C 61.02, H 4.36, N 1.24%.

**[*trans*-RuH(C≡Cpy-4)(dppe)$_2$]$_2$[PdCl$_2$] (5.21)**

Complex **5.21** was synthesized similar to the procedure for **5.17**, except that *trans*-[RuH(C≡Cpy-4)(dppe)$_2$] (**5.4**) was used instead of *trans*-[RuCl(C≡Cpy-4)(dppm)$_2$] (**5.1**). The yellow solid of **5.21** was isolated in 35%. $^1$H NMR (300 MHz, $CDCl_3$, 25°C): δ -9.75 (qn, $J_{P-H}$ = 19.4 Hz, 2H, Ru-*H*), 1.99 (m, 8H, C*H*$_2$), 2.43 (m, 8H, C*H*$_2$), 6.64 (d, $J_{H-H}$ = 6.8 Hz, 4H, py), 6.96-7.45 (m, 80H, Ph), 8.37 (d, $J_{H-H}$ = 6.8 Hz, 4H, py). $^{31}$P NMR (300 MHz, $CDCl_3$, 25°C): δ 69.1 (s, dppe).

$^{13}$C NMR (300 MHz, $CDCl_3$, 25°C): δ 151.0 (s, Ru-*C*), 138.3-125.7 (Ph & py), 32.8 (m, P-*C*$H_2$). Ru-C≡*C* could not be detected. ESI-MS: ($CH_2Cl_2$, 15 V, 150°C): m/z (fragment, relative intensity): 1002 ([RuH(dppe)$_2$(C≡Cpy) + H]$^+$, 100), 1108 ([RuH(dppe)$_2$(C≡Cpy-Pd) + H]$^+$, 35), 897 ([Ru(dppe)$_2$]$^{2+}$, 30). IR: ($CH_2Cl_2$) ν(C≡C) 2035 cm$^{-1}$ (s). Anal. Calcd for $C_{118}H_{106}Cl_2N_2PdRu_2P_8$: C 65.04, H 4.87, N 1.29%. Found: C 64.33, H 4.75, N 1.32%.

**[RuCp(C≡Cpy-4)(dppf)]$_2$[PdCl$_2$] (5.22)**

Complex **5.22** was synthesized similar to the procedure for **5.17**, except that [RuCp(C≡Cpy-4)(dppf)] (**5.7**) was used instead of *trans*-[RuCl(C≡Cpy-4)(dppm)$_2$] (**5.1**). The yellow solid of **5.22** was isolated in 55%. $^1$H NMR (300 MHz, $CDCl_3$, 25°C): δ 4.02 (s, 4H, dppf), 4.25 (s, 4H, dppf), 5.00 (s, 2H, dppf), 5.04 (s, 4H, dppf), 5.30 (s, 2H, dppf), 4.33 (s, 10H, Cp), 6.84 (d, $J_{H-H}$ = 6.8 Hz, 4H, py), 7.30-7.74 (m, 40H, Ph), 8.38 (d, $J_{H-H}$ = 6.8 Hz, 4H, py). $^{31}$P NMR (300 MHz, $CDCl_3$, 25°C): δ 55.7 (s, dppf). $^{13}$C NMR (300 MHz, $CDCl_3$, 25°C): δ 151.7 (s, Ru-*C*), 135.2 (Ph), 126.8 (Ph), 84.5 (Cp). Other carbon resonances could not be detected. ESI-MS ($CH_2Cl_2$, 15 V, 150°C): m/z (fragment, relative intensity): 1042 ([RuCp(C≡Cpy)(dppf)-PdCl-py)]$^+$, 100), 824 ([RuCp(C≡Cpy)(dppf) + H]$^+$, 35). IR ($CH_2Cl_2$): ν(C≡C) 2045 cm$^{-1}$(w). Anal. Calcd for $C_{92}H_{74}Cl_2Fe_2N_2PdRu_2P_4$: C 60.63, H 4.06, N 1.54%. Found: C 60.15, H 4.13, N 1.57%.

**[RuCp(C≡Cpy-4)(dppf)]$_2$[PtCl$_2$] (5.23)**

Complex **5.23** was synthesized similar to the procedure for **5.18**, except that [RuCp(C≡Cpy-4)(dppf)] (**5.7**) was used instead of *trans*-[RuCl(C≡Cpy-4)(dppm)$_2$] (**5.1**). The yellow solid of **5.23** was isolated in 40%. $^1$H NMR (300 MHz, $CDCl_3$, 25°C): δ 4.03 (s, 4H, dppf), 4.25 (s, 4H, dppf), 4.33 (s, 14H, dppf & Cp), 5.06 (s, 4H, dppf), 6.82 (d, $J_{H-H}$ = 6.9 Hz, 4H, py), 7.32-7.74 (m, 40H, Ph), 8.47 (d, $J_{H-H}$ = 6.9 Hz, 4H, py). $^{31}$P NMR (300 MHz, $CDCl_3$, 25°C): δ 55.7 (s, dppf). $^{13}$C NMR: (300 MHz, $CDCl_3$, 25°C): δ 151.7 (s, Ru-*C*), 133.8 (Ph), 127.3 (Ph), 85.2 (Cp). Other carbon resonances could not be detected. ESI-MS ($CH_2Cl_2$, 15 V, 150°C): m/z (fragment, relative intensity): 1912 ($[M]^+$, 15), 1130 ($[RuCp(C≡Cpy)(dppf)\text{-}PtCl\text{-}py)]^+$, 20), 1089 ($[RuCp(C≡Cpy)(dppf)\text{-}PtCl_2)]^+$, 20), 749 ($[RuCp(C≡C)(dppf)]^+$, 100), 721 ($[RuCp(dppf)]^+$, 65). IR ($CH_2Cl_2$): ν(C≡C) 2047 cm$^{-1}$(w). Anal. Calcd for $C_{92}H_{74}Cl_2Fe_2N_2PtRu_2P_4$: C 57.80, H 3.87, N 1.47%. Found: C 57.22, H 3.96, N 1.51%.

## 5.3.4 Syntheses of $d^6$ - $d^7$ - $d^7$ - $d^6$ Heterotetrametallic Complexes

### 5.3.4.1 Material information

$CH_3COONa$, $CH_3COOH$, $CH_3CH_2COOH$, $CH_3(CH_2)_3COOH$ and $C(CH_3)_3COOH$ were obtained from Aldrich and used as received. Dirhodium tetracarboxylates $[Rh_2(O_2CCH_2CH_3)_4]$,[204] $[Rh_2(O_2C(CH_2)_3CH_3)_4]$,[205] and $[Rh_2(O_2CCMe_3)_4]$[206] were prepared by ligand exchange reaction between $[Rh_2(O_2CCH_3)_4]$[207] and the corresponding fatty acid according to literature methods.

### 5.3.4.2 Syntheses

**[RuCp(C≡Cpy-4)(dppf)]$_2$[Rh$_2$(O$_2$CR)$_4$] (5.24 R = CH$_3$, 5.25 R = CH$_2$CH$_3$, 5.26 R = (CH$_2$)$_3$CH$_3$, 5.27 R = C(CH$_3$)$_3$).** Essentially the same procedures were applied to synthesize **5.24 – 5.27**; consequently, only the preparation of **5.24** is described in detail.

**[RuCp(C≡Cpy-4)(dppf)]$_2$[Rh$_2$(O$_2$CCH$_3$)$_4$] (5.24)**

[RuCp(C≡Cpy-4)(dppf)] (**5.7**) (82 mg, 0.1 mmol) and [Rh$_2$(O$_2$CCH$_3$)$_4$] (22 mg, 0.05 mmol) in THF (30 mL) was heated to reflux under an inert atmosphere of $N_2$ for 12 h. The red precipitate was collected and washed with $Et_2O$ for 3 times. Yield: 70 mg (67%). $^1$H NMR (300 MHz, $CDCl_3$, 25°C): δ 1.94 (s, 12H, C*H*$_3$), 4.02 (s, 4H, dppf), 4.26 (s, 4H, dppf), 4.34 (s, 4H, dppf), 5.25 (s, 4H, dppf), 4.39 (s, 10H, Cp), 7.31-7.86 (m, 44H, Ph & py), 9.04 (d, 4H, py). $^{31}$P NMR (300 MHz, $CDCl_3$, 25°C): δ 55.8 (s, dppf). $^{13}$C NMR (300 MHz, $CDCl_3$, 25°C): δ 191.7 (*C*O$_2$), 149.9 (Ru-*C*), 134.2-126.5 (Ph & py), 84.9 (Cp), 73.1-65.8 (Fc), 23.9 (*C*H$_3$). IR ($CH_2Cl_2$): ν(C≡C) 2063 (s), ν(C-O) 1591 (s), 1429 (m) cm$^{-1}$. Anal. calc. for $C_{100}H_{86}N_2O_8P_4Fe_2Rh_2Ru_2$: C 57.63, H 4.12, N 1.34%. Found: C 57.51, H 4.60, N 1.40%.

**[RuCp(C≡Cpy-4)(dppf)]$_2$[Rh$_2$(O$_2$CCH$_2$CH$_3$)$_4$] (5.25)**

The pale red product of **5.25** was isolated in 70% yield. $^1$H NMR (300 MHz, $CDCl_3$, 25°C): δ 0.98 (t, 12H, C*H*$_3$), 2.19 (q, 8H, C*H*$_2$), 4.02 (s, 4H, dppf), 4.27 (s, 4H, dppf), 4.34 (s, 4H, dppf), 5.27 (s, 4H, dppf), 4.38 (s, 10H, Cp), 7.29-7.87 (m, 44H, Ph & py), 8.98 (d, 4H, py). $^{31}$P NMR (300 MHz, $CDCl_3$, 25°C): δ 55.7 (s, dppf). $^{13}$C NMR (300

MHz, $CDCl_3$, 25°C): δ 194.7 (*C*$O_2$), 149.9 (Ru-*C*), 134.2-126.4 (Ph & py), 84.9 (Cp), 73.1-67.9 (Fc), 30.6 (*C*$H_2$), 10.4 (*C*$H_3$). IR ($CH_2Cl_2$): ν(C≡C) 2063 (s), ν(C-O) 1587(s), 1424 (m) $cm^{-1}$. Anal. calc. for $C_{104}H_{94}N_2O_8P_4Fe_2Rh_2Ru_2$: C 58.26, H 4.39, N 1.31%. Found: C 57.93, H 4.44, N 1.37%.

**[RuCp(C≡Cpy-4)(dppf)]$_2$[Rh$_2$(O$_2$C(CH$_2$)$_3$CH$_3$)$_4$] (5.26)**

The red product of **5.26** was isolated in 68% yield. $^1$H NMR (300 MHz, $CDCl_3$, 25°C): δ 0.84 (t, 12H, C*H*$_3$), 1.21 (m, 8H, $CH_3C$*H*$_2CH_2CH_2$), 1.48 (m, 8H, $CH_3CH_2C$*H*$_2CH_2$), 2.14 (t, 8H, $CH_3CH_2CH_2C$*H*$_2$), 4.02 (s, 4H, dppf), 4.27 (s, 4H, dppf), 4.34 (s, 4H, dppf), 5.29 (s, 4H, dppf), 4.38 (s, 10H, Cp), 7.30-7.90 (m, 44H, Ph & py), 8.95 (d, 4H, py). $^{31}$P NMR (300 MHz, $CDCl_3$, 25°C): δ 55.7 (s, dppf). $^{13}$C NMR (300 MHz, $CDCl_3$, 25°C): δ 193.9 (*C*$O_2$), 150.0 (Ru-*C*), 134.2-126.3 (Ph & py), 112.5 (Ru-C≡*C*), 84.9 (Cp), 73.1-68.0 (Fc), 37.0-13.8 ((*C*$H_2$)$_3$*C*$H_3$). IR ($CH_2Cl_2$): ν(C≡C) 2064 (s), ν(C-O) 1588 (s), 1418 (m) $cm^{-1}$. Anal. calc. for $C_{112}H_{110}N_2O_8P_4Fe_2Rh_2Ru_2$: C 59.63, H 4.88, N 1.24%. Found: C 59.29, H 4.97, N 1.27%.

**[RuCp(C≡Cpy-4)(dppf)]$_2$[Rh$_2$(O$_2$CC(CH$_3$)$_3$)$_4$] (5.27)**

The pale red product of **5.27** was isolated in 60% yield. $^1$H NMR (300 MHz, $CDCl_3$, 25°C): δ 0.98 (s, 36H, C*H*$_3$), 2.19 (q, 8H, C*H*$_2$), 4.03 (s, 4H, dppf), 4.28 (s, 4H, dppf), 4.36 (s, 4H, dppf), 5.30 (s, 4H, dppf), 4.38 (s, 10H, Cp), 7.28-7.90 (m, 44H, Ph & py), 8.74 (d, 4H, py). $^{31}$P NMR (300 MHz, $CDCl_3$, 25°C): δ 55.6 (s, dppf). $^{13}$C NMR (300 MHz, $CDCl_3$, 25°C): δ 198.1 (*C*$O_2$), 149.9 (Ru-*C*), 134.2-126.0 (Ph & py), 85.0 (Cp),

73.2-68.0 (Fc), 27.9 ($CH_3$). IR ($CH_2Cl_2$): ν(C≡C) 2065 (s), ν(C-O) 1584 (s), 1416 (m) $cm^{-1}$. Anal. calc. for $C_{112}H_{110}N_2O_8P_4Fe_2Rh_2Ru_2$: C 59.63, H 4.88, N 1.24%. Found: C 59.34, H 4.93, N 1.31%.

**[*trans*-RuCl(C≡Cpy-4)(dppm)$_2$]$_2$[Rh$_2$(O$_2$CR)$_4$] (5.28 R = CH$_3$, 5.29 R = CH$_2$CH$_3$, 5.30 R = (CH$_2$)$_3$CH$_3$, 5.31 R = C(CH$_3$)$_3$).** Complexes **5.28 – 5.31** were synthesized in a manner similar to that employed for **5.24 – 5.27**, except that *trans*-[RuCl(C≡Cpy-4)(dppm)$_2$] (**5.1**) was used instead of [RuCp(C≡Cpy-4)(dppf)] (**5.7**).

**[*trans*-RuCl(C≡Cpy-4)(dppm)$_2$]$_2$[Rh$_2$(O$_2$CCH$_3$)$_4$] (5.28)**

The light red complex **5.28** was isolated in 75% yield. $^1$H NMR (300 MHz, $CDCl_3$, 25°C): δ 1.94 (s, 12H, C$H_3$), 4.98 (s, 8H, P-C$H_2$-P), 6.22 (d, 4H, py), 7.14-7.48 (m, 80H, Ph), 8.75 (d, 4H, py). $^{31}$P NMR (300 MHz, $CDCl_3$, 25°C): δ -6.1 (s, dppm). $^{13}$C NMR (300 MHz, $CDCl_3$, 25°C): δ 191.8 ($CO_2$), 148.9 (Ru-*C*), 134.7-126.1 (Ph & py), 50.2 (P-$CH_2$-P), 23.9 ($CH_3$). IR ($CH_2Cl_2$): ν(C≡C) 2051 (s), ν(C-O) 1592 (s), 1430 (m) $cm^{-1}$. Anal. calc. for $C_{122}H_{108}Cl_2N_2O_8P_8Rh_2Ru_2$: C 59.63, H 4.40, N 1.14%. Found: C 58.75, H 4.67, N 1.17%.

**[*trans*-RuCl(C≡Cpy-4)(dppm)$_2$]$_2$[Rh$_2$(O$_2$CCH$_2$CH$_3$)$_4$] (5.29)**

The light red complex **5.29** was isolated in 70% yield. $^1$H NMR (300 MHz, $CDCl_3$, 25°C): δ 0.99 (t, 12H, C$H_3$), 2.20 (q, 8H, C$H_2$), 4.97 (s, 8H, P-C$H_2$-P), 6.19 (d, 4H,

py), 7.14-7.48 (m, 80H, Ph), 8.66 (d, 4H, py). $^{31}$P NMR (300 MHz, $CDCl_3$, 25°C): δ -6.1 (s, dppm). $^{13}$C NMR (300 MHz, $CDCl_3$, 25°C): δ 194.7 (*C*$O_2$), 149.0 (Ru-*C*), 134.6-125.9 (Ph & py), 112.1 (Ru-C≡*C*), 50.2 (P-*C*$H_2$-P), 30.6 (*C*$H_2$), 10.3 (*C*$H_3$). IR ($CH_2Cl_2$): ν(C≡C) 2072 (s), ν(C-O) 1587 (s), 1427 (m) cm$^{-1}$. Anal. calc. for $C_{126}H_{116}Cl_2N_2O_8P_8Rh_2Ru_2$: C 60.22, H 4.62, N 1.12%. Found: C 59.43, H 4.90, N 1.18%.

**[*trans*-RuCl(C≡Cpy-4)(dppm)$_2$]$_2$[Rh$_2$(O$_2$C(CH$_2$)$_3$CH$_3$)$_4$] (5.30)**

The light red complex **5.30** was isolated in 70% yield. $^1$H NMR (300 MHz, $CDCl_3$, 25°C): δ 0.87 (t, 12H, C*H*$_3$), 1.21 (m, 8H, $CH_3$C*H*$_2$$CH_2CH_2$), 1.46 (m, 8H, $CH_3CH_2$C*H*$_2$$CH_2$), 2.15 (t, 8H, $CH_3CH_2CH_2$C*H*$_2$), 4.97 (s, 8H, P-C*H*$_2$-P), 6.18 (d, 4H, py), 7.14-7.48 (m, 80H, Ph), 8.60 (d, 4H, py). $^{31}$P NMR (300 MHz, $CDCl_3$, 25°C): δ -6.1 (s, dppm). $^{13}$C NMR (300 MHz, $CDCl_3$, 25°C): δ 193.9 (*C*$O_2$), 148.9 (Ru-*C*), 134.6-125.8 (Ph & py), 42.0 (P-*C*$H_2$-P), 36.9-13.9 ((*C*$H_2$)$_3$*C*$H_3$). IR ($CH_2Cl_2$): ν(C≡C) 2072 (s), ν(C-O) 1587 (s), 1426 (m) cm$^{-1}$. Anal. calc. for $C_{134}H_{132}Cl_2N_2O_8P_8Rh_2Ru_2$: C 61.30, H 5.03, N 1.07%. Found: C 60.32, H 5.27, N 1.11%.

**[*trans*-RuCl(C≡Cpy-4)(dppm)$_2$]$_2$[Rh$_2$(O$_2$CC(CH$_3$)$_3$)$_4$] (5.31)**

The light red complex **5.31** was isolated in 66% yield. $^1$H NMR (300 MHz, $CDCl_3$, 25°C): δ 0.99 (s, 36H, C*H*$_3$), 4.96 (s, 8H, P-C*H*$_2$-P), 6.06 (d, 4H, py), 7.12-7.47 (m, 80H, Ph), 8.41 (d, 4H, py). $^{31}$P NMR (300 MHz, $CDCl_3$, 25°C): δ -6.0 (s, dppm). $^{13}$C NMR (300 MHz, $CDCl_3$, 25°C): δ 197.9 (*C*$O_2$), 148.8 (Ru-*C*), 134.8-125.3 (Ph & py),

50.2 (P-*C*$CH_2$-P), 27.8 (*C*$H_3$). IR ($CH_2Cl_2$): ν(C≡C) 2073 (s), ν(C-O) 1583 (s), 1416 (s) $cm^{-1}$. Anal. calc. for $C_{134}H_{132}Cl_2N_2O_8P_8Rh_2Ru_2$: C 61.30, H 5.03, N 1.07%. Found: C 61.23, H 4.90, N 1.16%.

**[*trans*-RuH(C≡Cpy-4)(dppe)$_2$]$_2$[Rh$_2$(O$_2$CR)$_4$] (5.32 R = $CH_2CH_3$, 5.33 R = $(CH_2)_3CH_3$, 5.34 R = $C(CH_3)_3$).** Complexes **5.32 – 5.34** were synthesized in a manner similar to that employed for **5.24 – 5.27**, except that *trans*-[RuH(C≡Cpy-4)(dppe)$_2$] (**5.4**) was used instead of [RuCp(C≡Cpy-4)(dppf)] (**5.7**).

**[*trans*-RuH(C≡Cpy-4)(dppe)$_2$]$_2$[Rh$_2$(O$_2$C$CH_2CH_3$)$_4$] (5.32)**

The light red complex **5.32** was isolated in 58% yield. $^1$H NMR (300 MHz, $CDCl_3$, 25°C): δ -9.93 (m, 2H, Ru-*H*), 1.05 (t, 12H, C*H*$_3$), 2.06 (s, 8H, P-C*H*$_2$-$CH_2$-P), 2.27 (q, 8H, $CH_2$), 2.56 (s, 8H, P-$CH_2$-C*H*$_2$-P), 7.00-7.49 (m, 84H, Ph & py), 8.98 (d, 4H, py). $^{31}$P NMR (300 MHz, $CDCl_3$, 25°C): δ 69.2 (s, dppe). $^{13}$C NMR (300 MHz, $CDCl_3$, 25°C): δ 194.9 (*C*$O_2$), 149.7 (Ru-*C*), 138.7-125.8 (Ph & py), 33.1-32.8 (P-*C*$H_2$-*C*$H_2$-P), 30.7 (*C*$H_2$), 10.4 (*C*$H_3$). IR ($CH_2Cl_2$): ν(C≡C) 2048 (s), ν(C-O) 1588 (s), 1426 (m) $cm^{-1}$. Anal. calc. for $C_{130}H_{126}N_2O_8P_8Rh_2Ru_2$: C 62.45, H 5.04, N 1.12%. Found: C 62.11, H 5.37, N 1.15%.

**[*trans*-RuH(C≡Cpy-4)(dppe)$_2$]$_2$[Rh$_2$(O$_2$C(CH$_2$)$_3$CH$_3$)$_4$] (5.33)**

The light red complex **5.33** was isolated in 63% yield. $^1$H NMR (300 MHz, $CDCl_3$,

25°C): δ -9.92 (m, 2H, Ru-*H*), 0.89 (t, 12H, C*H*$_3$), 1.24 (m, 8H, CH$_3$C*H*$_2$CH$_2$CH$_2$), 1.50 (m, 8H, CH$_3$CH$_2$C*H*$_2$CH$_2$), 2.20 (t, 8H, CH$_3$CH$_2$CH$_2$C*H*$_2$), 2.04 (d, 8H, P-C*H*$_2$-CH$_2$-P), 2.56 (s, 8H, P-CH$_2$-C*H*$_2$-P), 7.00-7.49 (m, 84H, Ph & py), 8.94 (s, 4H, py). $^{31}$P NMR (300 MHz, CDCl$_3$, 25°C): δ 69.2 (s, dppe). $^{13}$C NMR (300 MHz, CDCl$_3$, 25°C): δ 194.0 (*C*O$_2$), 149.7 (Ru-*C*), 138.7-125.8 (Ph & py), 33.1-32.8 (P-*C*H$_2$-*C*H$_2$-P), 37.1, 28.1-13.9 ((*C*H$_2$)$_3$*C*H$_3$). IR (CH$_2$Cl$_2$): ν(C≡C) 2048 (s), ν(C-O) 1588 (s), 1425 (m) cm$^{-1}$. Anal. calc. for C$_{138}$H$_{142}$N$_2$O$_8$P$_8$Rh$_2$Ru$_2$: C 63.45, H 5.44, N 1.07%. Found: C 63.05, H 5.52, N 1.10%.

**[*trans*-RuH(C≡Cpy-4)(dppe)$_2$]$_2$[Rh$_2$(O$_2$CC(CH$_3$)$_3$)$_4$] (5.34)**

The light red complex **5.34** was isolated in 60% yield. $^{1}$H NMR (300 MHz, CDCl$_3$, 25°C): δ -9.95 (m, 2H, Ru-*H*), 0.96 (s, 36H, C*H*$_3$), 2.02 (s, 8H, P-C*H*$_2$-CH$_2$-P), 2.52 (s, 8H, P-CH$_2$-C*H*$_2$-P), 6.98-7.47 (m, 84H, Ph & py), 8.68 (d, 4H, py). $^{31}$P NMR (300 MHz, CDCl$_3$, 25°C): δ 69.1 (s, dppe). $^{13}$C NMR (300 MHz, CDCl$_3$, 25°C): δ 197.9 (*C*O$_2$), 149.4 (Ru-*C*), 138.6-125.3 (Ph & py), 33.1-32.7 (P-*C*H$_2$-*C*H$_2$-P), 27.9 (*C*H$_3$). IR (CH$_2$Cl$_2$): ν(C≡C) 2049 (s), ν(C-O) 1584 (s), 1414 (m) cm$^{-1}$. Anal. calc. for C$_{138}$H$_{142}$N$_2$O$_8$P$_8$Rh$_2$Ru$_2$: C 63.45, H 5.44, N 1.07%. Found: C 63.11, H 5.30, N 1.07%.

# References


1 T. Verbiest, S. Houbrechts, M. Kauranen, K. Clays and A. Persoons, *J. Mater. Chem*., **1997**, 7, 2175.

2 M. M. Haley and R. R. Tykwinshi, *Carbon-Rich Compounds*, **2006**, p26-82, WILEY-VCH Verlagg GmbH & Co. KGaA.

3 *Nonlinear Optics of Organic Molecules and Polymers*, H. S. Nalwa, S. Miyata and Eds., CRC Press: Boca Raton, FL, **1997**.

4 C. E. Powell and M. G. Humphrey, *Coord. Chem. Rev.*, **2004**, 248, 725.

5 J. P. Morrall, G. T. Dalton, M. G. Humphrey and M. Samoc, *Adv. Organomet. Chem*., **2008**, 55, 61.

6 K. Onitsuka, N. Ohara, F. Takei and S. Takahashi, *Dalton Trans*., **2006**, 3693.

7 C. Olivier, B. Kim, D. Touchard and S. Rigaut, *Organometallics*, **2008**, 27, 509.

8 G. A. Koutsantonis, G. I. Jenkins, P. A. Schauer, B. Szczepaniak, B. W. Skelton, C. Tan and A. H. White, *Organometallics*, **2009**, 28, 2195.

9 I. O. Koshevoy, Y. C. Lin, A. J. Karttunen, P. T. Chou, P. Vainiotalo, S. P. Tunik, M. Haukka and T. A. Pakkanen, *Inorg. Chem*., **2009**, 48, 2094.

10 Y. Fan, L. Y. Zhang, F. R. Dai, L. X. Shi and Z. N. Chen, *Inorg. Chem*., **2008**, 47, 2811.

11 M. L. Muro, S. Diring, X. Wang, R. Ziessel and F. N. Castellano, *Inorg. Chem*., **2008**, 47, 6796.

12 J. R. Berenguer, B. G., J. Fernandez, J. Fornies and E. Lalinde, *Inorg. Chem*., **2009**, 48, 5250.

13 R. F. Winter and S. Záliš, *Coord. Chem. Rev.*, **2004**, 248, 1565.

14 L. Rigamonti, B. B., M. P. Cifuentes, R. L. Roberts, S. Petrie, R. Stranger, S. Righetto, A. Teshome, I. Asselberghs, K. Clays and M. G. Humphrey, *Inorg. Chem*., **2009**, 48, 3562.

15 S. Fraysse, C. Coudret and J. P. Launay, *J. Am. Chem. Soc.*, **2003**, 125, 5880.

16 N. Gauthier, C. Olivier, S. Rigaut, D. Touchard, T. Roisnel, M. G. Humphrey and F. Paul, *Organometallics*, **2008**, 27, 1063.

17 T. Y. Dong, S. F. Lin, C. P. Chen, S. W. Yeh, H. Y. Chen and Y. S. Wen, *J. Organomet. Chem*, **2009**, 694, 1529.

18 N. J. Long and C. K. Williams, *Angew. Chem. Int. Ed.*, **2003**, 42, 2586.

19 N. Gauthier, N. Tchouar, F. Justaud, G. Argouarch, M. P. Cifuentes, L. Toupeț, D. Touchard, J. F. Halet, S. Rigaut, M. G. Humphrey, K. Costuas and F. Paul, *Organometallics*, **2009**, 28, 2253.

20 Y. Zhu, O. Clot, M. O. Wolf and G. P. A. Yap, *J. Am. Chem. Soc.*, **1998**, 120, 1812.

21 S. K. Hurst, G. L. Xu and T. Ren, *Organometallics*, **2003**, 22, 4118.

22 R. T. Farley, Q. Zheng, J. A. Gladysz and K. S. Schanze, *Inorg. Chem.*, **2008**,

47, 2955.

23 R. Nast, *Angew. Chem. Int. Ed.*, **1960**, 72, 26.

24 R. Nast, *Coord. Chem. Rev.*, **1982**, 47, 89.

25 A. K. Bar, B. Gole, S. Ghosh and P. S. Mukherjee, *Dalton Trans*., **2009**, 6701.

26 W. Y. Wong and C. L. Ho, *Coord. Chem. Rev.*, **2006**, 250, 2627.

27 W. Y. Wong, *Coord. Chem. Rev.*, **2007**, 251, 2400.

28 K. M. C. Wong, C. K. Hui, K. L. Yu and V. W. W. Yam, *Coord. Chem. Rev.*, **2002**, 229, 123.

29 H. B. Xu, L. Y. Zhang, X. M. Chen, X. L. Li and Z. N. Chen, *Crystal Growth & Design*, **2009**, 9, 569.

30 M. P. Cifuentes, C. E. Powell, J. P. Morrall, A. M. McDonagh, N. T. Lucas, M. G. Humphrey, M. Samoc, S. Houbrechts, I. Asselberghs, K. Clays, A. Persoons and T. Isoshima, *J. Am. Chem. Soc.*, **2006**, 128, 10819.

31 M. G. Humphrey, C. E. Powell, M. P. Cifuentes, J. P. Morrall and M. Samoc, *In Metal-Containing and Metallosupramolecular Polymers and Materials*, **2006**, Vol. 928, p258.

32 R. Packheiser, P. Ecorchard, B. Walfort and Heinrich Lang, *J. Organomet. Chem*., **2008**, 693, 933.

33 S. Bolano, M. M. Rodriguez-Rocha, J. Bravo, J. Castro, E. Onate and M. Peruzzini, *Organometallics*, **2009**, 28, 6020.

34 M. Asay, B. Donnadieu, W. W. Schoeller and G. Bertrand, *Angew. Chem. Int.*

*Ed.*, **2009**, 48, 4796.

35 C. E. Powell, S. K. Hurst, J. P. Morrall, M. P. Cifuentes, R. L. Roberts, M. Samoc and M. G. Humphrey, *Organometallics*, **2007**, 26, 4456.

36 M. Samoc, J. P. Morrall, G. T. Dalton, M. P. Cifuentes and M. G. Humphrey, *Angew. Chem. Int. Ed.*, **2007**, 46, 731.

37 M. C. Lui, C. P. Chung, W. C. Chang, Y. C. Lin, Y. Wang and Y. H. Liu, *Organometallics*, **2009**, 28, 5204.

38 D. Touchard, P. Haquette, S. Guesmi, L. LePichon, A. Daridor, L. Toupet and P. H. Dixneuf, *Organometallics*, **1997**, 16, 3640.

39 D. Touchard, P. Haquette, N. Pirio, L. Toupet and P. H. Dixneuf, *Organometallics*, **1993**, 12, 3132.

40 A. M. McDonagh, C. E. Powell, J. P. Morrall, M. P. Cifuentes and M. G. Humphrey, *Organometallics*, **2003**, 22, 1402.

41 M. I. Bruce, K. Costuas, B. G. Ellis, J. F. Halet, P. J. Low, B. Moubaraki, K. S. Murray, N. Ouddaı, G. J. Perkins, B. W. Skelton and A. H. White, *Organometallics*, **2007**, 26, 3735.

42 S. Rigaut, D. Touchard and P. H. Dixneuf, *Coord. Chem. Rev.*, **2004**, 248, 1585.

43 C. Bianchini, P. Innocenti, M. Peruzzini, A. Romerosa and F. Zanobini, *Organometallics*, **1996**, 15, 272.

44 S. M. Yang, M. C. W. Chan, K. K. Cheung, C. M. Che and S. M. Peng, *Organometallics*, **1997**, 16, 2819.

45 H. Werner, A. Stark, M. Schulz and J. Wolf, *Organometallics*, **1992**, 11, 1126.

46 B. Xi, G. L. Xu, P. E. Fanwick and T. Ren, *Organometallics*, **2009**, 28, 2338.

47 V. W. W. Yam, W. Y. Lo, C. H. Lam, W. K. M. Fung, K. M. C. Wong, V. C. Y. Lau and N. Zhu, *Coord. Chem. Rev.*, **2003**, 245, 39.

48 I. Ara, N. Chaouche, J. Forniés, C. Fortuño, A. Kribii and A. Martín, *Eur. J. Inorg. Chem.*, **2005**, 3894.

49 T. Sue, Y. Sunada and H. Nagashima, *Eur. J. Inorg. Chem.*, **2007**, 2897.

50 H. Lang, D. S. A. George and G. Rheinwald, *Coord. Chem. Rev.*, **2000**, 206, 101.

51 P. Mathur, S. Chatterjee and V. D. Avasare, *Adv. Organomet. Chem.*, **2008**, 55, 201.

52 I. Y. Wu, J. T. Lin, J. Luo, S. S. Sun, C. S. Li, K. J. Lin, C. Tsai, C. C. Hsu and J. L. Lin, *Organometallics*, **1997**, 16, 2038.

53 D. Méry, L. P., C. Ornelas, J. Ruiz, S. Nlate, D. Astruc, J. C. Blais, J. Rodrigues, S. Cordier, K. Kirakci and C. Perrin, *Inorg. Chem.*, **2006**, 45, 1156.

54 M. I. Bruce, K. Costuas, T. Davin, B. G. Ellis, J. F. Halet, C. Lapinte, P. J. Low, M. E. Smith, B. W. Skelton, L. Toupet and A. H. White, *Organometallics*, **2005**, 24, 3864.

55 C. E. Powell, M. P. Cifuentes, M. G. Humphrey, A. C. Willis, J. P. Morrall and M. Samoc, *Polyhedron*, **2007**, 26, 284.

56 S. Houbrechts, K. Clays, A. Persoons, V. Cadierno, M. P. Gamasa and J. Gimeno, *Organometallics*, **1996**, 15, 5266.

57 R. L. Cordiner, M. E. Smith, A. S. Batsanov, D. Albesa-Jove, F. Hartl, J. A. K. Howard and P. J. Low, *Inorg. Chim. Acta*, **2006**, 359, 946.

58 F. E. Kühn, J. L. Zuo, F. F. de Biani, A. M. Santos, Y. Zhang, J. Zhao, A. Sandulache and E. Herdtweck, *New. J. Chem.*, **2004**, 28, 43.

59 M. Y. Choi, M. C. W. Chan, S. M. Peng, K. K. Cheung and C. M. Che, *Chem. Commun.*, **2000**, 1259.

60 A. Klein, O. Lavastre and J. Fiedler, *Organometallics*, **2006**, 25, 635.

61 R. L. Cordiner, D. Corcoran, D. S. Yufit, A. E. Goeta, J. A. K. Howard and P. J. Low, *Dalton Trans.*, **2003**, 3541.

62 M. I. Bruce, P. A. Humphrey, M. Jevric, B. W. Skelton and A. H. White, *J. Organomet. Chem.*, **2007**, 692, 2564.

63 M. I. Bruce, P. A. Humphrey, M. Jevric, G. J. Perkins, B. W. Skelton and A. H. White, *J. Organomet. Chem.*, **2007**, 692, 1748.

64 O. Lavastre, M. Even and P. H. Dixneuf, *Organometallics*, **1996**, 15, 1530.

65 O. Lavastre, J. Plass, P. Bachmann, S. Guesmi, C. Moinet and P. H. Dixneuf, *Organometallics*, **1997**, 16, 184.

66 M. I. Bruce, J. F. Halet, B. Le Guennic, B. W. Skelton, M. E. Smith and A. H. White, *Inorg. Chim. Acta*, **2003**, 350, 175.

67 L. Zhang, B. Xi, I. P. C. Liu, M. M. R. Choudhuri, R. J. Crutchley, J. B. Updegraff, J. D. Protasiewicz and T. Ren, *Inorg. Chem*, **2009**, 48, 5187.

68 V Guillaume and J. M. Tour, *Tetrahedronn Letters*, **2009**, 50, 1427.

69 Q. Y. Hu, W. X. Lu, H. D. Tang, H. H. Y. Sung, T. B. Wen, I. D. Williams, G. K. L. Wong, Z. Lin and G. Jia, *Organometallics*, **2005**, 24, 3966.

70 S. Rigaut, F. Monnier, F. Mousset, D. Touchard and P. H. Dixneuf, *Organometallics*, **2002**, 21, 2654.

71 J. L. Fillaut, J. Andrièès, J. Perruchon, J. P. Desvergne, L. Toupet, L. Fadel, B. Zouchoune and J. Y. Saillard, *Inorg. Chem.*, **2007**, 46, 5922.

72 J. P. L. Morrall, M. P. Cifuentes, M. G. Humphrey, R. Kellens, E. Robijns, I. Asselberghs, K. Clays, A. Persoons, M. Samoc and A. C. Willis, *Inorg. Chim. Acta*, **2006**, 359, 998.

73 M. I. Bruce, P. J. Low, F. Hartl, P. A. Humphrey, F. de Montigny, M. Jevric, C. Lapinte, G. J. Perkins, R. L. Roberts, B. W. Skelton and A. H. White, *Organometallics*, **2005**, 24, 5241.

74 C. W. Liu, Y. C. Lin, S. L. Huang, C. W. Cheng, Y. H. Liu and Y. Wang, *Organometallics*, **2007**, 26, 3431.

75 Y. H. Lo, Y. C. Lin, G. H. Lee and Y. Wang, *Eur. J. Inorg. Chem.*, **2004**, 4616.

76 M. P. Gamasa, J. Gimeno, B. M. Martín-Vaca, J. Borge, S. Garcíía-Granda and E. Pérez-Carreno, *Organometallics*, **1994**, 13, 4045.

77 M. I. Bruce, *Chem. Rev.*, **1991**, 91, 197.

78 M. I. Bruce, M. Jevric, G. J. Perkins, B. W. Skelton and A. H. White, *J. Organomet. Chem.*, **2007**, 692, 1757.

79 C. Y. Wong, M. C. W. Chan, N. Zhu and C. M. Che, *Organometallics*, **2004**, 23, 2263.

80 G. Q. Yin, Q. H. Wei, L. Y. Zhang and Z. N. Chen, *Organometallics*, **2006**, 25, 580.

81 H. Lang, R. Pachheiser and B. Walfort, *Organometallics*, **2006**, 25, 1836.

82 V. W. W. Yam, K. L. Cheung, E. C. C. Cheng, N. Zhu and K. K. Cheung, *Dalton Trans.*, **2003**, 1830.

83 C. S. Griffith, G. A. Koutsantoins, B. W. Skelton and A. H. White, *Chem. Commun.*, **2002**, 2174.

84 F. Paul, B. G. Ellis, M. I. Bruce, L. Toupet, T. Roisnel, K. Costuas, J. F. Halet and C. Lapinte, *Organometallics*, **2006**, 25, 649.

85 S. Rigaut, J. Perruchon, S. Guesmi, C. Fave, D. Touchard and P. H. Dixneuf, *Eur. J. Inorg. Chem.*, **2005**, 447.

86 S. K. Hurst, M. P. Cifuentes, J. P. L. Morrall, N. T. Lucas, I. R. Whittall, M. G. Humphrey, I. Asselberghs, A. Persoons, M. Samoc, B. Luther-Davies and A. C. Willis, *Organometallics*, **2001**, 20, 4664-4675.

87 M. A. Fox, R. L. Roberts, W. M. Khairul, F. Hartl and P. J. Low, *J. Organomet. Chem.*, **2007**, 692, 3277.

88 R. L. Cordiner, D. Albesa-Jove, R. L. Roberts, J. D. Farmer, H. Puschmann, D. Corcoran, A. E. Goeta, J. A. K. Howard and P. J. Low, *J.Organomet. Chem.*, **2005**, 690, 4908.

89 C. Y. Wong, C. M. Che, M. C. W. Chan, J. Han, K. H. Leung, D. L. Phillips,

K. Y. Wong and N. Zhu, *J. Am. Chem. Soc*., **2005**, 127, 13997.

90 C. M. Che, C. M. Ho and J. S. Huang, *Coord. Chem. Rev*., **2007**, 251, 2145.

91 Y. Zhu, D. B. Millet, M. O. Wolf and S. J. Rettig, *Organometallics*, **1999**, 18, 1930.

92 L. B. Gao, S. H. Liu, L. Y. Zhang, L. X. Shi and Z. N. Chen, *Organometallics*, **2006**, 25, 506.

93 C. E. Powell, M. P. Cifuentes, J. P. Morrall, R. Stranger, M. G. Humphrey, M. Samoc, B. Luther-Davies and G. A. Heath, *J. Am. Chem. Soc*., **2003**, 125, 602.

94 Rico Packheiser, M. Lohan, B. Bräuer, F. Justaud, C. Lapinte and H. Lang, *J. Organomet. Chem.*, **2008**, 693, 2898.

95 M. Samoc, N. Gauthier, M. P. Cifuentes, F. Paul, C. Lapinte and M. G. Humphrey, *Angew. Chem. Int. Ed.*, **2008**, 47, 629.

96 M. Samoc, N. Gauthier, M. P. Cifuentes, F. Paul, C. Lapinte and M. G. Humphrey, *Angew. Chem. Int. Ed.*, **2006**, 45, 7376.

97 S. Rigaut, C. Olivier, K. Costuas, S. Choua, O. Fadhel, J. Massue, P. Turek, J. Y. Saillard, P. H. Dixneuf and D. Touchard, *J. Am. Chem. Soc*., **2006**, 128, 5859.

98 K. M. C. Wong, L. L. Hung, W. H. Lam, N. Zhu and V. W. W. Yam, *J. Am. Chem. Soc*., **2007**, 129, 4350.

99 V. W. W. Yam, C. H. Tao, L. J. Zhang, K. M. C. Wong and K. K. Cheung, *Organometallics*, **2001**, 20, 453.

100 C. J. Adams and S. J. Pope, *Inorg. Chem*., **2004**, 43, 3492.

101 W. Y. Wong, K. Y. Ho, S. L. Ho and Z. Y. Lin, *J. Organomet. Chem.*, **2003**, 683, 341.

102 J. van Slageren, R. F. Winter, A. Klein and S. Hartmann, *J. Organomet. Chem.*, **2003**, 670, 137.

103 W. Lu, M. C. W. Chan, N. Zhu, C. M. Che, Z. He and K. Y. Wong, *Chem. Eur. J.*, **2003**, 9, 6155.

104 C. J. Adams, L. E. Bowen, M. G. Humphrey, J. P. L. Morrall, M. Samoc and L. J. Yellowlees, *Dalton Trans*., **2004**, 4130.

105 M. P. Cifuentes and M. G. Humphrey, *J. Organomet. Chem.*, **2004**, 689, 3968.

106 C. E. Powell, M. P. Cifuentes, A. M. McDonagh, S. K. Hurst, N. T. Lucas, C. D. Delfs, R. Stranger, M. G. Humphrey, S. Houbrechts, I. Asselberghs, A. Persoons and D. C. R. Hockless, *Inorgan. Chim. Acta*, **2003**, 352, 9.

107 I. R. Whittall, M. G. Humphrey, A. Persoons and S. Houbrechts, *Organometallics*, **1996**, 15, 1935.

108 S. K. Hurst, M. G. Humphrey, T. Isoshima, K. Wostyn, I. Asselberghs, K.Clays, A. Persoons, M. Samoc and B. Luther-davies, *Organometallics*, **2002**, 21, 2024.

109 W. Z. Chen and T. Ren, *Organometallics*, **2005**, 24, 2660.

110 M. I. Bruce, M. L. Cole, C. R. Parker, B. W. Skelton and A. H. White, *Organometallics*, **2008**, 27, 3352.

111 M. C. Puerta and P. Valerga, *Coord. Chem. Rev*., **1999**, 193-195, 977.

112 P. L. Low and M. I. Bruce, *Adv. Organomet. Chem.*, **2001**, 48, 71.

113 J. L. Zuo, E. Herdtweck, F. F. de Biani, A. M. Santosa and F. E. Kühn, *New J. Chem*., **2002**, 26, 889.

114 J. W. Ying and T. Ren, *J. Organomet. Chem*., **2008**, 693, 1449.

115 M. I. Bruce, M. Jevric, C. R. Parker, W. Patalinghug, B. W. Skelton, A. H. White and N. N. Zaitseva, *J. Organomet. Chem*., **2008**, 693, 2915.

116 R. Packheiser, P. Ecorchard, T. Rüffer, M. Lohan, B. Bräuer, F. Justaud, C. Lapinte and H. Lang, *Organometallics*, **2008**, 27, 3444.

117 C. Olivier, B. Kim, D. Touchard and S. Rigaut, *Organometallics*, **2008**, 27, 509.

118 P. J. Giordano and M. S. Wrighton, *J. Am. Chem. Soc.*, **1979**, 101, 2888.

119 D. Péron, A. Romero and P. H. Dixneuf, *Organometallics*, **1995**, 14, 3319.

120 R. H. Naulty, A. M. McDonagh, I. R. Whittall, M. P. Cifuentes, M. G. Humphrey, S. Houbrechts, J. Maes, A.Persoons, G. A. Heath and D. C. R. Hochless, *J. Organomet. Chem.*, **1998**, 563, 137.

121 G. J. Zhou, W. Y. Wong, Z. Lin and C. Ye, *Angew. Chem., Int. Ed*., **2006**, 45, 6189.

122 J. L. Fillaut, J. Perruchon, P. Blanchard, J. Roncali, S. Golhen, M. Allain, A. Migalsaka-Zalas, I. V. Kityk and B. Sahraoui, *Organometallics*, **2005**, 24, 687.

123 I. Y. Wu, J. T. Lin, J. Luo, C. S. Li, C. Tsai, Y. S. Wen, C. C. Hsu, F. F. Yeh

and S. Liou, *Organometallics*, **1998**, 17, 2188.

124 P. A. Humphrey, P. Turner, A. F. Masters, L. D. Field, M. P. Cifuentes, M. G. Humphrey, I. Asselberghs, A. Persoons and M. Samoc, *Inorg. Chim. Acta*, **2005**, 358, 1663.

125 J. K. Hino, L. D. Ciana, W. J. Dressick and B. P. Sullivan, *Inorg. Chem.*, **1992**, 31, 1072.

126 S. M. Frederichs, J. C. Luong and M. S. Wrighton, *J. Am. Chem. Soc.*, **1979**, 101, 7415.

127 J. V. Caspar and T. J. Meyer, *J. Phys. Chem.*, **1983**, 87, 952.

128 S. A. Moya, R. Pastene, H. Le Bozec, P. J. Baricelli, A. J. Pardey and J. Gimeno, *Inorg. Chim. Acta*, **2001**, 312, 7.

129 S. S. Sun and A. J. Lees, *J. Am. Chem. Soc.*, **2000**, 122, 8956.

130S. S. Sun, J. A. Anspach, A. J. Lees and P. Y. Zavalij, *Organometallics*, **2002**, 21, 685.

131 L. L. Ouh, T. E. Müller and Y. K. Yan, *J. Organomet. Chem.*, **2005**, 690, 3774.

132 C. Metcalfe, S. Spey, H. Adams and J. A. Thomas, *Dalton Trans.*, **2002**, 4732.

133 D. H. Gibson, J. G. Andino, S. Bhamidi, B. A. Sleadd and M. S. Mashuta, *Organometallics*, **2001**, 20, 4956.

134 D. H. Gibson, J. G. Andino and M. S. Mashuta, *Organometallics*, **2005**, 24, 5067.

135 V. Ferretti, P. Gilli, V. Bertollasi, G. Marangoni, B. Pitterri and G. Chessa, *Acta Cryst.*, **1992**, 48, 814.

136 J. Madureira, T. M. Santos, B. J. Goodfellow, M. Lucena, J. P. de Jesus, M. G. Santana-Marques, M. G. B. Drew and V. Félix, *Dalton Trans.*, **2000**, 4422.

137 L. E. Helberg, T. B. Gunnoe, B. C. Brooks, M. Sabat and W. D. Harman, *Organometallics*, **1999**, 18, 573.

138 J. L. Zuo, E. Herdtweck and F. E. Kühn, *Dalton Trans.*, **2002**, 1244.

139 M. Ferrer, L. Rodríguez, O. Rossell, J. C. Lima, P. Gómez-Sal and A. Martín, *Organometallics*, **2004**, 23, 5096.

140 F. A. Cotton and T. R. Felthouse, *Inorg. Chem.*, **1981**, 20, 600.

141J. E. Fiscus, S. Shotwell, R. C. Layland, M. D. Smith, H. C. zur Loye and U. H. F. Bunz, *Chem. Commun.*, **2001**, 2674.

142 M. Mikuriya, D. Yoshioka and M. Handa, *Coord. Chem. Rev.*, **2006**, 250, 2194.

143 W. M. Xue and F. E. Kühn, *Eur. J. Inorg. Chem.*, **2001**, 2041.

144 W. M. Xue, F. E. Kühn, E. Herdtweck and Q. Li, *Eur. J. Inorg. Chem.*, **2001**, 213.

145 Q. Ge and T. S. A. Hor, *Dalton Trans.*, **2008**, 2929.

146 G. B. Deacon and R. J. Phillips, *Coord. Chem. Rev.*, **1980**, 33, 227.

147 S. A. Johnson, H. R. Hunt and H. M. Neumann, *Inorg. Chem.*, **1963**, 2, 960.

148 A. Endres and G. Maas, *Tetrahedron*, **2002**, 58, 3999.

149 W. M. Xue, F. E. Kühn and E. Herdtweck, *Polyhedron*, **2001**, 20, 791.

150 J. E. Fiscus, S. Shotwell, R. C. Layland, M. D. Smith, H. C. zur Loye and U. H. F. Bunz, *Chem. Commun.*, **2001**, 2674 and references cited therein.

151 J. K. Kera, J. Bacsa, B. W. Smucker and K. R. Dunbar, *Eur. J. Inorg. Chem.*, **2004**, 368.

152 F. Barcelo, F. A. Cotton, P. Lahuerta, R. Llusar, M. Sanau, W. Schwotzer and M. A. Ubeda, *Organometallics*, **1986**, 5, 808.

153 F. P. Pruchnik, A. Jutarska, Z. Ciunik and M. Pruchnik, *Inorg. Chim. Acta*, **2003**, 350, 609.

154 F. Estevan, P. Lahuerta, J. Latorre, E. Peris, S. G. Granda, F. G. Beltrán, A. Aguirre and M. A. Salvadó, *Dalton Trans.*, **1993**, 1681.

155 Skoog, et. al., *Principles of Instrumental Analysis. 6th ed. Thomson Brooks/Cole.*, **2007**, 169.

156 B. Babgi, L. Rigamonti, M. P. Cifuentes, T. C. Corkery, M. D. Randles, T. Schwich, S. Petrie, R. Stranger, A. Teshome, I. Asselberghs, K. Clays, M. Samoc and M. G. Humphrey, *J. Am. Chem. Soc.*, **2009**, 131, 10293.

157 M. Ferrer, A. Gutiérrez, L. Rodríguez, O. Rossell, J. C. Lima, M. Font-Bardia and X. Solans, *Eur. J. Inorg. Chem.*, **2008**, 2899.

158 Q. Ge, G. T. Dalton, M. G. Humphrey, M. Samoc and T. S. A. Hor, *Chem. Asian J.*, **2009**, 4, 998.

159 M. A. Fox, R. L. Roberts, W. M. Khairul, F. Hartl and P. J. Low, *J. Organomet. Chem.*, **2007**, 692, 3277.

160 N. J. Long, C. K. Wong and A. J. P. White, *Organometallics*, **2006**, 25, 2525.

161 R. L. Cordiner, D. Albesa-Jové, R. L. Roberts, J. D. Farmer, H. Puschmann, D. Corcoran, A. E. Goeta, J. A. K. Howard and P. J. Low, *J. Organomet. Chem.*, **2005**, 690, 4909.

162 M. L. Kuznetsov and A. J. L. Pombeiro, *Dlaton Trans.*, **2003**, 738.

163 K. M. C. Wong, W. S. Tang, X. X. Lu, N. Zhu and V. W. W. Yam, *Inorg. Chem.*, **2005**, 44, 1492.

164 K. L. Cheung, S. K. Yip and V. W. W. Yam, *J. Organomet. Chem.*, **2004**, 689, 4451.

165 W. M. Xue, M. C. W. Chan, Z. M. Sun, K. K. Cheung, S. T. Liu and C. M. Che, *Organometallics*, **1998**, 17, 1622.

166 G. Zhang, J. Zhao, G. Raudaschl-Sieber, E. Herdtweck and F. E. Kühn, *Polyhedron*, **2002**, 21, 1737.

167 V. Cadierno, S. Conejero, M. P. Gamasa and J. Gimeno, *Organometallics*, **1999**, 18, 582.

168 M. Sheik-Bahae, A. A. Said, T. Wei, D. J. Hagan and E. W. van Stryland, *IEEE J. Quantum Electr.*, **1990**, 26, 760.

169 A. M. McDonagh, M. P. Cifuentes, I. R. Whittall, M. G. Humphrey, M. Samoc, B. Luther-Davies and D. C. R. Hockless, *J. Organomet. Chem.*, **1996**, 526, 99.

170 S. K. Hurst, M. P. Cifuents, A. M. McDonagh, M. G. Humphrey, M. Samoc,

B. Luther-Davies, I. Asselberghs and A. Persoons, *J. Organomet. Chem*., **2002**, 642, 259.

171C. Feuvrie, O. Maury, H. L. Bozec, I. Ledoux, J. P. Morrall, G. T. Dalton, M. Samoc and M. G. Humphrey, *J. Phys. Chem. A*, **2007**, 111, 8980.

172 M. Samoc, A. Samoc, B. Luther-Davies, M. G. Humphrey and M. S. Wong, *Opt. Mater*., **2002**, 21, 485.

173 D. Milam, *Appl. Opt.* **1998**, 37, 546.

174 M. A. Fox, R. L. Roverts, T. E. Baines, B. Le Guennic, J. F. Halet, F. Hartl, D. S. Yufit, D. Albesa-Jove, J. A. K. Howard and P. J. Low, *J. Am. Chem. Soc.*, **2008**, 130, 3566.

175 T. Cardolaccia, A. M. Funston, M. E. Kose, J. M. Keller, J. R. Miller and K. S. Schanze, *J. Phys. Chem. B*, **2007**, 111, 10871.

176 C. Lapinte, *J. Organomet. Chem.*, **2008**, 693, 793.

177 A. E. Dray, F. Wittmann, R. H. Friend, A. M. Donald, M. S. Khan, J. Lewis and B. F. G. Johnson, *Synth. Met.*, **1991**, 41, 871.

178 S. C. F. Lam, V. W. W. Yam, K. M. C. Wong, E. C. C. Cheng and N. Zhu, *Organometallics*, **2005**, 24, 4298.

179 F. E. Kühn, J. L. Zuo, F. F. de Biani, A. M. Santos, Y. Zhang, J. Zhao, A. Sandulache and E. Herdtweck, *New. J. Chem*., **2004**, 28, 43.

180 S. P. Cummings, Z. Cao, C. W. Liskey, A. R. Geanes, P. E. Fanwick, K. M. Hassell and T. Ren, *Organometallics*, **2010**, 29, 2783.

181 M. I. Bruce, A. Burgun, C. R. Parker and B. W. Skelton, J. Organomet.

Chem., 2010, 695, 619.

182 (a) Y. Wu, J. T. Lin, J. Luo, S. S. Sun, C. S. Li, K. J. Lin, C. Tsai, C. C. Hsu and J. L. Lin, *Organometallics*, **1997**, 16, 2038; (b) The reported redox potential of 0.56 V ($Ru^{II/III}$) and 0.94 V ($Fe^{II/III}$) vs ferrocene has been converted to be referenced to SCE.

183 (a) C. E. Powell, M. P. Cifuents, J. P. Morrall, R. Stranger, M. G. Humphrey, M. Samoc, B. Luther-Davies and G. A. Heath, *J. Am. Chem. Soc.*, **2003**, 125, 602; (b) The reported redox potentials of 0.50 V ($Ru^{II/III}$) in *trans*-[$RuCl_2(dppe)_2$] and 0.56 V ($Ru^{II/III}$) in *trans*-[$RuCl(CCPh)(dppe)_2$] vs ferrocene has been converted to be referenced to SCE.

184 (a) R. H. Naulty, A. M. McDonagh, I. R. Whittall, M. P. Cifuentes, M. G. Humphrey, S. Houbrechts, J. Maes, A.Persoons, G. A. Heath and D. C. R. Hochless, *J. Organomet. Chem.*, **1998**, 563, 137; (b) The reported redox potentials of 0.53 V ($Ru^{II/III}$) in *trans*-[$RuCl_2(dppm)_2$] and 0.57 V ($Ru^{II/III}$) in *trans*-[$RuCl(dppm)_2(CCC_5H_4N\text{-}2)$] vs ferrocene has been converted to be referenced to SCE.

185 A. M. McDonagh, M. P. Cifuentes, M. G. Humphrey, S. Houbrechts, J. Maes, A. Persoons, M. Samoc and B. Luther-Davies, *J. Organomet. Chem.*, **2000**, 610, 71.

186 (a) S. K. Hurst, M. P. Cifuentes, J. P. L. Morrall, N. T. Lucas, I. R. Whittall, M. G. Humphrey, I. Asselberghs, A. Persoons, M. Samoc, B. Luther-Davies and A. C. Willis, *Organometallics*, **2001**, 20, 4664; (b) The reported redox

potential of 0.55 V ($Ru^{II/III}$) vs ferrocene has been converted to be referenced to SCE.

187 R. H. Naulty, M. P. Cifuentes, M. G. Humphrey, S. Houbrechts, C. Boutton, A. Persoons, G.. A. Heath, D. C. R. Hockless, B. Luther-Davies and M. Samoc, *Dalton Trans.*, **1997**, 4167.

188V. W. W. Yam, K. M. C. Wong, S. H. F. Chong, V. C. Y. Lau, S. C. F. Lam, L. Zhang and K. K. Cheung, *J. Organomet. Chem*., **2003**, 670, 205.

189 S. C. Rasmussen, S. E. Ronco, D. A. Mlsna, M. A. Billadeau, W. T. Pennington, J. W. Kolis and J. D. Petersen, *Inorg. Chem.*, **1995**, 34, 821.

190 K. Kalyanasundaram, *J. Chem. Soc., Faraday Trans.*, **1986**, 82, 2401.

191 (a) W. M. Xue, F. E. Kühn, E. Herdtweck and Q. Li, *Eur. J. Inorg. Chem*., **2001**, 213; (b) The reported redox potential of 1.36 V ($Rh_2^{IV/V}$) vs ferrocene has been converted to be referenced to SCE.

192 (a) W. M. Xue and F. E. Kühn, *Eur. J. Inorg. Chem.*, **2004**, 2041; (b) The reported redox potentials of 0.52 V ($Rh_2^{IV/V}$) in $[Fc(C{\equiv}Cpy\text{-}4)]_2[Rh_2(O_2CCH_3)_4]$ and 0.48 V ($Rh_2^{IV/V}$) in $[Fcpy\text{-}4]_2[Rh_2(O_2CCH_3)_4]$ vs ferrocene has been converted to be referenced to SCE.

193 SMART & SAINT Software Reference Manuals, Version 5.611, Siemens Energy & Automation, Inc., Analytical Instrumentation, Madison, WI, **1996**.

194 G. M. Sheldrick, *SADABS, a software for empirical absorption correction*, University of Göttingen, **1993**.

195 G. M. Sheldrick, *SHELXTL, version 5.03, Siemens Energy & Automation, Inc., Analytical Instrumentation, Madison, WI,* **1996**.

196 J. Chatt, B. L. Shaw and A. E. Field, *J. Chem. Soc*., **1964**, 3466.

197 B. P. Sullivan and T. J. Meyer, *Inorg. Chem.*, **1982**, 21, 1037.

198 M. T. Bautista, E. P. Cappellani, S. D. Drouin, R. H. Morris, C. T. Schweitzer, A. Sella and J. Zubkowski, *J. Am. Chem. Soc*., **1991**, 113, 4876.

199 M. Sato and M. Sekino, *J. Organomet. Chem*., **1993**, 444, 185.

200 M. I. Bruce, C. Hameister, A. G. Swincer and R. C. Wallis, *Inorg. Synth*., **1982**, 21, 78.

201 S. P. Schmidt, W. C. Trogler and F. Basolo, *Inorg. Synth*., **1990**, 28, 160.

202 E. Hevia, J. Pérez and V. Riera, *Inorg. Chem.*, **2002**, 41, 4673.

203 G. K. Anderson and M. Lin, *Inorg. Synth.*, **1990**, 28, 60.

204 J. Kitchens and J. L. Bear, *Thermochim. Acta*, **1970**, 1, 537.

205 A. M. Girond-Godquin and J. C. Marchon, *J. Phys. Chem.*, **1986**, 90, 5502.

206 K. Das, K. M. Kadish and J. L. Bear, *Inorg. Chem.*, **1978**, 17, 930.

207 G. A. Rempel, P. Legzdius, H. Smith and G. Wilkinson, *Inorg. Synth*., **1972**, 13, 90.